



Summary Report for Work Package 3.1.2

Investigation of Super-Conducting Direct Drive Generators

Agreement n.:	308974
Duration	November 2012 – October 2017
Co-ordinator:	DTU Wind



The research leading to these results has received funding from the European Community's Seventh Framework Programme FP7-ENERGY-2012-1-2STAGE under grant agreement No. 308974 (INNWIND.EU).

PROPRIETARY RIGHTS STATEMENT

This document contains information, which is proprietary to the "INNWIND.EU" Consortium. Neither this document nor the information contained herein shall be used, duplicated or communicated by any means to any third party, in whole or in parts, except with prior written consent of the "INNWIND.EU" consortium.

Document information

Document Name:	Summary Report for Work Package 3.1.2 – Investigation of HTS Super-Conducting Direct Drive Generators
Document Number:	Deliverable D 3.1.2
Author:	Arwyn Thomas & Ziad Azar
Document Type	Report
Dissemination level	Public
Review:	Arwyn Thomas & Ziad Azar
Date:	26/01/2016 - Revised July 2016
WP:	3. Electromechanical Conversion
Task:	3.1.2: Design of Superconducting Direct-Drive Generators for Wind Turbines
Approval:	Approved by Author and Asger B Abrahamsen

INTRODUCTION	5
1 SUMMARY OF PHASE A	5
2 SUMMARY OF PHASE B.....	5
3 OUTCOMES AND DISCUSSION.....	6
4 RECOMENDATIONS FOR FUTURE PROJECTS.....	7
APPENDIX A – SMART DELIVARABLES FOR WORK PACKAGE 3.1.2	8



INTRODUCTION

This summary report highlights the outcomes of Phases A and B in the work package 3.1.2. It also contains a discussion of the outcomes and whether the criteria for continuing to Phases C and D are achieved. The details of Phase A – D and the gate requirements are in Appendix A.

1 SUMMARY OF PHASE A

Phase A of work package 3.1.2 was to design and manufacture a field coil out of high temperature superconducting (HTS) 2nd generation tape (YBCO), to demonstrate a practical field coil delivering the required magnetic field at 30K. The work was contracted to Siemens CT, which did the design, manufacturing and testing of the coils. Having done the design process, they achieved in manufacturing 8 test coils, 5 of which failed during testing, leaving 3 to be used in the final field coil, Figure 1.

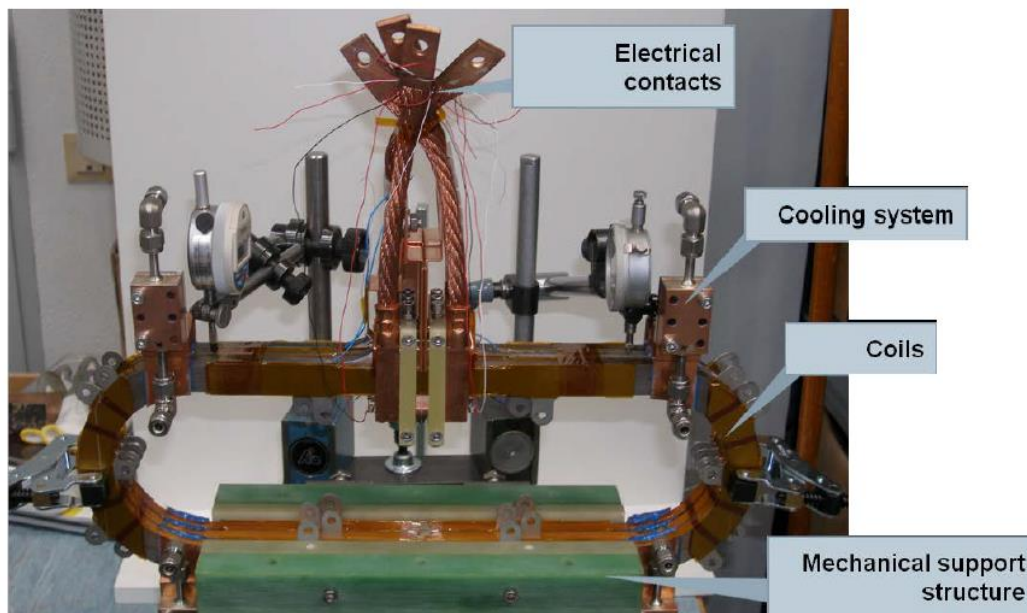


Figure 1. Final field coil before testing of critical current

During the final testing, one of the coils failed with the consequences unknown, although it is speculated that the mechanical forces were the likely cause. By extrapolating the measured current profile it is anticipated that the coil would achieve its designed critical current.

The designed HTS field coils were feasible to the critical currents and magnetic field required at 30K. However the thermal management of the coils needs careful consideration, to minimise the temperature gradient across the coils causing mechanical stress in the HTS tapes. The mechanical brittleness of the coils also poses issues in fault conditions when the HTS field coil can be subjected to large transient forces.

2 SUMMARY OF PHASE B

Phase B of the work package 3.1.2, was to utilise the technical data obtained from Phase A to generate a viable direct-drive generator design to compete with current permanent magnet generator design.

An initial study presented a cost optimised HTS generator topology is required to have an iron cored stator and rotor, illustrated in figure 2, to minimise the required HTS tape in the field winding. Following, a cost optimised design for a 10 and 20 MW generators were presented along with a medium voltage converter topology and excitation voltage supply design. The dimensions of the design are sensitive to the cost of the superconducting tape, with more expensive tape yielding larger diameter and heavier designs,

PROPRIETARY RIGHTS STATEMENT

This document contains information, which is proprietary to the "INN WIND.EU" Consortium. Neither this document nor the information contained herein shall be used, duplicated or communicated by any means to any third party, in whole or in parts, except with prior written consent of the "INN WIND.EU" consortium.

due to lower pole numbers and maximising torque through diameter increase. As the cost of the tape decreases, its proportion to the other active material components can be increased, increasing the pole number and decreasing the generator volume and weight.

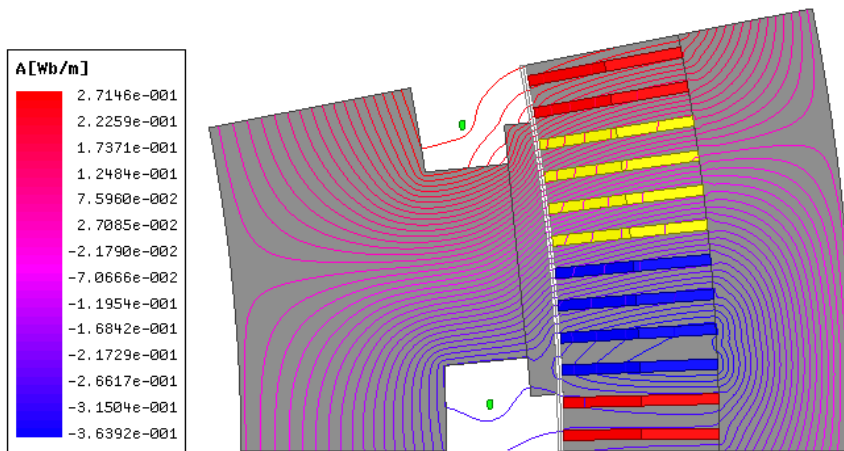


Figure 2. Cross section of the HTS generator (flux plot under load)

Several fault conditions were analysed and it is clear that the design of the exciter can significantly improve the fault mode conditions under converter short-circuit, either minimising the torque pulsations or the force seen by the HTS field coils.

3 OUTCOMES AND DISCUSSION

The outcomes of Phase B showed that a cost optimised design for the direct drive generator can be achieved, although it did not compete with the current costs of the current state of the art permanent magnet direct drive generators. Figure 3 shows the cost profile of a cost optimised HTS DD generator versus the current state of the art generator, showing that the superconducting tape needs to achieve a cost parity of €10/m or less before it can compete (allowing for 30% extra cost for the cryo-cooler). The future projections of the HTS tapes does not estimate that the tapes will achieve this cost parity by 2020, therefore the criteria for advancing to Phases C and D are not met.

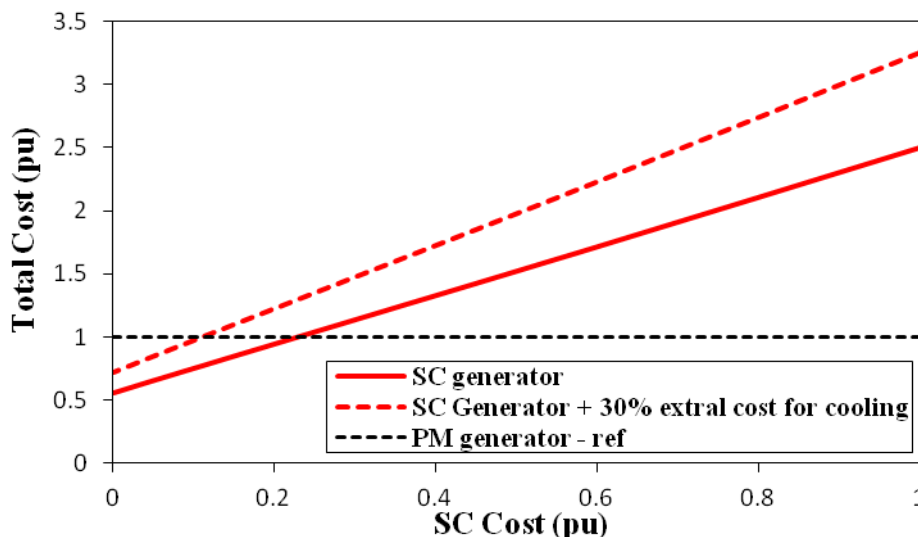


Figure 3. Comparison of active material costs for the HTS and PM DD generators

The mass of the generator was also increased, due to the low relative pole number of the HTS DD generator, this will add cost to the construction of the generator. As the cost of the superconducting material is decreased, the cost optimised generator design can increase the number of poles, allowing for a decrease in the active material mass as shown in figure 4. However, due to the utilisation of rotor pole

steel, to minimise the HTS material content, it is not anticipated to reduce the generator mass compared to current PM DD generator topologies utilising surface mounted magnet designs.

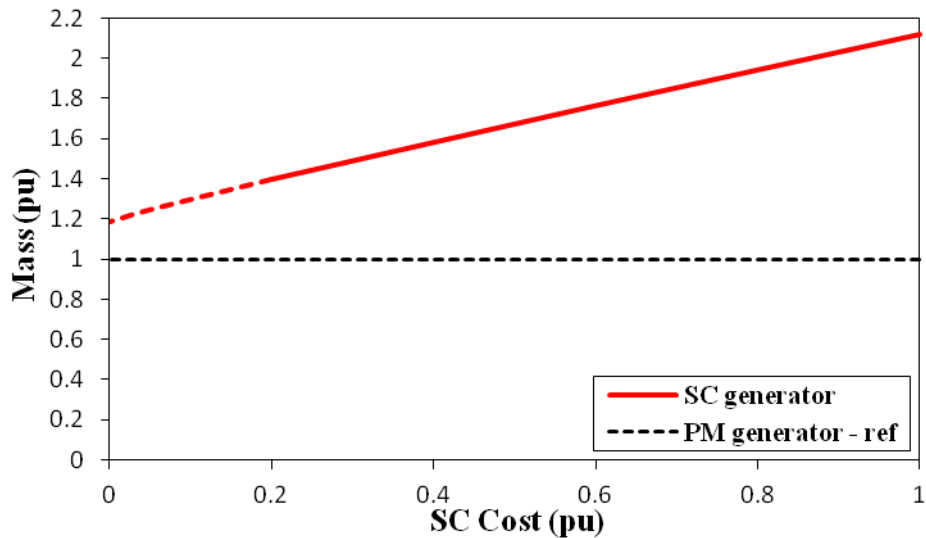


Figure 4. Comparison of mass versus HTS tape cost for cost optimised generator design

The low pole number also poses a challenge for the converter due to the low fundamental electrical frequency. The low frequency will cause thermal fluctuation in the diodes in between the electrical cycles, causing fatigue on the wire bonding and reducing the lifetime. Therefore the converter needs to be increased to reduce the relative device rating and increasing the overall cost of the converter.

4 RECOMENDATIONS FOR FUTURE PROJECTS

Having shown a feasible electromagnetic design optimised for active material costs, future projects should focus on the integration of a field winding and cryo-cooling system, to deliver a cost optimised solution, operation and maintenance and fault conditions. In the opinion of the authors, these are the biggest technical barrier for HTS DD generators.

APPENDIX A – SMART DELIVARABLES FOR WORK PACKAGE 3.1.2

Deliverable No: 3.12	Title: Industrial demonstration of superconducting generator
Month Due: 34	Participants: Siemens Wind Power (SWP) & DTU
Brief Description (3 lines): SWP will design, construct and test a down-scaled superconducting direct drive generator pole targeted at the 3-6 MW direct drive nacelle structure currently equipped with permanent magnets. The performance indicators such as size, weight, efficiency and cost will be extrapolated to P = 10-20 MW from the demonstration and provide input to the INN WIND.EU consortium for assessment of the turbine concepts investigated.	
Specific targets: The work has been organized in the following phases, which are described in tables below: Phase A – Design and test of down scaled race track coil Phase B – Extrapolation of performance indicators to P=10-20 MW generators Phase C - Design and test of downsized, segmented cryostat Phase D - Rotation test of segmented cryostat and test of cryosystem reliability	
Measure of success: A series of Go/No Go criteria have been formulated between then phases: Phase A: 1) Is the superconducting wind turbine drive train design basis available? 2) Functional test race track coil available? Phase B: 1) Is the CoE of the SC generators lower than the SWP DD drive train solution at P = 20 MW in 2020? 2) The project will end if the CoESC is higher than CoESWP,DD in 2020. Phase C: 1) Did the magnetic flux density, current density of coil, operation temperature and heat flow into the cryostat meet the targets? 2) Did airgap flux- and force density between down-sized segmented cryostat and stator segment meet targets? Phase D: 1) Is the total loss associated with the cryogenic system and operating the superconducting coils limited to about 1% of the power of the P = 10-20 MW direct drive generators? 2) Determine reliability and availability of system It should be noted that the INN WIND.EU budget will only cover Phase A and B, where as additional funding will be found for Phase C and D if the CoE target is obtained.	

Participant contributions

Siemens Wind Power: Execution of Phase A-D.

DTU: Discussion of the technology, targets for demonstrator and evaluation of performance indicators.

Phase A – Design and test of down scaled race track coil

Objective

Provide data base and design basis for conceptual design of a 10 – 20 MW superconducting wind turbine drive train.

Task

- 1) Make rough concept design of the system illustrated on figure 1 for $P = 10\text{-}20$ MW.
- 2) Design and construction of a down-sized race track coil based on the 2G coated conductor high temperature superconductor tape.
Targets: Size: width \sim PM pole of SWP 3.0-101 & length $\sim 2 \times$ width.
 $B_{\text{centre}} = 1.5$ T, $B_{\text{max,superconductor}} = 2.5$ T (to be confirmed) at $T = 30$ K.
- 3) Design a segmented cryostat and design one cryostat segment capable of holding the down-sized 2G race track coil.
- 4) Design a down-sized stator structure suited for the higher magnetic flux density.
- 5) Test the race track coil using liquid neon cooling to $T = 30$ K in a laboratory cryostat (@ Siemens CT) and determine if the target operation magnetic flux density, the tape current density and the hoop forces were obtained by the coil support structure at the operation temperature. Make initial investigation of AC losses in the race track coil due to ramping of field and current as well as harmonics superimposed on the DC excitation current of the coil.

DTU, SWP:

- Project Management
- Steering Committee
- Coil dimensions, rough concept design, evaluation of results

Deliverables

- Functional coil
 - Interface, framed
- Test results
 - AC losses, field, temperature, power
- FE model
- Tape properties incl. the price/ cost
 - mechanical, electric, magnetic, cost, access, forecast

Time Schedule:

Summer 2013 - Final delivery end of Sept. 2014 by Siemens CT

Resources/ Budget

459.000,- EUR (415.000,- to Siemens CT; 44.000,- to Siemens Wind Power)

Go/ NoGo criteria

- Is the superconducting wind turbine drive train design basis available?
- Functional test race track coil available?

Phase B – Extrapolation of performance indicators to P=10-20 MW generators

Objective

Design of superconducting wind turbine drive train (10 – 20 MW) and calculate CoE

Task

- 1) Use race-track coil demonstration to extrapolate size, weight, efficiency to P=10-20 MW.
- 2) Design of superconducting wind turbine drive train on the basis of SWP DD concept.
- 3) Investigate state-of-the-art cryogenic cooling systems and estimate CAPEX and OPEX.
- 4) Estimate Cost of Energy of SC generators at P = 10-20 MW.
- 5) Estimate delta AEP, delta Cost and delta CoE (superconducting wind turbine drive train compared with the standard SWP DD concept)

DTU, SWP:

- Project Management
- Steering Committee
- Detailed concept design of the SC drivetrain, evaluation of results, calculation of CoE (delta between SC and permanent magnet generator)

Deliverables

- 10-20 MW extrapolation
- 2 times cryo concept design (for the big and the small coil)
- System design for a turbine
- Estimate delta of AEP, Cost, CoE
- Reliability, availability evaluation
- Delta CAPEX and delta OPEX

Time Schedule

August 2014 to December 2015

Resources/ Budget

392.423,- EUR (Siemens Wind Power)

Go/ NoGo criteria

- Is the CoE of the SC generators lower than the SWP DD drive train solution at P = 20 MW in 2020?
- The project will end if the CoESC is higher than CoESWP,DD in 2020.

Phase C - Design and test of downsized, segmented cryostat

Objective

Design, test and validation of segmented cryostat concept

Task

- 1) Construct a down sized segmented cryostat which can hold the race track coil of phase A.
- 2) Test the race track coil in the segmented cryostat using a flow of first liquid nitrogen (LN₂) T = 77 K and then liquid helium (LHe) T = 4.2 K to determine the magnetic flux density, the tape current density and the heat flow into the cryostat at operation temperature.
- 3) If the segmented cryostat proved operational then construct the down-sized stator segment designed in phase A.
- 4) Measure the static force density between the segmented cryostat holding the down-sized race track coil and the stator segment.

Deliverables

- Operating results
 - field
 - power
 - temperature
 - structural behaviour
- Coil/ stator test result
 - field intensity/ density
 - loads
 - air gap distance
- Update FE model, update CoE and estimate reliability/availability of the concept

Time Schedule

December 2015 – June 2015

Resources/ Budget

Tbd

Go/ NoGo criteria

- Did the concept work?
- Did the magnetic flux density, current density of coil, operation temperature and heat flow into the cryostat meet the targets?
- Did airgap flux- and force density between down-sized segmented cryostat and stator segment meet targets?

Phase D - Rotation test of segmented cryostat and test of cryosystem reliability

Objective

Design, test and validation of the SC concept in a rotational test

Task

- 1) Design and mount of segmented cryostat from phase B on rotating frame.
- 2) Design layout of cryogenic transfer lines from segmented cryostat to rotation coupling and cryocoolers.
- 3) Design current leads and slip rings or brushless excitation of superconducting coils.
- 4) Determine the mechanical loads that the above components will experience in a 10-20 MW turbine and examine if the components all comply with these.

- 5) If found feasible from the above load analysis then construct the rotation frame and mount the segmented cryostat of phase C, transfer lines, rotation coupling, excitation and cryocoolers.
- 6) Examine system performance by performing selected load cases.
- 7) Investigate reliability of system by running the system for extended periods.

Deliverables

To be discussed

Time Schedule

June 2015 – December 2015

Resources/ Budget

Tbd

Evaluation

- Is the total loss associated with the cryogenic system and operating the superconducting coils should be limited to about 1% of the power of the $P = 10\text{-}20$ MW direct drive generators.
- Determine reliability and availability of system

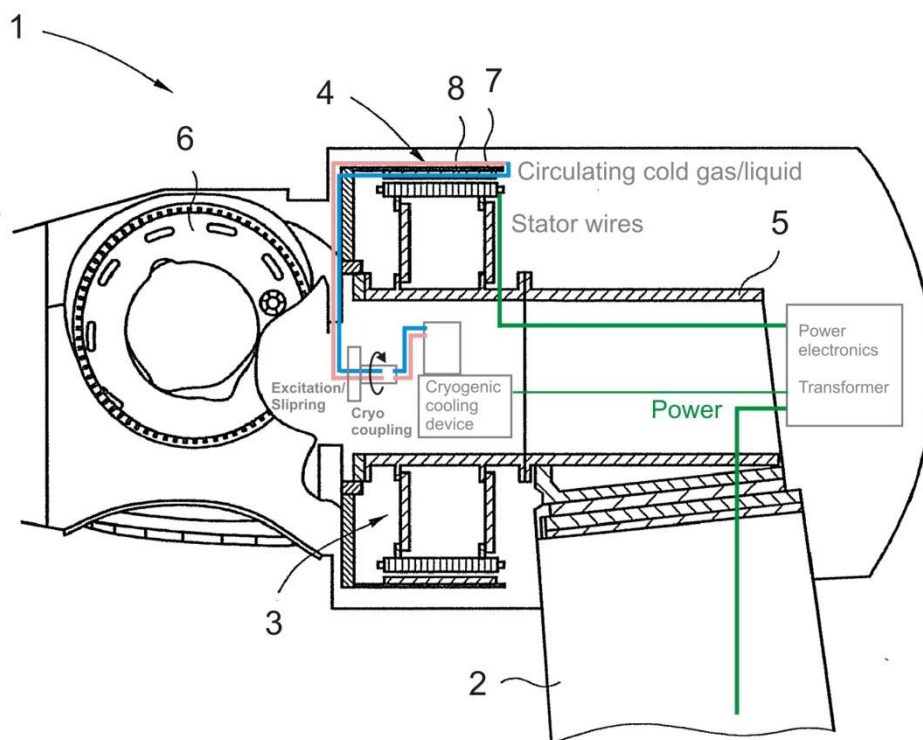


FIGURE 1: Illustration of the Siemens Wind Power concept of changing the current permanent magnet direct drive generator into a superconducting version, where the permanent magnets are replaced by superconducting race track coils. The philosophy of the concept is to have no machinery (cold heads and compressors) in the rotating frame and to use high temperature superconductors in order to obtain the simplest cryogenic system and thereby increase the reliability. The nacelle drawing is reproduced from J. K. Booth, U.

Eriksen, J. B. Nielsen and H. Stiesdal, "Wind turbine with a generator", US 2012/0217752 A1.

Phase A – Design of HTS field coil for direct drive generator for wind turbine

Agreement n.:	308974
Duration	November 2012 – October 2017
Co-ordinator:	DTU Wind

The research leading to these results has received funding from the European Community's Seventh Framework Programme FP7-ENERGY-2012-1-2STAGE under grant agreement No. 308974 (INN WIND.EU).



Document information

Document Name:	Phase A – Design of HTS field coil for direct drive generator for wind turbine
Document Number:	Deliverable D ...
Author:	Arwyn Thomas
Document Type	Report
Dissemination level	Choose an item.
Review:	Ziad Azar
Date:	26/01/2016
WP:	3.1.2
Task:	HTS field coil design for superconducting wind turbine generator
Approval:	Approved by Author

TABLE OF CONTENTS

TABLE OF CONTENTS	16
1 INTRODUCTION	17
2 FIELD COIL DESIGN	18
2.1 GEOMETRY AND HTS TAPE	18
2.2 ELECTROMAGNETIC	19
2.3 MECHANICAL	19
2.4 THERMAL	21
3 COIL CONSTRUCTION	22
4 TESTING	23
4.1 LOW TEMPERATURE QUALITY TESTING	23
4.2 30K COIL TESTING	23
4.3 AC LOSS TESTING	24
5 RESULTS AND CONCLUSION	27
6 CHAPTER 4	ERROR! BOOKMARK NOT DEFINED.
7	27
7.1 FIRST PARAGRAPH	ERROR! BOOKMARK NOT DEFINED.
7.1.1 xxxx	<i>Error! Bookmark not defined.</i>

5 INTRODUCTION

This report presents the work done in the design, manufacture and testing of a field coil using second generation high temperature superconducting (2G-HTS) tape (GdBCO). This work was conducted by a third party, Siemens Corporate Technology (CT), who have experience in manufacturing field coils from HTS tapes, minimising the risk to the project.

The field coil designed is representative of the dimensions required for a field coil of a full scale synchronous generator in order to validate the manufacturing large coils required for direct drive wind turbine generators, Fig. 1. The scope of the project was limited to manufacturing of the field coil itself and its validation; the manufacturing of a cryogenic system was not considered at this stage.

The target rating for the coil was to achieve 1.15T in the centre of the coil conducting 650A at 30K. The electromagnetic, thermal, mechanical and electrical design was undertaken to achieve this outcome. The construction method used was a wet-winding method in which individual coils are formed on a mandrill, and the final field coil is made up of a stack of 3 coils.

Having manufactured the coils, they were tested at different temperatures, initially 77K for qualification testing and then to 30K for validation testing using DC current. The final field coil was also tested under AC current conditions to measure the losses incurred in the event of transient currents.

6 FIELD COIL DESIGN

6.1 Geometry and HTS Tape

The coil geometry is based on a racetrack shape to emulate the Lorentz forces experienced in a field coil. The construction of the final field coil is made up of individual coils stacked on top of each other. This required the contacts to be aligned between each coil layer, therefore the central coil is wound in reverse to allow easy connection. The designed inductance of the field coil is 42.3mH.

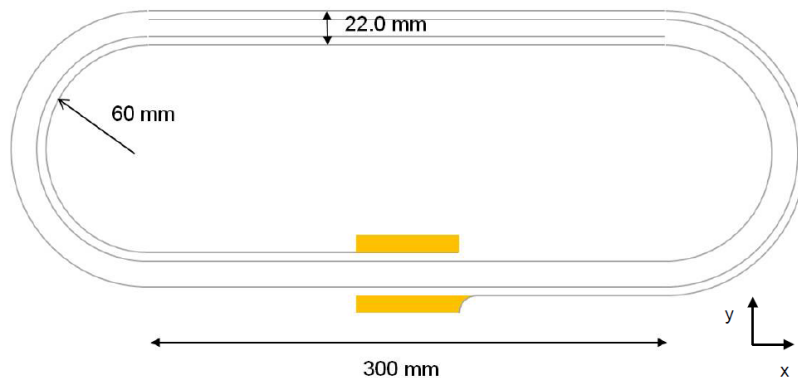


Fig. 1 Geometry layout of HTS coil with position of electrical contacts

The coils are wound from 2G-HTS tape, Fig. 2, which is engineered to support the delicate superconducting ceramic material GdBCO. When the tape is received from the supplier it is tested for critical current and uniform thickness before it is used in the coils to ensure consistent quality.



Fig. 2 Schematic of HTS tape. Buffer and cap layers not shown for simplicity

The performance of the tape can be seen in Fig. 3, in which the critical current has been measured at different temperature from the maximum superconducting temperature of 77K down to 10K. The approximate working point for a synchronous generator requires the tape to be cooled to 30K.

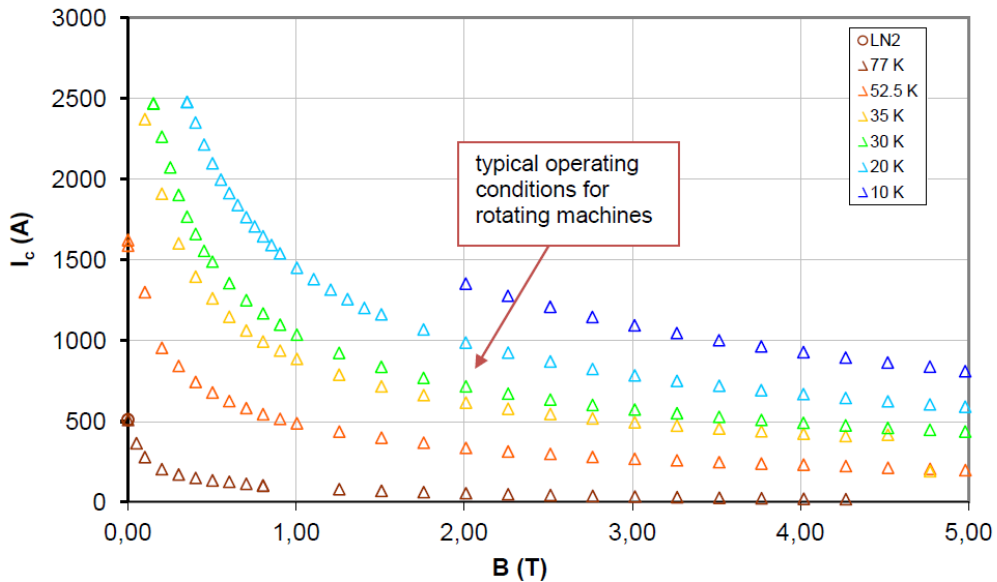


Fig. 3 Typical critical current plot (versus B-field and temperature) of HTS tape.

6.2 Electromagnetic

Electromagnetic finite element analysis of the coil was done to ensure the critical current of the tape would not be exceeded at the applied self-field normal to the tapes surface and temperature. The magnetic field within the tape reaches approximately 2.35T resulting in a field at the centre of the coil of 1.15T.

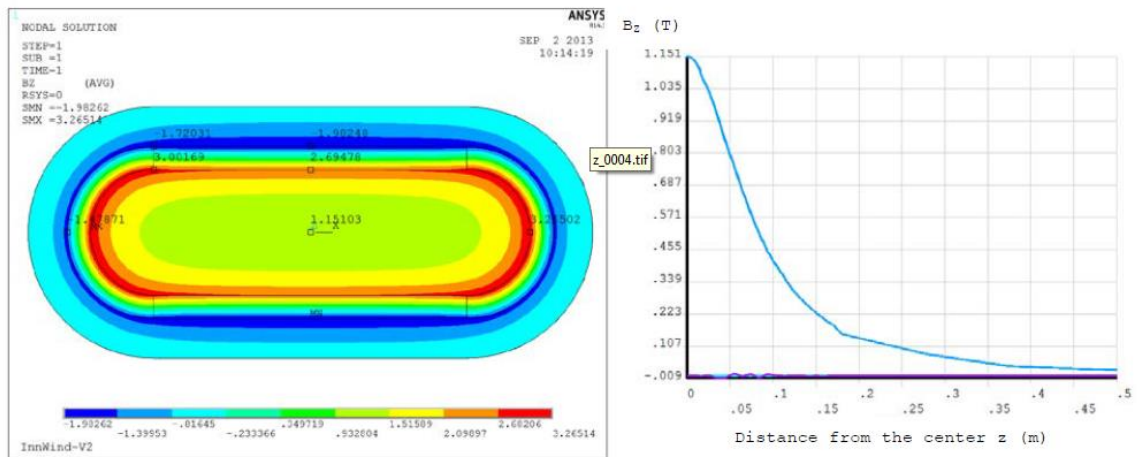


Fig. 4 FE plot of magnetic field applied to the coil

6.3 Mechanical

During operation with high current density associated with superconducting tapes, a significant Lorentz force will be acting on the race-track shaped coil, requiring that it can withstand the forces without significant deformation. Fig. 5 shows the coil deformation when the rated current of 650A is supplied, causing the side of the coils to deform by 4mm. This deformation is unacceptable due to potential tape damage and vibration when AC current is applied. Fig. 5 also shows the forces in a cross section of the field coil during operation, showing there is a significant squeezing force applied to the tapes. This must be design so that the tapes are not damaged as a

result. Fig. 6 shows the coil deformation when the sides of the coil is supported, by using FRP material on the outer surfaces, reducing the coil deformation to 0.05mm which is acceptable to this project.

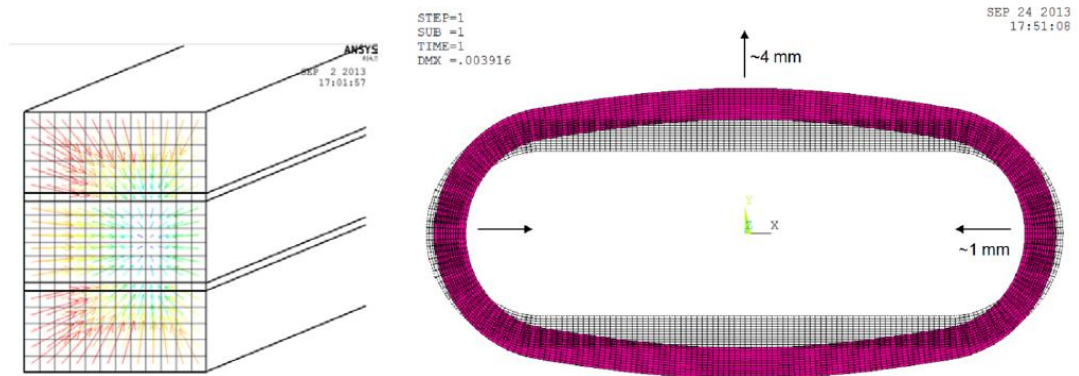


Fig. 5 forces in coil cross section and coil deformation under rated current

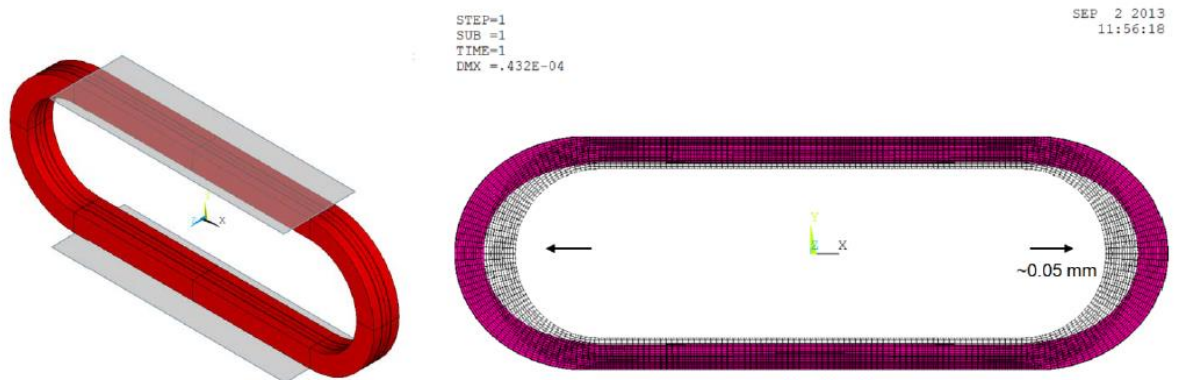


Fig. 6 Deformation in supported coil at rated current

The forces acting on the coil material are shown in Fig. 7, with the maximum von Mises stress occurring within the coil sides. The peak stress is 27.3MPa which is within the design limits for the conductor material.

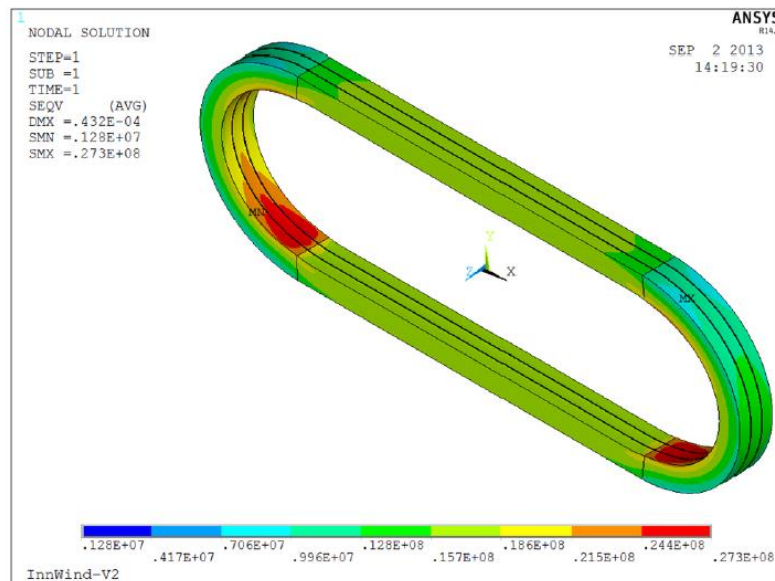


Fig. 7 Force distribution in coils under full load current

6.4 Thermal

The thermal design of the coil is done to ensure the whole coil remains within the required working temperature during worst case conditions. In the simulation, cooling contacts are placed on the end coil regions and heat is then conducted from the centre of the racetrack coil to the cooling contacts. Having applied the relevant thermal conductivities and loss density, Fig. 8 shows the coil remains below 30K during these conditions, with approximately 2K temperature variation across the coil.

In the final design the coil is cooled by 4 cooling contacts at the corners by liquid Neon. The cooling contacts were moved due to issues with eddy losses at the coil end locations.

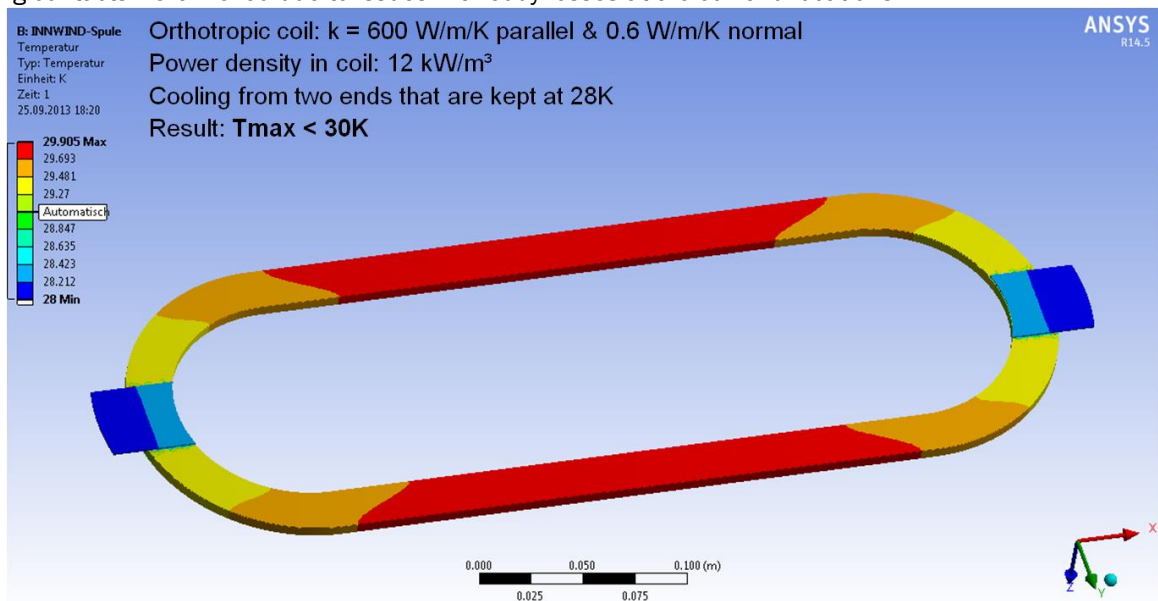


Fig. 8 Thermal distribution in the field coil under load with conduction cooling at ends of race track (blue)

7 COIL CONSTRUCTION

The tape was form wound with the addition of adhesive and Kapton tape to provide bonding and turn to turn insulation. Each coil has 102 turns, with 8 coils constructed (numbered 1 to 8), from which the 3 were then selected for the final field coil test. For testing, several voltage taps were connected to the current connector to monitor individual coils. Thermocouples were also embedded into the coils to monitor temperature

Fig. 9 shows the complete construction of the coils, with mechanical support and cooling contacts.

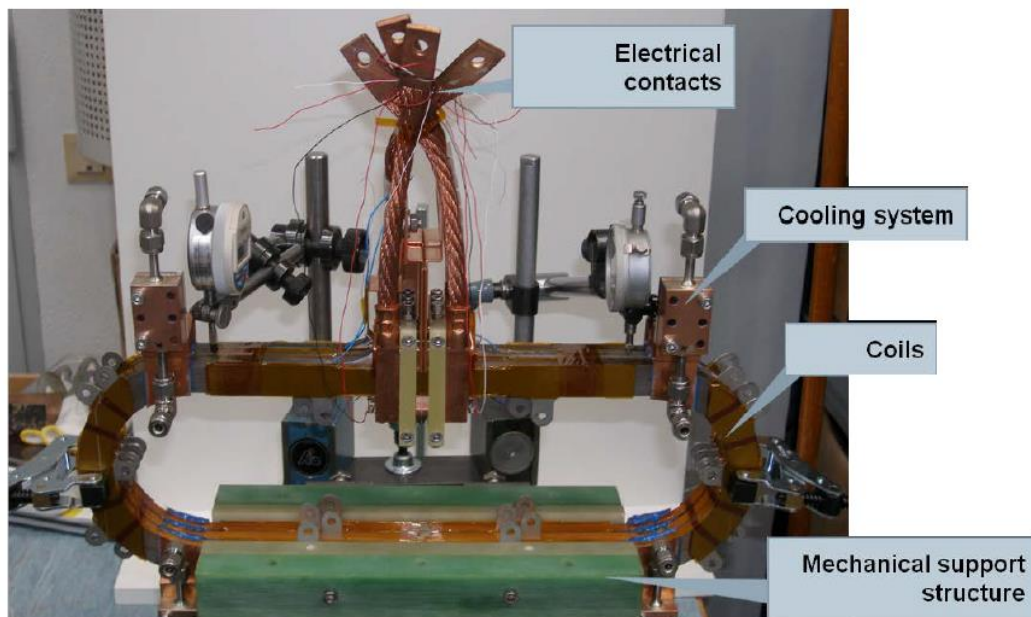


Fig. 9 Picture of the finished field coil with support structure, cooling contacts and current leads

8 TESTING

8.1 Low Temperature Quality Testing

Once the individual coils were manufactured, they were quality tested in liquid nitrogen to check the critical current (I_c) of the coils at 77K, which is just below the superconducting threshold. Coils #1 and #2 were cooled down from room temperature to 77K within the space of 10-15mins, which resulted in inhomogeneous thermal contraction rates, which possibly resulted in defects within the coils. The later coils were cooled at a much slower rate to reduce this risk.

The measured V-I characteristics of all 8 coils is shown in Fig. 10, whereby it is clear that coils #1, #2 and #5 do not exhibit superconducting characteristics. The other 5 coils fulfilled the $1\mu\text{V}/\text{cm}$ criteria at the expected current rating and therefore pass the test.

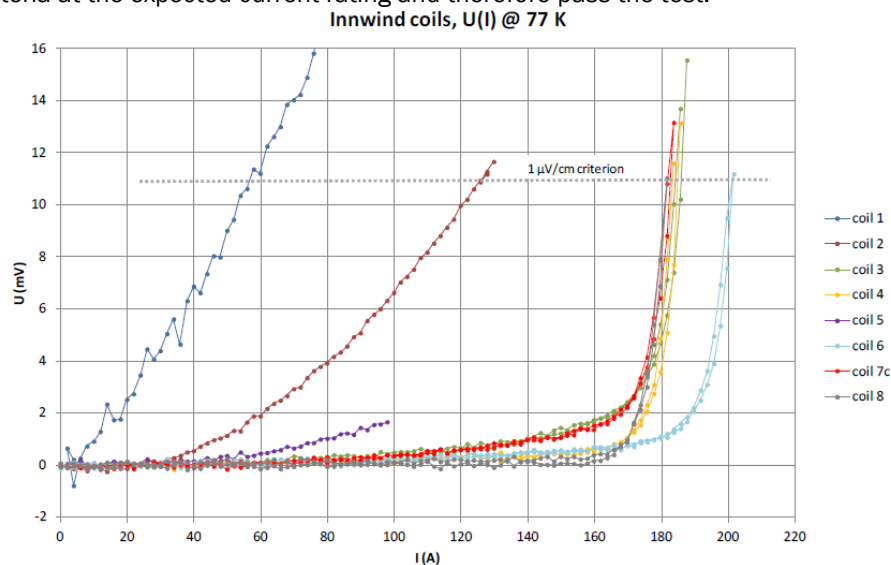
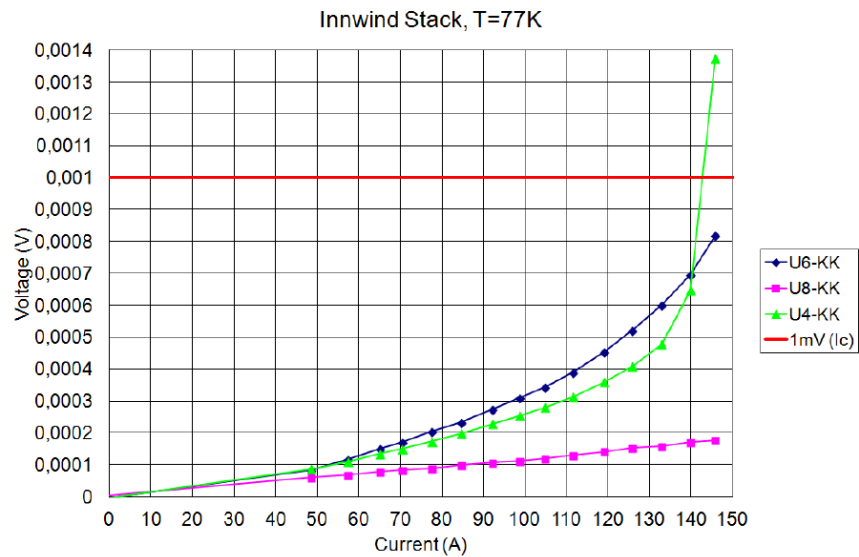


Fig. 10. V-I curve for the 8 coils tested at 77K

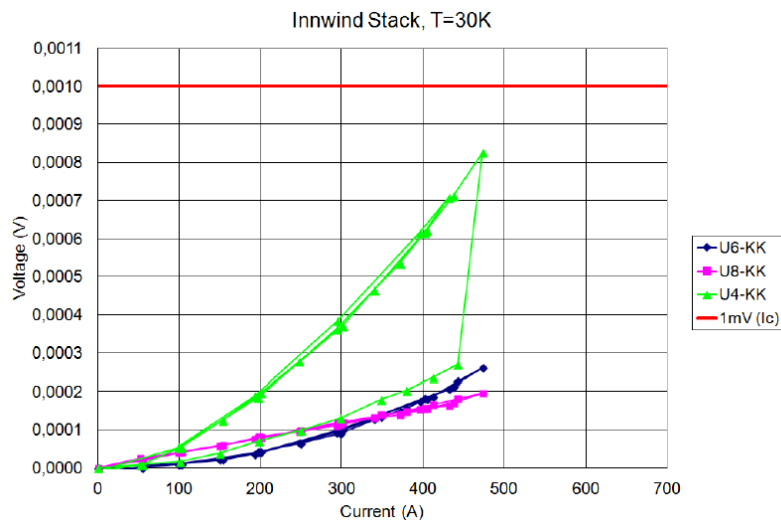
8.2 30K Coil Testing

For the 30K test, 3 coils (#4, #6 and #8) were chosen to create the fields coil, as they performed best in the qualification tests. To test the final set-up, they were initially tested at 77K and achieve the required performance as shown in Fig. 11 a). Next they were cooled down to the operating temperature of 30K, and the current was incrementally increased. In this case coil #4, has a sudden increase in voltage from 0.25mV to 0.8mV at 450A, Fig. 11 b). The current was ramped down and then up again, however the higher coil resistance persisted in coil #4. This resulted in the field coil not being able to achieve its design current rating of 650A at 30K.

Due to lack of time on the project there was no time to replace coil #4 with another coil to complete the testing.



a)



b)

Fig. 11 V-I characteristics of the field coil under different temperatures

8.3 AC Loss Testing

The AC loss tests were conducted at 30K, to measure a range of potential AC current amplitudes and frequency. The measurement of the losses in the tape is difficult due to the cold copper components used for the copper stabiliser on the tape, current leads, cooling contacts and the surrounding metallic components which will induce eddy current losses in the electromagnetic field applied. These losses are mostly impossible to separate from the actual AC loss components of the superconducting material.

The measured range of currents and frequencies are shown below;

- 0-350A DC
- 10-100A AC
- 0.05 – 3Hz frequency

The AC current is applied onto the DC current to simulate current ripples under operation of the field coil. Unfortunately due to the damage sustained in the field coil, it was not possible to measure up to the design DC current of 650A.

The frequency range is limited by the available voltage supply of the AC voltage source and the large inductance of the field coil. It was originally intended to measure up to 6Hz, which is estimated to be the fundamental frequency of a wind turbine generator with a pole number of ~18.

The losses are measured electrically using a wattmeter to measure the supplied power. Fig. 12 shows the measured results for the different ranges and frequencies on a logarithmic graph. As expected the losses follow the eddy loss square law which is illustrated in Fig. 13. This indicates that a majority of the losses are induced as eddy current losses in the cold copper components within the field coil set up. The in house calculation software, LOCSWING, developed to calculate the AC losses within the superconducting tapes generally underestimates the losses within the field coil, suggesting higher losses due to other cold copper components also. The peak loss of 7W is easily removed by the cryogenic cooling system, and the measure temperature variation in the coil is less than 2K.

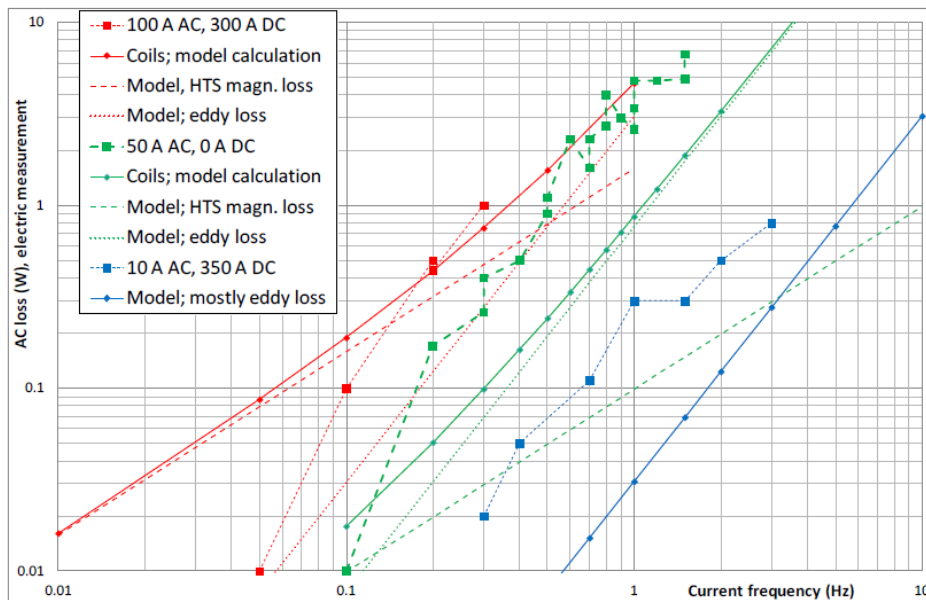


Fig. 12 Measured and calculated AC loss in field coils

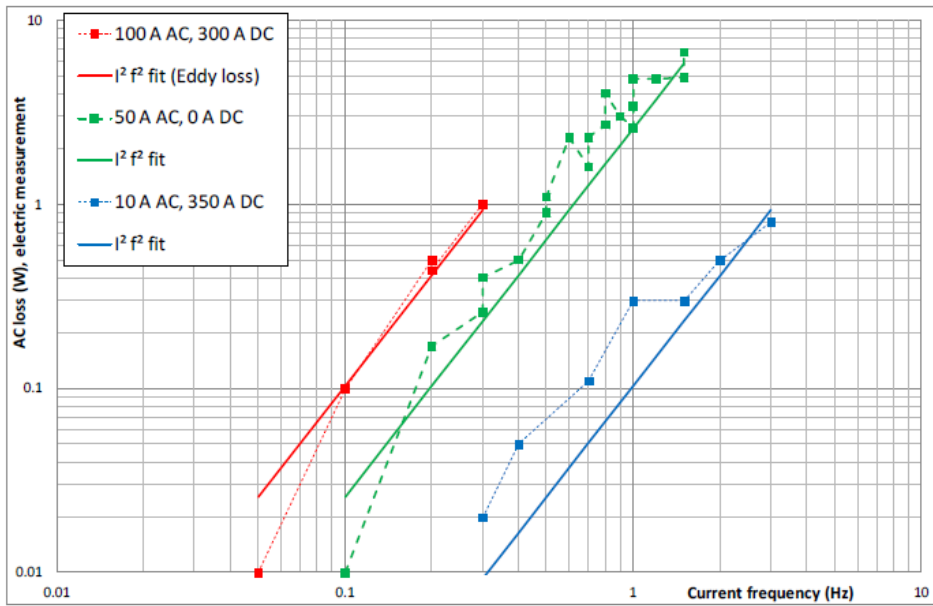


Fig. 13 Measured AC loss plotted with Eddy loss curve fit $P=C \cdot I_{ac}^2 \cdot f^2$
 ($C=1.03 \text{mW}/(\text{A}^2 \cdot \text{Hz}^2)$)

9 CONCLUSION

A field coil of representative dimensions and magnetic field required for a wound field synchronous machine has been design built and tested. The material used is the state of the art 2G -HTS tape (GdBCO) with a working temperature of 30K. 8 coils of 102 turns were manufacture and tested in liquid nitrogen with 5 surviving to the low temperature testing stage.

Three of the best performing coils were then selected to be put into the field coil, which was then tested at 77K and then at 30K. Unfortunately during the ramping up of the current at 30K, coil #4 suffered a partial failure which resulted in the rated current of 650A not being achievable at 30K. When the V-I characteristics is extrapolated from before the failure, the coil design should be able to deliver the require current.

The AC losses were then tested in the coil, by applying an AC current to the field winding. This was done to validate the calculated superconducting tape losses and to see the required cooling power that a cryogenic cooling system would need to apply. The peak loss for the field coil was approximately 7W, with approximately half of those losses coming from the cold copper components and surrounding test equipment.



PROPRIETARY RIGHTS STATEMENT

This document contains information, which is proprietary to the "INN WIND.EU" Consortium. Neither this document nor the information contained herein shall be used, duplicated or communicated by any means to any third party, in whole or in parts, except with prior written consent of the "INN WIND.EU" consortium.

Phase B - Design of Superconducting Direct Drive Generators for Wind Turbines (10-20MW)

Agreement n.:	308974
Duration	November 2012 – October 2017
Co-ordinator:	DTU Wind

The research leading to these results has received funding from the European Community's Seventh Framework Programme FP7-ENERGY-2012-1-2STAGE under grant agreement No. 308974 (INNWIND.EU).



Document information

Document Name:	Phase B - Design of Superconducting Direct-Drive Generators for Wind Turbines (10-20 MW)
Document Number:	Deliverable D ...
Author:	Ziad Azar
Document Type	Report
Dissemination level	Choose an item.
Review:	Arwyn Thomas
Date:	26/01/206
WP:	3.1.2
Task:	Design of Superconducting Direct-Drive Generators for Wind Turbines
Approval:	Approved by Author

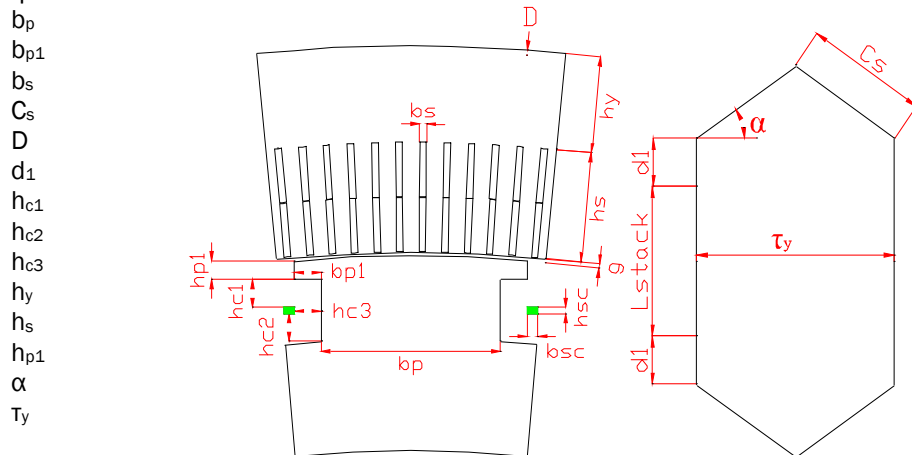
NOMENCLATURE	36
INTRODUCTION	37
CHAPTER 1: LITERATURE REVIEW.....	39
1 INTRODUCTION	39
2 CLASSIFICATION OF SC GENERATOR TOPOLOGIES	42
2.1 FULLY AND PARTIALLY SC GENERATORS	42
2.2 AIR-CORE AND IRON-CORE ROTORS	43
2.3 AIR-CORE AND IRON-CORE STATORS	45
2.4 ROTATING ARMATURE AND ROTATING FIELD WINDING	46
2.5 CLASSIFICATION OF OTHER TOPOLOGIES WITH STATIONARY FIELD WINDING	47
2.5.1 <i>Homopolar SC generator</i>	47
2.5.2 <i>Flux-switching SC generator</i>	48
2.5.3 <i>Magnetic gear</i>	49
3 CHALLENGES OF SC GENERATOR COMMERCIALIZATION.....	49
3.1 RELIABILITY OF CRYOGENIC SYSTEM.....	49
3.1.1 <i>Rotating Seal</i>	49
3.1.2 <i>Cryocooler</i>	50
3.2 PRICE OF SC MATERIAL	50
3.3 AC LOSS IN FIELD COIL	51
3.4 OTHER CHALLENGES.....	51
4 EXCITATION SYSTEM.....	51
5 CONVERTERS	52
5.1 POWER CONVERTERS FOR WIND TURBINES.....	53
5.1.1 <i>Two-level power converter (2L BTB)</i>	53
5.1.2 <i>Multilevel power converter</i>	53
5.1.3 <i>Matrix converter</i>	56
5.1.4 <i>Current source converters</i>	57
5.1.5 <i>Comparison of power electronic converters for wind applications</i>	57
5.1.6 <i>Power converters for low inductance applications</i>	58
CHAPTER 2: GENERATOR DESIGN.....	61
1 INTRODUCTION	61
2 COMPARISON OF TORQUE-SC QUANTITY CHARACTERISTICS BETWEEN SC GENERATORS WITH DIFFERENT TOPOLOGIES.....	61
2.1 INTRODUCTION	61
2.2 OPTIMIZATION METHOD.....	61
2.3 RESULTS	61
3 DESIGN AND ANALYSIS OF SC GENERATOR WITH IRON-CORE STATOR AND ROTOR TOPOLOGY.....	62
3.1 INFLUENCE OF POLE NUMBER AND STATOR OUTER DIAMETER ON PERFORMANCES	62
3.1.1 <i>Optimization Method</i>	62
3.1.2 <i>Results</i>	65
3.1.3 <i>Determination of Pole Number and Stator Outer Diameter</i>	68
3.1.4 <i>Influence of SC Material Price</i>	69
3.2 INFLUENCE OF SC AREA PER POLE ON PERFORMANCES	70
3.3 INFLUENCE OF POLE WIDTH ON PERFORMANCES	72

4	ANALYSIS OF ELECTROMAGNETIC PERFORMANCES	75
4.1	FINAL DESIGN	75
4.2	LOSSES AND EFFICIENCIES	77
4.3	FIELD HARMONICS IN SC COIL	78
4.4	FORCES ON ROTOR COMPONENTS UNDER RATED OPERATION	80
4.5	PERFORMANCES UNDER 3-PHASE SHORT-CIRCUIT FAULT OPERATION	82
4.5.1	<i>Results with Voltage Excitation Source</i>	83
4.5.2	<i>Results with Current Excitation Source</i>	85
5	DESIGN OF CRYOGENIC SYSTEM AND HEAT CALCULATION	86
5.1	DESIGN OF CRYOGENIC SYSTEM	86
5.2	CALCULATION OF HEAT	87
6	SCALING UP TO 20MW	89
6.1	STRATEGY I	89
6.2	STRATEGY II	90
6.3	SUMMARY	93
7	CONCLUSIONS	94
	CHAPTER 3: CONVERTER DESIGN	97
1	INTRODUCTION	97
2	10 MW DESIGN	97
2.1	INTRODUCTION	97
2.2	ARMATURE CONVERTER	98
2.2.1	<i>Comparison between the 2 and 3-level back to back converter</i>	99
2.2.2	<i>Semiconductors</i>	102
2.2.3	<i>Passive components</i>	106
2.2.4	<i>DC-Link design</i>	107
2.2.5	<i>Other components</i>	107
2.2.6	<i>Efficiency</i>	107
2.2.7	<i>Energy calculations</i>	108
2.2.8	<i>Cost analysis</i>	109
2.3	FIELD CONVERTER	110
3	20 MW CONVERTER	112
4	CONCLUSIONS	115
	CHAPTER 4: POTENTIAL WORK	117
	REFERENCES	119
	APPENDIX I. CHARACTERISTIC OF SC MATERIAL	129
	APPENDIX II. SPECIFICATIONS OF LAMINATION	131
	APPENDIX III. REQUIREMENTS OF 10MW DIRECT-DRIVE SC GENERATORS	133
	APPENDIX IV. DESIGN AND ANALYSIS OF SC GENERATOR WITH AIR-CORE STATOR AND ROTOR TOPOLOGY	135
IV.1	INFLUENCES OF PARAMETERS ON TORQUE CAPABILITY	135
IV.2	INFLUENCE OF STATOR SLOT WIDTH	135
IV.3	INFLUENCE OF STATOR SLOT WIDTH	137
IV.4	INFLUENCE OF STATOR YOKE THICKNESS	138
IV.5	INFLUENCE OF SC COIL PITCH	140

IV.6 INFLUENCE OF COPPER LOSS.....	141
IV.7 INFLUENCE OF POLE NUMBER.....	142
IV.A. Determination of SC current density.....	142
IV.B. Influence on torque.....	143
IV.C. Influence on torque per generator volume	143
IV.D. Influence on torque per SC volume	144
IV.E. Influence on torque per iron mass	145
IV.F. Summary	146
IV.8 INFLUENCE OF SC COIL WIDTH TO HEIGHT.....	147
APPENDIX V. COMPARISON BETWEEN SC GENERATORS WITH IRON-CORE STATOR AIR-CORE ROTOR AND AIR-CORE STATOR AIR-CORE ROTOR TOPOLOGIES	149
APPENDIX VI. ANALYSIS OF SC GENERATORS WITH IRON-AIR-COMBINED TEETH.....	153
VI.1 SC GENERATOR WITH AIR-CORED ROTOR.....	153
VI.2 SC GENERATOR WITH IRON-CORED ROTOR.....	155

NOMENCLATURE

A_s	Electrical load	A/m
B_s	Flux density in the middle of armature winding	T
b_{sc}	Width of SC coil	mm
D_s	Diameter of armature winding	m
g	Length of airgap	mm
h_{sc}	Height of SC coil	mm
h_{yi}	Height of stator yoke	mm
J_a	Current density of armature winding	A/mm ²
J_{sc}	Current density of SC coil	A/mm ²
k_w	Armature winding factor	
L, L_{stack}	Stack length	m
L_{ef}	Effective length of stack	m
L_{half_turn}	Length of half turn of stator coil	mm
p	Number of pole pairs	
P_{Cu}	Stator copper loss	kW
q	Number of slots per pole per phase	
S_{sc}	Area of SC coil cross section	mm ²
S_{slot}	Area of one stator slot	mm ²
T	Electromagnetic torque	Nm
η	Efficiency	%



INTRODUCTION

Due to the high current density and almost zero loss of SuperConducting (SC) material, SC electrical machines have higher torque, power density and, higher efficiency than conventional Permanent Magnet (PM) and field-excited machines. Extensive studies have been conducted on SC generators for many applications which have tough requirements for the size and weight of machines, such as wind turbine and ship propulsion, etc. The purpose of this report is mainly the design and analysis of 10-20MW SC generators for direct-drive off-shore wind turbines.

This report is organised in four chapters as follows:

Chapter 1 covers the literature review focusing on the main topologies of SC generators and the power electronic converters associated to them for wind power generation.

In chapter 2, the performances of the four major SC generator topologies, i.e. iron-core stator and rotor, air-core stator and rotor, and iron-core stator and air-core rotor are compared. Based on the comparison, the iron-core stator and rotor topology is determined, since it has the highest SC material utilization. Then the influences of pole number, stator outer diameter and pole width on performances and costs are investigated, and the final electromagnetic design of 10MW SC generator is determined. After that, the electromagnetic performances are analysed, including losses and efficiency, field harmonics in SC coils, forces on rotor components, etc. In addition, the performances of generator under three-phase short-circuit fault operation are also analysed. Finally, the 10MW SC generator is scaled to 20MW.

Chapter 3, focuses on the design of the armature power converter for the SC generator designed in chapter 2. To achieve a satisfactory design the numbers of levels of the converter (2-levels and 3 levels) are compared. Then 23 different IGBTs and 3 different diodes are taken into account for the converter design. The output filter design of converter for the generator side is also designed to reduce the harmonics produced by the modulation strategy. After the design of the filter and the analysis of all the semiconductors several options are presented for the final design and their efficiency is calculated and compared. Finally the energy calculation and cost analysis for the whole drive train (generator and power converter) are carried out. A study of the field converter for the field converter of the SC machine is also done. As in chapter 2, the last part of the chapter 3 is scaling up the 10 MW power converter design to 20 MW.

Finally, chapter 4 shows the future potential work.

CHAPTER 1: LITERATURE REVIEW

10 INTRODUCTION

Due to the high current density and almost zero loss of SC material, the SC electrical machines have higher torque and power density, and higher efficiency than PM and field-excited machines. Snitchler et al. [SNI11] compared the size and weight between PM and SC direct-drive 10MW wind turbines. The optimum weight for a 10 MW direct drive PM generator is larger than 300 tons with an air gap diameter larger than 10 meters. By comparison, a 10 MW SC machine has an optimum outer diameter in the 4.5 to 5 meter range. The projected weight is approximately 150 to 180 tons. The torque densities of PM and field-excited machines are about 30-40Nm/kg (32Nm/kg according to [SNI11] and 40Nm/kg [KEY11]) and 15Nm/kg (Enercon-E112 [KEY11]), respectively. The available torque densities of SC generators in literature are also listed in Table 1-Table 3. In summary, the torque density of SC electrical machines is about 2 and 5 times of that for PM and field-excited electrical machines respectively.

The first SC electrical machine was proposed by Stekly et al. [STE64] in 1964. Some of the major SC generators, including partially SC, fully SC and homopolar SC generators, etc., are summarised in Table 1-Table 3. Most of the SC generator projects were terminated or suspended in the late 1980s due the global economic crisis. All of the SC generators during that period adopted the low temperature SC material NbTi. The high temperature SC (HTS) material is adopted by most of the SC generators after 2000. However, there are still no commercialized SC generators, mainly due to:

- High cost of SC material
- Reliability of cryogenic system

Compared with PM and field-excited machines, the SC electrical machines have higher torque and power density, and higher efficiency.

Table 1. Summary of partially SC generators (SC material as the field winding, copper as the armature winding)

Country	Affiliation	Year	Power	Speed (r.p.m.)	SC material	Feature	Torque density (Nm/kg)	Reference
USA	MIT	1970	0.045MW	360	NbTi			[THU70] [THU71] [WOO71]
USA	MIT	1973	2-3 MVA	3600	NbTi			[KIR73] [BEJ77]
USA	MIT	1979	10 MVA	3600	NbTi			[SMI79] [ULA80] [MIN81] [SMI95]
USA	Westinghouse	1973	5 MVA	3600	NbTi			[BRE73] [FAG73] [HUL73] [CHA74]
USA	Westinghouse	1977	5-10 MVA	12,000	NbTi	For air force	10.9	[BLA77] [PAR75]
USA	Westinghouse	1979	300 MVA	3600	NbTi	Planned		[PAR79] [FLI81] [YIN81]
USA	Westinghouse	1979	1200 MVA	3600	NbTi	Planned		[PAR79]
USA	AMSC	2001	5000hp	1800	HTS			[GAM02]
USA	AMSC	2011	36.5MW	120	HTS	9-phase For ship propulsion	39	[GAM11] [JEN12]
USA	AMSC, Alstom	2005	5MW	230	HTS	For ship		[SNI05]

						propulsion		
USA	GE	1981	20 MW	3600	NbTi	For utility		[LAS81] [FEA85] [KEI85]
USA	GE	1980	20 MW	High	NbTi	For air force		[GAM80]
USA	GE	2003	1.8MVA	3600	HTS			[ACK03]
USA	GE	2003	100MVA		HTS			[ACK03]
USA	GE	2013	10MW	10	NbTi	For wind turbine	66	[FAI12] [STA13]
USA	AMSC	2011	10MW	10	YBCO	For wind turbine	55-66	[SNI11] [ONL14b]
USA	Rockwell	1996	200hp	1800	BSCCO			[ZHU00] [SCH97] [UMA06]
USA	Rockwell	1996	1000hp	1800	BSCCO			[ZHU00] [SCH97]
USA	Rockwell	2000	5000hp			Planned		[ZHU00]
Japan	Hitachi Ltd.	1980	50MVA	3600	NbTi		3.98	[MAK80] [YAM84] [MAK87] [TAK89]
Japan	Hitachi Ltd.	1980	1000MVA	3600	NbTi	Planned		[MAK80] [YAM89]
Japan	Toshiba	1986	3MVA	3000	NbTi			[KUM86] [KUM87]
Japan	Toshiba	1986	1000MVA		NbTi	Planned		[KUM86]
Japan	Kyoto University, Seikei University, Saga University, etc.	1983	0.02MVA	1800	NbTi			[MUT83] [OKA85a] [OKA85b] [ISH88] [OKA87]
Japan	Super GM, etc.	1991-1999	70MVA	3000	NbTi			[OHA91] [YOS91] [MAT94] [YAM93] [TAK95] [INO94] [UED99] [HIR96] [SHI99a] [SHI99b]
Japan	Super GM, etc.	2003	200-600MW	3600	NbTi	Planned		[NIS03]
Japan	Kyushu University	2007	15kW	360	YBCO	Iron-core Rotating-inside-armature	0.44	[IWA07]
Germany	Technical University of Munich	1984-1989	0.32MVA	3000	NbTi			[BRA84] [BIS89]
Germany	KWU, Siemens	1983	400-1000MVA	3000	NbTi	For utility		[INT83]
Germany	Siemens	2003	0.4MVA	1500	Bi2223			[FRA03]
Germany	Siemens	2006	4MVA	3600	Bi2223		1.54	[FRA06] [NIC07]
Korea	Changwon	1999-	0.03MVA	1800	NbTi			[CHU99]

	National University, etc.	2000						[BAI00] [J000]
Korea	Electrotechnology Research Institute, etc.	2005	100 hp	1800	Bi2223			[KW005]
UK	University of Southampton	2007-2011	100 kW	3600	Bi2223			[MOS07] [BAI11] [BAI09] [GOD09] [SHI02] [SHI04] [LUK09] [BAI13] [LUK08]
France	Alstom	1981	250 MW		NbTi			[GIL81]
France	Alstom	1981	1200 MW		NbTi	Planned		[GIL81]
France	Laboratory of Electrotechnique	1979	0.5 MW	3000	NbTi			[BRU79] [BRU86]
Europe	Converteam	2007	8 MW	12	YBCO	For wind turbine	63.6	[LEW07]

Table 2. Summary of fully SC generators (SC material for both field and armature windings)

Country	Affiliation	Year	Power	Speed (r.p.m.)	SC material	Feature	Reference
France	Alstom, CNRS-CRTBT, etc.	1989	20kVA	3000	NbTi		[TIX91] [BRU89]
Japan	Yokohama National University, etc.	1992	30kVA	1500	NbTi		[TSU92] [TSU93] [CHE95]
Japan	Saga University	1992	20kW	1500	NbTi		[MUT92]
Japan	Seikei University	2000	0.3kW	2000	NbTi	15-phase	[SEK00] [NOM02]
USA	AML	2014	10MW		MgB2	For wind turbine	[ONL14a]

Table 3. Prototyped or being prototyped homopolar SC generators

Country	Affiliation	Year	Power	Speed (r.p.m.)	SC material	Feature	Torque/power density	Reference
China	Wuhan Marine Electrical Propulsion Research Institute	1996	300kW	1,300	NbTi	Ship propulsion		[GE96]
Russia	Moscow Aviation Institute	1992	480kW	10,000	NbTi		1.01Nm/kg 1.06kW/kg	[ALI92]
USA	GE	2009	1.3MW	10,000	BCCCO/ YBCO	Ship propulsion	8.4Nm/kg 8.8kW/kg	[SIV09]
USA	GE	2009	5MW	35,000	BCCCO/ YBCO	Ship propulsion	2.5 Nm/kg 9.17kW/kg	[SIV09]

11 CLASSIFICATION OF SC GENERATOR TOPOLOGIES

11.1 Fully and partially SC generators

A superconducting generator is classified as fully superconducting when both the armature and the field windings are made of superconductors (Fig. 1.a) [TSU92]. On the other hand, a partially superconducting generator has its DC field windings made of superconducting materials and its armature windings are made of conventional copper (Fig. 1.b).

Suitable superconducting materials for superconducting machines are classified in two big categories: LTS and HTS. Although the use of LTS superconductors have been successfully used in AC applications, their use for large superconducting wind turbines is difficult due to their high cooling requirements and their low magnetic field endurance. Hence, researchers have focused on the use of HTS materials to design new superconducting generators.

The ideal situation would be the use of fully superconducting generators since they allow a high power density [BAR05] what leads to a considerable reduction of weight -around 50% of the weight of a partially SC machine [SNI10]. Furthermore, in fully SC generators the air gap is smaller than partially SC generators since there is no need of insulation between the rotor and stator. The direct consequence of a smaller air gap is the need of less superconductor wires.

On the other hand, the use of HTS brings the problem of AC losses. The design of a fully SC generator is not realistic until a new type of superconductors is developed to overcome the high AC losses in both stator and rotor [TER12]. Moreover, winding stators with flat HTS wires complicates the effective use of the available space at the stator. Finally the high cooling needs of fully SC generators and price of HTS wires make their design inadvisable at the present time.

Since the use of fully SC machines is impractical for the aforementioned reasons, the partially SC topology is now the most used for large wind turbine generators.

The disposition of superconducting wires in the rotor -field- improves the flux density in the air gap compared to conventional machines whereas the current density in the armature winding is similar. In spite of the fact that partially SC generators still use HTS wires for their field windings, with proper shielding, the AC losses are endurable.

The key design for partially SC generators is their superconducting rotor since it requires to be cooled to cryogenic temperatures. The use of a cryogenic cooling system in the rotor forces designers to design a rotating transfer coupling to transfer the coolant from the rotating part to the stationary part of the cooling system. This coupling system increases the cost of the generator and reduces its reliability since a failure in it prevents the operation of the machine.

Comparing with partially SC generators, the advantages and disadvantages of fully SC generators are as follows:

Advantages of fully SC generator:

- 1) Higher torque density, due to the higher electric load, which can be explained from (Fig. 1). The estimated weight of 10MW 10rpm fully SC generator designed by S. S. Kalsi [KAL14] is 52.5t, which is about 1/3 of partially SC generator (150 to 180t [SNI11]).

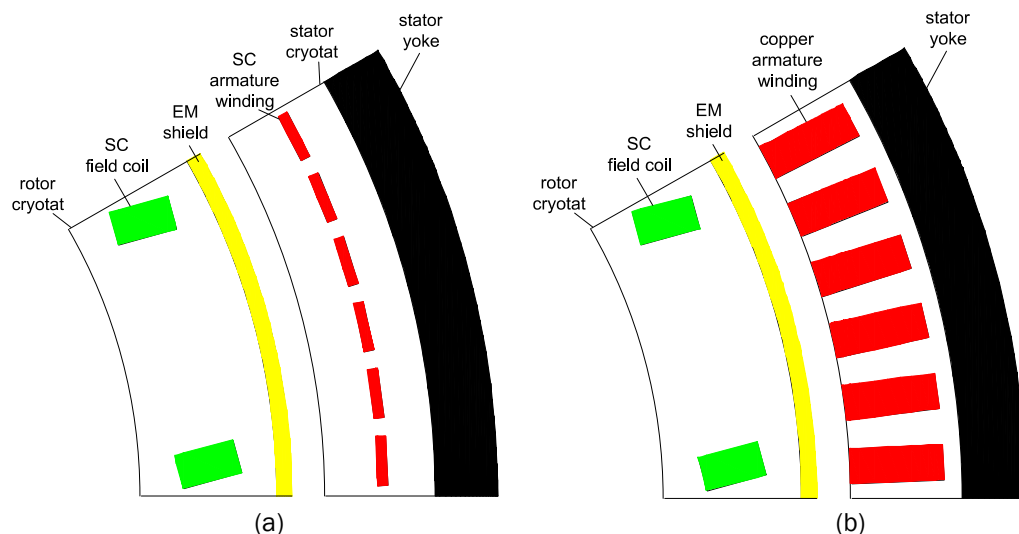


Fig. 1 (a) Fully and (b) partially SC generators.

- 2) Higher efficiency, due to the much smaller conduction loss in the armature winding;
- 3) Lower fault quantities, in terms of current, field and torque, due to the larger synchronous reactance x_d ;
- 4) Airgap length has the potential to be smaller, because the thermal insulation between stator and rotor has the possibility to be removed. It should be mentioned that if the stator and rotor are cooled with two separate cryogenic vessels, the airgap length is larger in fact [SWA14].

Disadvantages of fully SC generator:

- 1) Larger power of cryogenic system, because both the armature and field winding need to be cooled to 4-5K (for LTS) or 20-30K (for MgB₂). In addition, the AC loss in armature winding favours to increases the power of cryogenic system.
- 2) Complicated structure of cryogenic system, due to the existence of both rotating and stationary SC coils.
- 3) Electric stability is poorer, due to the larger x_d , in other words, due to more coupling between field coil and armature.
- 4) Immaturity of SC material, which can produce less AC loss caused AC current and field.

$$T \propto k_w B_s A_s D_s L_{ef} \quad (1)$$

where B_s , A_s and D_s are the flux density, electric load, diameter at the armature winding mean radius, k_w is the winding factor, L_{ef} is the effective machine length. Besides the prototyped or being prototyped fully SC generators listed in 0, some of the conceptual designs were carried out by S. S. Kalsi et al. [KAL14], Y. Terao et al. [TER12] and Y. C. Liang et al. [LIA14].

The partially SC generators are the most widely developed topology nowadays. There exist extensive conceptual designs in literature (S. Fukui et al. [FUK11], H. Tsukiji et al. [TSU01], R. Shafaie et al. [SHA13] [SHA14a] [SHA14b], M. F. Hsieh et al. [HSI13], H. J. Sung et al. [SUN13], H. Yamasaki et al. [YAM14], R. H. Qu et al. [FAN14] [WAN14a] [LIU14a] [LIU14b] [ZHU14], Y. Xu et al. [XU14] etc.). The influences of winding topology (multi-phase or fractional slot) on damper and field winding harmonic losses were investigated by J. Wang et al. [WAN13] [WAN14b] and J. H. Seo et al. [SEO14]. The effect of material on damper loss was investigated by H. C. Jo et al. [JO14]. Some optimal field winding shape, which can improve the voltage amplitude and reduce THD were proposed in [WEN14] [KIM14]. K. Choi et al. [CHO14] proposed a dual field winding structure, which can confine the flux path through the armature winding, and further to improve the stator voltage amplitude to a large extent. However, it has complicated structure, with dual-stator.

11.2 Air-core and iron-core rotors

Depending on materials used for the construction of the stator or rotor they can be classified as air or iron cored, Fig. 2. When the stator teeth or the rotor core material is ferromagnetic, they are known as iron cored machines. Otherwise, they are known as air cored machines.

Air cored rotor machines are popular in large wind turbines since it greatly reduces the total weight of the machine. However, the use of air cored rotors increases the reluctance of the magnetic circuit and more HTS wires are needed to keep the same flux density than in an iron cored rotor [KLA07].

The synchronous reactance of air cored rotors is smaller than iron cored rotors, therefore the transient stability of an air cored rotor generator is better than the iron ones [GAM06]. The disadvantages of air cored rotors are their higher peak torque and current when a short circuit happens. Furthermore, the electromagnetic forces directly applied to the superconducting coils leads to more complex support systems for the superconducting coils [GIE08].

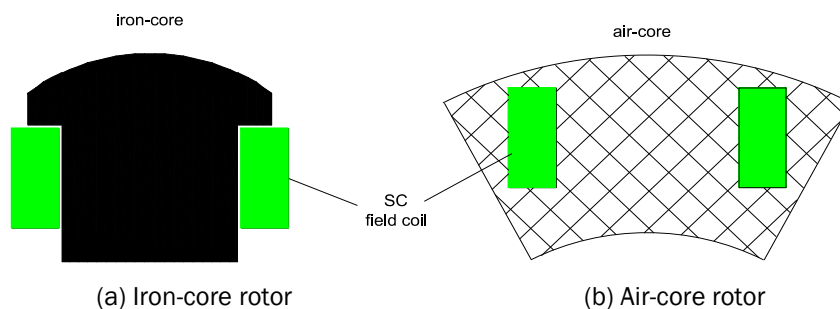


Fig. 2 (a) Iron-core and (b) air-core rotors.

On the other hand, iron cored rotors need less HTS wires and have better superconducting coil performances. As disadvantages the iron cored rotors have higher synchronous reactance and the total weight of the machine greatly increases. Moreover, steel suitable for the required environment of HTS wires is expensive and rare [TON10] and it might be subjected to Eddy current losses.

Iron cored rotors can be categorised according to how they are cooled. If a rotor is cooled together with the superconducting coils, it is known as a cold rotor. However, if a rotor is thermally insulated and kept at room temperature, it is known as warm rotor.

Cold rotors have the advantage of simpler structures if compared to warm rotors. However, cold rotors require an increase of the cooling capacity since the whole rotor has to be cooled and their cooling time is longer than in warm rotors. Special steels are also needed since conventional steels cannot work properly at cryogenic temperatures. Additionally, an auxiliary torque transmission is needed to transfer the mechanical power from the shaft to the rotor which increases heat leakage due to the difference in temperature between the rotor and the auxiliary transmission. Finally, cryogenic environments favour the existence of Eddy currents hence losses in cold rotors tend to be higher than in warm rotors.

On the other hand, warm rotors have low cold mass and do not need special steels for their core. Furthermore, their cooling times are shorter and require smaller cooling capacities. Regarding the Eddy currents, their values are reduced since the rotor works at room temperature. The main concerns for warm rotors are mainly two: the design of their support structure, which is more complicated than the cold rotors, and the heat leakage, also present in cold rotors, since there is still a difference of temperature between the superconducting coils and the rotor core.

Concerning stator configurations, the air gap armature winding is widely used in HTS machines since there is a high flux density in the armature [KAL02], which would saturate the iron teeth, and to avoid teeth harmonics [WU11]. The absence of iron teeth eliminates the cogging torque and air gap flux harmonics and vibrations are reduced [SNI10] but Eddy currents and circulating current losses are increased [KLA07]. AC losses can be reduced by the use of Litz wire although it is more expensive and difficult to manufacture than the classical copper wires [WU11]. The use of iron cored armatures is possible in wind generators due to the low frequencies they are subjected to. The optimal iron teeth are thinner than in conventional stators with a width ratio of slot to tooth pitch in the range from 0.65 to 0.9 [SNI10b]. The use of iron teeth reduces the complexity of the stator manufacture process and its price [FRA08].

Most of the developed SC generators adopt air-core in order to improve the airgap flux density and reduce the total mass. Comparing with SC generator with air-core rotor, the iron-core topology has following advantages and disadvantages:

Advantages of iron-core rotor:

- 1) Lower SC quantity due to higher SC utilization. It is said that 1/2-2/3 SC material was saved by utilizing iron-core rotor [QU13], if the required flux density is not so large (2/3 was saved, with flux density in the field coil 1.5T [BAI05]). The magnetic reluctance of flux path can be reduced by adopting iron-core, if the required flux density in the airgap is not too large. The effect of SC reduction is obvious with the flux-density in the iron $\leq 2T$ [KLA07], another reason is that flux path can be confined by the iron to improve the utilization of flux. The third reason is that the SC current density can be higher, due to lower flux density acting on the SC. It is because much of the flux is confined in the iron-core.
- 2) Less complicated SC coil supporting structure (for cold rotor iron-core), because the force does not act directly on the SC coils.
- 3) Capability of higher speed (for cold rotor iron-core), because the force does not act directly on the SC coils and robust rotor structure.
- 4) Lower fault quantities (current, field, torque etc.), due to the higher x_d , caused by lower magnetic reluctance in the iron.

Disadvantages of iron-core rotor:

- 1) Lower torque density, due to the limited flux density by the iron and higher density of iron.
- 2) Higher weight, due to the existence of iron.
- 3) The other disadvantages depend on whether it is cold rotor iron-core or warm rotor iron-core, as shown in Fig. 3. If it is cold rotor iron-core, the cold mass is quite large. Consequently, the power of cryogenic system is large and cooling down time is long. If it is warm rotor iron-core, the support system is complicated.

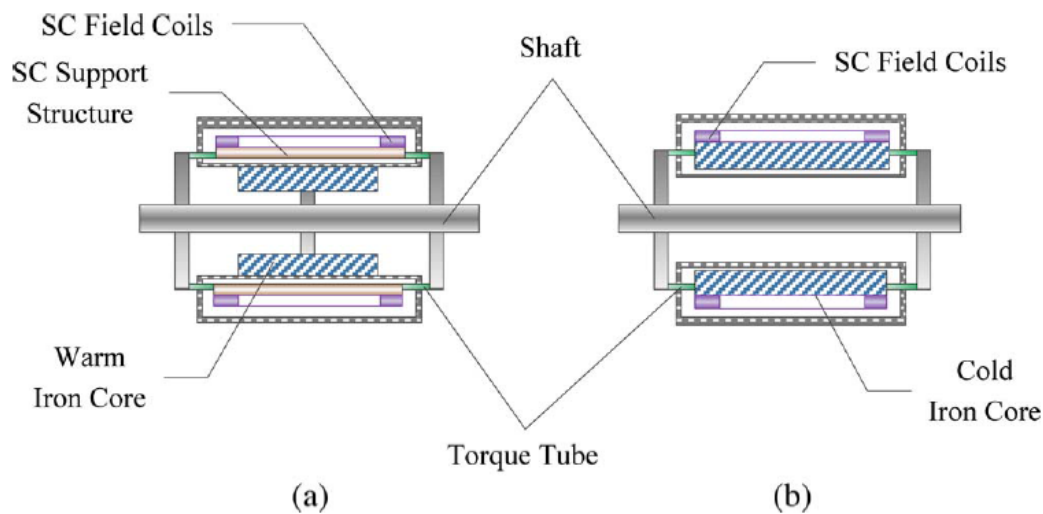


Fig. 3 Warm and cold rotor iron-core topologies. (a) Warm rotor iron-core. (b) Cold rotor iron-core. [QU13]

A 100kW iron-core rotor SC generator was prototyped by M. K. Al-Mosawi et al. [MOS05] [WEN09] [WEN11]. A rotating inside armature winding iron-core SC motor was prototyped by M. Iwakuma et al. [IWA07]. Some conceptual designs have been conducted by H. Yamasaki et al. [YAM14], G. Q. Zhang et al. [ZHA07], R. H. Qu et al. [FAN14] [WAN14a] [LIU14a] [LIU14b] [ZHU14].

11.3 Air-core and iron-core stators

The air-core and iron-core stators are shown in Fig. 4. Comparing with SC generator with iron-core stator, the air-core stator topology has the following advantages and disadvantages:

Advantages of air-core stator:

- 1) No cogging.
- 2) Less vibration.
- 3) Less iron loss.

Disadvantages of air-core stator:

- 1) Higher eddy current and circulating current losses in the armature winding, due to more transverse flux components acting directing on armature winding. Usually, litzwire can be employed. However, it is more complicated and expensive and leads to lower filling factor.
- 2) Larger pulsation forces on armature winding, thus, the mechanical support for the armature winding should be designed carefully.
- 3) Higher weight due to existence of stator iron

The iron-core stator topology is widely adopted in literature [MOS05] [WEN09] [WEN11] [IWA07] [ZHA07] [FAN14] [WAN14a] [LIU14a] [LIU14b]. The 10MW 10rpm SC generator being developed by GE also adopts iron-core stator [STA13].

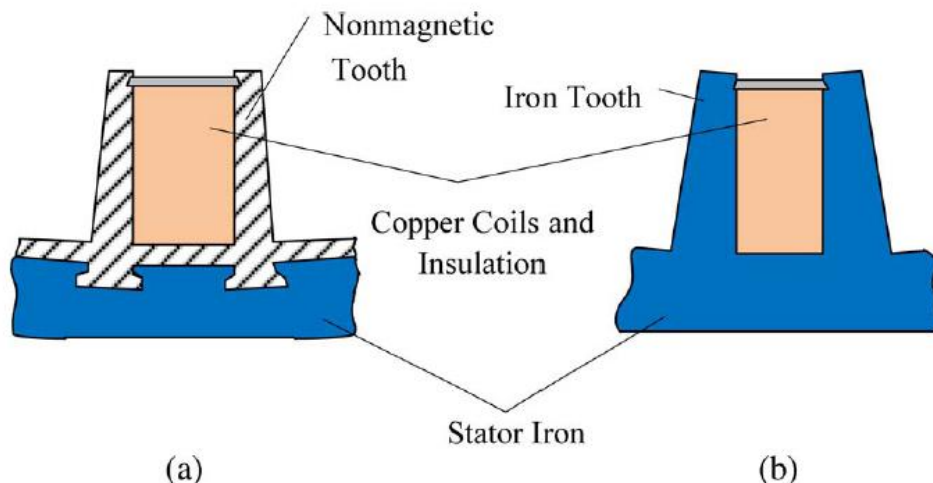


Fig. 4 Air-core and iron-core stators. (a) Air-core stator. (b) Iron-core stator. [QU13]

11.4 Rotating armature and rotating field winding

In a rotating armature AC generator (Fig. 5) the stator provides a stationary electromagnetic field whereas the rotor, acting as the armature, rotates in it. The output voltage is taken from the rotor by the slip rings and brushes and can be transferred to an external circuit.

In a rotating field AC generator (Fig. 6) a direct current is passed through the windings on the rotor by means of slip rings and brushes creating a similar effect than if the rotor was a permanent magnet. As the rotor turns, alternating voltages are induced in the stator windings. A difference from the rotating armature machines, the output power is taken from stationary windings which can be connected through fixed terminals.

When designing a partially SC synchronous machine is desirable to have the SC field coils stationary (rotating armature generator) since the cooling system is associated with them and without rotation, the design of SC coils is less challenging.

The main advantage of the rotating armature concept is that it allows the use of LTS coils to create the field therefore the partially SC generator cost is reduced.

On the other hand, the transference of large currents through the sliding contacts is one of the main drawbacks. Furthermore the design of the armature is much more complicated than in field rotating generators.

In spite of the fact of the above comments, it has to be noticed that it is easier to transfer electric power through sliding contacts than cooling a rotor.

Regarding the rotating field concept it has to be said that it is still popular in partially SC generators.

The advantages of this configuration are the easier design of the armature compared to the rotating armature configuration and its permissiveness to higher current and flux density since the problems with the slip rings are avoided. The stator cooling systems are also easier to be build.

Among the disadvantages, there is a challenge to improve the cooling systems for the SC field coils since they are rotating with the rotor. If the cooling systems are improved, the rotating field topology can have a better performance than the rotating armature topology.

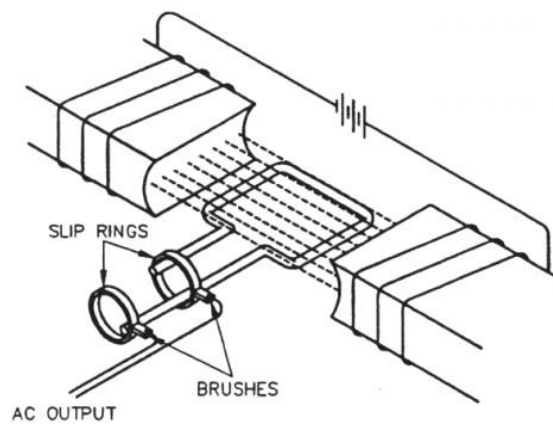


Fig. 5 Rotating armature AC generator [ASO14]

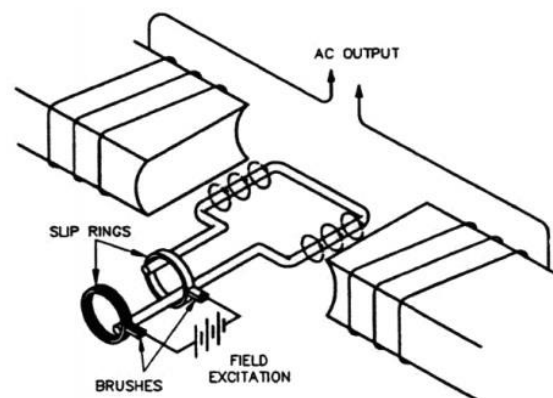


Fig. 6 Rotating field AC generator [ASO14]

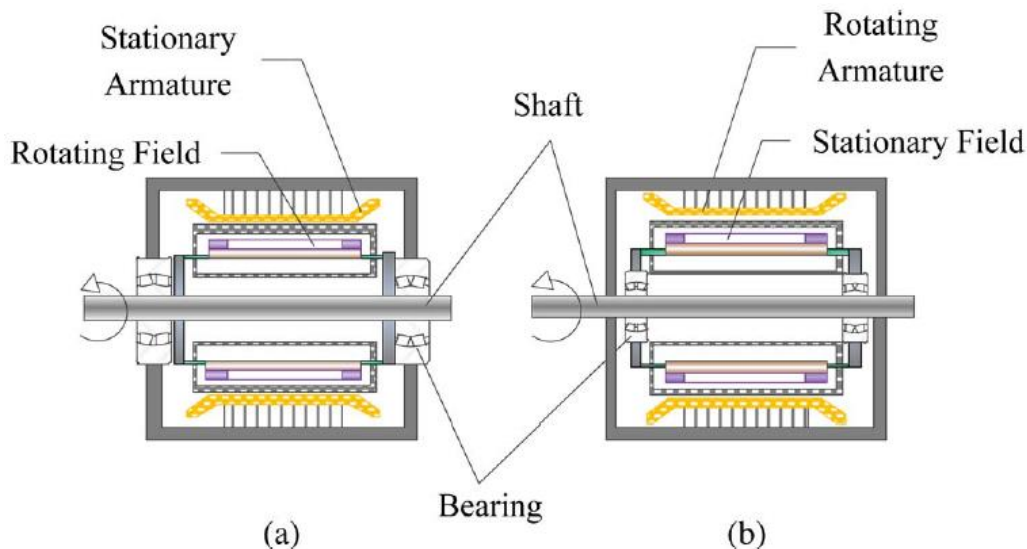


Fig. 7 Rotating armature and rotating field winding topologies. (a) Rotating armature winding. (b) Rotating field winding. [QU13]

The rotating armature and rotating field winding topologies are shown in Fig. 7. Comparing with rotating field winding, the rotating armature topology with stationary field winding has the following advantages and disadvantages:

Advantages of rotating armature:

- 1) Higher reliability of cryogenic system, because there is no need for rotating seals, which is a major hurdle preventing SC wind turbine development.
- 2) Higher reliability of SC coils, because the SC coils are stationary and there is no centrifugal force acting on them and less mechanical vibrations.
- 3) Higher reliability of supporting system, because it is stationary.

Disadvantages of rotating armature:

- 1) Existence of slip ring and brushes for the armature winding. However, it is less concerned for low speed applications, such as wind turbine.

The rotating armature concept is a very competitive candidate for SC generator for wind turbine application. The rotating armature SC electrical machines were prototyped by Z. Stekly et al. [STE64], M. Iwakuma et al. [IWA07]. The prototyping of 10MW rotating armature SC generator for wind turbine application is under way by GE.

11.5 Classification of other topologies with stationary field winding

11.5.1 Homopolar SC generator

The main feature of Homopolar Superconducting Synchronous Machines (HSSM) is their stationary superconducting field winding which eliminates the need for a transfer coupling between the rotor and the stationary cooling system. As a consequence, the design of the cooling and excitation systems are simplified.

Furthermore, the flux penetrating into the superconducting winding is minimized by the rotor magnetic core and the wire requirement is minimum due to the small air gap.

Another advantage of HSSM is that the superconducting coils do not have to endure centrifugal forces since no electromagnetic torque is acting on them.

All the aforementioned advantages make HSSM very robust and low cost machines with only one big disadvantage which is their high weight due to the large mass of the rotor core compared to other machines.

A homopolar SC generator is shown in Fig. 8.

Advantages of homopolar SC generator:

- 1) Higher speed, due to the robust rotor structure and less rotor iron loss.
- 2) Higher power density, due to the possibility of high speed.
- 3) Higher reliability of cryogenic system, because there is no need for rotating seals and the cryostat is stationary, without 'g' forces.

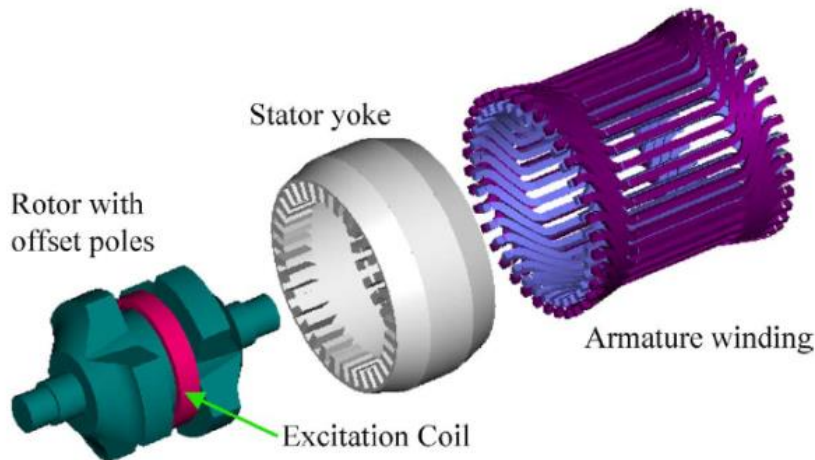


Fig. 8 Schematic of homopolar inductor alternator [SIV07]

- 1) Higher reliability of SC coils, because there is no centrifugal force, which is extremely serious for high speed applications.
- 2) Higher reliability of supporting system, because it is stationary.

Disadvantages of homopolar SC generator:

- 1) Lower torque density, because 1) the iron limits the flux density in the airgap, 2) more leakage flux between poles
- 2) Higher weight, due to the existence of iron-core.

The already prototyped and being prototyped homopolar SC generators have been summarized in Table 3. A new rotor topology of this kind of generator was proposed by Y. J. Hwang et al. [HWA13].

O. Keysan and M. A. Mueller proposed a 6MW 12rpm axial-flux homopolar bipolar SC generator [KEY11]. The torque density is 35.7Nm/kg, which is slightly lower than a PMG. It has the field winding in the stator, and the rotor field is produced by rotor modulation. The rotor iron loss is supposed to be large.

11.5.2 Flux-switching SC generator

Y. J. Hwang et al. [HWA14] conducted a conceptual design of 15MW 900rpm flux switching SC generator Fig. 9. The advantages and disadvantages of this type of machine are as follows:

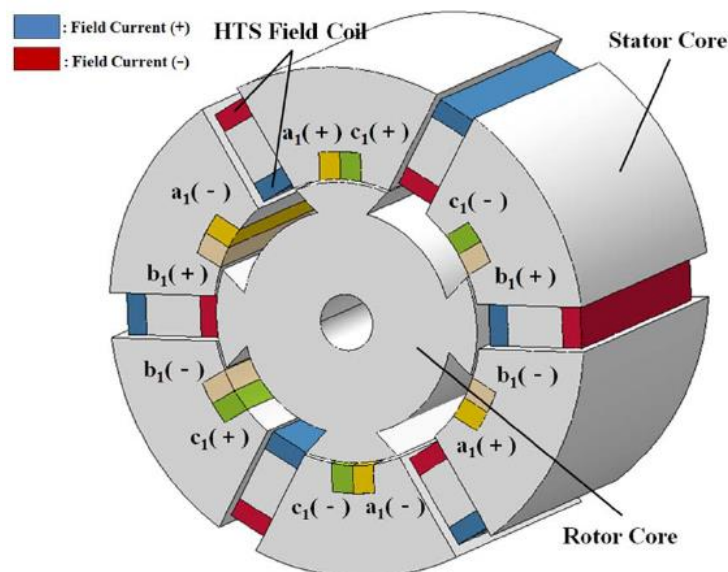


Fig. 9 Topology of flux-switching SC generator, [HWA14]

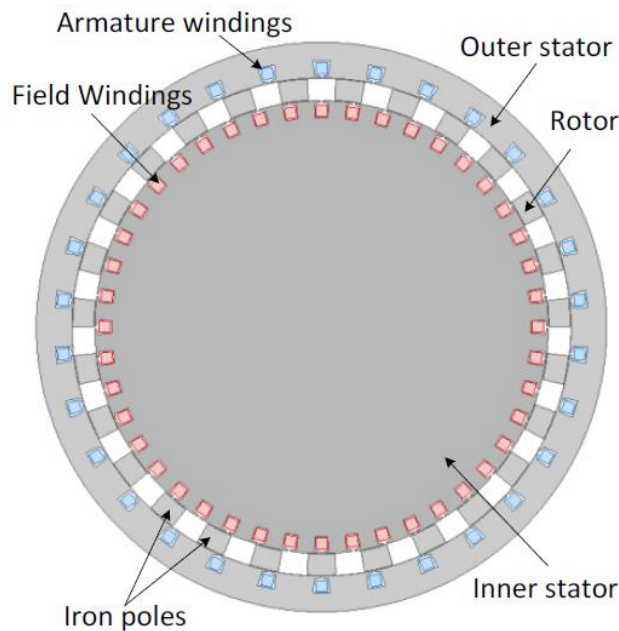


Fig. 10 Topology of SC magnetic gear [LIU14c]

Advantages of flux-switching SC generator:

- 1) Higher reliability of cryogenic system, because there is no need for rotating seals and the cryostat is stationary, without 'g' forces.
- 2) Higher reliability of SC coils, because there is no centrifugal force, which is extremely serious for high speed applications.
- 3) Higher reliability of supporting system, because it is stationary.

Disadvantages of homopolar SC generator:

- 1) Lower torque density, because the iron limits the flux density.
- 2) Higher weight, due to the high density of iron-core.
- 3) Larger rotor iron loss.

Although its rotor has robust structure, which is suitable for high speed, the rotor iron loss does not favour to the increase of speed.

11.5.3 Magnetic gear

Y. L. Liu et al. [LIU14c] conducted a conceptual design of SC magnetic gear Fig. 10. The advantages and disadvantages of this type of machine are as follows:

Advantages of SC magnetic gear:

- 1) Higher reliability of cryogenic system, because there is no need for rotating seals and the cryostat is stationary, without 'g' forces.
- 2) Higher reliability of SC coils, because there is no centrifugal force, which is extremely serious for high speed applications.
- 3) Higher reliability of supporting system, because it is stationary.

Disadvantages of SC magnetic gear:

- 1) Lower torque density, because the iron limits the flux density.
- 2) Higher weight, due to the high density of iron-core.
- 3) Larger rotor iron loss.

12 CHALLENGES OF SC GENERATOR COMMERCIALIZATION

12.1 Reliability of Cryogenic System

12.1.1 Rotating Seal

A major challenge of SC generator is the complicated cryogenic system as a result of transferring the coolant from the stationary compressor to the rotating cryostat and rotating seals

[QU13]. The key strategy to improve the reliability of cryogenic system is to avoid the rotating seals connecting the rotating part (cryogenic tubes in cryostat) and stationary part (tubes connected to condenser and cold head), which is a source of failures to the wind turbine. The strategies to avoid rotating seals are as follows:

- Adopting rotating armature topology [STA13] [IWA07]. The rotating armature topology is a very competitive candidate, and it is adopted by GE [STA13]. It is because it is easier to transfer electric power than cryogenic fluids to a rotor [QU13]. It is said in [STA13] that the reason why it was discarded before is due to immaturity of slip ring system for larger current, and the slip ring system is not a problem now since GE has resolved successfully with their 100MVA brush system for a variable frequency transformer. Besides the slip ring system, the other problems with rotating armature topology are difficult of building stator's cooling system etc.
- Adopting new machine topologies with stationary SC coils, such as homopolar, switching flux, double-stator double-fed generators, etc., which have been summarized in section 11.5.
- Adopting on-board cryogenic system, which means the cryogenic system is rotating with the rotor [WON05]. G. Snitchler proposed a cryogenic system with the cold heads mounted on the rotor for the low speed wind turbine application [SNI10]. However, this technology is not mature yet, mainly due to the immaturity of cryocooler, which can withstand the centrifugal force [ZHU14].

12.1.2 Cryocooler

The mostly widely used cryocooler, Gifford-McMahon (G-M) cycle, is off-the-shelf. However, the efficiency is low (typical efficiencies for commercial products around 10~15% [KOS12]) and it needs maintenance every 9~18 months [QU13]. The strategies to improve the reliability and capability are:

- Mult-cryocoolers.
- Development of new types of cryocoolers, such as Stirling cryocooler and pulse tube cryocooler, etc. Stirling cryocooler has higher efficiency and longer lifetime than G-M cryocoolers, but they are more expensive. It is said the Stirling cryocoolers are beginning to replace the G-M cryocoolers [QU13]. The pulse tube cryocooler has a longer lifetime, but its lower efficiency, smaller capacity and higher cost than G-M cryocooler limit its application at present.

12.2 Price of SC Material

The high price of SC material is an important hurdle preventing the commercializing of SC generator. The strategies to reduce the SC cost are as follows:

- Utilizing LTS instead of HTS (GE [STA13], R. Qu et al. [FAN14] [WAN14a] [LIU14a] [LIU14b] [ZHU14]). The price of LTS is much less than HTS, as listed in Table 4. The problems for utilization of LTS are 1) High cost of cryogen, because the liquid He (LHe) has to be utilized, which is more costly than Nitrogen or air. 2) Larger power of cryocoolers, which influences the overall efficiency and size of generator. Usually, the cryocooler efficiency decreases and power increases as the temperature decreases [QU13]. Consequently, HTS is preferable to LTS. However, with the technical progress in recent years, the gap of required cryogenic power for LTS and HTS is not as large as before.
- Utilizing iron-core instead of air-core. 1/2-2/3 SC material can be saved by utilizing iron-core rotor [QU13], if the required flux density is not so large (2/3 was saved, with flux density in the field coil 1.5T [BAI05]). The effect on SC reduction is obvious with the flux-density in the iron \leq 2T [KLA07]. The iron-core SC generator researches have been summarized in section 11.2.
- Optimizing SC coil shape to improve the field utilization [WEN14] [KIM14] [CHO14].

Table 4. *Prices of SC materials, [QU13]*

LTS	HTS (1G)_BSCCO	HTS (2G)_YBCO
1\$/kAm	50\$/kAm	10-15\$/kAm

12.3 AC Loss in Field Coil

The SC coil can be easily damaged by the heat power in the coil. Thus, the AC losses in steady and transient operation due to the alternative field should be minimized. The strategies are as follows:

- Adopting electromagnetic shield (EM shield)/damper between armature and field winding. The damper is extensively adopted in literature, and the AC losses in SC coils can be reduced to an acceptable level by utilizing damper.
- Utilizing multi-phase armature winding. J. Wang [WAN13] [WAN14b] investigated the influence of multi-phase armature winding topology on damper loss. It is said the damper loss can be reduced by almost 90% under rated load operation by adopting 9-phase 20 electrical degree shift winding topology [WAN13]. It should be applicable for field coils as well. In this way, there may be no need to separate the damping shell and cryostat to prevent the heat from conducting to the cryostat, which simplifies the structure of damper and cryostat. In fact, the damper and cryostat shell are adjacent (Qu et al. [ZHU14]) and even combined (GE [FAI12]) in many designs.

The SC coil which can withstand high AC current and field is the key for the development of fully SC generators.

12.4 Other Challenges

- 1) SC support system.
- 2) Torque transfer assembly, consisting of drive shaft, coil supporter, torque tube and interconnection assembly, in which the most important and difficult part is the torque tube.
- 3) Excitation system. The rotating transformer excitation system and flux pump are two most widely used excitation systems until now. However, more efforts are still needed for successful application in SC wind turbine [QU13].

These parts in SC generator have to satisfy electrical, mechanical and thermal requirement. Take torque tube, it has to transfer torque from warm shaft to cryogenic coil assembly, as well as reduce the heat leakage from shaft to coil assembly.

13 EXCITATION SYSTEM

The excitation system of SC generators requires special attention since the resistance in a SC generator is very low and a small change in the supply voltage will greatly modify the value of the field current [UMA02]

Furthermore, the value of the inductance of SC field coils is usually high with a low resistance. Such a combination leads to a long time constant, hence, to change the field current in a reasonable time a high voltage is needed [FRA08].

Another key thing is the amount of harmonics -quality- in DC current that flow through the field coils since the more harmonics it has, the higher AC losses of SC materials. As a consequence, the use of current as a control variable in the excitation system is more suitable than voltage.

The use of slip rings has reliability and heat leakage problem [TSU97a], [TSU97b] brushless excitation systems are under research and two methods have been proposed: a rotating transformer with a complex control system and a flux pump.

The rotating transformer excitation system only appears in some patents [GOL02], [CRA11]. The main advantage of this system is less heat load since the current flows intermittently. Main drawbacks of this system are: the reliability and availability of the switching devices, the difficulty in the maintenance since the cooling system has to be open and the needed quenching protection in the rotating transformer.

The flux pump system offers the possibility of using a higher field current in the SC field coils with low heat leak [ISH08] with also a higher efficiency and reliability than the rotating transformer excitation system. The use of a flux pump system reduces the synchronous reactance in the wind generator, hence the voltage control and the dynamic stability of the SC wind turbine is improved [MUT94].

Regardless of the excitation system chosen, more efforts have to be done to achieve a successful application in SCDD generators.

14 CONVERTERS

Wind turbine systems have a set of optimal operational conditions (frequency, voltage, etc.) which present good energy capture efficiency but may not directly match the grid specifications. Power electronic converters are used to provide the connection between the generation units and the grid to achieve high efficiency and meet the grid requirements.

Power electronic technology has seen a rapid development in recent years since its performance is continuously being improved while cost are falling.

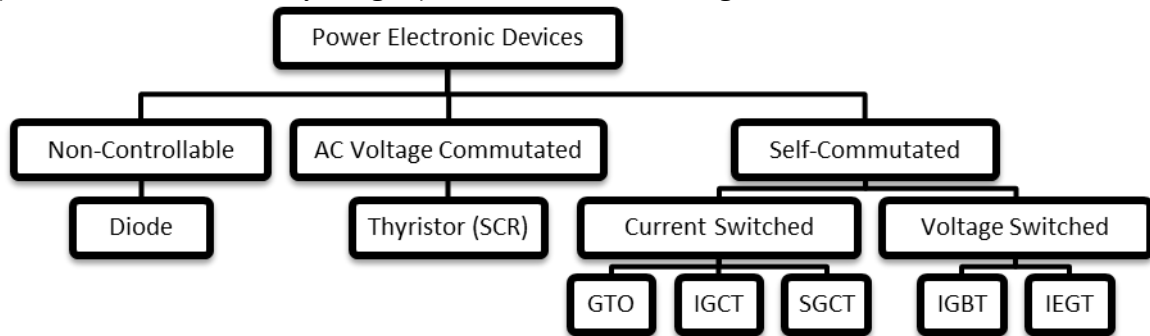


Fig. 11 Classification of the semiconductors for power electronic devices

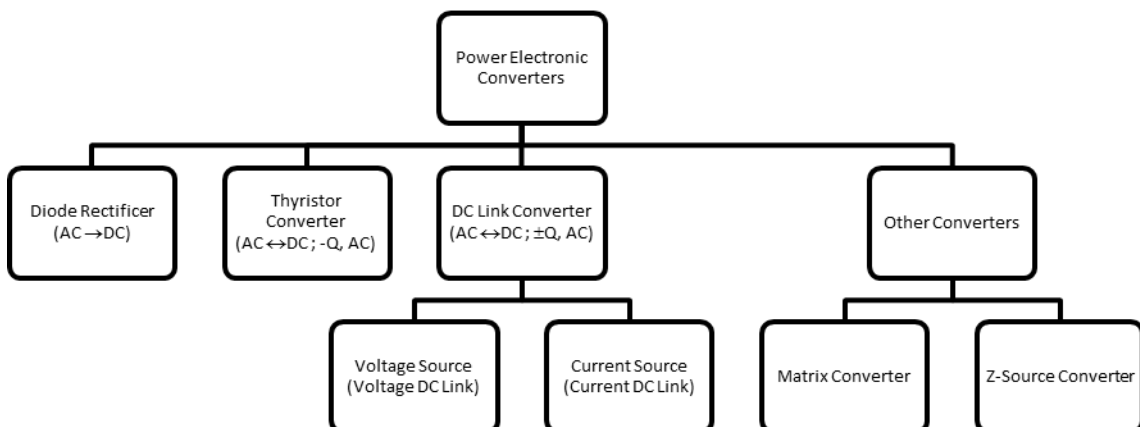


Fig. 12 Classification of power electronic converters

Semiconductors are the basic power electronic components and act as switches in power electronic circuits whose main parameters are the breakdown voltage and the rated current.

Semiconductors may be classified as non-controllable, AC voltage-commutated and self-commutated semiconductors. The self-commutated power semiconductor devices may be divided into current-switched and voltage switched devices Fig. 11.

The advantage of current switched devices is their lower conduction losses than voltage switched devices but as disadvantage their switching losses are higher.

Two of the most common switching devices (voltage switched) are Insulated Gate Bipolar Transistor (IGBT) and Insulated Gate Commutated Thyristor (IGCT). The advantages of IGCT compared to IGBT are its lower voltage drop on conduction and its higher current rating. On the other hand IGBT has a better maximum switching frequency that may allow the improvement of the harmonic performance, compared to IGCT, at the expense of higher switching losses.

IGBT is available at voltage ratings up to 4500 V and current ratings up to 3000 A and IGCT are available at 6000 V and 6000 A. Compared to Gate Turn-Off thyristor (GTO), IGBT and IGCT are cheaper and have better specifications. It is expected that IGBT will replace GTO at the low and medium power applications and IGCT will replace them in higher power range.

Power converters are built with semiconductors and may be classified as shown in Fig. 12.

A diode rectifier can only convert AC power into DC power. A thyristor can transfer active power in both directions but consumes inductive reactive power. Besides, a thyristor is not able to control the reactive power.

Self-commutated converters may transfer active power in both directions and can also control the AC reactive power in both directions. The most common self-commutated converters are DC link and may be classified into two types: Voltage Source Converter (VSC) and Current Source Converter (CSC). The self-commutated converters usually adopt Pulse Width Modulation (PWM) methods and high frequency harmonics and interharmonics may appear in the range of some kHz. In spite of that, these harmonics are relatively easy to be removed with the use of small filters.

The use of PWM techniques in VSC allow the control of the power losses, harmonics, dynamic requirements, etc. in power electronic devices and may be classified as voltage control PWM and current control PWM.

The voltage control methods produce a controllable AC voltage waveform whereas current control methods generate a desired AC current waveform.

For large wind turbines, the converter can be built with either high voltage devices or with a number of low voltage converters.

14.1 Power converters for wind turbines

The performance of power converters plays a key role in the operation of the wind turbines. Some promising converter topologies are described in the following sections.

Further information can be found in [ZHU13a] and [ZHU13b], where a thorough work of power electronics for high power wind energy has been done.

14.1.1 Two-level power converter (2L BTB)

Pulse Width Modulation-Voltage Source Converter with two level output voltage (2L PWM-VSC) is the most frequently used three-phase power converter topology in the range of 3MW [BLA13]. The configuration of the 2L PWM-VSC is usually in back to back structure with a transformer on the grid side as shown in Fig. 13.

The 2L-BTB is a simple solution with few components that has been proven as robust and reliable. However, the increase of voltage and power range of wind turbines increases its switching losses and makes its structure more complicated (necessity of paralleled or series switches) [ROD07].

Another drawback is the higher stress that produces to the generator and transformer due its steep dv/dt character that requires the use of output filters [IOV08].

The 2L-BTB converter topology is the most used in Double Fed Induction Generator (DFIG) wind turbines [CHE09].

14.1.2 Multilevel power converter

Multilevel converters are mainly used in the 3 MW to 10 MW range for variable speed full-scale power converter wind turbines due the inconveniences that 2L-BTB have to achieve acceptable performances in that range of power [KOU10].

The most promising topologies of multilevel converters are described in the following subsections.

14.1.2.1 Three-level neutral point diode clamped back to back topology (3L NPC-BTB)

Three-level Neutral Point diode Clamped topology is one of the most commercialised multilevel converters in the market. It is usually known as 3L NPC-BTB. It is usually configured as back to back structures in wind turbines Fig. 14.

The advantage of the 3L NPC-BTB is its higher voltage and less dv/dt compared to the two-level topology.

As a drawback it has the mid-point voltage fluctuation of DC bus. However this problem has been extensively researched and is considered solved by controlling of redundant switching status.

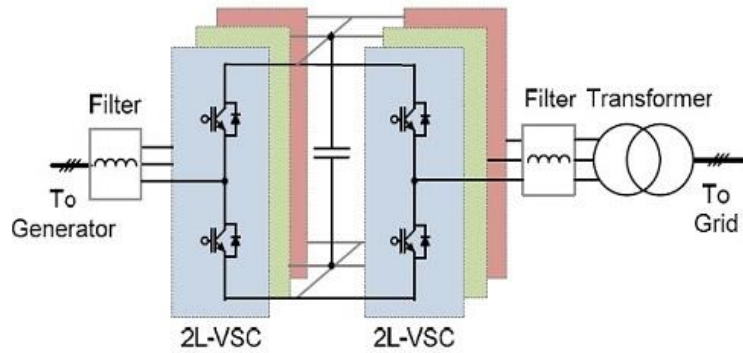


Fig. 13 Two-level back-to-back voltage source converter for wind turbines (2L BTB) [BLA10]

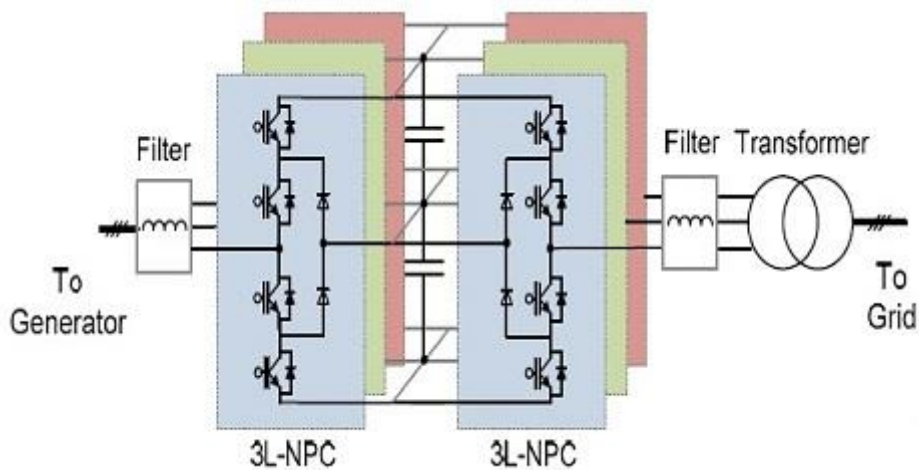


Fig. 14 Three-level Neutral Point Clamped back-to-back converter for wind turbines (3L-NPC BTB) [BLA10]

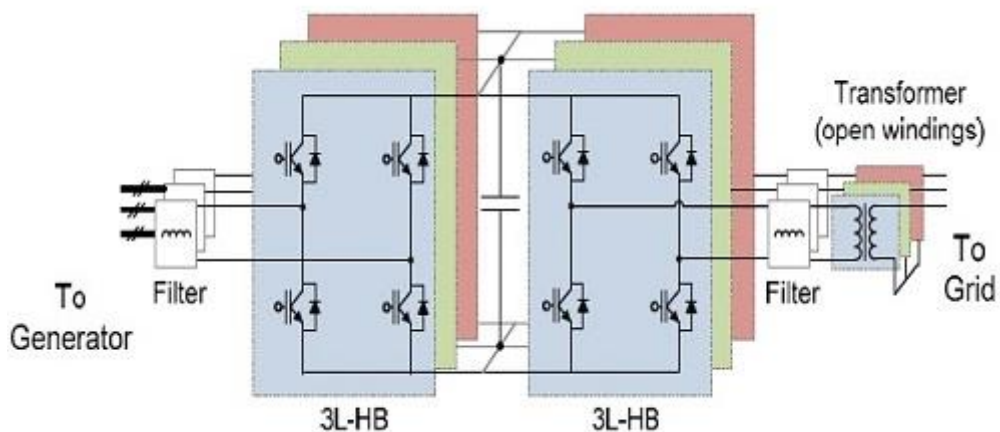


Fig. 15 Three-level H-bridge back-to-back converter for wind turbines (3L-HB BTB) [BLA10]

A second drawback is unequal use of the outer and inner switching devices in a switching arm [ROD10].

14.1.2.2 Three level H-bridge back to back topology (3L HB-BTB)

The 3L-HB BTB solution is composed of two H-bridge converters which are configured as back to back structure as shown in Fig. 15.

The performance of 3L-HB BTB is similar to 3L NPC BTB solution but the unequal loss distribution and clamped diodes are eliminated. In this topology a more efficient and equal usage of switching devices could be acquired, as well as higher designed power capacity [SEN09].

Since only half of the DC bus voltage is needed in 3L NPC BTB compared to 3L NPC BTB, there are less series connection capacitors and no midpoint in DC bus, therefore the size of DC link capacitors can be highly reduced.

The 3L HB-BTB solution needs open windings structure in the generator and transformer in order to achieve isolation between each phase. The advantage of open windings is that it enables a relative isolated operation of each phase, therefore the system is fault tolerant in the event two phases of the generator or the generator side are broken. The disadvantage is the need of double cable length to connect it with generator and transformer, hence extra cost, weight, loss and inductance in the cables are the major drawback.

14.1.2.3 Five-level H-bridge back to back topology (5L-HB BTB)

The 5LHB BTB converter is composed of two back to back H-bridge converters making use of 3L-NPC switching arms as shown in Fig. 16. It is an extension of 3L HB BTB and shares the same special requirements for open-winding generator and transformer.

With the same voltage rating switching devices, 5L-HB BTB can achieve a five level output voltage, and double voltage amplitude compared to the 3LHB BTB solution. Therefore it requires a smaller output filter and less current rating in the switching devices as well as in the cables [SEN09].

Compared to 3L HB BTB the 5L HB BTB converter introduces more switching devices, which could reduce the reliability of total system. As in the 3L HB BTB topology, the problems of unequal loss distribution as well as larger DC link capacitors are the major drawbacks.

14.1.2.4 Three-level Neutral point diode clamped topology for generator side and five level H-bridge topology for grid side (3L NPC+5L HB)

Output quality requirement of grid side are much stricter than those of the generator side [CHE09]. To achieve a good performance in both side with the lowest costs, a back to back converter with 3L NPC topology in the generator side and a 5L HB topology on the grid side is proposed Fig. 17.

The result of this configuration is a performance similar to a 3 NPC BTB on the grid side and a performance similar to a 5 HB BTB on the grid side.

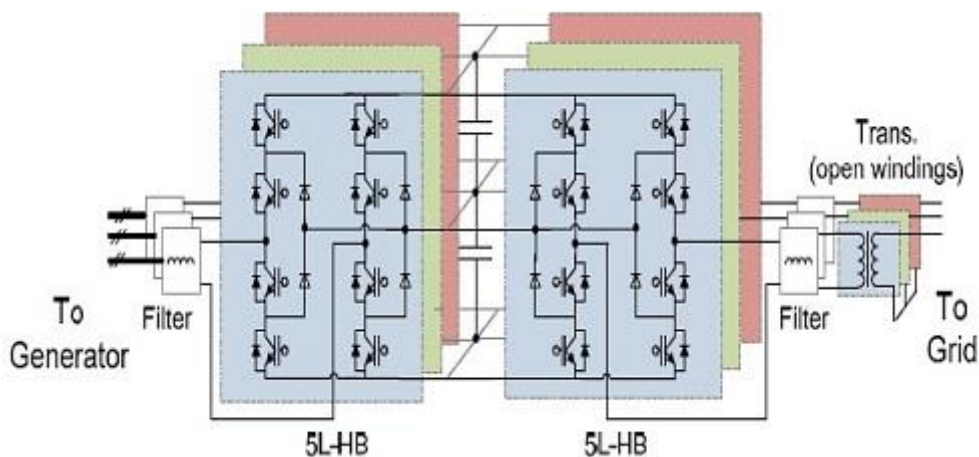


Fig. 16 Five-level H-bridge back-to-back converter for wind turbines (5L- HB BTB) [BLA10]

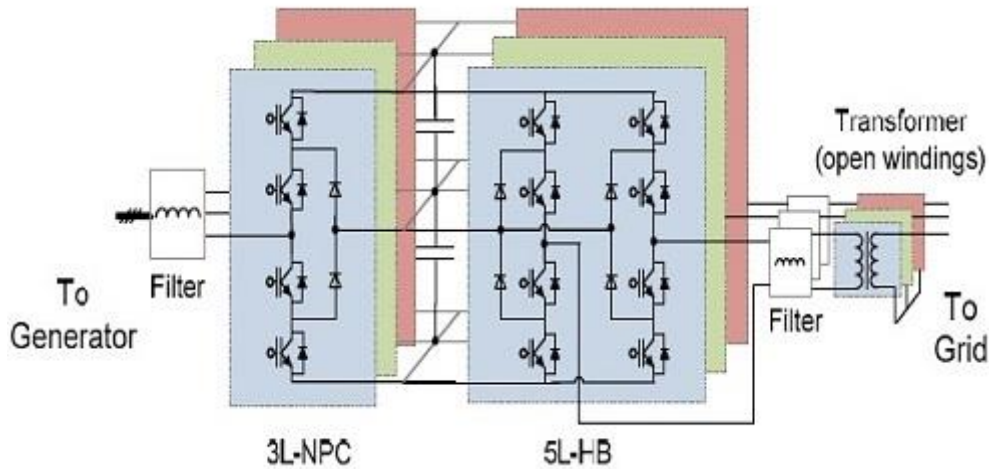


Fig. 17 Three-level Neutral Point Clamped and five-level H-bridge converter for wind turbines (3L-NPC + 5L-HB) [BLA10]

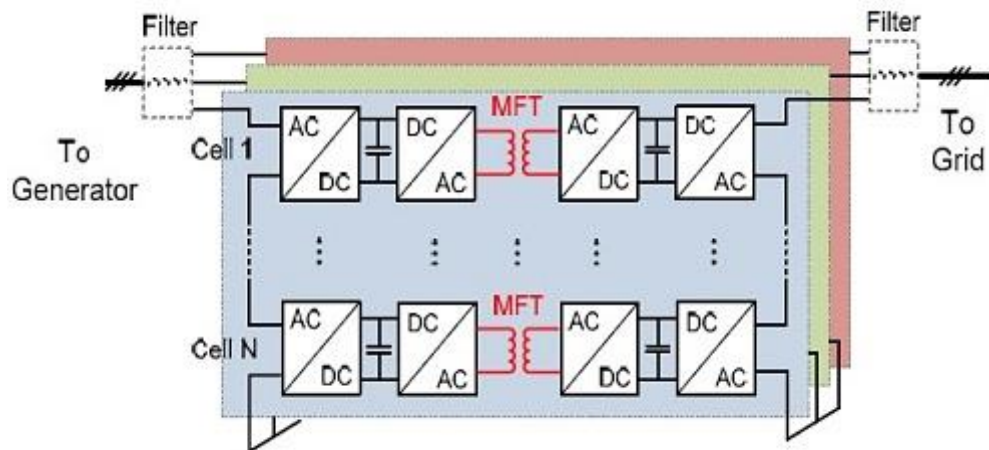


Fig. 18 Cascade H-bridge back-to-back converter for wind turbines with Medium Frequency Transformer (CHB-MFT) [BLA10]

14.1.2.5 Cascaded H-bridge back to back converter with medium frequency transformers (CHB-MFT)

Until now, one of the most commercialised cascaded converter cells multilevel topologies is Cascaded H-Bridge (CHB) converter. However, their use requires an isolated DC link for each converter cell. This feature results in a complex multi-pulse transformer on the generator side, resulting in larger weight and volume converters [KOU10].

To overcome such inconveniences a configuration based on a back to back CHB converter structured with galvanic insulated DC/DC converters as interface has been proposed Fig. 18.

The advantages of the use of DC/DC converters with Medium Frequency Transformers (MFT) that operate from several kHz is their reduced size. Furthermore, it might be directly connected to the transmission power grid with high output voltage quality, hence the need for filter design is almost inexistent.

On the other hand, as a drawbacks, the large amount of power semiconductors as well as auxiliary components needed reduces the converter's reliability as well as increases its cost.

14.1.3 Matrix converter

Matrix converters are considered as AC-AC devices. Their features, such as bidirectional power flow, sinusoidal input/output currents, controllable power factor, are well documented in [WHE02].

Although the tremendous interest achieved by the matrix converter, its use in real applications is limited [WHE02] since they are technically much more complicated [CHE09]. Moreover, matrix converters neither benefit from ripple reduction nor reduced Eddy currents [MIN07].

A good review of control and modulation methods, such as scalar techniques, PWM, Direct Torque Control (DTC) and predictive control, for Matrix converters can be found in [ROD12].

Despite that there is no intrinsic limitation to the power of a matrix converter, not many matrix converter has been reported to be constructed. A 150 kVA matrix converter for military applications [POD05], a 50 kVA for a PMSG [HOJ13], for some residential wind turbines [WAN09] and for a 7.5 kW converter [IBA12] are the main matrix applications at the present time. The real challenge of the matrix converter is, therefore, to be accepted in the market.

14.1.4 Current source converters

All commercially available variable speed wind turbine technologies make use of a VSC converters. Only Rockwell has been trying to apply its PWM Current Source Converter (CSC) to variable speed wind turbines.

The main advantages of CSC are the inherent back to back operation and the reduced Electromagnetic Interference (EMI) problems.

As a drawbacks CSC has a worse performance than VSC. Moreover, the power factor achieved with CSC at low speeds is not in the required range by the grid codes. To improve the power factor performance better and more complex control techniques must be developed [BAD09].

14.1.5 Comparison of power electronic converters for wind applications

A summary of the advantages and disadvantages of the power electronic converters for wind applications is shown in Table 5.

Table 5. *Advantages and disadvantages of power electronic converters solutions for wind turbines [BLA10] [BAD09] [MIN07]*

Configuration	Advantages	Disadvantages
2 Level Back to Back	<ol style="list-style-type: none"> Commercialised Simple solution Robust Reliable 	<ol style="list-style-type: none"> Steep dv/dt Need of large output filters Low power Low voltage
3 Level Neutral Point Diode Clamp Back to Back	<ol style="list-style-type: none"> Most commercialised High power High voltage Less dv/dt 	<ol style="list-style-type: none"> Midpoint voltage fluctuation of DC bus. Unequal use and losses of switches
3 Level H-Bridge Back to Back	<ol style="list-style-type: none"> Higher design capacity More efficiency Less capacitors No midpoint DC bus Isolation of each phase 	<ol style="list-style-type: none"> Double cable length Heavier More expensive More losses Higher inductance
5 Level H-Bridge Back to Back	<ol style="list-style-type: none"> Higher output voltage Smaller output filter Less current rating switches Thinner cables 	<ol style="list-style-type: none"> More switching devices Poor reliability Unequal distribution of use of switches Large capacitors
3 Level Neutral Point Diode Clamped + 5 Level H-Bridge	<ol style="list-style-type: none"> Adapts to the more stricter requirements of the grid 	<ol style="list-style-type: none"> Same as 3L NPC and 5L HB
Cascaded H-Bridge Back to Back with Medium Frequency Transformer	<ol style="list-style-type: none"> Small transformer High output quality 	<ol style="list-style-type: none"> Isolated DC for each converter cell. Expensive

		3. Reduced reliability
Matrix Converter	<ol style="list-style-type: none"> 1. Bidirectional power 2. Sinusoidal input/output currents 3. Controllable power factor 	<ol style="list-style-type: none"> 1. Technically complicated 2. Not accepted in the market 3. No experience for high power applications 4. Current ripple 5. Eddy currents
Current Source Converters	<ol style="list-style-type: none"> 1. Inherent back to back operation 2. Reduced EMI problems 	<ol style="list-style-type: none"> 1. Not commercially used in variable speed wind turbines 2. Worse performance than VSC 3. Do not meet the grid codes for low speeds

Table 6. Comparison of the multilevel solutions for wind turbines

Configuration	2 Level Back to Back	3 Level Neutral Point Diode Clamp Back to Back	3 Level H-Bridge Back to Back	5 Level H-Bridge Back to Back	3 Level Neutral Point Diode Clamped + 5 Level H-Bridge	Cascaded H-Bridge Back to Back with Medium Frequency Transformer
Output voltage levels	2	3	3	5	3/5	2N+1
IGBT number	4	8	8	16	12	16N
Diode number	4	12	8	24	17	16N
Max. Output voltage	2 V_{switch}	4 V_{switch}	4 V_{switch}	8 V_{switch}	4/8 V_{switch}	8N V_{switch}
Fault tolerant ability	No	No	Limited	Limited	No	Yes
Filter size	Large	Medium	Medium	Small	Medium/Small	No need
Transformer size	Large					Small

Table 7. Comparison of multilevel converters for low inductance machines [MIN07]

Topology	Current Ripple	THD	Price
2 Level Back to Back	100 %	1	1 p.u.
3 Level Back to Back	50%	0.51	1.25 p.u.
4 Level Back to Back	33%	0.38	1.70 p.u.
5 Level Back to Back	25%	0.27	2.15 p.u.

Since the VSC are the most predominant topologies in the market a comparison of the elements necessary for each converter as well as the maximum output voltage, fault tolerant ability, filter size and transformer size are summarised in 0.

14.1.6 Power converters for low inductance applications

The application of VSC to low inductance machines is difficult to implement due the high current ripple for common frequencies (2-10 kHz) as a consequence of the low value of the

inductance. High current ripple values are unacceptable in the vast majority of applications as it degrades torque control and reduces the efficiency of the system [LUD12].

Current solutions for this problem is the use of external line reactors, high switching frequencies or a combination of both.

The use of external line reactors to increase the inductance of the system brings problems since the external line reactors are bulky, increase cost and reduce reliability of the system.

High switching frequencies (>20 kHz) are possible in low power applications, but for high power application, switches cannot achieve such frequencies and losses are too high.

In [MIN07] has been stated that the use of multilevel converters can improve current ripple and harmonic distortion for low inductance machines. The inconvenience of using multilevel converters is the increase of cost and reduction of the reliability of the system.

A comparison between multilevel back to back converters of 2, 3, 4 and 5 levels, taking the 2 level back to back converter as a reference, is shown in Table 7.

CHAPTER 2: GENERATOR DESIGN

1 INTRODUCTION

In this chapter, the SC generator is designed and the performances are analysed. Firstly, the performances of three major SC generator topologies, i.e. iron-core stator and rotor, air-core stator and rotor, and iron-core stator and air-core rotor, etc., are compared, in terms of torque-SC quantity characteristic. Based on the comparison, the iron-core stator and rotor topology is determined, since it has the highest SC material utilization. Then the influences of pole number, stator outer diameter and pole width on performances and costs are investigated, and the final electromagnetic design of 10MW SC generator is determined. Based on the final design, the electromagnetic performances are analysed, including losses and efficiency, field harmonics in SC coils, forces on rotor components, etc. In addition, the performances of generator under three-phase short-circuit fault operation are also analysed. Finally, the 10MW SC generator is scaled to 20MW.

2 COMPARISON OF TORQUE-SC QUANTITY CHARACTERISTICS BETWEEN SC GENERATORS WITH DIFFERENT TOPOLOGIES

2.1 Introduction

For the design of SC generator in this project, much attention should be paid to the cost of generator, because the cost of SC material is too high (In this report, a kind of YBCO SC material is utilized with quotation 100€/m). In this report, the feasible topology is determined from the view of SC material cost.

There are three major topologies for SC generators for wind turbines, i.e. air-core stator air-core rotor, iron-core stator air-core rotor, and iron-core stator iron-core rotor, etc., as shown in Fig. 19. The torque-SC quantity characteristics of the three topologies will be compared in this chapter, which can supply some guidelines for the determination of topology.

2.2 Optimization Method

The parameters of these topologies are listed in Table 8. For each design, the stator slot height and width, and stator yoke thickness are globally optimized to maximum the torque capability. The J - B characteristic of SC material is shown in Appendix I. During the optimization, the current density of SC coil always operates with a safety margin of 22%.

Table 8. Parameters of SC generator

Parameters	Air-core stator air-core rotor	Iron-core stator air-core rotor	Iron-core stator iron-core rotor
Stator outer diameter D (m)	7	7	7
Stack length L (m)	1	1	1
Stator copper loss P_{cu} (kW) (without end winding)	274	274	274
Stator current density (A/mm ²)	3.5	3.5	3.5
Pole/slot number $2p/Q$	32/576	32/576	32/576
Packing factor	0.6	0.6	0.6
Airgap length g (mm)	80	80	9

2.3 Results

The variations of torque capability with SC area per pole for the three topologies are shown in Fig. 20. The torque-SC quantity characteristic of iron-core stator and rotor topology becomes saturated, as S_{sc}/pole increases, due to the saturation of iron. The characteristics of air-core rotor topologies are much harder, because less iron is utilized. The torque capability of iron-core stator and rotor topology are higher than that of air-core rotor topologies, and the advantage is more significant with when S_{sc}/pole is small. Due to the high cost of SC nowadays, a small quantity of SC

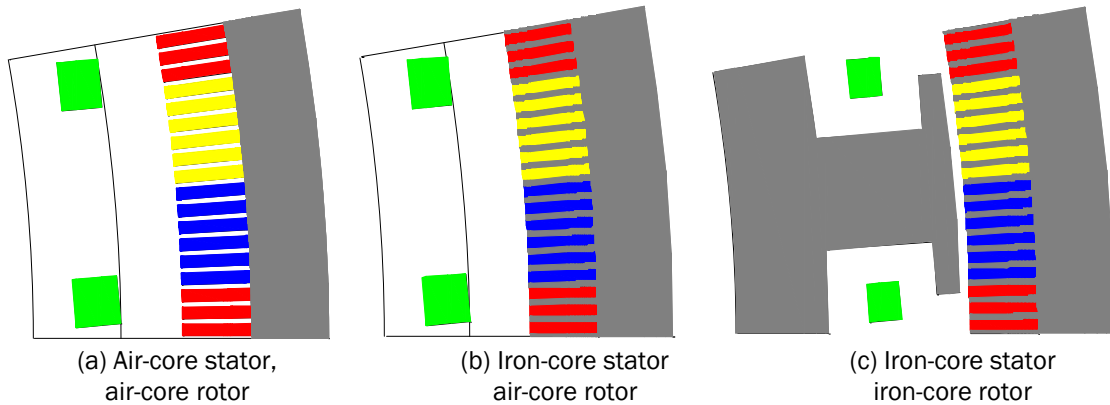


Fig. 19 SC generators with different topologies. (a) Air-core stator, air-core rotor, (b) Iron-core stator, air-core rotor and (c) Iron-core stator, iron-core rotor

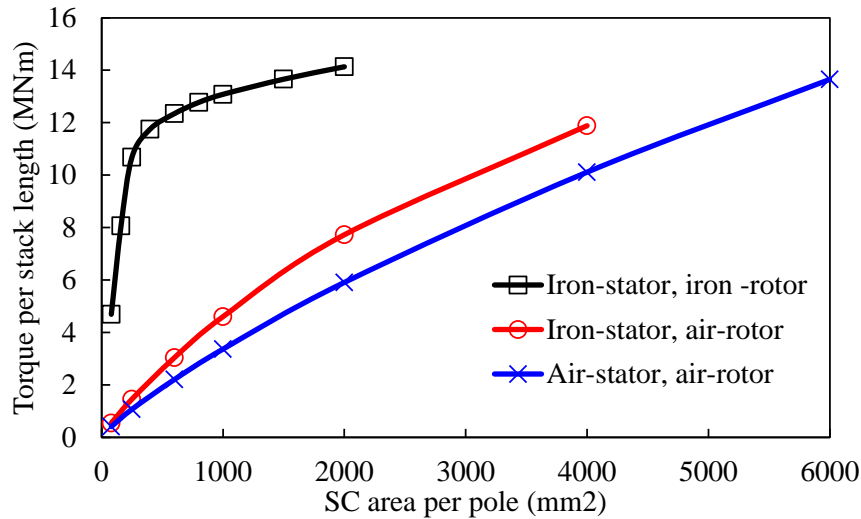


Fig. 20 Variations of torque with SC area per pole, $D=7\text{m}$, $P_{Cu}/\text{stack length}=274\text{kW}$, $J_a=3.5\text{A}/\text{mm}^2$, for each S_{sc}/pole , the stator slot height and width, and stator yoke thickness are optimized.

is preferable. Thus, iron-core stator and rotor topology is favourable in this project. However, as the cost of SC reduces, air-core rotor topologies may be better, since they have great advantage over generator weight.

3 DESIGN AND ANALYSIS OF SC GENERATOR WITH IRON-CORE STATOR AND ROTOR TOPOLOGY

Since, the iron-core stator and rotor topology has been determined, the design and analysis for this topology are conducted in this chapter.

3.1 Influence of Pole Number and Stator Outer diameter on Performances

3.1.1 Optimization Method

Finite element analysis software MAXWELL is utilized for torque calculation and $i_d=0$ control is adopted. The major dimensional parameters of SC generator are shown in Fig. 21.(a). Some of them are determined in advance, which are listed in Table 9, in order to simplify the optimization. The stator yoke thickness h_y , stator slot width and area b_s and S_{slot} are globally optimized for each specific stator outer diameter D and pole number $2p$. The optimization target is to achieve the 10.5MNm electromagnetic torque with the shortest stack length L_{stack} . During the optimization process, the efficiency is fixed to be 95.5%, with only the stator DC copper loss considered. The torque and efficiency are based on the requirements of 10MW generator for direct-drive wind turbines, which are shown in Appendix III. The total length of half turn stator coil, L_{half_turn} , which involves the end winding length, is (2).

$$L_{half,turn} = L_{stack} + 2d_1 + 2C_s$$

$$C_s = \frac{\tau_y}{2 \cos \alpha} \quad (2)$$

$$\cos \alpha = \sqrt{1 - \sin^2 \alpha} = \sqrt{1 - \left(\frac{b_s}{b_s + b_\tau} \right)^2}$$

where b_s is stator slot width, b_τ is the average width of stator tooth, and d_1 , C_s , τ_y , α are shown in Fig. 21(b).

For a SC conductor, the critical engineering current density, flux densities (components perpendicular and parallel to the surface of SC tapes respectively) and temperature are always interrelated. In this optimization, the temperature is assumed to be 30K, and only the perpendicular flux density B_\perp is considered, since B_\perp is more dominant for the influence on current density. When a current density J is imposed on the SC coil, there will produce a self-induced field. The variation of induced maximum B_\perp in SC with J is shown as the blue dashed line in Fig. 22, which is linear and termed as load $J-B_\perp$. The red dashed line in the figure is the $J-B_\perp$ characteristic of SC involving a 22% safety margin. The J for the cross point of load $J-B_\perp$ and $J-B_\perp$ characteristic is determined as the operation current density of SC coil, in order to fully and safely utilize the SC material.

The optimization procedure is shown in Fig. 23. It should be mentioned that the appropriate operation J_{sc} for different designs are not different a lot. The two processes for checking the $J-B_\perp$ relationship can be eliminated, after the initial check, in order to reduce the work amount.

It should be mentioned that the $S_{sc}/pole$ (200mm²) is determined, according to the torque- S_{sc} characteristic in Fig. 22. It is around the saturation point.

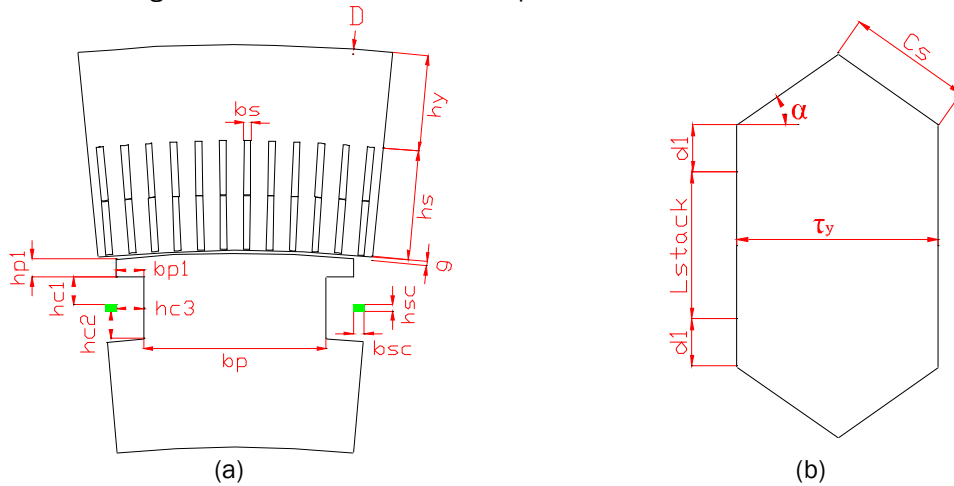


Fig. 21 Parameters of SC generator

Table 9. Parameters of 10MW SC generator

Power (MW)	10
Speed (rpm)	9.6
Torque (MNm)	10.5
Efficiency η (%)	95.5
h_{p1} (mm)	40
b_{p1} (mm)	60
h_{c1} (mm)	60
h_{c2} (mm)	60
h_{c3} (mm)	60
g (mm)	$2+0.001 \times D$
b_{sc} (mm)	12.6
h_{sc} (mm)	8
h_{c3} (mm)	60
Packing factor k_{pac}	0.6
Stator current density J_a (A/mm ²)	3.5

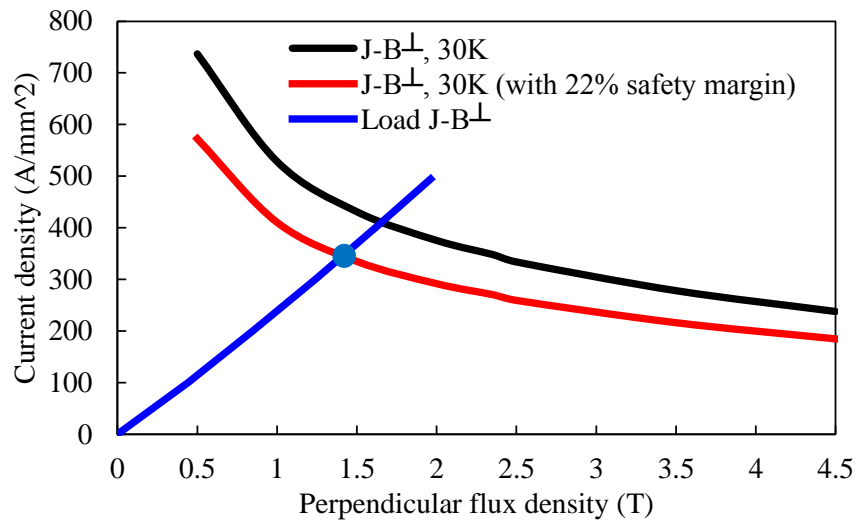


Fig. 22 Variations of current density with perpendicular flux density in SC, B_{\perp} is the amplitude of flux density perpendicular to the surface of SC tapes, Load $J-B_{\perp}$ is the variation of current density with maximum self-induced B_{\perp} in SC.

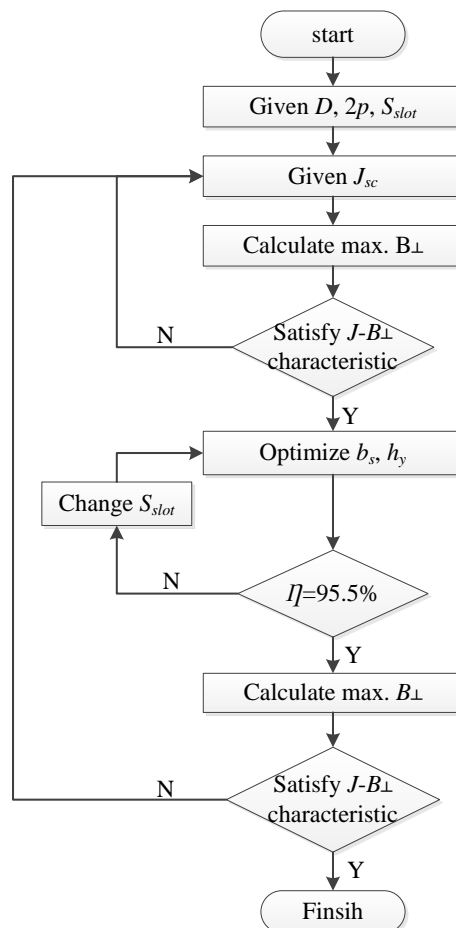


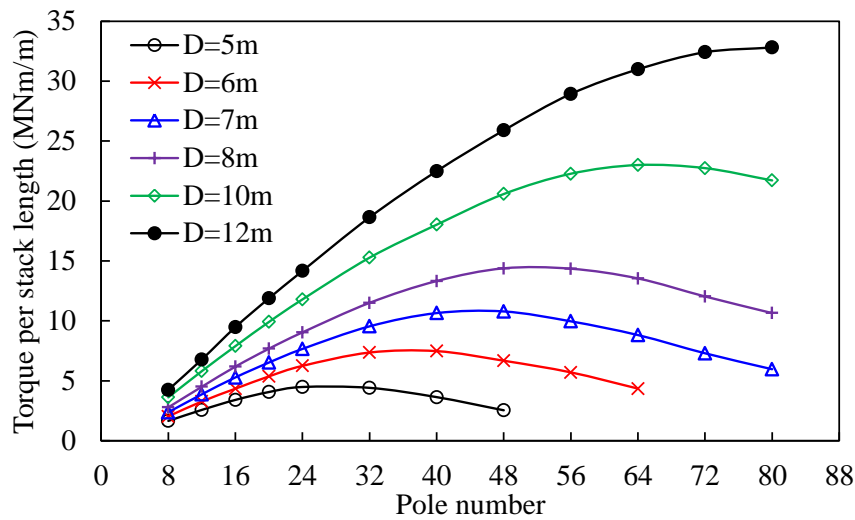
Fig. 23 Optimization procedure.

3.1.2 Results

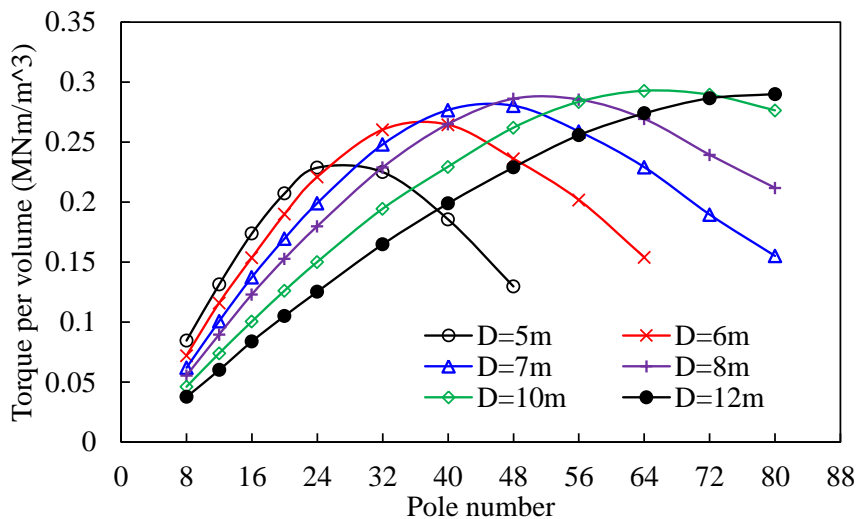
3.1.2.1 Torque and Torque per Generator Volume

Usually, as the pole number $2p$ increases, the armature end winding length decreases. It tends to fully utilize the armature winding and increase the torque, when the total copper loss is constant. However, as $2p$ increases, the total area of cryostats along circumferential direction increases linearly, which tends to reduce the total flux through the air gap, and further reduce the torque. Thus, there should be an optimal $2p$ to achieve the maximum torque. The variations of torque per stack length with pole number for different stator outer diameters are shown in Fig. 24.(a). At the beginning, the influence of $2p$ on end winding length is significant, and the torque increases. As $2p$ increases, the influence on end winding length becomes gradually less, and the torque starts to reduce.

The variations of torque per generator active volume with $2p$ for different stator outer diameters are also shown in Fig. 24.(b). The optimal $2p$ for torque per volume is the same as that for torque per stack length. In addition, the optimal $2p$ increases with stator outer diameter.



(a) Torque per stack length.



(b) Torque per generator active volume.

Fig. 24 Variations of torque per stack length and per generator volume with pole number for different stator outer diameters.

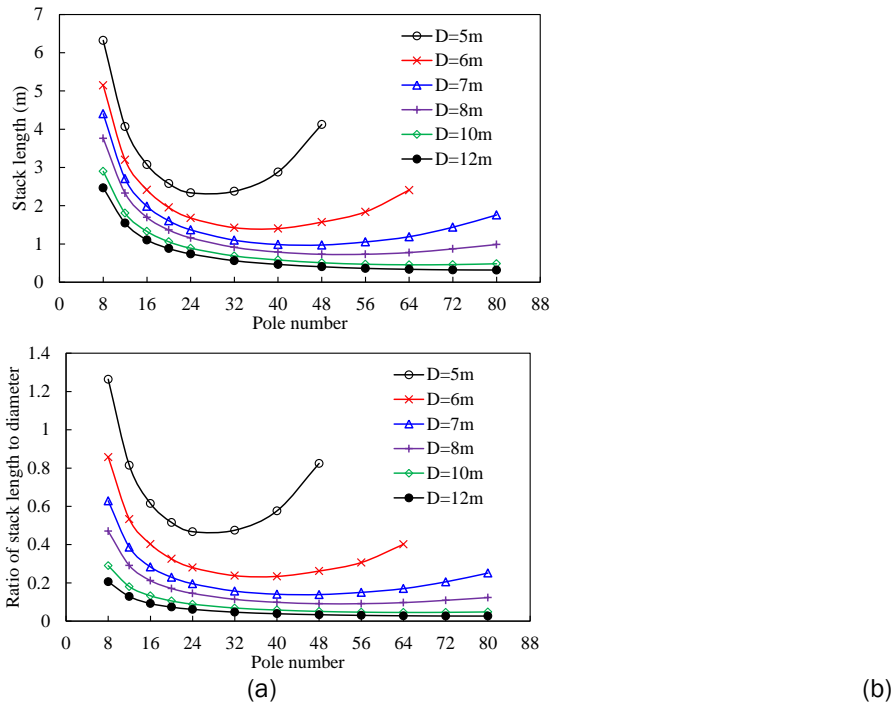


Fig. 25 Variations of stack length and ratio of stack length to stator outer diameter with pole number for different stator outer diameters, torque=10.5MNm.

3.1.2.2 Stack Length

The variations of stack length with pole number for different stator outer diameters to achieve 10.5MNm torque are shown in Fig. 25. In order to achieve the target torque, the stack length is usually shorter for a large stator outer diameter. In other words, the generator becomes flatter as stator outer diameter increases.

3.1.2.3 Torque per Generator Iron Mass

As $2p$ increases, the stator yoke thickness always decreases and the iron mass per stack length decreases, as shown in Fig. 26.(a). The torque per iron mass is shown in Fig. 26.(b). There exists an optimal $2p$ for torque per mass, and it should be between the optimal $2p$ for torque and for mass. Since the optimal $2p$ for mass is close to an infinite large value, the optimal $2p$ for torque per mass is always larger than that for torque per stack length.

3.1.2.4 Torque per SC Length

The SC length increases linearly with $2p$, as shown in Fig. 27.(a), since the SC area per pole is fixed in the optimization. The SC coil end length is not considered in Fig. 27.(b). When the torque in Fig. 24.(a) is divided by the SC length, the torque per SC length is obtained, as shown in Fig. 27.(b). The optimal $2p$ for maximum torque per SC length should be between the optimal $2p$ for torque and SC length. Since the optimal $2p$ for SC length is close to zero, the optimal $2p$ for torque per SC length is always smaller than that for torque.

In order to accurately estimate the SC utilization, the SC coil end length has to be considered. The total end length $L_{sc(end)}$ for a SC coil is

$$L_{sc(end)} = \pi \tau_{sc} \quad (3)$$

where τ_{sc} is the pitch of SC coil. The torque per SC total length can be obtained by

$$\frac{\tau}{L_{sc(total)}} = \frac{\tau}{L_{sc(stack)}} \frac{L_{sc(stack)}}{L_{sc(total)}} \quad (4)$$

where $L_{sc(stack)}$ and $L_{sc(total)}$ are the SC coil straight and total length respectively. Variations of $L_{sc(stack)}/L_{sc(total)}$ and $T/L_{sc(total)}$ with $2p$ for different stator outer diameters to achieve 10.5MNm torque

are shown in Fig. 28.(a) and Fig. 28.(b) respectively. $L_{sc(stack)}/L_{sc(total)}$ becomes smaller as stator outer diameter increases, because the generator becomes flatter. The shapes of $T/L_{sc(total)}$ curves are not quite different from those in Fig. 27.(b), however, the relative positions of these curves are changed, due to the influence of $L_{sc(stack)}/L_{sc(total)}$.

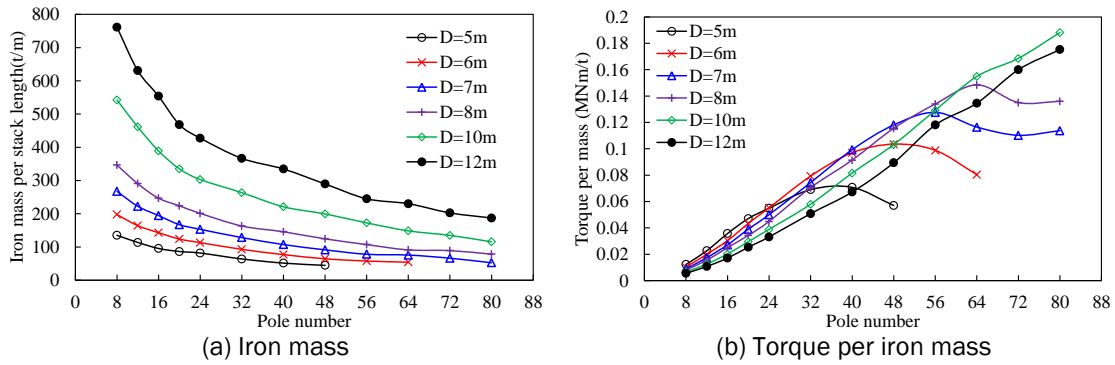


Fig. 26 Variations of iron mass and torque per iron mass with pole number for different stator outer diameters.

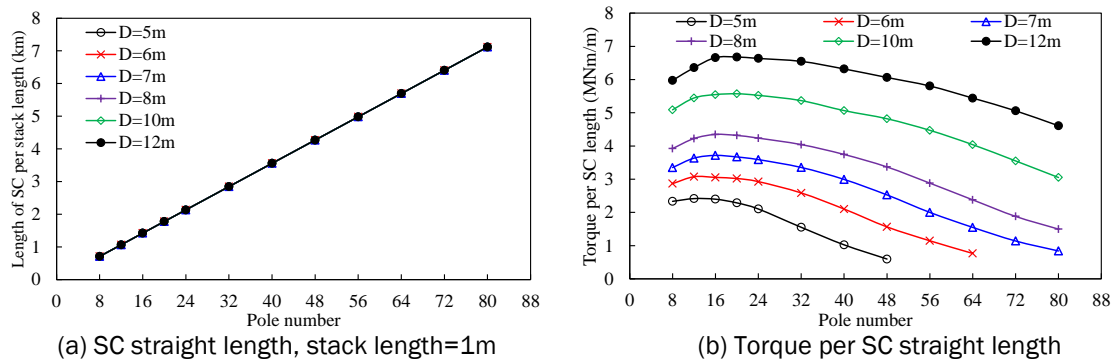


Fig. 27 Variations of SC length and torque per SC length with pole number for different stator outer diameters, the end SC coil length is not considered.

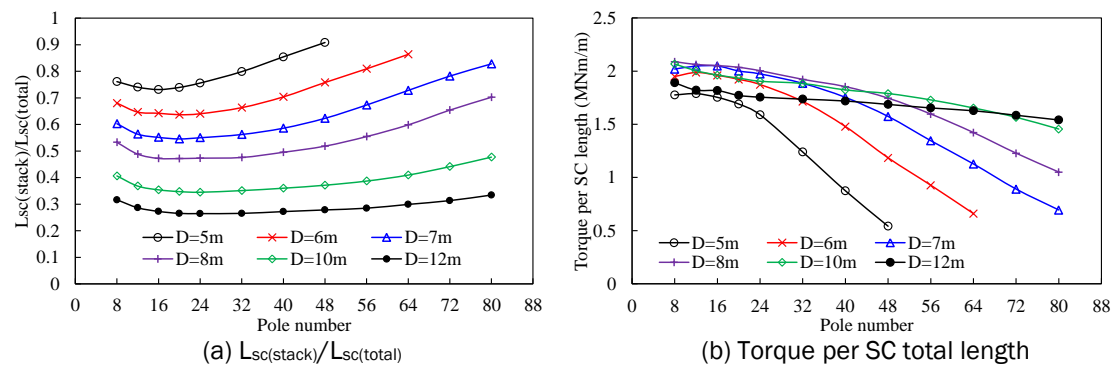


Fig. 28 Variations of ratios of SC coil straight length to total length and torque per SC length with pole number for different stator outer diameters, torque=10.5MNm.

3.1.2.5 Costs

The costs of SC material, iron and copper, and total cost are shown in Fig. 29. As $2p$ increases, the iron cost decreases, because the stator and yoke thickness become narrower, Fig. 29.(c). During the optimization, the total copper loss and stator current density are fixed, thus, the total copper quantity is fixed. Consequently, the copper loss is constant Fig. 29.(d). The SC cost increases with $2p$, because the SC utilization becomes lower, Fig. 28 (b). As $2p$ increases, the total cost decreases at the beginning, due to the influence of iron cost. After some point, the total cost increases, due to the increase of SC cost. It can be seen that the SC cost dominates the total cost.

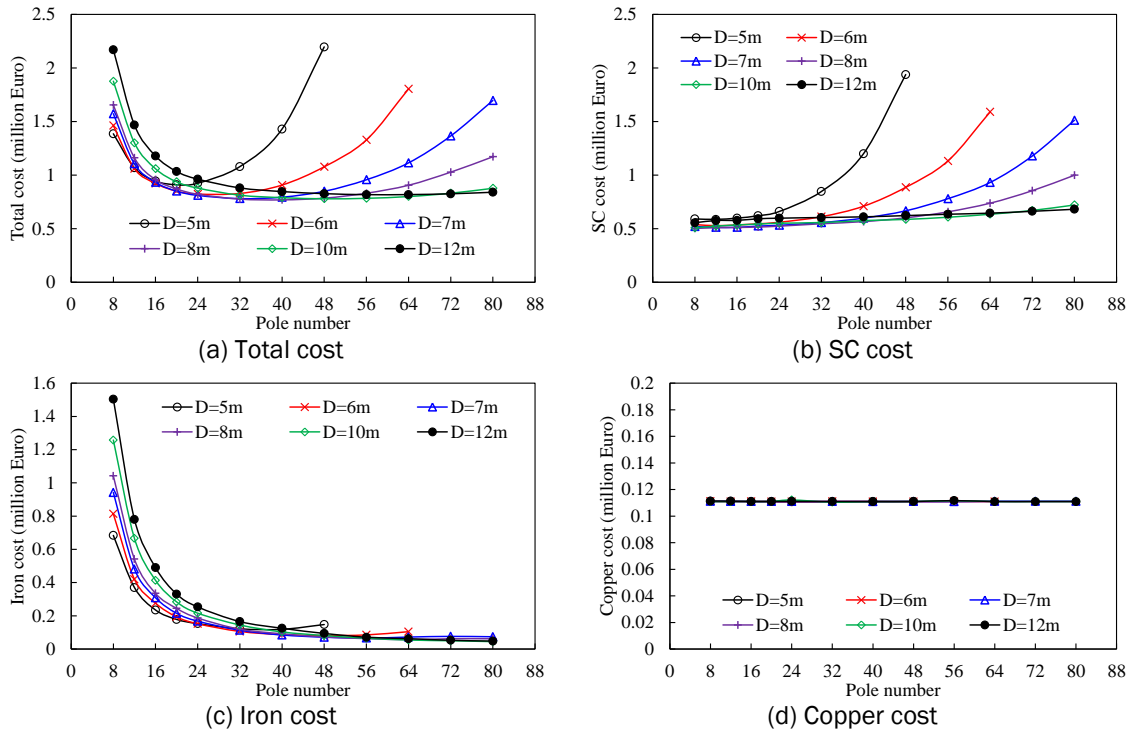


Fig. 29 Variations of material cost with pole number for different stator outer diameters, torque=10.5MNm.

3.1.3 Determination of Pole Number and Stator Outer Diameter

The pole number and stator outer diameter of 10MW SC generator should be determined from the view trade-off between cost, generator volume and weight. The variations of cost, volume and weight with $2p$ and D are shown in Fig. 30. Some combinations of $2p$ and D are given: 1) $D=6m$ $2p=24$, 2) $D=7m$ $2p=32$; 3) $D=8m$, $2p=40$.

Finally, $D=7m$ $2p=32$ are chosen.

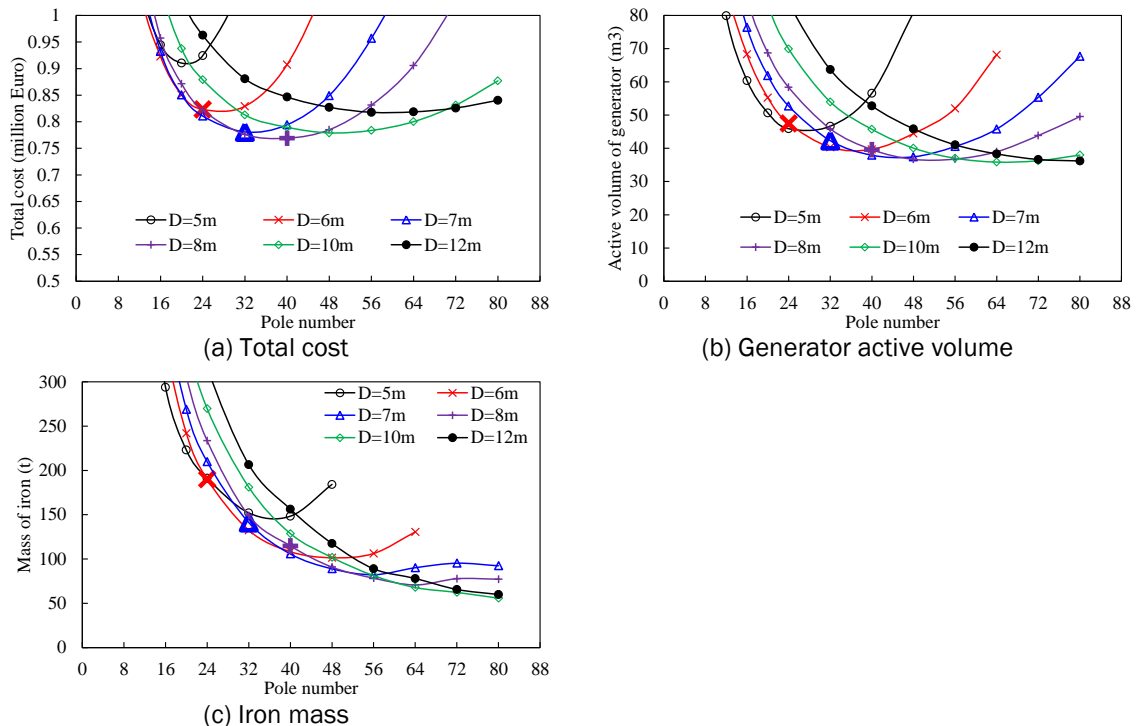


Fig. 30 Variations of active material cost, generator active volume and iron mass with pole number for different stator outer diameters, torque=10.5MNm.

3.1.4 Influence of SC Material Price

Nowadays, the price of SC material is quite high, ~100€/m. It is expected that the price can drop extensively in the further. The influence of SC price on performances is investigated. The price of SC material will only influence the price of total costs, as shown in Fig. 31. For the same stator outer diameter, the optimal pole number tends to increase, as the price of SC material reduces, due to the higher utilization of SC material.

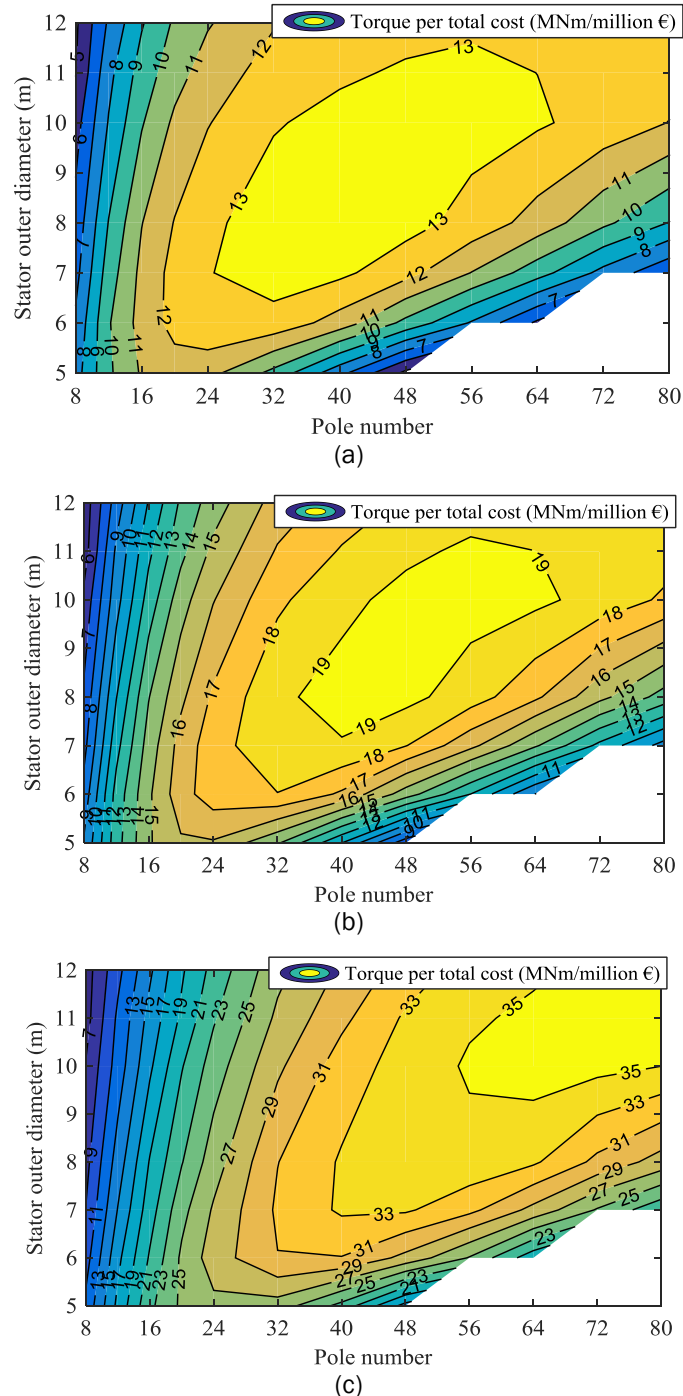


Fig. 31 Torque per active material total costs, (a) SC=100€/m, (b) SC=60€/m, (c) SC=20€/m.

3.2 Influence of SC Area per Pole on Performances

In this section, the influence of SC coil area per pole on performances is investigated. The investigation is based on the determined design in last section, with $D=7\text{m}$ and $2p=32$. For each area, the generator will be re-optimized. The optimization process is the same as that in section 3.1.1.

A. No-load Flux density

The distributions of flux density for SC generators with different pole width are shown in Fig. 32. The flux density in the pole is $\sim 1.4\text{T}$, when $S_{sc}/\text{pole}=40\text{mm}^2$. It is $\sim 2\text{T}$, when $S_{sc}/\text{pole}=120\sim 400\text{mm}^2$. The waveforms and spectrums of flux density in the airgap are shown in Fig. 33.

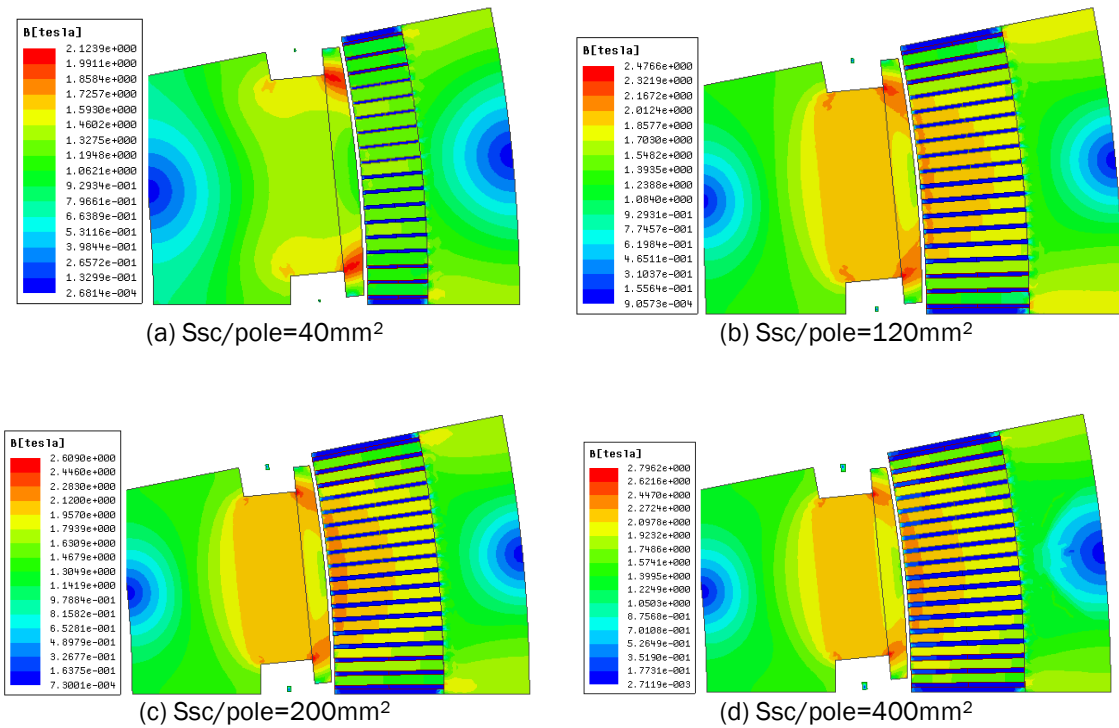


Fig. 32 Cross sections of optimized generators

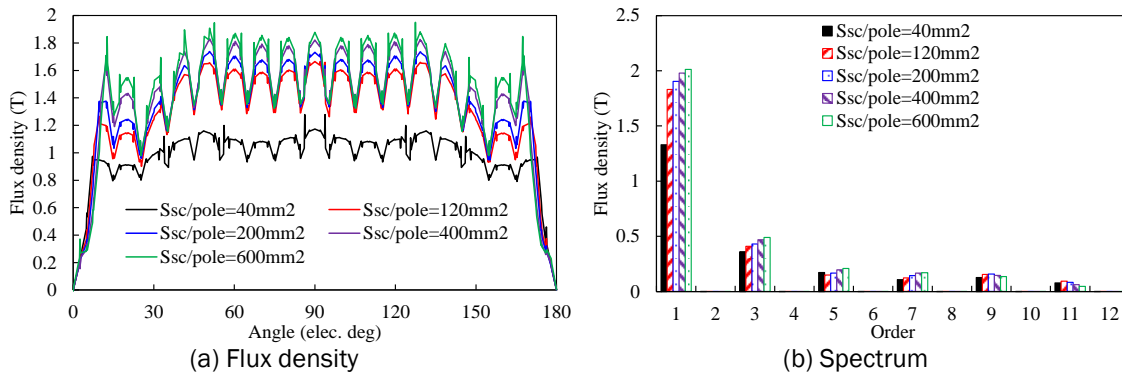


Fig. 33 Waveforms and spectrums of flux density in the airgap.

B. Torque

The variation of torque with S_{sc}/pole is shown in Fig. 34. The torque increases with the area. However, the increases tends to be saturated after some point.

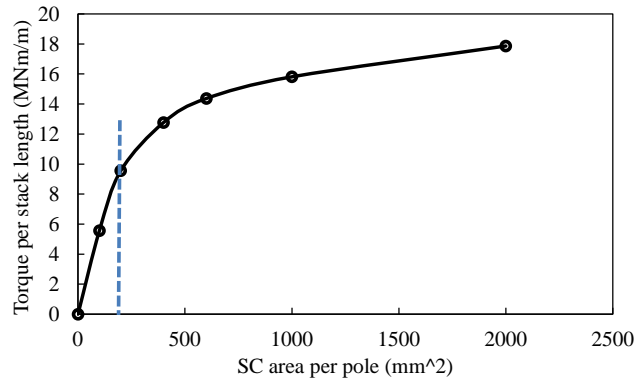


Fig. 34 Variations of generator dimensions with SC area per pole, $T=10.5\text{MNm}$.

C. SC Length

The variations of SC wire length with S_{sc}/pole are shown in Fig. 35. The length increases with area.

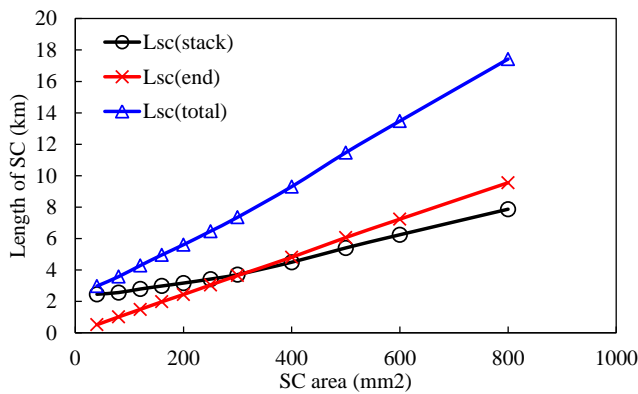


Fig. 35 Variations of SC wire length with SC area per pole, $T=10.5\text{MNm}$.

D. Weight

The variations iron and copper masses with S_{sc}/pole are shown in Fig. 36. The iron mass decrease as the SC coil area reduces.

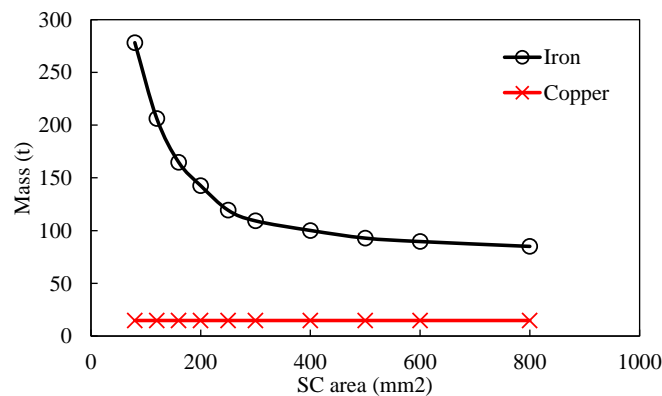


Fig. 36 Variations of iron and copper masses with SC area per pole, $T=10.5\text{MNm}$.

E. Cost

The variations costs with S_{sc}/pole are shown in Fig. 37. As the area increase, iron cost reduces, while the SC material cost increases. Overall, the total cost increases.

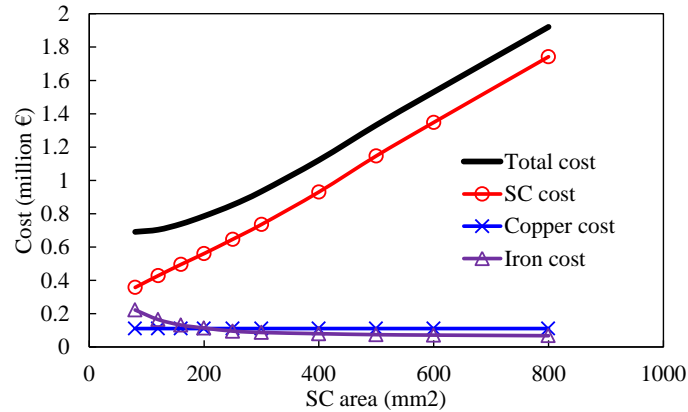


Fig. 37 Variations of iron and copper masses with SC area per pole, $T=10.5\text{MNm}$.

F. Determination of SC Area

The variations cost, iron mass and active volume with S_{sc}/pole are shown in Fig. 38. Three S_{sc}/pole are suggested, from the view of tradeoff between cost, iron mass and stack length. Finally, $S_{sc}/\text{pole}=200\text{mm}^2$ is determined.

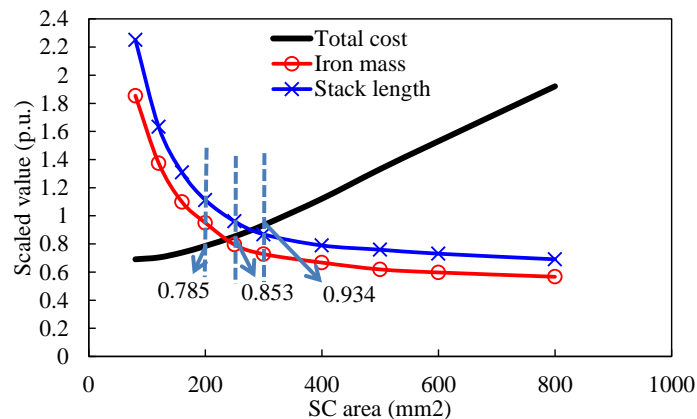


Fig. 38 Variations of cost, iron mass and active volume with SC coil area per pole, torque= 10.5MNm , base values: cost=1 million €, mass=150t, Length=1m

3.3 Influence of Pole Width on Performances

In this section, the influence of pole width on performances is investigated. The investigation is based on the determined design in last section, with $D=7\text{m}$ and $2p=32$. For each pole width, the generator will be re-optimized. The optimization process is the same as that in section 3.1.1.

A. No-load Flux density

The distributions of flux density for SC generators with different pole width are shown in Fig. 39. The flux densities in the rotor pole for different pole width are close, $\sim 2.0\text{-}2.2\text{T}$. Consequently, the design with a larger pole width tends to have more major flux, as shown in Fig. 40.

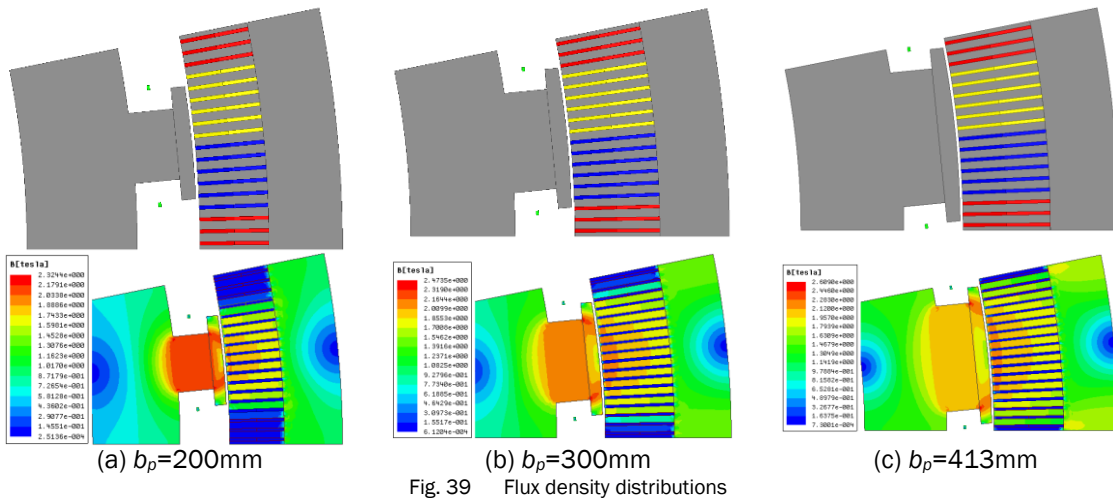


Fig. 39 Flux density distributions

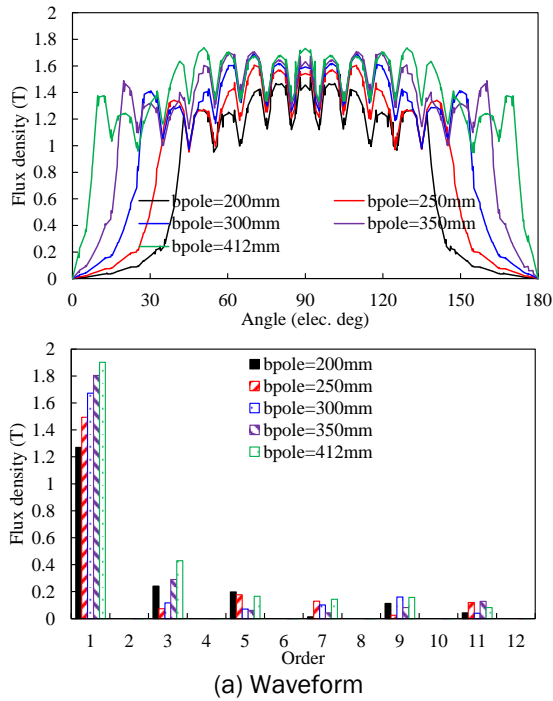


Fig. 40 Waveforms and spectrums of flux density in the airgap.

B. Torque

Because the fundamental flux density increases with pole width, as shown in Fig. 40, the torque capability increases with pole width, Fig. 41.a. Thus, the stack length can be reduced to achieve 10.5 MNm torque, as shown in Fig. 41.b.

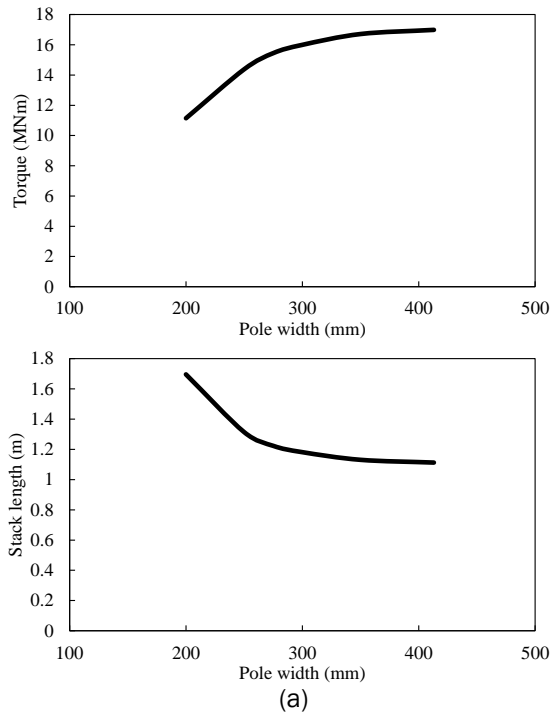


Fig. 41 A) Variation of torque with pole width, $L=1.8\text{m}$. b) Variation of stack length with pole width, $T=10.5\text{MNm}$

C. SC Length

The variation of SC length with pole width is shown in Fig. 42. The length of SC wire straight part decreases as b_p increases, due to reduction of stack length, Fig. 41. However, the SC wire end length will increase with b_p . Consequently, there exists an optimal b_p to achieve the shortest SC wire total length, as shown in Fig. 42.

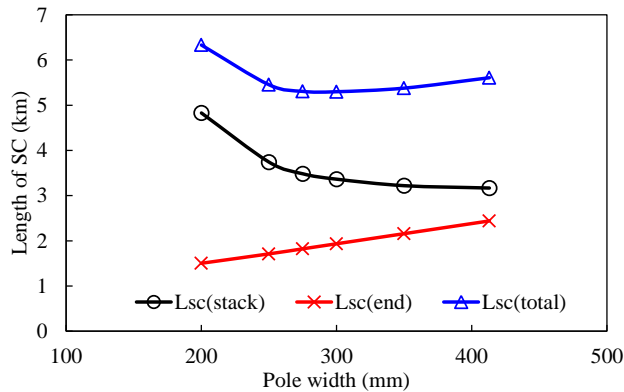


Fig. 42 Variations of SC length with pole width, $T=10.5\text{MNm}$.

D. Costs

The variations of costs are shown in Fig. 43. The SC cost accounts for most of the total cost. Consequently, the trend of the total cost variation is similar to that of SC cost, and there is an optimal pole width to achieve the minimum total cost. Copper cost is constant, because the total copper quantity is fixed.

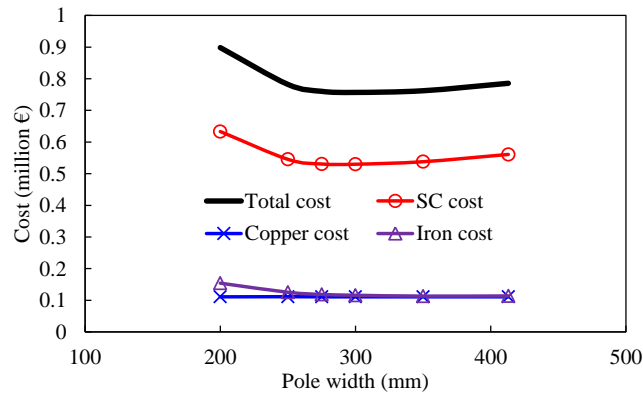


Fig. 43 Variations of cost with pole width, T=10.5MNm.

E. Determination of Pole Width

The proper pole width should be determined from the view of trade-off between cost, weight and generator length, etc., as shown in Fig. 44.

Finally, $b_p=300\text{mm}$ is chosen.

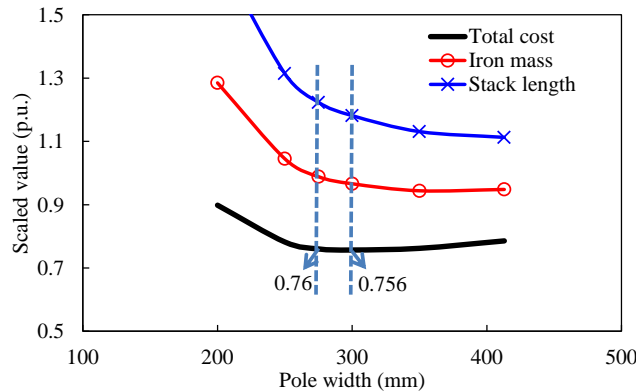


Fig. 44 Variations of total cost, iron mass and stack length with pole width, T=10.5MNm, base values: cost=1 million €, mass=150t, Length=1m.

4 ANALYSIS OF ELECTROMAGNETIC PERFORMANCES

4.1 Final Design

The specifications of finally designed SC generator are listed in Table 10. The flux lines and distribution of flux density are shown in Fig. 45. The flux density in the air gap, no load phase voltage, rated torque and cogging torque are shown in Fig. 46-Fig. 49

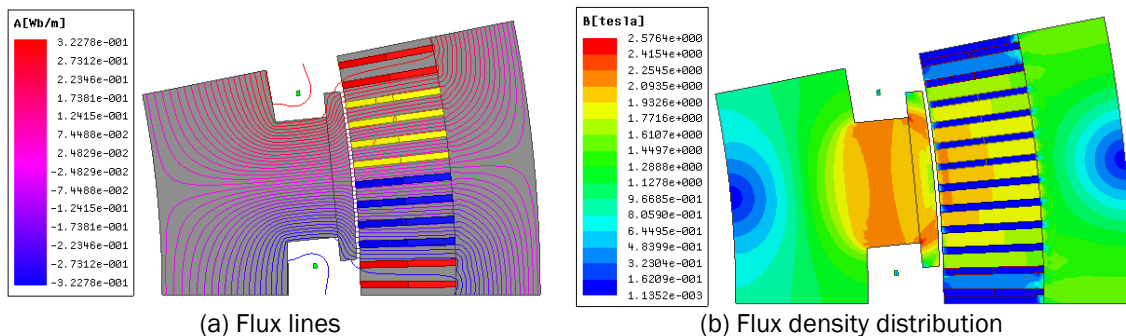


Fig. 45 Flux lines and flux density distribution under no load operation.

Table 10. Parameters of 10MW SC generator with iron-core stator and rotor topology

Stator outer diameter D	7m
Stack length L	1.2m

Speed n	9.6rpm
Torque T_{em}	10.5MNm
Line voltage U_{ab} (no load)	3,130Vrms
Stator phase current I_a	2200Arms
Stator current density J_s	3.5A/mm ²
Stator phase resistance R_s	0.0313Ω
Copper loss P_{Cu} (DC loss)	454Kw
Stator slot packing factor	0.6
Number of poles $2p$	32
Number of stator slots Q	384
Air gap length g	9mm
SC current density J_{sc}	340A/mm ²
SC area per pole	200mm ²
Length of SC wire	5.348km
Dimensions of cross section of SC coil	12.65mm×7.9mm
Stator yoke thickness h_{yl}	210mm
Stator slot dimension	16mm×238.7mm
Ampere turns of SC per pole	34,000AT
Max. B_{\perp} in SC	1.348T
Torque ripple (peak to peak)	2.8%
Type of stator core	Iron-core
Type of rotor core	Iron-core
Cost of SC (million €)	0.534
Cost of Cu (million €)	0.117
Cost of iron (million €)	0.112
Cost of total (million €)	0.764

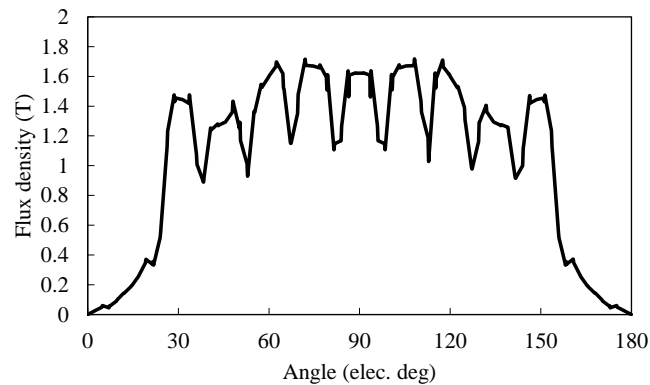


Fig. 46 Flux density in the air gap.

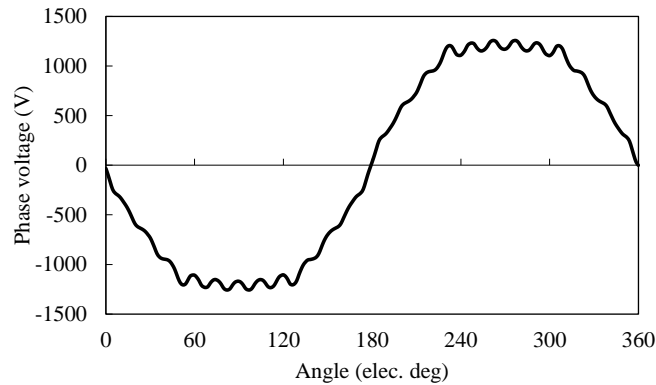


Fig. 47 No load phase voltage.

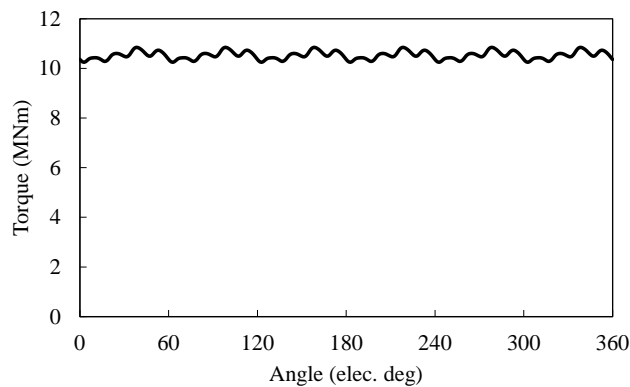


Fig. 48 Rated torque.

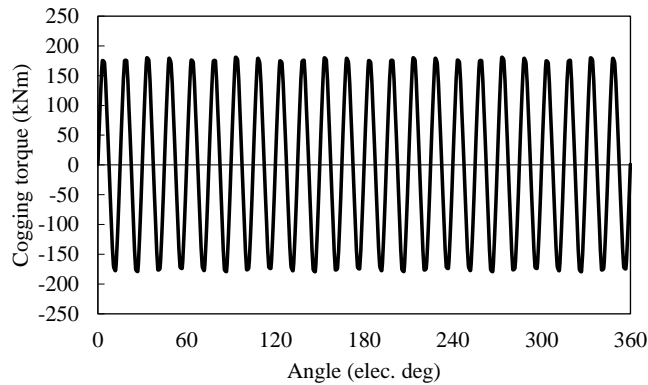
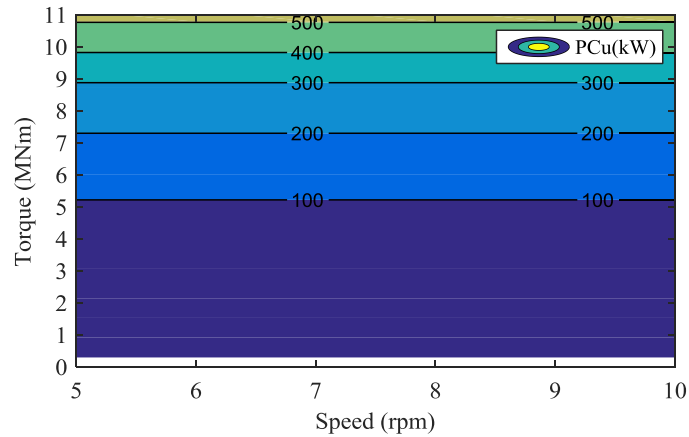


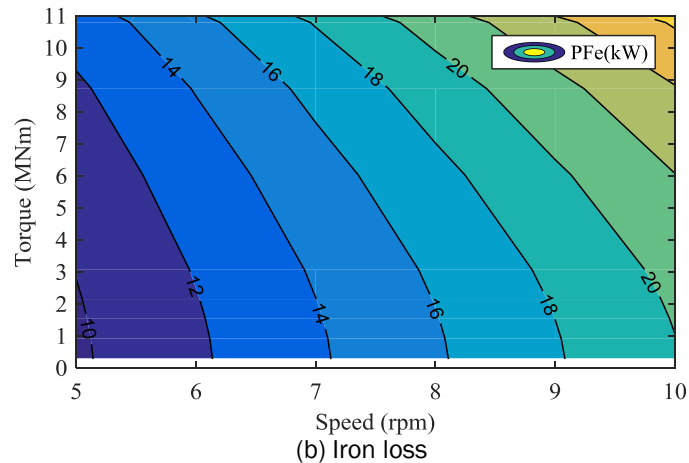
Fig. 49 Cogging torque.

4.2 Losses and Efficiencies

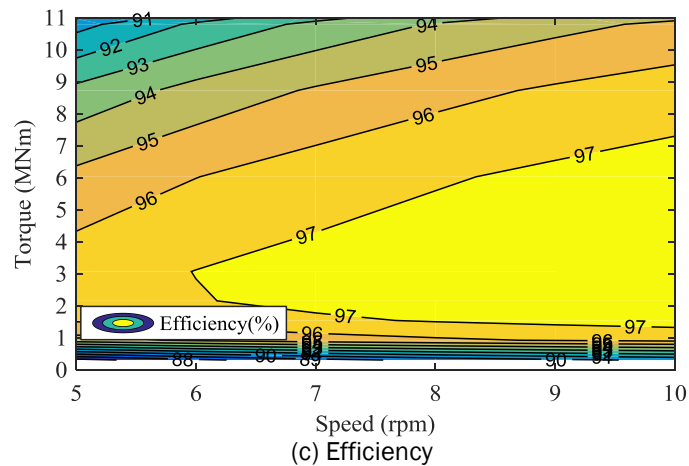
Based on the final design in section 4.1, the losses and efficiencies for different speed and torque are calculated, as shown in Fig. 50. The steel grad is 50JN600, whose specifications are shown in Appendix II. FE analysis software MAXWELL is utilized for the iron loss calculation. The copper loss, iron loss and cryocooler power (14.9kW) are calculated. It is found that the copper loss is much larger than iron loss, due to the low speed of direct-drive generator. The process of calculating cryocooler power will be presented in section 5.2.d.



(a) Copper loss, with end-winding considered, $R_a=0.0313 \Omega$ (@130°C)



(b) Iron loss

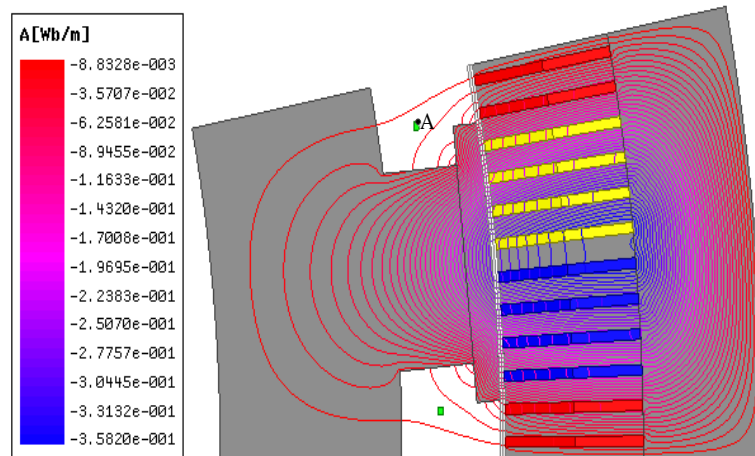


(c) Efficiency

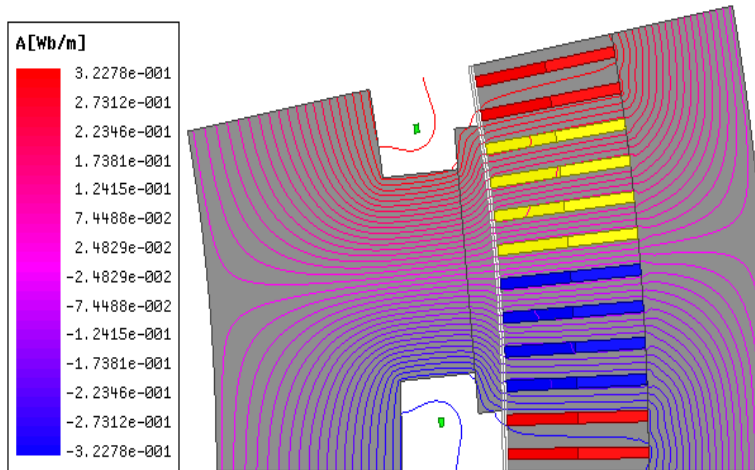
Fig. 50 Losses and efficiencies of SC generator with different speed and electromagnetic torque

4.3 Field Harmonics in SC Coil

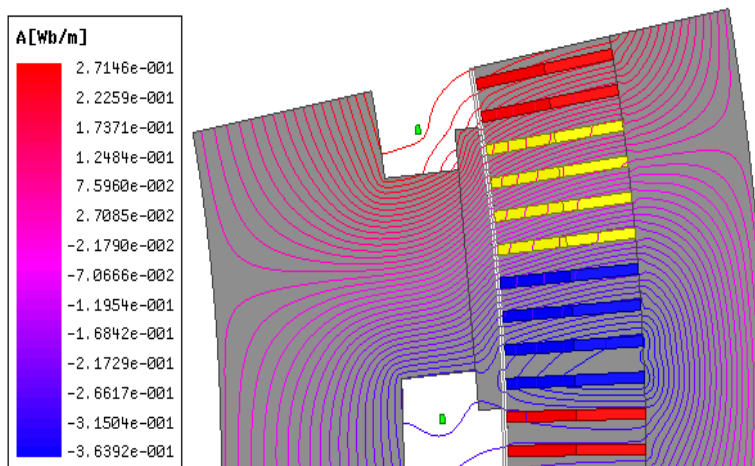
The analysis of field harmonics in SC coil is conducted for generator with different excitation conditions, i.e. with only armature current, with only field current, and with both field and armature current, etc. In this way, it is easier to find the origin of field harmonics in SC coil. The flux lines under the three different excitation conditions are shown in Fig. 51.



(a) $i_q=2200*1.414A$, $i_d=0$, $I_{sc}=0$

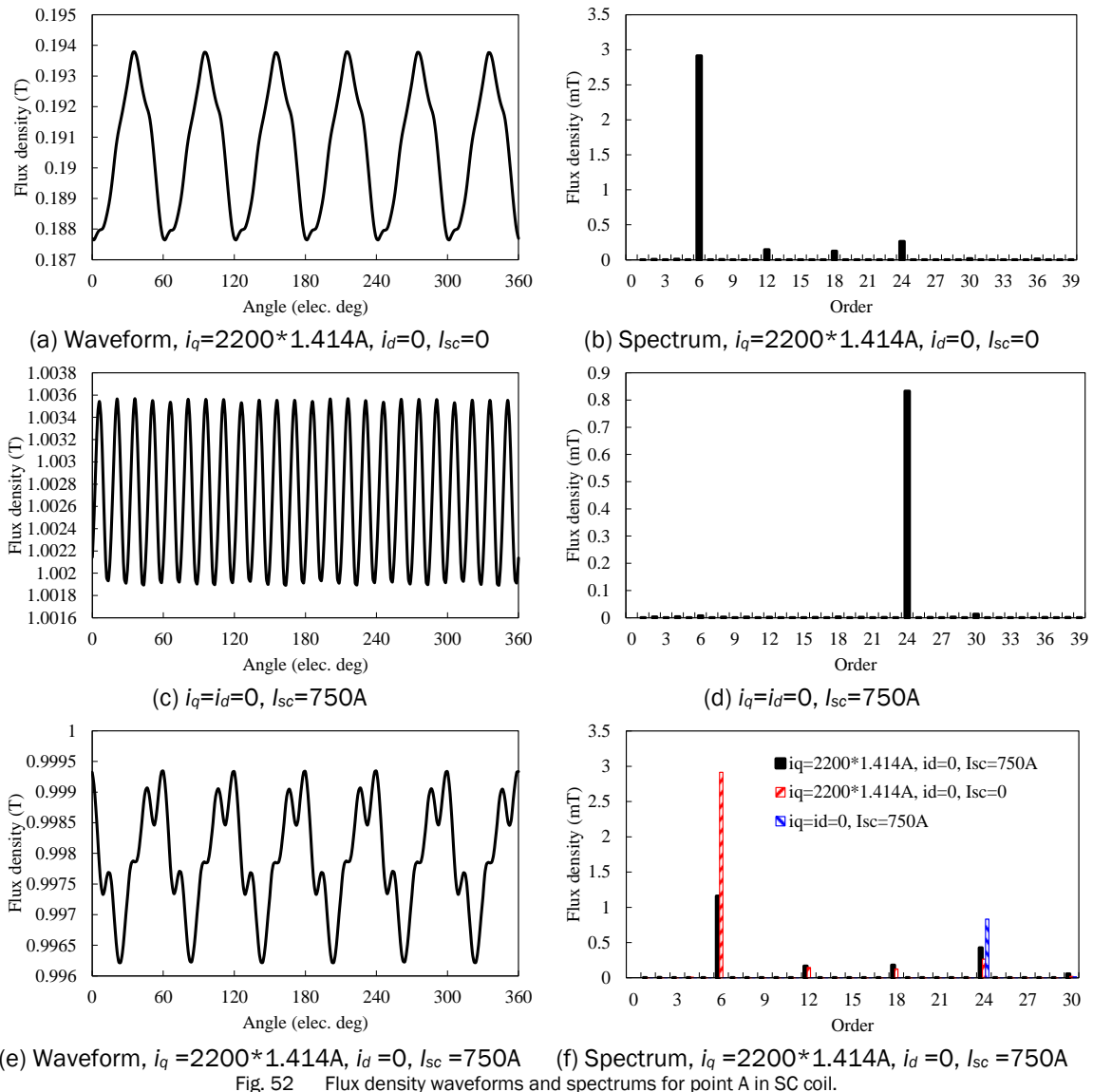


(b) $i_q=i_d=0$, $I_{sc}=750A$



(c) $i_q=2200*1.414A$, $i_d=0$, $I_{sc}=750A$

Fig. 51 Flux lines



The flux density waveforms and corresponding spectrums for point A in SC coil are shown in Fig. 52. When the generator is only excited by armature current, the induced field harmonics are mainly 6th and 24th, as shown in Fig. 52.(a). It is due to the 6th and 24th MMF harmonics of armature winding. When the generator is only excited by field current, there is only 24th field harmonics in SC coil, as shown in Fig. 52.(b), which is due to the slot opening. When the generator is excited by both armature and field current, the major field harmonics in SC coil are 6th and 24th, as shown in Fig. 52.(c). It is found that the 6th harmonic is due to the MMF harmonic of armature winding, and the 24th is mainly due to the slot opening.

4.4 Forces on Rotor Components under Rated Operation

The force analysis is conducted on three components of rotor, i.e. SC, RSC, and rotor iron, etc., as shown in Fig. 53. For each component, the radial and tangential forces are calculated respectively. The results are shown in Fig. 55. The total force on SC is larger than that on RSC, because the flux density on SC is larger than that on RSC, Fig. 54. The forces on SC and RSC are much smaller than those on rotor iron. The major torque of iron-core stator and rotor topology is mainly due to the tangential force on rotor iron. For the rotor iron, the radial force is much larger than tangential force.

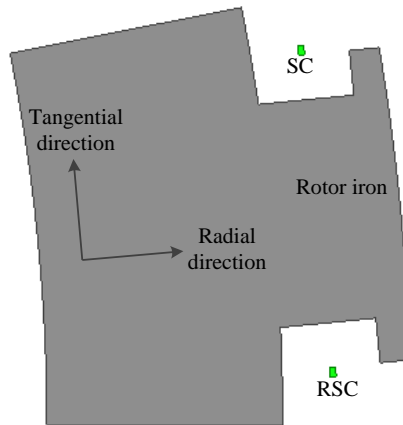


Fig. 53 Cross section of rotor.

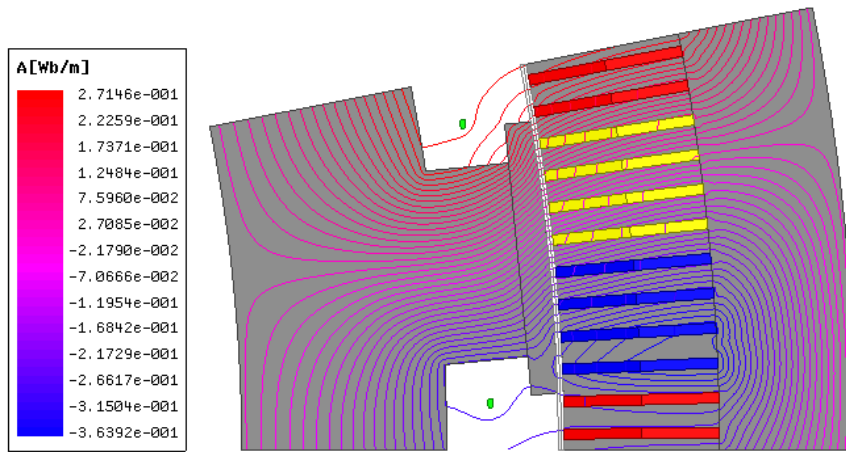
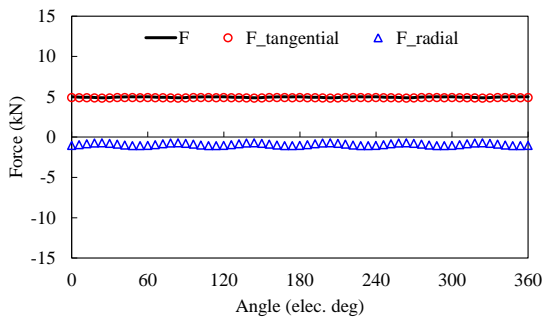
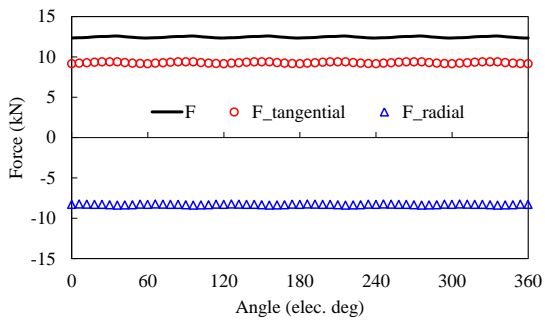
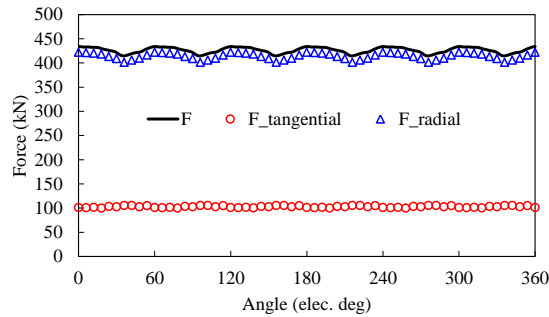


Fig. 54 Flux lines under rated operation



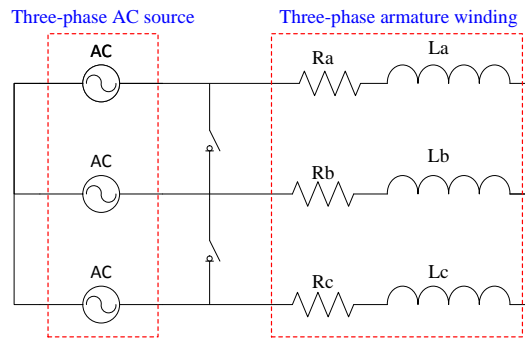
(a) SC

(b) RSC

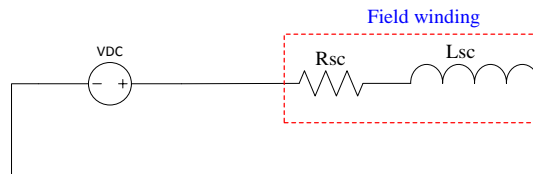


(c) Rotor iron

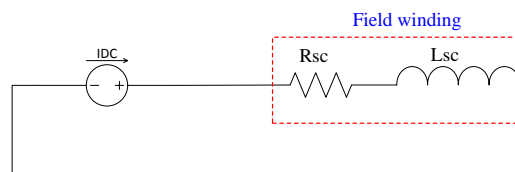
Fig. 55 Forces on rotor components.



(a) Armature winding



(b) Field winding with voltage source



(c) Field winding with current source

Fig. 56 Connections of armature and field windings.

4.5 Performances under 3-Phase Short-Circuit Fault Operation

Among the usually-confronted faults, three-phase short-circuit is the most stressful. In this section, the analysis of performances under fault operation is conducted respectively for two conditions, i.e. the field winding is excited by current and voltage sources.

The generator is modelled by the finite element analysis software MAXWELL. The connections of armature and field winding with a voltage excitation source are shown in Fig. 56.(a) and (b). The modelling of generator with a current excitation source is the same as that with a voltage excitation source, except that the voltage source in Fig. 56.(b) is replaced by a current source, as shown in Fig. 56.(c). Before the short-circuit fault arises, the generator operates at rated status, with rated three-phase currents imposed on the armature winding and switches off. At 0.43s, the switches are turned on to simulate symmetric three-phase short-circuit fault. In the simulation, the rotor speed is assumed to be fixed 9.6rpm in order to simplify the modelling. In real case, it varies with time, which is not only related with the generator, but also with the blade and associated speed-governing

system. The modelling for the whole system is difficult. However, since the inertia of the whole system is quite large for a direct-drive wind turbine and the fault usually endures for quite a short time, it is reasonable to assume that the speed is not changed.

4.5.1 Results with Voltage Excitation Source

The responses of torque, armature and field current, and field flux linkage are shown in Fig. 57- Fig. 59. After some fluctuations, these electromagnetic quantities tend to be steady. The steady short-circuit electromagnetic torque is close to zero, because when three-phase short-circuit fault arises, the torque-produced power is only consumed inside the machine on the copper loss, which is quite a small value, compared with the rated power. The steady short-circuit stator current is increased, but mainly for demagnetization of field winding, which can be seen from the dq -axis components in Fig. 58 (b). The d -axis is aligned with the rotor flux direction. During the period of short-circuit fault, the field winding flux is always constant, as shown in Fig. 59, which can be explained from (5).

$$\frac{d\psi}{dt} + R \cdot i = u \quad (5)$$

where ψ , R , i and u are the rotor flux linkage, resistance, current and voltage respectively. For SC winding, $R \cdot i$ can be removed. Consequently, ψ is constant due to the constant voltage source. In order to keep constant flux linkage, a larger short-circuit steady field current, as shown in Fig. 59, is required to eradicate the increased stator d -axis current. For the electromagnetic and mechanical design of a generator, more attention should be paid to the peak fault quantities, which are produced in the period of fluctuation. In this simulation, the peak torque, stator phase and field currents are about 5.5, 3.2 and 5.4 times of rated values respectively. It is worth mentioning that the design of SC winding is especially challenging, due to the high short-circuit current, Fig. 59, which can easily quench the SC material.

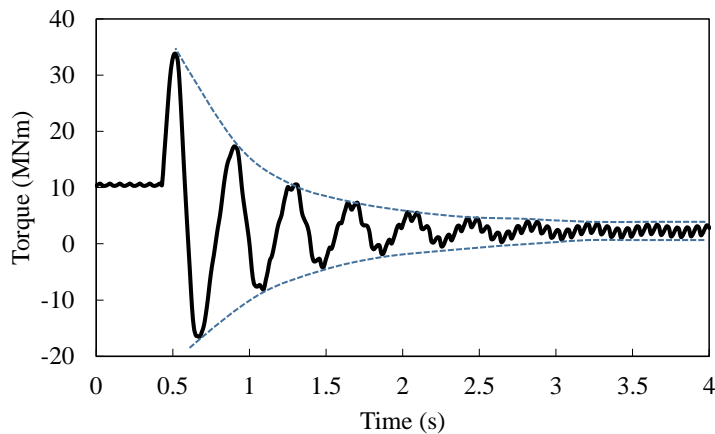


Fig. 57 Variation of torque with time.

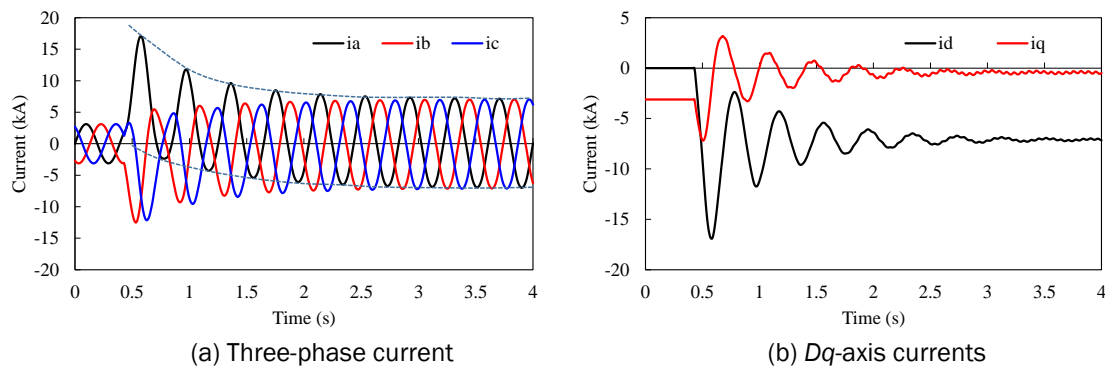


Fig. 58 Variations of armature currents.

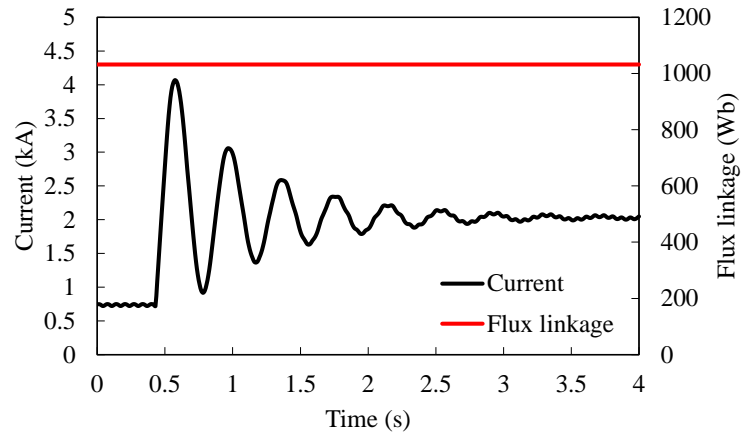


Fig. 59 Variation of field current and flux linkage with time.

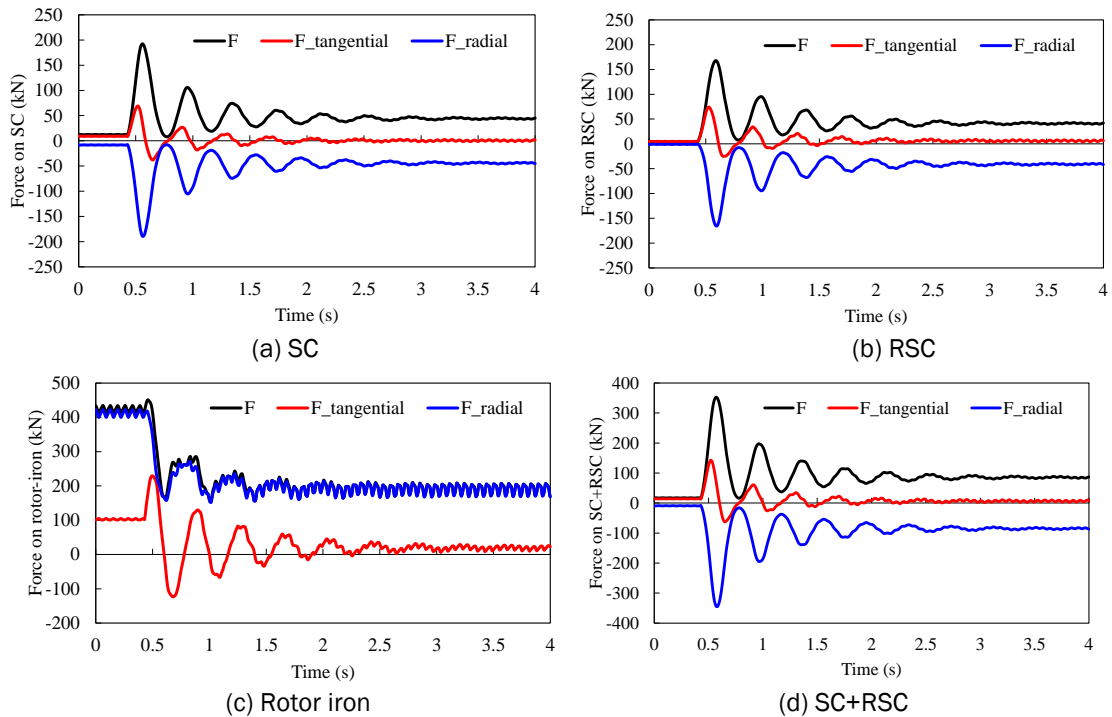


Fig. 60 Forces on rotor components.

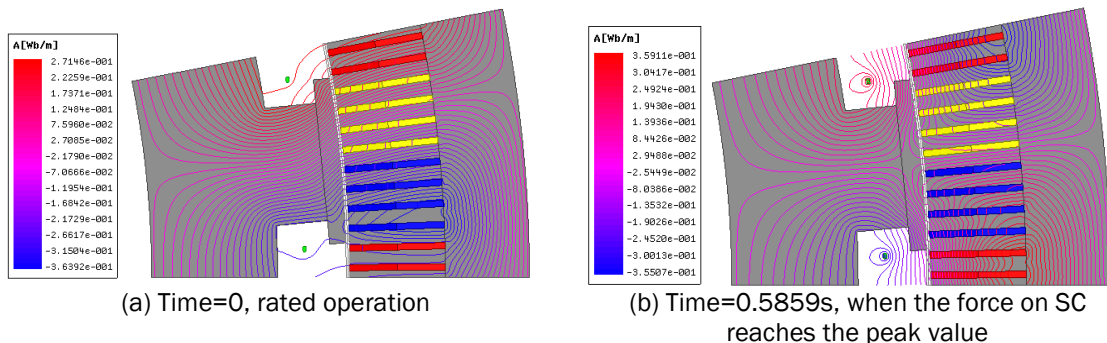


Fig. 61 Flux lines at different time.

The forces on three rotor components, i.e. SC, RSC and rotor iron, etc., are shown in Fig. 60. When the generator is under rated operation, most of the force is on the rotor iron instead of SC coils. Consequently, the SC coils are quite safe from the view of mechanical performance, and the

design for SC coil supporters are not challenging. However, after short-circuit fault arises, the forces on SC coils increase quite a lot, with the peak fault forces on SC and RSC 15 and 33 times of rated values respectively. The significant increase is due to the increase of both flux density and current in SC coils, as shown in Fig. 59 and Fig. 61. The force on rotor iron increases little, because the rotor iron is already quite saturated under rated operation, and the flux through it cannot increase a lot under fault conditions.

4.5.2 Results with Current Excitation Source

The responses of torque, stator current and field current and flux linkage, and forces on rotor components of the generator with a current excitation source are shown in Fig. 62-Fig. 65. The trends of these quantity variations are similar to those with a voltage excitation source. However, the peak fault torque, stator and field currents, and force on SC coils are much smaller. The increase of stator current is the most significant, but just 1.5 times of rated value, and the increase of other quantities can be ignored, which means that the performances of a generator with a current excitation source are much better than that with a voltage excitation source. Thus, if some current-limiting strategies are imposed on the field winding, the performances of generator under fault operations can be improved quite a lot, and the design of SC generator can be less stressful.

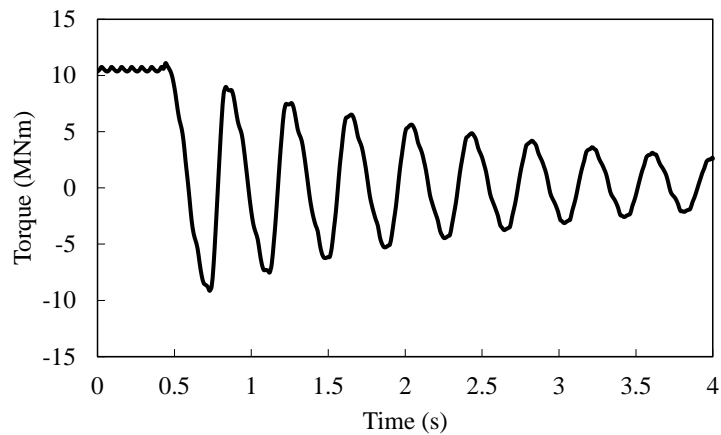


Fig. 62 Variation of torque with time.

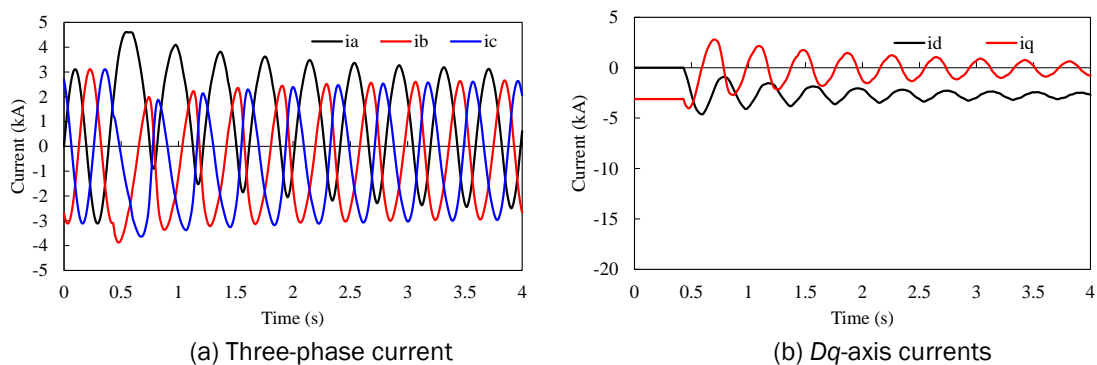


Fig. 63 Variations of armature currents.

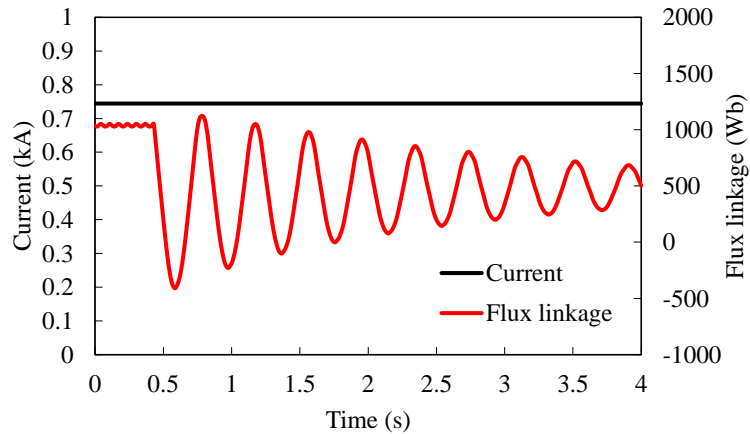


Fig. 64 Variation of field current and flux linkage with time.

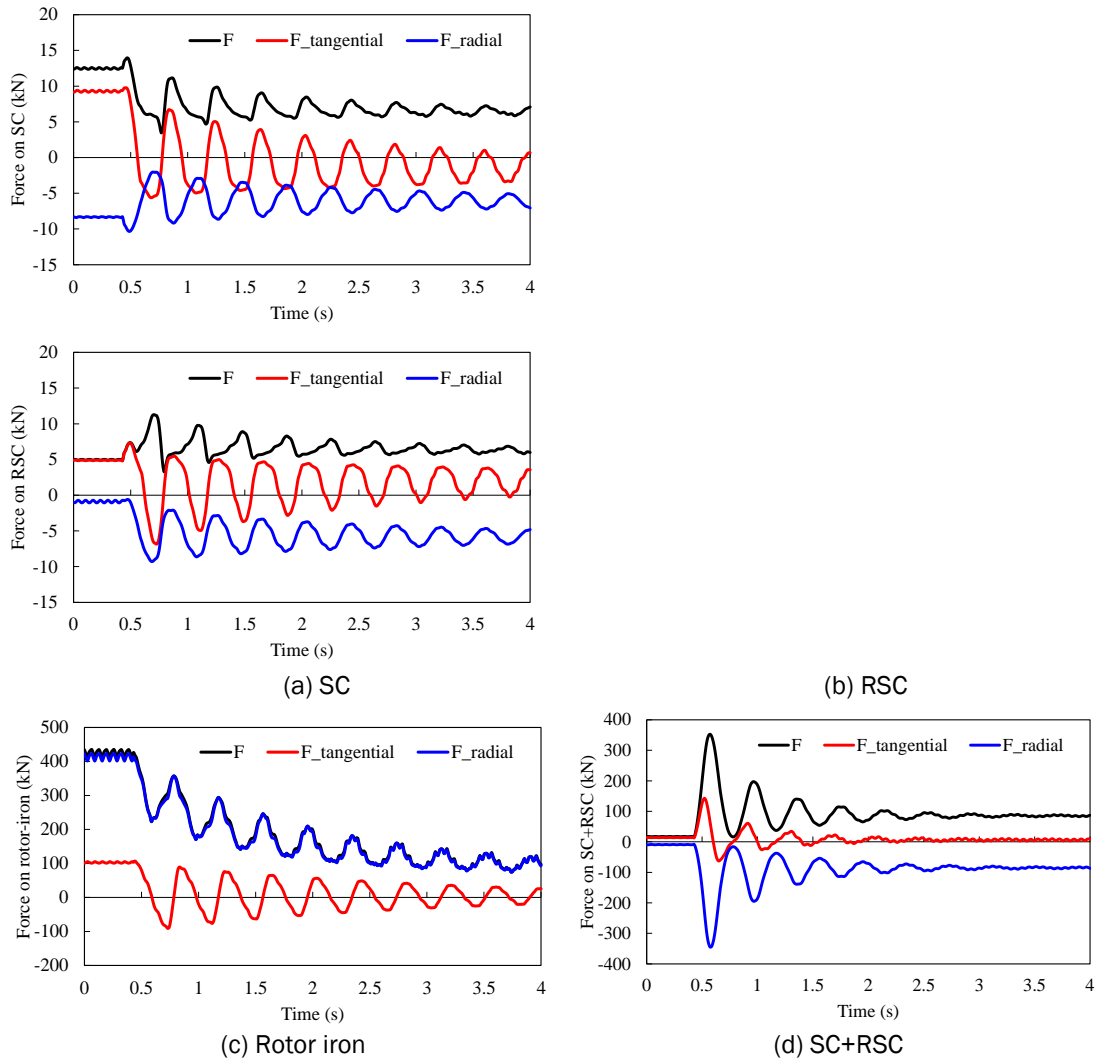


Fig. 65 Forces on rotor components.

5 DESIGN OF CRYOGENIC SYSTEM AND HEAT CALCULATION

5.1 Design of Cryogenic System

The cryogenic system design is shown in Fig. 66, and it is mainly referred to the design in [KAR14]. The outer box thickness is assumed 15mm to satisfy the mechanical requirement. The

inner box thickness is assumed 20mm to accommodate cooling channels. The distance between outer and inner boxes is assumed 25mm to accommodate MLI layers & Vacuum. The materials of outer and inner boxes are stainless steel.

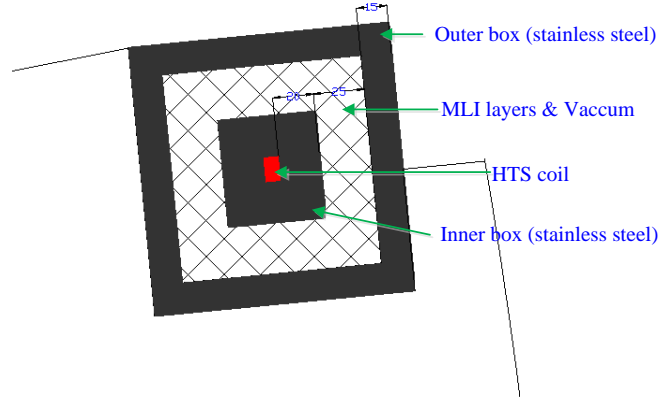


Fig. 66 Cross section of rotor pole cryostat

5.2 Calculation of Heat

A. Radiation Heat

$$q = \frac{\sigma(T_1^4 - T_2^4)}{\frac{1}{\alpha_1} + \frac{1}{\alpha_2} - 1} \quad (6)$$

$$Q = \frac{A}{N_i + 1} \cdot q \quad (7)$$

Equations (6) and (7) allow the radiation heat calculation [ZHU14], where q is heat transfer per m^2 (W/m^2), σ is Stefan-Boltzmann constant which is $5.67 \cdot 10^{-8} (W \cdot m^{-2})$, α_1 and α_2 are thermal emissivity of outer and inner box surfaces respectively, T_1 and T_2 are temperatures of outer and inner box surfaces respectively (K), which are assumed 350K and 40K respectively, Q is the heat transfer (W), A is the area (m^2). N_i is the number of MLI ($N_i = 30$ in [ZHU14], with 30 layers of MLI with a total thickness of 1cm wrapped on the thermal shield). This equation is utilized to calculate the heat transfer between two parallel infinitely-large surfaces.

Table 11. Emissivity of some materials [ZHU14]

	Polished Stainless steel	Polished copper	Polished aluminium
Emissivity α	0.2	0.1	0.05

B. Residual Gas Conduction Heat

$$q = \eta_g P_g (T_1 - T_2) \quad (8)$$

$$Q = A \cdot q \quad (9)$$

[KAR14] where η_g is estimation of residual gas viscosity (W/m^2PaK), P_g is the vacuum pressure level (Pa). η_g and P_g are assumed 0.5 W/m^2PaK and $1e-5$ torr (0.001333Pa) respectively [KAR14].

C. Conduction Heat Leak of Current Leads [KAL11]

Current leads are the connection between the SC coils and the excitation source. The total heat, including Joule heat and conduction heat is

$$Q = \frac{\rho LI^2}{A} + \frac{KA\Delta T}{L} = \left(\sqrt{\frac{\rho LI^2}{A}} - \sqrt{\frac{KA\Delta T}{L}} \right)^2 + 2I\sqrt{\rho K\Delta T} \quad (10)$$

where I is the current in the lead, L is the length of lead, ρ is the average resistivity of the lead material, K is the average thermal conductivity of the lead material, $\Delta T = (T_1 - T_2)$.

To achieve minimum Q , $\left(\sqrt{\frac{\rho LI^2}{A}} - \sqrt{\frac{KA\Delta T}{L}} \right)^2 = 0$, i.e. thermal conduction heat equals to Joule heat. Consequently, the following equations are given as

$$\frac{L}{A} = \frac{1}{I} \sqrt{\frac{k}{\rho}} \Delta T \quad (11)$$

which gives the optimal ratio of lead length to area in terms of the minimum heat. Consequently,

$$Q = I \sqrt{\rho k \Delta T} \quad (12)$$

For the design in this report, $I=750A$, average ρ is $0.04 \cdot 10^{-6} \Omega/m$ (the material of leads is brass), $K=100W/m/K$. Usually, there are two leads in total. Consequently, $Q=107.3W$.

D. Power of Cryocoolers

A typical cryogenic system is shown in in Fig. 67. The efficiency of an ideal process in Fig. 67 (called Carnot efficiency) is

$$\eta_{Carnot} = \frac{T_C}{T_A - T_C} \quad (13)$$

Then, Carnot power is

$$P_{Carnot} = Q_c \left(\frac{T_A}{T_C} - 1 \right) \quad (14)$$

A real cryogenic system typically runs at a fraction (less than 10% and up to 30%) of Carnot efficiency due to losses in compressors and heat exchanger effectiveness, etc. Assuming that the cryocoolers used for the design in this report run 20% of Carnot efficiency, the power of cryocoolers are $186.2 \cdot 1.5 \cdot (350/30-1)/20\% = 14.896kW$ (coefficient 1.5 stands for 50% safety margin).

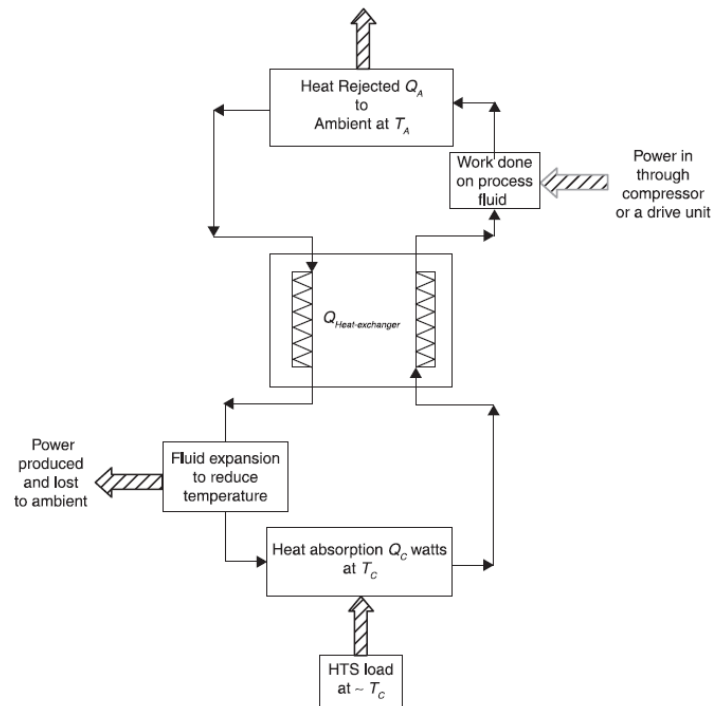


Fig. 67 A typical cryogenic system [MEL12].

E. Results

Table 12. Heats in SC coils

Heat source	Value
Radiation heat (W)	73.78@30K
Residual gas(W)	5.16@30K
Current leads(W)	107.3@30K
Total (W)	186.2@30K

6 SCALING UP TO 20MW

The specifications of 20MW SC generator are listed in Appendix III, which are summarized in Table 13. The torque of 20MW generator is almost three times of that of 10MW. The scaling-up will be carried out by two strategies:

- Strategy I: Increasing of S_{SC} , based on the design in Chapter 2, section 3, with $D=7m$ and $2p=32$.
- Strategy II: Optimization of D , $2p$ and S_{SC} , in order to obtain an optimal compromise between cost, generator volume and weight.

Table 13. Specifications of 10MW and 20MW SC generators

	10MW	20MW
Speed (rpm)	9.6	6.8
Electromagnetic torque (MNm)	10.5	30

6.1 Strategy I

The design of 10MW SC generator has been finished in Chapter 2, section 3. The stator outer diameter ($D=7m$) and pole number ($2p=32$) are kept the same in this section. The generators with different $S_{SC}/pole$ are optimized. The optimization process is the same as that in Chapter 2, section 3.1.1. The cross sections of optimized generators are shown in Fig. 68. The variation of torque per stack length with $S_{SC}/pole$ is shown in Fig. 69. The torque increases with $S_{SC}/pole$, however, the increase will become saturated after some point. The stack lengths to achieve 30 MNm torque are shown in Fig. 70. It decreases as $S_{SC}/pole$ increases, due to the increase of torque per stack length.

Finally, $1000mm^2$ is determined.

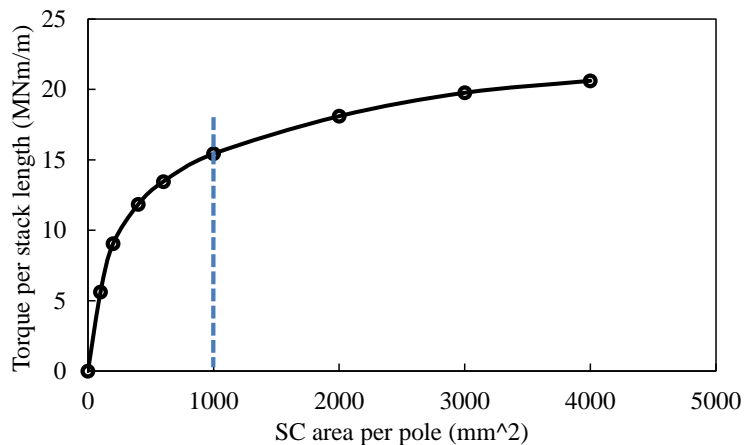
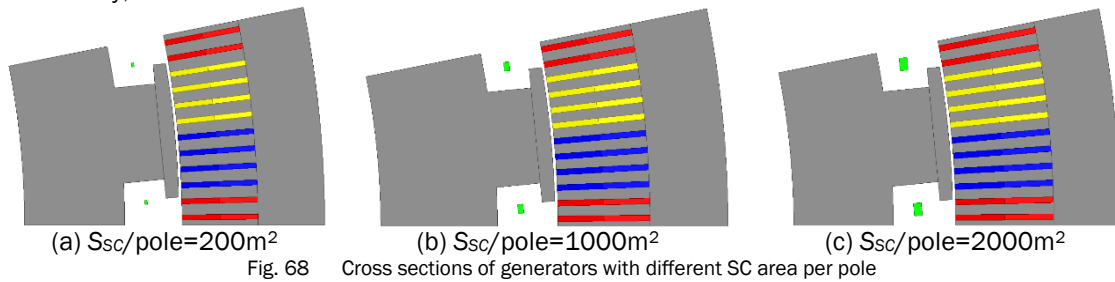


Fig. 69 Variation of torque with SC area per pole.

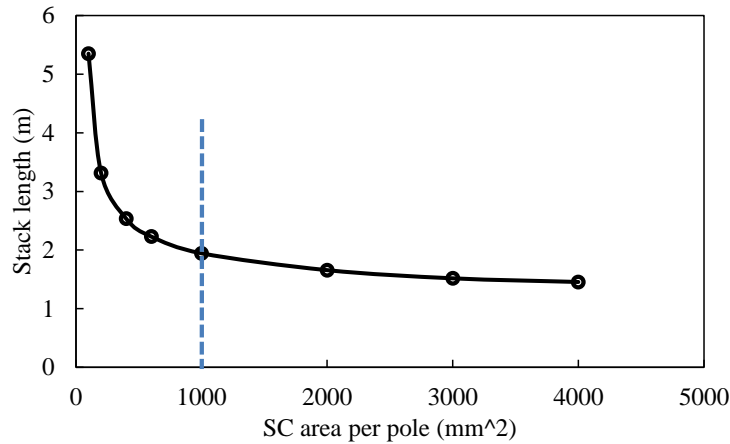


Fig. 70 Variation of stack length with SC area per pole, T=30 MNm.

6.2 Strategy II

In this section, the 20MW SC generator is designed by optimizing stator outer diameter, pole number and SC area per pole. The process is the same as that in Chapter 2, section 3.1. The torque per stack length, torque per generator volume, torque per iron mass, torque per SC length, and costs are shown in Fig. 71-Fig. 77. The trends of these variations are the same as those in Chapter 2, section 3.1.2.

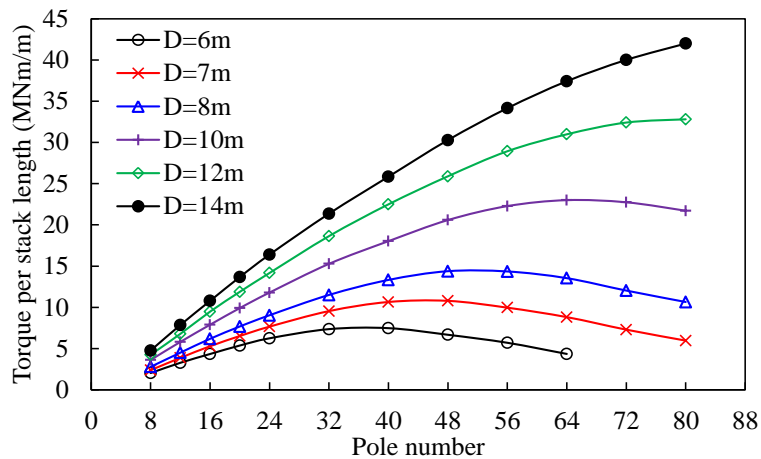


Fig. 71 Variations of torque with pole number for different stator outer diameters, L=1m.

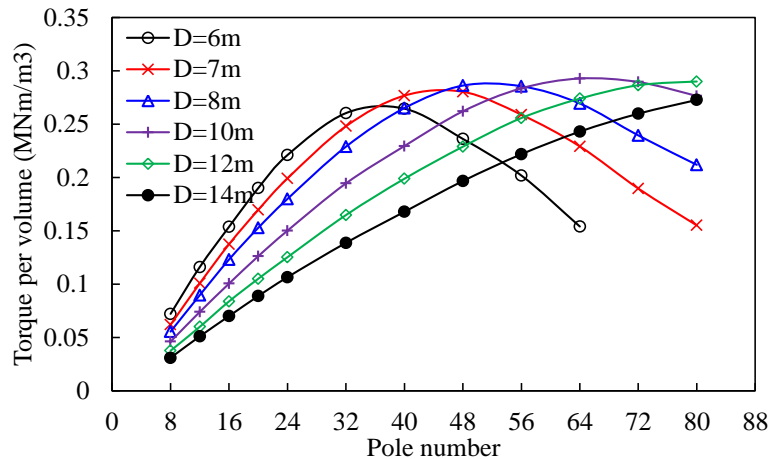


Fig. 72 Variations of torque per generator volume with pole number for different stator outer diameters, without SC end length.

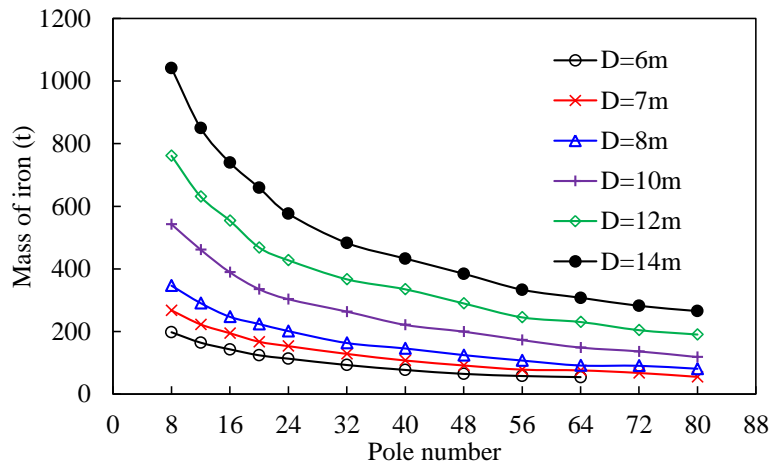


Fig. 73 Variations of iron mass with volume with pole number for different stator outer diameters, L=1m.

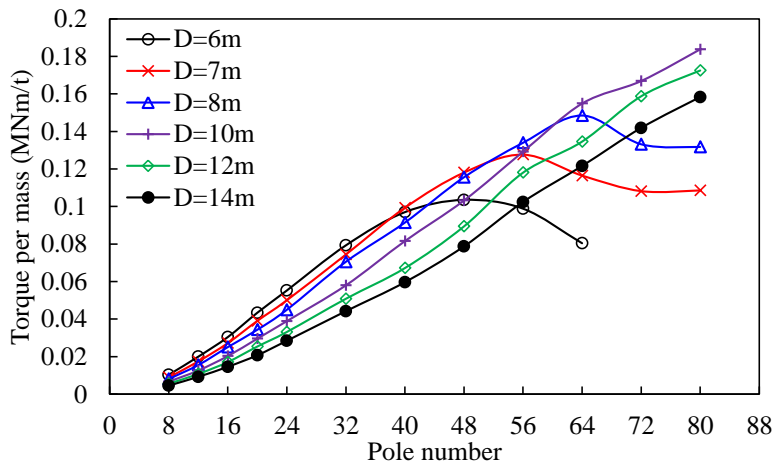


Fig. 74 Variations of T/M_{iron} with volume with pole number for different stator outer diameters, without SC end length.

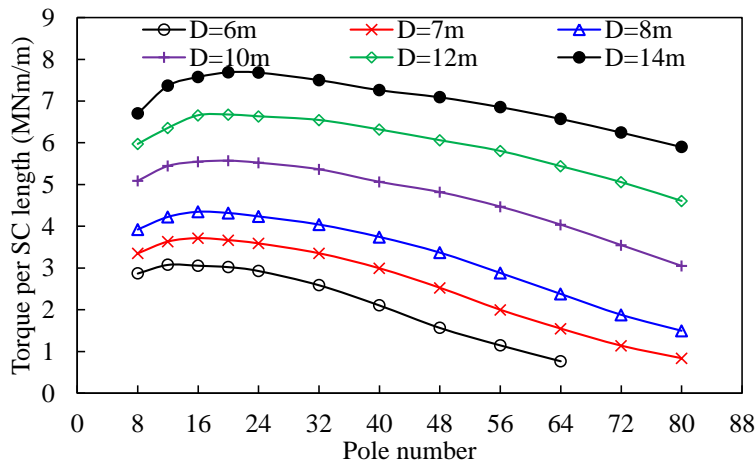


Fig. 75 Variations of torque per SC length with pole number for different stator outer diameters, without SC end length.

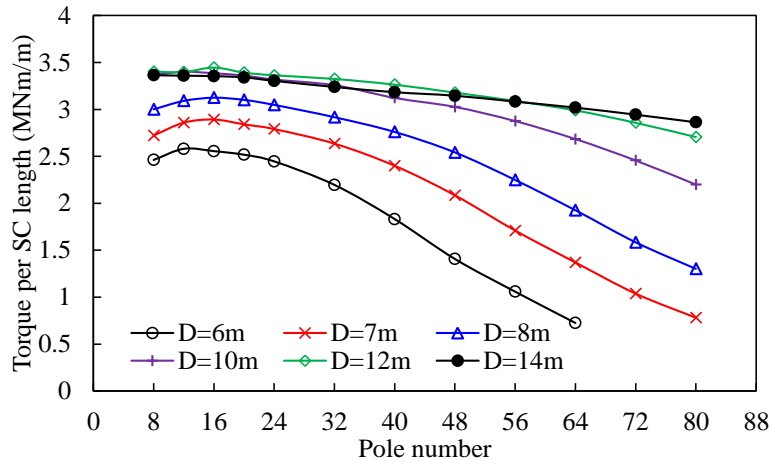


Fig. 76 Variations of torque per SC length (total length) with pole number for different stator outer diameters, $T=30\text{MNm}$.

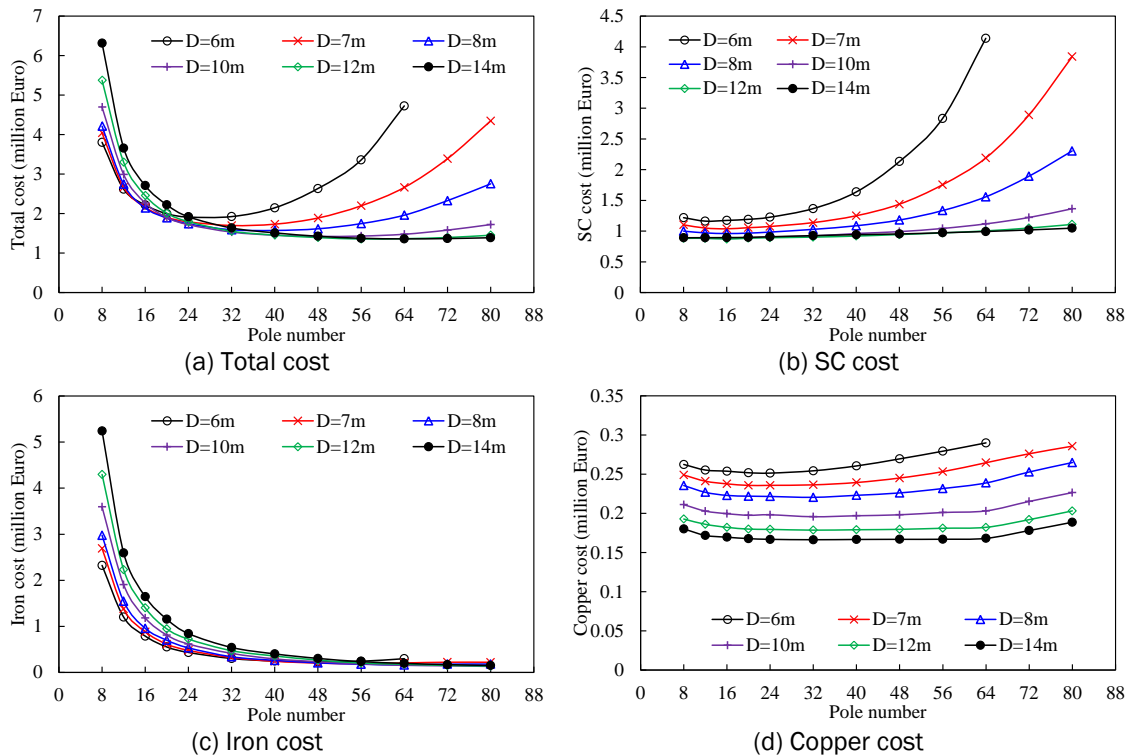


Fig. 77 Variations of costs with pole number for different stator outer diameters, $T=30\text{ MNm}$.

The variations of cost, volume and weight with $2p$ and D are shown in Fig. 78. Some combinations of $2p$ and D are suggested: 1) $D=11\text{m}$ $2p=54$, 2) $D=11\text{m}$ $2p=64$; 3) $D=11\text{m}$, $2p=72$; 4) $D=12\text{m}$, $2p=64$; 5) $D=12\text{m}$, $2p=72$.

Finally, $D=11\text{m}$ $2p=64$ are determined.

The variation of torque with S_{sc}/pole is also checked, as shown in Fig. 79. $S_{sc}/\text{pole}=200\text{mm}^2$ is reasonable, since it is around the saturation point.

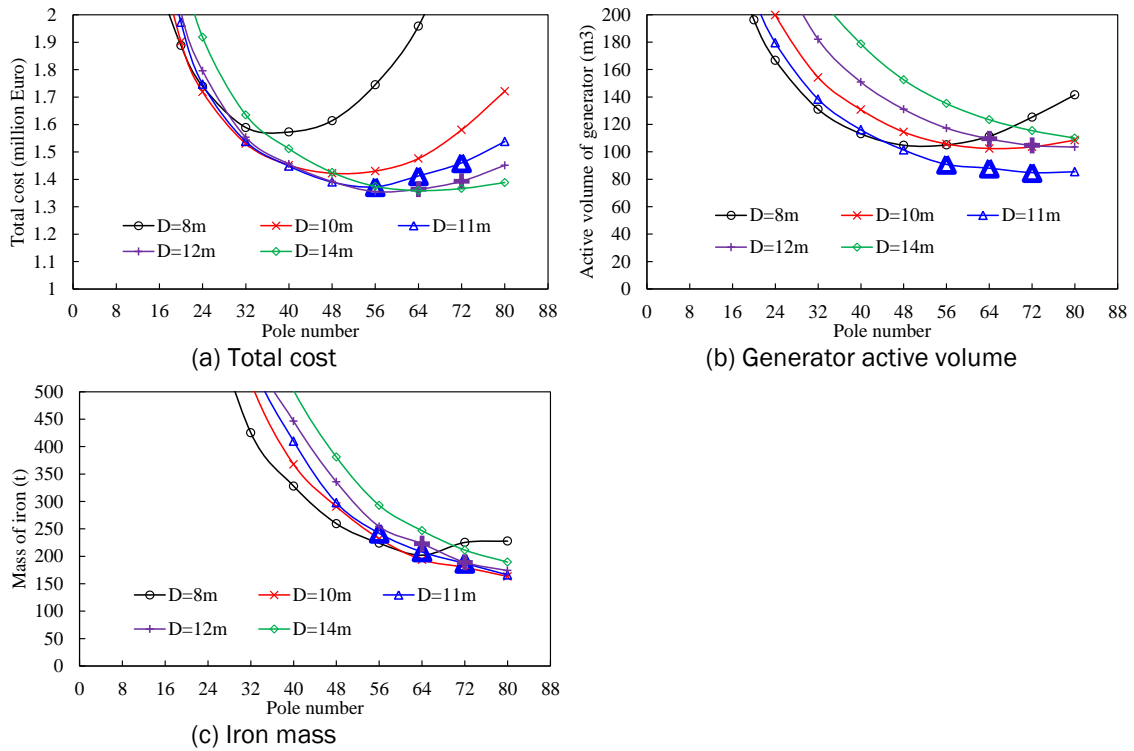


Fig. 78 Variations of active material cost, generator active volume and iron mass with pole number for different stator outer diameters, torque=30MNm.

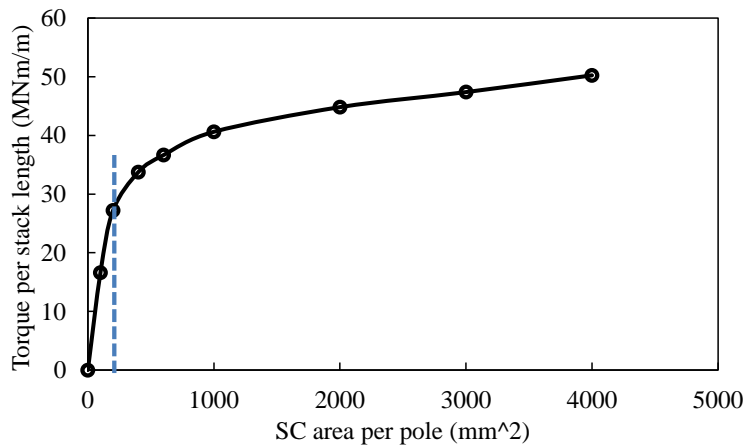


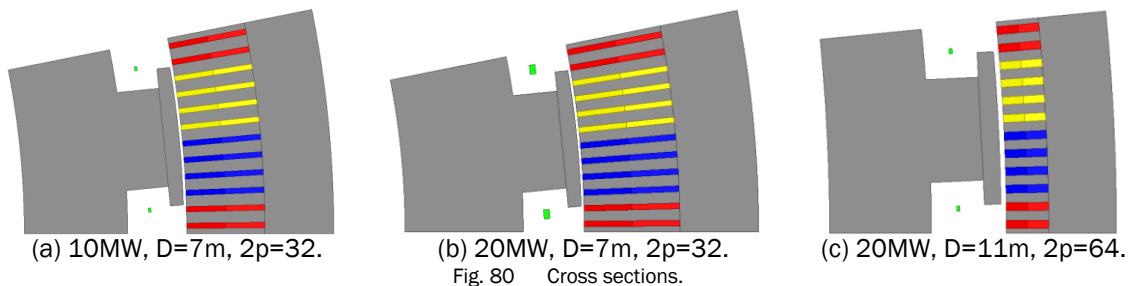
Fig. 79 Variation of torque with SC area per pole, L=1m.

6.3 Summary

The cross sections and specifications of 10MW and 20MW SC generators are shown in Fig. 80 and Table 14. 20MW-I has the advantage of smaller stator outer diameter. But the cost is almost three times of that of 20MW-II, due to the large quantity of SC wire. Since the stator outer diameter, pole number and $S_{sc}/pole$ are all optimized for 20MW-II, the cost of 20MW-II is much lower.

Table 14. Specifications of 10MW and 20MW SC generators

	10MW	20MW-I	20MW-II
Stator outer diameter D (m)	7	7	11
Stack length L (m)	1.2	1.95	1.16
Speed n (rpm)	9.6	6.8	6.8
Torque T_{em} (MNm)	10.5	30	30
Stator current density J_s (A/mm ²)	3.5	3.5	3.5
Stator slot packing factor	0.6	0.6	0.6
Number of poles 2p	32	32	64
Number of stator slots Q	384	384	768
Air gap length g (mm)	9	9	13
SC current density J_{sc} (A/mm ²)	340	273	340
SC area per pole (mm ²)	200	1000	200
Length of SC wire (km)	5.35	39.2	10.54
Ampere turns of SC per pole (AT)	34,000	136,500	34,000
Type of stator core	Iron-core	Iron-core	Iron-core
Type of rotor core	Iron-core	Iron-core	Iron-core
Volume of generator (m ³)	42.3	68.7	100.5
Mass of Iron (t)	141	271.9	208
Cost of SC (million €)	0.543	3.92	1.054
Cost of Cu (million €)	0.117	0.215	0.192
Cost of iron (million €)	0.112	0.217	0.166
Cost of total (million €)	0.764	4.35	1.412



7 CONCLUSIONS

A. Comparison between different topologies

There are mainly three SC generator topologies for wind turbines, i.e. air-core stator air-core rotor, iron-core stator air-core rotor, and iron-core stator iron-core rotor, etc. By comparing the torque-SC quantity characteristic, the following conclusions can be obtained:

- The torque increases with SC quantity. For iron-core stator and rotor topology, the increase becomes saturated after some point, due to the saturation of iron.
- The characteristics of air-core rotor topologies are much harder, because less iron is utilized.
- The torque capability of iron-core stator and rotor topology are higher than that of air-core rotor topologies, and the advantage is more significant with when S_{sc}/pole is small. Due to the high cost of SC nowadays, the iron-core stator and rotor topology is favourable. As the cost of SC reduces, air-core rotor topologies may be better, since they have great advantage over generator weight.

B. Influence of pole number and stator outer diameter

Based on the iron-core stator and rotor topology, the influences of pole number and stator outer diameter on performances are investigated. In general, it can be concluded that:

- There exists optimal pole numbers $2p$ for SC material utilization, generator volume and mass respectively. The optimal $2p$ is dependent on stator outer diameter.
- The following relationship always exists:
 $2p$ (for SC utilization) $<$ $2p$ (for generator volume) $<$ $2p$ (for generator mass).

C. Performances under rated operation

Through the analysis of performances of SC generator with iron-core stator and rotor topology under rated operation, it can predict:

- The copper loss is much larger than iron loss and cryocooler power. The quite small iron loss is due to the low speed of direct-drive wind turbine.
- If the generator is only excited by armature current, there exist phase belt and tooth field harmonics in SC coil, which are due to corresponding MMF harmonics of armature winding. If the generator is only excited by field current, there is only tooth field harmonics in SC coil, which is due to the slot opening. If the generator is excited by both armature and field current, the major field harmonics in SC coil are phase belt and tooth harmonics. The phase belt harmonic is due to the MMF harmonic of armature winding, and the tooth harmonic is mainly due to the slot opening.
- The forces on SC coil are much smaller than those on rotor iron. The major torque of iron-core stator and rotor topology is mainly due to the tangential force on rotor iron. For the rotor iron, the radial force is much larger than tangential force.

D. Performances under three-phase short-circuit operation

The analysis of performances of SC generator under three-phase short-circuit operation is conducted with voltage and current excitation sources respectively.

D.1. Performances with voltage excitation source

- The peak torque, stator phase and field currents are about 5.5, 3.2 and 5.4 times of rated values respectively. It is worth mentioning that the design of SC winding is especially challenging, due to the high short-circuit current, which can easily quench the SC material.
- After short-circuit fault arises, the forces on SC coils increase quite a lot, with the peak fault force 33 times of rated value. The significant increase is due to the increase of both flux density and current in SC coils. The force on rotor iron increases little, because the rotor iron is already quite saturated under rated operation, and the flux through it cannot increase a lot under fault conditions.

D.2. Performances with current excitation source

- The responses of torque, stator current and field current and flux linkage, and forces on rotor components of the generator with a current excitation source are similar to those with a voltage excitation source. However, the peak fault torque, stator and field currents, and force on SC coils are much smaller. The increase of stator current is the most significant, but just 1.5 times of rated value, and the increase of other quantities can be ignored, which means that the performances of a generator with a current excitation source are much better than that with a voltage excitation source. Thus, if some current-limiting strategies are imposed on the field winding, the performances of generator under fault operations can be improved quite a lot, and the design of SC generator can be less stressful.

CHAPTER 3: CONVERTER DESIGN

8 INTRODUCTION

Wind energy is considered as one of the most promising renewable sources. It is expected that direct drive wind turbine generators with large power ratings will reduce the cost of wind farms, especially for offshore wind farms. Therefore, Electrically Excited Synchronous Generators (EESG) with 10 MW rating power and above are of great interest.

The scheme of the Wind Energy Conversion System (WECS) is shown in Fig. 81. A WECS is composed mainly by 3 parts:

- Electrically Excited Synchronous Generators (EESG)
- Armature power converter
- Field converter

A WECS is usually connected to the grid through a transformer.

In this chapter a 10 MW armature converter is designed and then scaled up to 20 MW. The armature converter controls the delivered power from the generator to the grid adjusting the voltage and frequency. The design of 10 MW and 20 MW armature converters focuses on the calculation of the number of IGBTs and diodes necessary to build up the converter, the generator output filter, cost of armature power converter and an energy analysis.

The field converter supplies the necessary current to feed the generator field. Different field converter topologies and its control are discussed.

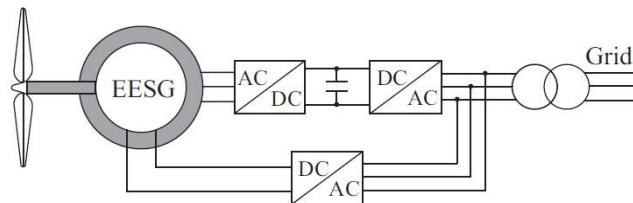


Fig. 81 Scheme of an EESG [CHE14]

9 10 MW DESIGN

9.1 Introduction

The design of a 10 MW armature converter for a superconducting EESG involves the study of the following points:

- Determination of the number of levels of the converter.
- Study of the necessary semiconductors (IGBTs and diodes).
- Generator output filter design.
- Determination of the efficiency of the drive train (EESG and converter).
- Drive train cost analysis.

For the design of the field converter it is necessary to determine study:

- Topology of the system.
- Study of the necessary semiconductors.

The current document follows the structure showed above focusing on the details for each of the aforementioned bullets points.

The design of the armature converter begins deciding the necessary number of levels for it. Therefore, the advantages and disadvantages of converters with 2 and 3-levels are discussed in detail.

The second step is to determine the semiconductors, rated current and rated voltage, and the necessary amount of them to build up the armature converter. In this step, 23 different IGBTs and 3 different diodes are considered.

In order to guarantee a low torque ripple and harmonics, an output generator filter is necessary. Its design is discussed after the selection of the semiconductors.

The fourth step is to determine the efficiency of the designed system and carry out a cost analysis to choose the best option.

Regarding the design of the field converter, its design is carried out by discussing the best topology for it and the necessary amount of semiconductors.

9.2 Armature converter

The design of the armature converter for a 10 MW superconducting generator in wind turbine conditions is developed in the current section. The main specifications for the design of the power converter are its AC line-to-line voltage (V_{ll}), which corresponds with the line-to-line voltage of the superconducting generator, and power (P_n).

The peak current that the power converter has to endure is another necessary specification for the design of the power converter. Its value is directly derived from the AC line-to-line voltage and power:

$$I_p = \frac{\sqrt{2} \cdot P_n}{\sqrt{3} \cdot V_{ll}} \quad (15)$$

The AC line-to-line voltage and power are imposed parameters from the generator design. Their values are 3.3 kV for the AC line-to-line voltage and 10 MW for the power. Hence, from (15) the peak current (I_p) is calculated and it takes the value of 2.47 kA. The main specifications for the design of the armature power converter are summarised in Table 15

Two armature converter topologies are studied. Fig. 82 and Fig. 83 show the studied Back-To-Back (BTB) Voltage Source Converters (VSCs) configurations for wind turbine systems.

Fig. 82 shows a two-level VSCs converter which is the most used in wind power industry for low voltage. The basic two level VSC is composed of six switches and the voltage applied on each switch is equal to the DC-link voltage (V_{dc}).

Fig. 83 shows a three-level Neutral Point Clamped (NPC) converter. The basic three-level NPC converter is composed of 12 switches and 6 diodes. The voltage applied on each switch and diode is half of the DC-link voltage.

Regardless of the chosen topology converter, a BTB converter is composed of the generator side converter and grid side converter. The generator is connected to the grid via the BTB power converter and transformer. Normally, the generator side converter is used to keep the DC-link voltage constant whereas the generator converter controls the power supplied by the generator to the grid. In order to reduce the current THD at the generator and grid side, filters are also equipped.

Table 15. Main specifications for the design of an armature converter to feed a 10 MW direct drive superconducting generator for wind applications

Converter capacity P_n (MW)	AC voltage V_{ll} (kV)	Peak current I_p (kA)
10	3.3	2.47

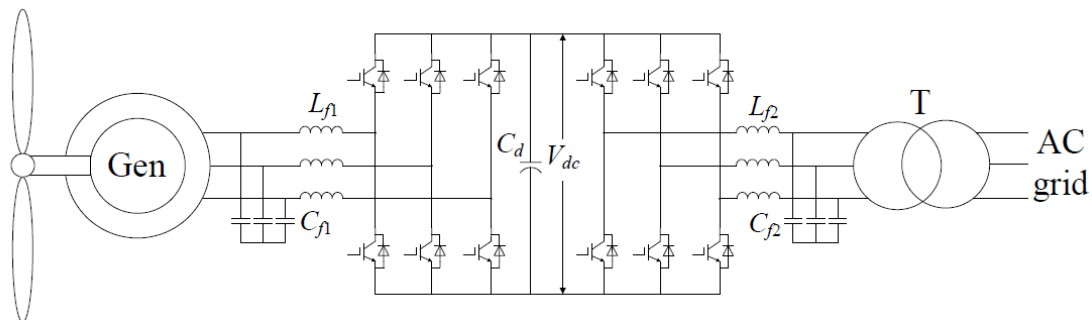


Fig. 82 2-level back to back voltage source converter [INN14]

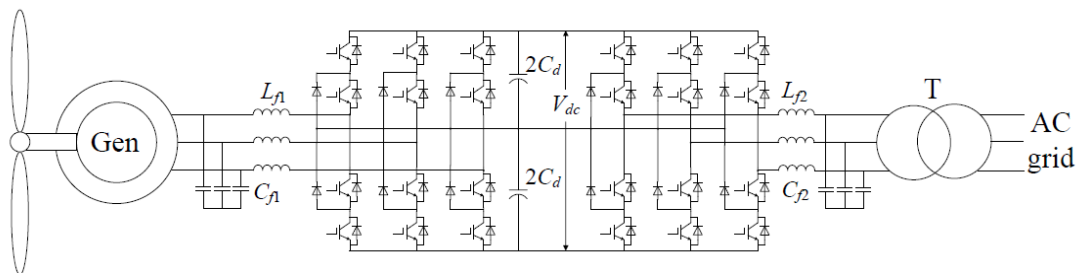


Fig. 83 3-level back to back neutral point clamped voltage source converter [INN14]

The control strategy for both studied converters is vector control with the switching technique of Space Vector PWM (SVPWM). The SVPWM is the most widely used modulation technique since it gives a higher level of fundamental voltage compared with the classical Sinusoidal PWM (SPWM). The comparison between SVPWM and SPWM shows that the SVPWM is the best and the most reliable of both techniques since it enables an efficient use of the DC link, reduces the Total Harmonic Distortion (THD), improves the Power Factor (PF) and reduces the switching losses [BOS06].

9.2.1 Comparison between the 2 and 3-level back to back converter

In 2-level VSCs the voltage waveform is produced by using SVPWM with only two voltage levels. As a consequence, the output voltage is distorted (high values of THD). On the other hand, in 3-level VSCs the output voltage is less distorted (smaller values of THD) thanks to the more steps to create the output voltage [BOS06].

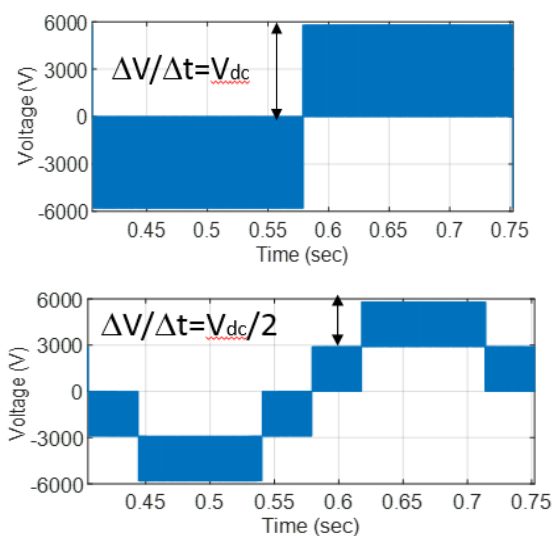
The effect described in the above paragraph can clearly be seen in Fig. 84, where the output for the two level converter looks like a rectangular signal (Fig. 84.left) whereas the voltage for the three level converter resembles more to a sinusoidal wave (Fig. 84.right). Moreover, a three level converter has a lower dv/dt (Fig. 84.rigth) than a two level converter. In particular, a switch in a three level converter has to endure half of the voltage than a switch in a two level converter for the same DC-link voltage.

The direct consequence of a better output voltage is a better output current (Fig. 85 right) for the 3 level converter (smaller current ripple, red line) than for the 2 level converter although the fundamental evolution of the current seems to be the same for a complete period (Fig. 85 left).

The final consequence of the current ripple is a higher ripple at the power (torque) of a generator when it is fed by a two level converter than when it is fed by a three level converter (Fig. 86).

The torque ripple is not only affected by the converter topology. It is also affected by the fed generator, the switching sequence and switching frequency which also affect to the efficiency of the system [BOS06]. The generator is an input for the design of the converter, whereas the switching sequence and frequency are parameters that the designer of the converter has to set. Therefore the switching sequence and switching frequency are further investigated for both two and three level converter topologies.

Regarding the switching sequence, it is worth noticing that there is only one reasonable possibility to synthesize the voltage vector for the two level converter, whereas for the three level converter there are many possibilities. Hence, the unique switching sequence for the two level converter is studied and four different switching sequences are taken into account for the three level converter.



(a) (b)
Fig. 84 a) 2-level VSC output voltage and b) 3-level VSC output voltage

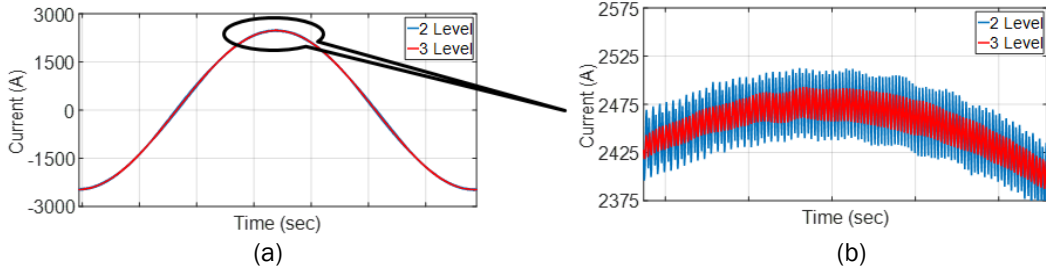


Fig. 85 Output current for a (a) 2 and 3-level converter and (b) zoom at the currents

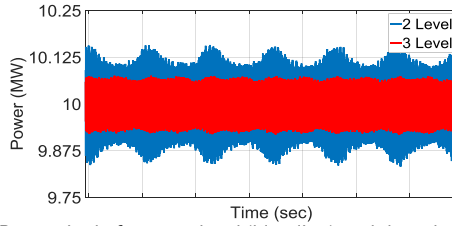


Fig. 86 Power ripple for a two level (blue line) and three level (red line) VSC

The studied switching sequences and their diagrams are shown in Table 17 and in Table 16 for the two level and three level converter respectively.

Table 16. Switching sequences for a three level BTB converter

Topology	Sector	Region	Sequence	Diagram
3 level - v1	Odd	1L	0-1-1;00-1;000;100	
		1H	00-1;000;100;110	
		2L	0-1-1;00-1;10-1;100	
		2H	110;100;10-1;00-1	
		3	0-1-1;1-1-1;10-1;100	
	Even	4	00-1;10-1;11-1;110	
		1L	-10-1;00-1;000;010	
		1H	00-1;000;010;110	
		2L	-10-1;00-1;01-1;010	
		2H	110;010;01-1;00-1	
3 level - v2	Odd	1	0-1-1;00-1;000;100;110	
		2	0-1-1;00-1;10-1;100;110	
		3	0-1-1;1-1-1;10-1;100	
		4	00-1;10-1;11-1;110	
	Even	1	-10-1;00-1;000;010;110	
		2	-10-1;00-1;01-1;010;110	
		3	00-1;01-1;11-1;110	
		4	-10-1;11-1;01-1;010	
3 level - v3	Odd	1	-1-1-1;0-1-1;00-1;000;100;110;111	
		2	0-1-1;00-1;10-1;100;110	
		3	0-1-1;1-1-1;10-1;100	
		4	00-1;10-1;11-1;110	
	Even	1	-1-1-1;00-1;-10-1;000;110;010;111	
		2	00-1;-10-1;01-1;110;010	
		3	00-1;11-1;01-1;110	

		4	-10-1;01-1;-11-1;010	
3 level - v4	Odd	1	-1-1-1;0-1-1;00-1;000;100;110;111	
		2	0-1-1;00-1;10-1;100;110	
		3	0-1-1;1-1-1;10-1;100	
		4	00-1;10-1;11-1;110	
	Even	1	-11-1;-10-1;00-1;000;010;110;111	
		2	-10-1;00-1;01-1;010;110	
		3	00-1;01-1;11-1;110	
		4	-10-1;-11-1;01-1;010	

Table 17. Switching sequence for a two level BTB converter

Topology	Sector	Sequence	Diagram
2 level	Odd	000; 100; 110; 110	
	Even	000; 010; 110; 111	

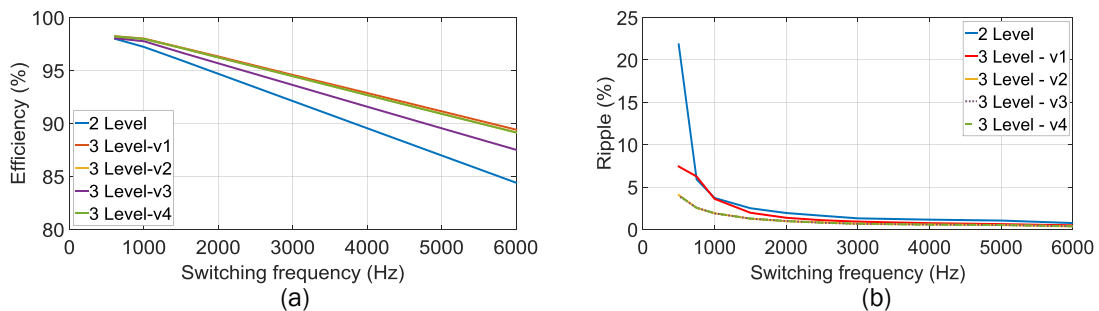


Fig. 87 (a) Efficiency and (b) torque ripple vs. switching frequency for different converter topologies (two and three level) and different switching sequences.

Several simulations for each switching sequence and converter topology are carried out for different values of switching frequencies (from 600 Hz to 6000 Hz). These simulations show the evolution of the efficiency and torque ripple versus the studied switching sequences and switching frequency. Fig. 87 shows the efficiency (left) and torque ripple (right) evolution versus the switching frequency for a two and three level converter topology for the switching sequences described in Table 17 and Table 16.

The analysis of the carried out simulations show that the evolution of the efficiency is mainly linear for high switching frequencies (above 1 kHz) regardless the chosen topology (Fig. 87, left). The reason is that switching losses are predominant over conduction losses for high switching frequencies.

The use of different converter levels shows that 3-level converters have a better performance than 2-level converters for the same switching frequency regardless of the chosen switching sequence for the 3-level converter (Fig. 87, left). Among the 3-level converter switching sequences, it is concluded that option 'v3' has a poorer performance than the rest of 3-level switching sequences (Fig. 87, left).

Focusing now on the evolution of the torque ripple (Fig. 87, right) it is concluded that the torque ripple for 2-level converter is much higher than for 3-level converters. The conclusion of the analysis of the four different switching sequences for the 3-level converter shows that the torque ripple for option 'v1' is much higher than the rest of the options.

Table 18 shows the values of torque ripple and efficiency for the two converter topologies (2 and 3-level) and the four different switching sequences for the 3-level converter topology for a switching frequency of 600 Hz. The use of 600 Hz as switching frequency is due efficiency reasons,

higher switching frequencies reduce the efficiency, and technical reasons, lower switching frequencies increase the torque ripple and as a consequence the cost of the output current filter. Torque ripple values are unacceptable regardless the converter topology and switching sequence since its minimum value is 3.95% and the specifications limit the torque ripple value up to 1%. As a consequence, the use of current output filters to improve the torque ripple is mandatory. The design of the current output filter is described in 9.2.3.1

The comparison of the torque ripple and efficiency between the 2 and 3-level converter shows that 3-level converters are better in both aspects (better torque ripple and better efficiency) than the 2-level converter. Furthermore, the huge torque ripple for the 2-level converter requires the use of large current output filters which cost is unacceptable. Therefore, the use of 2-level converters is discarded for the design of the armature converter and it will not be considered further in future analysis.

Regarding the 3-level converter, the chosen switching sequence is 'v2'. Switching sequence 'v2' is chosen over the other options since it has a better torque ripple and efficiency than options 'v1' and 'v3' and it performs better than option 'v4' for low power loads.

After the analysis of the 2 and 3-level converter topologies, with different switching sequences, and different switching frequencies it is concluded that the converter that will be designed will be a 3-level converter, operated at a switching frequency of 600 Hz with the switching sequence v2.

Table 18. Torque ripple and efficiency values for 600 Hz switching frequency for a 2 and 3 level BTB converter topology with different switching sequences

Topology	Torque ripple (%)	Efficiency (%)
2 Level	21.83	98.04
3 Level - v1	7.43	98.10
3 Level - v2	4.06	98.16
3 Level - v3	3.95	98.08
3 Level - v4	4.05	98.16

9.2.2 Semiconductors

To determine the number of semiconductors for a power converter it is necessary to know the following parameters:

- Voltage of DC-Link (V_{dc})
- Converter power (P_n)
- Converter topology
- Chosen switch (V_{ce} and I_{ce})

Equations to calculate the number of IGBTs in series and in parallel for a 3-level converter are the following [HIT09]:

$$IGBT_{series} = \text{ceil} \left(\frac{V_{dc}}{V_{ce}} \right) \quad (16)$$

$$IGBT_{parallel} = \text{ceil} \left(\frac{\sqrt{2} \cdot I_{rms}}{0.7 \cdot D \cdot I_{ce}} \right) \quad (17)$$

Where

$$D = \left(1 + \frac{(n-1)(1-\alpha/100)}{1+\alpha/100} \right) / n \cdot 100 \quad \begin{cases} \alpha = \text{voltage unbalance (15\%)} \\ n = \text{number of switches in parallel} \end{cases} \quad (18)$$

The value of the DC-Link depends on the line to line voltage (V_{ll}) according to:

$$V_{DC-Link} = V_{ll} \cdot \sqrt{2} \cdot 1.15 \quad (19)$$

Since the line-to-line voltage has been set as 3.3 kV, the necessary value of the DC-Link is:

$$V_{DC-Link} = 3300 \cdot \sqrt{2} \cdot 1.15 = 5366.9 \approx 5400 \text{ V} \quad (20)$$

The value of I_{rms} is worked out from the value of the rated power (P_n) as:

$$I_{rms} = \frac{P_n}{\sqrt{3} \cdot V_{ll}} = \frac{10 \cdot 10^6}{\sqrt{3} \cdot 3300} = 1749.5 \text{ A} \quad (21)$$

The value of D is calculated as an iterative process. Values of I_{ce} and V_{ce} depend on the chosen IGBT for the design. For the design of the 3-level converter 23 different switches, listed on Table 19, are considered. Three different diodes, listed on Table 20, are also considered for the three level converter design. Equation (16) and (17) are applied for the 23 different IGBTs and 3 diodes. The amount of necessary devices, in series and in parallel, cost per switch and total cost for the semiconductor for a 3-level BTB converter are shown in 0 and Table 22 for the considered IGBTs and diodes, respectively.

Table 19. IGBTs considered for the design of a 3-level BTB converter

V_{ce}	I_{ce}	V_{ce}	I_{ce}	V_{ce}	I_{ce}	V_{ce}	I_{ce}
1.2 kV	0.15 kA	1.7 kV	0.4 kA	3.3 kV	0.4 kA	6.5 kV	0.6 kA
	0.4 kA		0.6 kA		0.8 kA		
	0.6 kA		0.8 kA		1 kA		
	0.8 kA		1.2 kA		1.2 kA		
	1.2 kA		1.6 kA		1.5 kA		
	1.6 kA		1.8 kA				
	1.8 kA		2.4 kA				
	2.4 kA		3.6 kA				
	3.6 kA						

Table 20. Diodes considered for the design of a 3-level BTB converter

V_{ce}	I_{ce}
1.7 kV	0.8 kA
1.7 kV	3.6 kA
3.3 kV	1.2 kA

Table 21. Summary of amount of IGBTs, in series and parallel, cost per IGBT and total cost for a 3-level BTB converter

V_{ce}	I_{ce}	IGBT _{series}	IGBT _{parallel}	Total IGBT	€/IGBT	Cost (€)
1200	150	5	32	3840	85.51	328366.1
1200	400	5	12	1440	117.22	168799.7
1200	600	5	8	960	423.56	406613.8
1200	800	5	6	720	622.82	448429
1200	1200	5	4	480	755.38	362584.3
1200	1600	5	3	360	755.38	271938.2
1200	1800	5	3	360	1148.08	413310.2
1200	2400	5	2	240	978.00	234719.5
1200	3600	5	1	120	1343.19	161182.6
1700	400	4	12	1152	877.95	1011403
1700	600	4	8	768	940.48	722287.1
1700	800	4	6	576	1063.05	612315.6
1700	1200	4	4	384	1190.62	457196.5
1700	1600	4	3	288	1118.07	322003.6
1700	1800	4	3	288	1398.22	402687.9

1700	2400	4	2	192	1510.78	290070.1
1700	3600	4	1	96	1792.06	172037.4
3300	400	2	12	576	986.85	568423.3
3300	800	2	6	288	1181.31	340216.1
3300	1000	2	5	240	1563.07	375137.3
3300	1200	2	4	192	1752.63	336505.3
3300	1500	2	3	144	2102.70	302789.1
6500	600	1	8	192	2668.62	512375.8

Table 22. Summary of amount of diodes, in series and parallel, cost and total cost for a 3-level back to back converter

V_{ce}	I_{ce}	Diode _{series}	Diode _{parallel}	Total Diode	€/Diode	Cost (€)
1700	800	4	6	288	144.84	41715.07
1700	3600	4	1	48	939.77	63152.54
3300	1200	2	4	96	1037.52	139442.7

Among all the possible designs (0) the four cheapest options are preselected for further investigation. The chosen IGBTs, their number in series and parallel, cost per unit and total cost are summarised in Table 23.

Table 23. Preselected switches for a 10 MW 3-level BTB power converter design

V_{ce}	I_{ce}	IGBT _{series}	IGBT _{parallel}	Total IGBT	€/IGBT	Cost (€)
1200	3600	5	1	120	1343.19	161182.6
1200	400	5	12	1440	117.22	168799.7
1700	3600	4	1	96	1792.06	172037.4
1700	2400	4	2	192	1510.78	290070.1

Table 24. Devices chosen for further study of the converter design

Device	V_{ce}	I_{ce}
IGBT	1200	3600
IGBT	1700	2400
IGBT	1700	3600
Diode	1700	800

Among the four preselected switches, the option 1200 V x 400 A is discarded since it has too many switches. Switch 1700 V x 2400 A is chosen in order to compare it with a previous converter design [INN14] since it was the selected switch.

Among the three available diodes to design the converter a similar reasoning is followed. Therefore, the chosen diode is 1700 V x 800 A since its price is around 33% cheaper than the second best option 1700 V x 3600 A, although it needs a larger number of diodes to build up the converter.

The design process of the converter continues with a further study of three different IGBTs and one diode. The chosen semiconductors are shown in Table 24.

There is no standard way to calculate the number of switches in series and in parallel since there are always some safety margins than can be adjusted by the designer. Therefore equation (16) and (17) can be rearranged into

$$IGBT_{series} = \text{ceil} \left(k \frac{V_{DC}}{V_{ce}} \right) \quad (22)$$

$$IGBT_{parallel} = \text{ceil} \left(k' \frac{I_{rms}}{I_{ce}} \right) \quad (23)$$

According to values of k and k' the number of switches for a converter with the same power and DC-link is different. Two different values for k and k' are taken into account as pre-designs for the final power converter. Values of k and k' are shown in Table 25. Values of k and k' for option A correspond to [INN14] whereas option B correspond to [HIT09].

Equation (22) and (23) are applied to the semiconductors in Table 24 and two new designs per IGBTs are considered. The number of semiconductors for each option are shown in Table 26.

Table 25. K and K' constants for determining the number of IGBT in series and parallel

Option	k	k'
A	0.8	2.5
B	1	2.33

Table 26. Pre-designs for a 10MW 3-level back to back converter

Design	Option	IGBT					Diode				
		V_{ce} (kV)	I_{ce} (kA)	Series	Parallel	Total	V_f (kV)	I_f (kA)	Series	Parallel	Total
1	A	1.2	3.6	5	1	120	1.7	0.8	4	6	288
2	B	1.2	3.6	5	1	120	1.7	0.8	4	6	288
3	A	1.7	2.4	3	2	144	1.7	0.8	3	6	216
4	B	1.7	2.4	3	2	192	1.7	0.8	4	6	288
5	A	1.7	3.6	3	1	72	1.7	0.8	3	6	216
6	B	1.7	3.6	4	1	96	1.7	0.8	4	6	288

Table 27. Final designs for a 10 MW 3-level back to back converter

Design	Option	IGBT					Diode				
		V_{ce} (kV)	I_{ce} (kA)	Series	Parallel	Total	V_f (kV)	I_f (kA)	Series	Parallel	Total
1	A	1.2	3.6	5	1	120	1.7	0.8	4	6	288
2	A	1.7	2.4	3	2	144	1.7	0.8	3	6	216
3	B	1.7	2.4	3	2	192	1.7	0.8	4	6	288
4	A	1.7	3.6	3	1	72	1.7	0.8	3	6	216

5	B	1.7	3.6	4	1	96	1.7	0.8	4	6	288
---	---	-----	-----	---	---	----	-----	-----	---	---	-----

It is worth noticing that, in general, option A is less conservative than option B since for the same semiconductor the design requires less devices (Table 26). However, designs 1 and 2 need the same amount of devices, hence only five final designs (Table 27) are considered for the 10 MW BTB converter.

9.2.3 Passive components

The cost of the passive components in the configurations of the BTB power converters are investigated and compared with previous designs [INN14]. Passive components mainly includes the filter inductor, the filter capacitor and the DC-link capacitor.

9.2.3.1 Filter design

The filter is usually adopted in industry to reduce the harmonics around the switching frequency and multiples of the switching frequency at the generator side and the grid side of the BTB power converter. The design of the filter is closely related to switching frequency, which value is set at 600 Hz.

During the design of the filter some design criteria should be specified to meet the generator side and grid side requirements. Here, the THD of the generator side current is limited less than 3.5%. The filter capacitor value is limited by the decrease of the power factor at the rated power, which is generally less than 5%.

The calculation of the filter is carried out by applying equations (24)-(28) [REZ14], [WEI10]. The value of the calculated filter is shown in Table 28 and compared with the value for the filter in [INN14]. Prices for three-phase filter inductor and filter capacitor are shown in Table 29

Simulations are run to calculate the effectiveness of the filter and it turns out that the value of the THD current is 5.51% before the filter and it is reduced to 0.20% after the filter.

$$C_f = k \cdot \frac{\sqrt{2} \cdot P_n}{3 \cdot V_{ph}} L_{grid} = \frac{\sqrt{\frac{1}{k_a^2} + 1}}{C_f \cdot \omega_s^2} \quad (24)$$

$$L_{inv} = \frac{V_{DC}}{16 \cdot f_s \cdot \Delta i} \quad (25)$$

$$L_{grid} = \frac{\sqrt{\frac{1}{k_a^2} + 1}}{C_f \cdot \omega_s^2} \quad (26)$$

$$\omega_{res} = \sqrt{\frac{L_{inv} + L_{grid}}{L_{inv} \cdot L_{grid} \cdot C_f}} \quad (27)$$

$$R = \frac{1}{6 \cdot \pi \cdot f_{res} \cdot C_f} \quad (28)$$

Table 28. Filter values for the generator side 10 MW 3-level back to back converter

Parameters	Value	[INN14]
C_f	0.8 mF	0.8 mF
L_{inv}	1.1 mH	1 mH
R	0.31 Ω	0.37 Ω

Table 29. Reference price for filter [INN14]

Filter	Type	Price (k€)
Three-phase filter inductor	0.33 mH/2.4 kA	16
Three-phase filter capacitor	150 μ F/3 kV	1.8
	75 μ F/6 kV	3.6

9.2.4 DC-Link design

The DC-link capacitor for a 3-level back to back converter can be designed [ZEN07]:

$$C_d = \frac{P_n}{2 \cdot f_s \cdot V_{dc} \cdot \Delta u} \quad (29)$$

where P_n is the rated power of converter, Δu is voltage ripple, f_s is the switching frequency and V_{dc} is the DC-link voltage. The capacitor ripple is limited under 1%.

Price for DC-link capacitors are shown in Table 30.

Table 30. Price and features for DC-link capacitors [INN14]

Type	Capacitance (μF)	Voltage (kV)	Price (€)
AVX FFLI6B3007KJE	3000	0.8	288.4
AVX FFLI6U1607KJE	1600	1.15	217.49

9.2.5 Other components

9.2.5.1 Cooling system cost

The cost of the cooling system is estimated based on the maximum power loss of the power converter. The cooling system cost for per loss is assumed as 800€/kW. Based on the power converter efficiency results [INN14].

9.2.5.2 Mechanical cost

Mechanical system cost is estimated about 40% of the total cost excluding the cooling system [INN14].

9.2.6 Efficiency

The 10 MW superconducting generator with the five different converter configurations (Table 27) are modelled and simulated with the time-domain simulation tool Simulink Matlab.

The 10 MW superconducting generator parameters are shown Table 31. Semiconductors losses, conduction and switching losses, are implemented in the model. During the simulation semiconductor's currents are calculated and used for power losses calculation with the IGBT and diode data sheet.

Conduction losses are calculated by multiplying the I_c current with the U_{ce} voltage in the datasheet to get the conduction losses dependent on the current I_c for the operating current. This way creates a 2nd order curves based on the datasheet curves which can be approximated very accurately described as [DR005]

$$P_C = a \cdot I_c^2 + b \cdot I_c \quad (30)$$

Where a and b are derived by curve fitting.

In power electronics switching losses typically contribute to a significant amount to the total system losses. Therefore omitting switching losses in the calculation cannot be neglected. Switching losses are calculated through its dependency with the blocking voltage and current since it comes from the datasheet and they can be described as [DR005]

$$P_{S,ON} = a' \cdot I_c^3 + b' \cdot I_c^2 + c' \cdot I_c \quad (31)$$

$$P_{S,OFF} = a'' \cdot I_c^3 + b'' \cdot I_c^2 + c'' \cdot I_c \quad (32)$$

As for the conduction losses a' , a'' , b' and b'' are derived by curve fitting.

Total losses of the system will be

$$P_{Total} = P_C + P_{S,ON} + P_{S,OFF} \quad (33)$$

Table 32 shows the value of torque ripple, efficiency and cost for each of the final designs from Table 27. Among the five options, two of them are chosen for a further analysis. The chosen options are design 2 (IGBT 1700 V x 2400 A IGBT), since it has the best efficiency, 98.23%, and design 4 (IGBT 1700 V x 3600 A), since it is the cheapest option, 218 k€.

Table 31. 10 MW superconducting generator parameters for simulations

Parameter	Iron Cored
-----------	------------

Nominal power (kW)		10
Nominal voltage (V)		3300
Nominal frequency (Hz)		2.56
Nominal field current (A)		753
Stator	Core type	Iron
	Rs (pu)	0.0302
	LI (pu)	0.0129
	Lmd (pu)	0.0160
	Lmq (pu)	0.0182
Field	Core type	Iron
	Rf' (pu)	0.0001
	Llfd'(pu)	0.0115
Pole pairs		16

Table 32. Number of IGBTs and diodes, in series and parallel, torque ripple, efficiency and cost for the final converter designs

Design	IGBT					Diode					Torque ripple	η	Cost
	V _{ce} (kV)	I _{ce} (kA)	S	P	T	V _f (kV)	I _f (kA)	S	P	T	%	%	k€
1	1.2	3.6	5	1	120	1.7	0.8	4	6	288	0.19	97.70	260
2	1.7	2.4	3	2	144	1.7	0.8	3	6	216	0.20	98.23	307
3	1.7	2.4	3	2	192	1.7	0.8	4	6	288	0.20	98.01	390
4	1.7	3.6	3	1	72	1.7	0.8	3	6	216	0.19	98.16	218
5	1.7	3.6	4	1	96	1.7	0.8	4	6	288	0.19	97.88	272

Key: S = Series; P = Parallel; T = Total

9.2.7 Energy calculations

In order to discern which is the best option among the two last candidates, IGBT 1700 V x 2400 A and IGBT 1700 x 3600 A, it is necessary to carry out an energy study to determine the return of the investment for each option.

The necessary inputs to carry out the energy study are the following:

- Wind distribution for a specific area and height.
- Mechanical power curve of the generator.
- Generator efficiency curve.
- Power converter efficiency curve.

The wind energy distribution (Fig. 88.left) and the generator mechanical power curve (Fig. 88.right) for the energy analysis are taken from [INN14a]. The generator, power converter and drive train efficiency curves versus wind speed are shown in Fig. 89 (left) for the IGBT 1700 V x 3600 A. Fig. 89 (right) shows the energy distribution per year versus wind speed for the same IGBT.

The total amount of energy per year for the both IGBTs considered is shown in Table 33 and compared with the energy values reported in [INN14] where an IGBT 1700 V x 2400 A is chosen for the design of the converter.

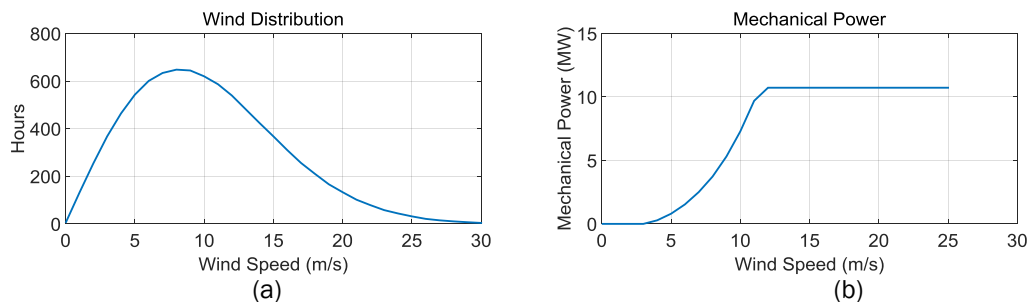


Fig. 88 (a) Wind distribution for energy calculations, height 90 m, and (b) generator mechanical power versus wind speed

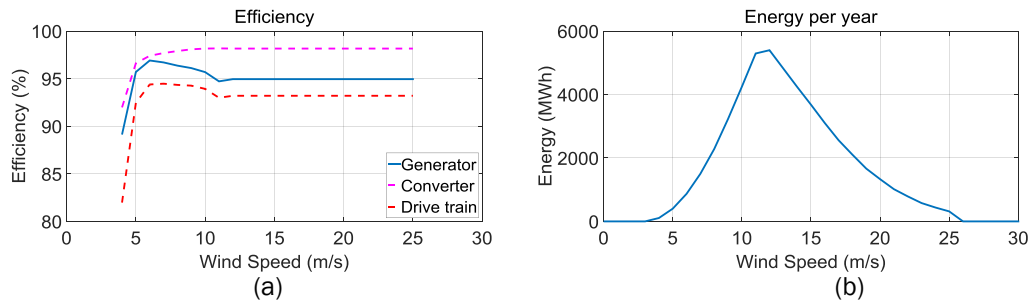


Fig. 89 (a) Generator, converter and drive train efficiency and (b) energy distribution per year vs. wind speed for a converter designed with an IGBT 1700 V 3600 A

Table 33. Summary of energy for each option

Switch	Energy (GWh/year)	Energy (GWh/year) [INN14]
1700 V - 2400 A	49.963	49.300
1700 V - 3600 A	49.953	

Table 34. Main parameters of the final design for a 10 MW 3-level BTB converter

IGBT					Diode					Ripple	η	Cost	Energy/year
V_{ce} (kV)	I_{ce} (kA)	S	P	T	V_f (kV)	I_f (kA)	S	P	T	%	%	k€	(GWh/year)
1.7	3.6	3	1	72	1.7	0.8	3	6	216	0.19	98.16	218	49.953

Key: S = Series; P = Parallel; T = Total

The conclusions of the analysis of the energy per year for each IGBT are the following:

- Both new designed converters, built up with IGBT 1700 V x 2400 A and IGBT 1700 V x 3600 A, generate 1.32% more energy (~0.65 GWh/year) than previous designs from [INN14].
- The new designed converter is 30% more expensive (95000€) than previous designs from [INN14] when the same switch, IGBT 1700 V x 2400 A, is used to build up the converter.
- A converter with IGBT 1700 V x 3600 A produces 0.001% less energy (0.01 GWh) per year than a converter with IGBT 1700 x 2400 A but it is 29% cheaper (89000 €).
- The new designed converter with IGBT 1700 V x 3600 A is 0.75% cheaper (6000 €) than previous designs from [INN14], where IGBT 1700 V x 2400 A is used.

As a consequence of the above statements, the chosen switch for the final 10 MW 3-level BTB converter for a superconducting wind generator is the IGBT 1700 V x 3600 A with the diode 1700 V x 800 A.

Main parameters of the converter design (number of IGBTs and diodes in series and parallel, torque ripple, efficiency, cost and energy per year) are summarised in Table 34.

9.2.8 Cost analysis

After the design of the superconducting generator and the armature power converter, a cost analysis of the drive train is carried out.

Three parameters are calculated to evaluate the viability of the drive train. The studies cost parameters are:

- Energy cost
- Cost of energy
- Cost of energy (with discount rate)

The energy cost defined as

$$\text{Energy Cost} = \frac{\text{Drive train cost}}{\text{Energy per year}} \quad (34)$$

The drive train cost includes the cost of the power converter and the generator. A breakdown of the cost for the drive train is shown in Table 35. Values of DC-link, grid filter, cooling system and mechanical cost come from [INN14]. The total value of the drive train is 1.55 M€, Table 35, and the amount of energy produced per year is 49.953 GWh, Table 34.

The second parameter is the cost of energy per the total life of the windmill defined as:

$$CoE = \frac{\text{Windmill cost}}{25 \text{ years energy}} \quad (35)$$

The windmill cost includes the drive train cost and adds 30 M€ which account for the foundations, tower and the rest of costs do not considered for the drive train. Therefore the total windmill cost is 31.55 M€.

Finally the third parameter is the cost of energy with a discount rate of 8%. The cost of energy with discount rate is taken into account to consider the decrease of the current value of the investment in a future since a cash flow today is more valuable than an identical cash flow in the future [BER14]. The derated energy value for 25 years with a discount rate of 8% is 575.90 GWh.

Table 35. Total cost of the designed 10 MW drive train

		Cost (M€)
Generator cost	Iron	0.112
	Copper	0.117
	SC	0.535
Total generator		0.764
Converter cost	Switches	0.160
	Generator filter	0.058
	DC Link*	0.152
	Grid filter*	0.089
	Cooling system*	0.143
	Mechanical cost*	0.184
Total converter		0.786
Total drive train		1.55

*Cost from [INN14]

Table 36. Cost parameters for the 10 MW drive train

	Requirement	Value
Target Energy Cost (€/MWh/year)	-	31.04
Cost of energy (€/kW)	0.05	0.025
Cost of energy (€/kW) [Discount rate = 8%]	0.05	0.055

$$CoE_{DR} = \frac{\text{Windmill cost}}{\text{Energy per year} \cdot \sum_1^{25} (1 + DR)^{-(n-1)}} \quad (36)$$

Table 36 summarises the values of the three cost parameters and compare them with the set requirements. The new designed converter achieves the set requirement, 0.05 €/kW, since its value is 0.025 €/kW. On the other hand, the value of the cost of energy with a discount rate of 8% is 10% higher than the set requirement, 0.05 €/kW versus 0.055 €/kW.

9.3 Field converter

An EESG, unlike Permanent Magnet Synchronous Generators (PMGS), does not requires permanent magnets in its rotor. However, for the generation of the magnetic field in an EESG a DC current at their excitation is required. To deliver the necessary DC current at their excitation it is necessary a DC source. The DC source is usually an AC/DC converter which has to be designed for each machine according to its specific circumstances.

An initial study for the design of the field converter is carried out. The design of the field converter begins discussing what the most suitable topology is. The main possible topologies for a field converter are (Fig. 90):

- AC/DC controlled converter
- AC/DC uncontrolled converter
- AC/DC uncontrolled converter + DC/DC buck controlled converter
- DC/DC buck controlled converter

One of the main characteristics of the AC/DC one step controlled converter topology (Fig. 90.a) is its boost nature. Furthermore, the main advantages of the AC/DC controlled converter topology are its simplicity (build up with IGBTs) and capacity to regulate the DC voltage supplied to the generator field winding.

The boost nature of the AC/DC controlled converter turns into a disadvantage for this specific application due to the superconducting nature, very low resistance and high inductance, of the field winding of the EESG. As a consequence of the superconducting nature of the field winding, it has to be fed with a very low voltage.

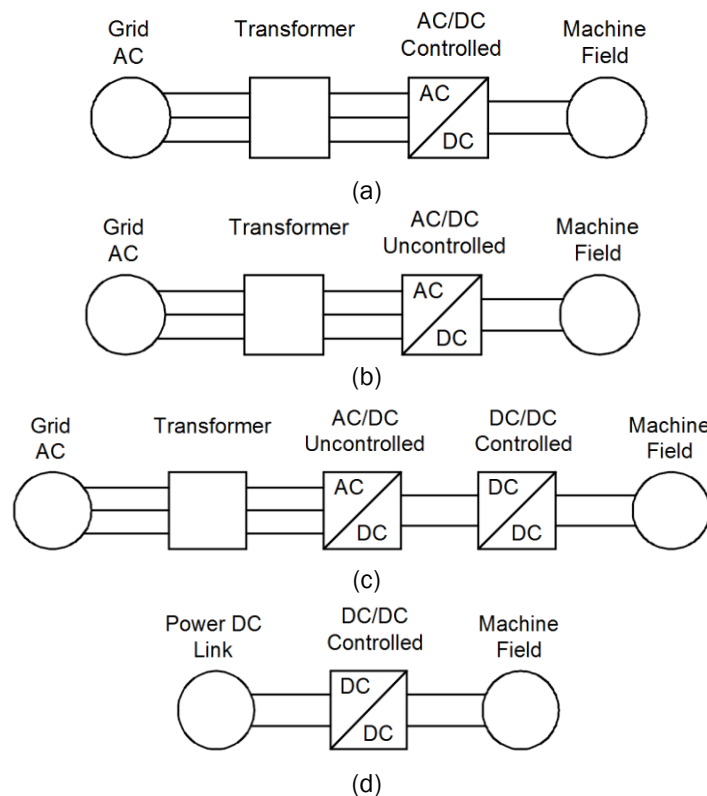


Fig. 90 Field converter topologies. (a) AC/DC controlled converter (b) AC/DC uncontrolled converter (c) AC/DC uncontrolled converter + DC/DC controlled converter and (d) DC/DC controlled converter

For optimal operation the DC-link voltage of the converter has to be kept constant. Moreover, to keep the input currents sinusoidal, the rectifier needs to operate in the linear PWM mode. The maximum line-to-line voltage to maintain linear PWM operation is given by [BHO97]

$$V_{ll} = \frac{\sqrt{3}}{2 \cdot \sqrt{2}} \cdot V_{DC} \quad (37)$$

Since the value of the V_{DC} has to be very small due the lack of resistance of the field winding, the line-to-line voltage (V_{ll}) has to be even smaller. Hence, the line-to-line voltage has to be reduced with a transformer to unpractical values, therefore the use of an AC/DC controlled converter is discarded.

The second proposed option is an AC/DC one step uncontrolled converter topology (Fig. 90.b). AC/DC uncontrolled converters are very similar to AC/DC controlled converters but they lack the capacity of regulating the DC voltage. The value of the DC voltage in an AC/DC uncontrolled transformer is set by the peak value of the input voltage, set by the transformer relation. As for the

previous converter, the main challenge comes due to the superconducting field winding, which requires very low voltage, and makes the use of AC/DC one step converters unpractical.

Since one step AC/DC converters are unable to provide a very low DC voltage, the combination of an AC/DC converter with a DC/DC converter is considered (Fig. 90.c). The advantages of this topology is that the AC/DC converter can be uncontrolled since its only function is provide an acceptable DC voltage to the DC/DC converter. The input DC value for the DC/DC converter is set by the peak line-to-line voltage and it will be adjusted by the transformer connected to the input of the AC/DC uncontrolled converter.

The DC/DC converter topology will be set in buck configuration. The use of a DC/DC converter has many advantages since the input DC/DC voltage may contain a small ripple and the output voltage (or current) can be easily controlled with a very low ripple.

On the other hand, the use of a two steps converter increases the price of the device. It also requires a bigger effort to design a control scheme which increases the price of the device.

In order to reduce the cost of the field converter, the first step of the two steps converter is replaced by taking the DC input to the DC/DC converter stage directly from the BTB armature converter (Fig. 90.d). Taking the DC input voltage from the power DC link might seem an advantage

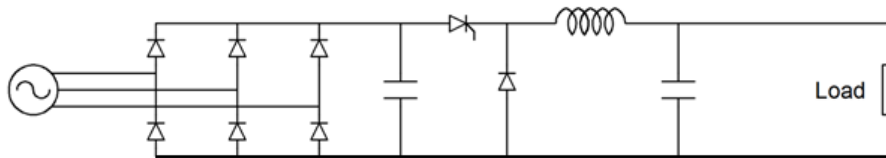


Fig. 91 AC/DC uncontrolled converter with a DC/DC buck converter to feed the field winding of the superconducting EESG

since the AC/DC uncontrolled converter is not needed. However, it turns out that the power DC-link voltage is much higher than the required output voltage for the field winding and the voltage requirements for the semiconductors of DC/DC buck converter become higher, highly increasing the price of the proposed topology.

The discussion of the advantages and disadvantages of each topology reveals that the best topology among the four possibilities is topology three (AC/DC uncontrolled + DC/DC buck converter). A more detailed scheme of the topology is shown in Fig. 91.

Once the topology has been set two control strategies in steady state are studied: (i) voltage control and (ii) current control.

Results from simulations show that voltage control is unable to set the right value since its response turns instable. On the other hand, current control has a satisfactory response achieving the set current value with no ripple. The lack of ripple in the system is due the high inductance of the superconducting field winding.

10 20 MW CONVERTER

After the study of the 10 MW drive train, the system needs to be scaled up to 20 MW. As a consequence, it is necessary to set again the input parameters. The scaling up process begins with the determination of the scaled up generator speed and mechanical power versus wind speed.

The new generator speed is scaled up as a linear relationship between the rated speeds of the 10 MW and 20 MW generators, according to:

$$\text{Speed}_{20MW} = \frac{\text{Rated Speed}_{20MW}}{\text{Rated Speed}_{10MW}} \cdot \text{Speed}_{10MW} \quad (38)$$

The 10 MW generator rated speed is 9.6 r.p.m. whereas the 20 MW generator rated speed is 6.8 r.p.m. The mechanical speed versus wind speed for the 10 MW generator is an input from [INN14a]. The result of (38) is plotted on Fig. 92 (left), where the solid blue line stands for the generator speed for the 10 MW generator and the solid red line for the 20 MW generator.

A similar process is done to scale up the mechanical power. In this case the relationship to scale up the mechanical power follows:

$$\text{Power}_{20MW} = 2 \cdot \text{Power}_{10MW} \quad (39)$$

In Fig. 92, the evolution of the mechanical power for the 10 MW generator [INN14a] is compared to the mechanical power for the 20 MW versus the wind speed.

The scaling up process repeats the same steps done for the design of the converter for the 10 MW generator. Therefore, 23 different IGBTs and 3 different diodes are analysed to determine which the best options for building up a BTB converter for the 20 MW generator are.

The value of the line-to-line voltage is a parameter that affects the converter design. Two line-to-line voltages, 3.3 kV and 6.6 kV, are considered for the design of the new converter and compared with the results presented in [INN14] for a generator with 6.6 kV line-to-line voltage.

Table 37 summarises the best five options for both 3.3 kV and 6.6 kV line to line voltages, showing the chosen IGBTs, the necessary number of switches in series and in parallel, total number of switches, price and efficiency comparing them with the previous design from [INN14].

Among the options shown in Table 37, IGBT 1200 V x 400 A is discarded for both line-to-line voltages since the total amount of switches for a 20 MW converter is too high.

The comparison among the rest of options for the 3.3 kV and 6.6 kV line-to-line voltages reveals that converters for the 3.3 kV line-to-line voltage are more expensive than converters for 6.6 kV.

The comparison of the proposed designs for the 3.3 kV line-to-line voltage are a little bit more expensive than the previous design, whereas the proposed designs for the 6.6 kV line-to-line voltage are a little bit cheaper.

Regarding the efficiency, there are no big differences among the proposed designs for 3.3 kV and 6.6 kV line-to-line voltages since they have similar efficiency values than previous designs (~98%).

Table 37. Summary of the best five options for a 20MW 3-level BTB converter for a 3.3 kV and 6.6 kV line-to-line voltage

Power (MW)	Voltage (kV)	Device	Voltage (V)	Current (A)	Series	Parallel	Total switches	Price (M€)	Efficiency (%)
20 MW	3.3 kV	IGBT	1200	400	5	24	2880	0.421	
		IGBT	1200	2400	5	4	480	0.553	98.11
		IGBT	1200	3600	5	3	360	0.567	98.13
		IGBT	1700	3600	4	3	288	0.600	97.81
		IGBT	1700	2400	4	4	384	0.664	97.87
	Diode	1700	800	4	12	576			
	6.6 kV	IGBT	1200	3600	9	1	216	0.363	98.16
		IGBT	1700	3600	7	1	168	0.374	98.26
		IGBT	1200	400	9	12	2592	0.377	
		IGBT	1200	2400	9	2	432	0.495	98.22
IGBT		1700	2400	7	2	336	0.581	98.36	
Diode	1700	800	7	6	504				
20 MW [INN14]	6.6 kV	IGBT	1700	2400	6	2	288	0.498	~98
		Diode	1700	800	6	6	432		

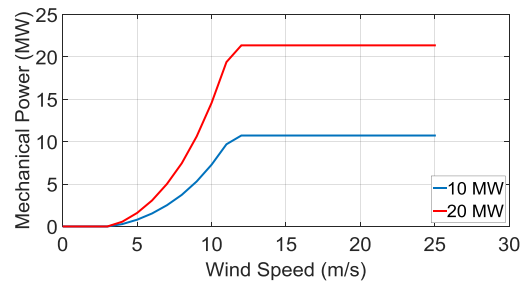
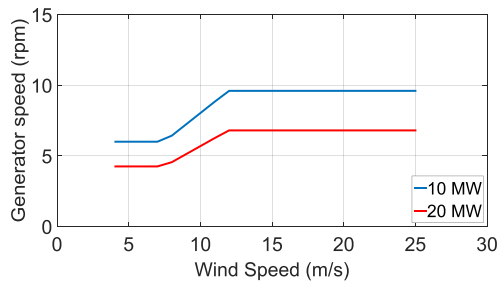


Fig. 92 10 MW (blue line) and scaled up 20 MW (red line) (a) generator speed and (b) mechanical power vs. wind speed

Since price of semiconductors is not decisive to discern which line-to-line voltage is the optimum, the price of the generator side filter and DC-link are considered in the process.

A generator side filter and DC-link are calculated for each line-to-line voltage and compared with the previous design (Table 38).

Total price for the generator grid side and DC-link for 3.3 kV line-to-line voltage is much higher, around 3 times higher, (1.144 M€) than for the 6.6 kV line-to-line voltage (0.398 M€). Hence, the 3.3 kV line-to-line voltage is discarded and the system will be designed for a 6.6 kV.

At this point, the scaling up process requires to decide which one of the four remaining options is the best for building up the 20 MW BTB converter. To decide which the best option is, an energy per year production analysis is carried out. Results for the energy production, price of the semiconductors and total number of switches for each possible option are shown in Table 39. The cost of the DC link, generator and grid filter, cooling system and mechanical cost are the same for each option so they are not considered in the analysis since they will not affect the results.

Among all the options shown in Table 39, the option chosen is the IGBT 1700 V x 3600 A. The reason for its selection are the following:

- IGBT 1700 V x 3600 A is the second option at producing energy per year. It produces 0.041 GWh/year less (0.001% less) than IGBT 1700 V x 2400 A but it is 0.207 M€ cheaper (36% cheaper).
- IGBT 1700 V x 3600 A is the second cheapest option by only 11 k€.
- IGBT 1700 V x 3600 A needs less semiconductors devices (168, at least 29% less semiconductors) than the rest of the options. Therefore the likelihood of having a failure in the semiconductors is smaller than in the other options.

Due the above reasons, the chosen IGBT for the design of the 20 MW BTB converter is IGBT 1700 V x 3600 A. The number of diodes has not been taken into account at the economical comparison since all the options are designed with the same diode, 1700 V x 800 A, then it does not affect the result of the design. The necessary amount of diodes for the converter is 504.

Table 38. Filter generator side and DC-link values and cost for 3.3 kV and 6.6 kV line-to-line voltage for 20 MW 3-level BTB converters

Power (MW)	Voltage (kV)	Generator side				DC Link		Total (M€)
		Inductor (mH)	Inductor price (M€)	Capacitor (mF)	Capacitor Price (M€)	Capacitor (mF)	Capacitor Price (M€)	
20 MW	3.3 kV	0.5	0.048	1.1	0.013	57.2	1.082	1.144
	6.6 kV	2.27	0.110	0.28	0.013	14.3	0.275	0.398
20 MW [INN14]	6.6 kV	2.3	0.112	0.45	0.021	12.5	0.242	0.375

Table 39. Remaining options for the 20 MW 3-level BTB converter design

Power (MW)	Voltage (kV)	Voltage (V)	Current (A)	Energy (GWh/year)	Switches cost (M€)	Switches (units)
20 MW	6.6 kV	1200	2400	100.722	0.495	432
		1200	3600	100.658	0.363	216
		1700	2400	100.777	0.581	336
		1700	3600	100.736	0.374	168
[INN14]	6.6 kV	1700	2400		0.498	288

Table 40. Total cost of the designed 20 MW drive train

		Cost (M€)
Generator cost	Iron	0.166
	Copper	0.192
	SC	1.054
Total generator		1.412
Converter cost	Switches	0.374
	Generator filter	0.124
	DC Link	0.275
	Grid filter*	0.100

	Cooling system*	0.320
	Mechanical cost*	0.332
Total converter		1.525
Total drive train		2.937

*Cost from [INN14]

Table 41. Cost parameters for the 20 MW drive train

	Requirement	Value of design
Target Energy Cost (€/MWh/year)	-	29.16
Cost of energy (€/kW)	0.05	0.019
Cost of energy (€/kW) [Discount rate = 8%]	0.05	0.041

Finally, as for the 10 MW drive train, the economical parameters are calculated. Table 40 shows the breakdown of the cost of the 20 MW drive train. The cost parameters are shown in Table 41.

For both cost of energy parameters, a cost of 45M€ has been considered for the foundations, tower and rest of the costs not considered for the drive train.

11 CONCLUSIONS

The current sections summarises the main parameters of the designed drive train (Table 42).

Table 42. Summary of the main parameters for both the 10 MW and 20 MW designed drive trains

Parameter	10 MW	20 MW	Difference
Energy cost (€/MWh/year)	31.04	29.16	-6%
Cost of energy (€/kW) [INN WIND]	0.025	0.019	-24%
Cost of energy (€/kW) [Discount rate = 8%]	0.055	0.041	-25.45%
Generator cost (M€)	0.764	1.412	84.82%
Power Electronics cost (M€)	0.786	1.525	94.02%
Foundations cost + Turbine cost (M€)*	30	45	50%
Total cost (M€)	31.55	47.93	51.92%
Drive train efficiency (%)	98.16	98.26	0.1%
Energy per year (GWh)	49.953	100.736	101.66%

Conclusions of the current work for an increase of 100% in the power drive (from 10 MW to 20 MW):

- Energy cost decreases 6% (31.04 vs. 29.16 €/MWh/year).
- Cost of energy decreases 24% (0.025 vs. 0.019 €/kW).
- Cost of energy with a discount rate of 8% decreases 25.45% (0.055 vs. 0.041).
- Generator cost increases 84.82 %.
- Power electronics cost increases 94.02%.
- With an increase of 50% at the foundation and turbine cost, the total windmill cost increases 51.92%
- Drive train efficiency remains constant (98.16% vs. 98.26%) regardless the power of the drive train.
- The energy per year increases 101.66% (49.953 GWh vs. 100.736 GWh).

CHAPTER 4: POTENTIAL WORK

A. Design and analysis of Air-core rotor topology

With a small quantity of SC material, the advantage on torque capability of iron-core stator and rotor topology is significant. Consequently, the iron-core stator and rotor topology is determined, due to the high price of SC material nowadays. However, as SC material price reduces, the air-core rotor topology may become favourable, because it has great advantage on generator weight.

B. Influence of rotor pole shaping on performance

For the design of SC generator in this report, it is assumed that the air gap length between stator and rotor pole is uniform. In other words, the rotor pole is not shaped. In fact, the rotor pole shaping has some influences on performances, such as torque capability, torque ripple and iron loss, etc.

C. Detailed design of cryogenic system

The cryostat is initially designed and the thermal load is roughly calculated in this report. The more detailed design of cryogenic system and thermal load calculation can be as future work.

D. Design of SC coil supporting and torque transfer components

The basic electromagnetic design of SC generator is finished in this report. However, there are still some crucial components without design, such as SC coil supporting and torque transfer components, etc. For these components, the mechanical design is more important.

E. Detailed design of the field converter

The field converter is initially designed in this report. A more detailed design of it can be seen as future work since its behaviour in transient state has not been analysed yet.

F. Current limiters for the field converter

The SC features of a material depend on their temperature, magnetic field and current density. In the event of a short circuit, the field current may be higher than the maximum current density that the SC material can endure. Therefore current limiters may be researched in order to keep the SC material in the superconducting region.

G. Design of the armature converter with high voltage IGBTs

New high voltage IGBTs start to be available in the market. At the present time, neither prices nor features of them were available. The design of the armature converter with the new high voltage IGBTs would be worth trying.

H. Study of the influence of the converter level in the performance of the drive train

In the current report only 2 and 3-level BTB converters have been considered for the converter design. The use of higher level converters might improve the system if the DC voltage can be kept constant, which is the major challenge of higher level converters.

REFERENCES

- [ACK03] R. Ackermann, J. Alexander, A. Gadre, T. Laskaris, K. Sivasubramaniam, J. Urbahn, R. Nold, and L. Tomaino, "Testing of a 1.8 MVA high temperature superconducting generator," presented at the *IEEE Power Engineering Soc. Annual Meeting, Emerging Technologies Panel Session*, Toronto, ON, Canada, 2003
- [ALI92] B. L. Aliyevsky, B. A. Bazarnov, A. M. Oktyabrsky, N. N. Popov, A. G. Sherstuk, and D. P. Shopen, "Superconductor homopolar machines with liquid-metal contacts," *IEEE Trans. Magn.*, vol. 28, no. 1, pp. 287-290, Jan. 2009.
- [ASO14] Basic AC electrical generators, American Society of Power Engineers, 2014
- [BAD09] B. Badrzadeh, M. MacDonald, "Alternatives for high-power power electronic converters, switching devices and electric machines for very large wind farms: A technological and market assessment", *European Wind Energy Conference and Exhibition (EWEC 2009)*, Marseille, France, 12 pp, March 2009
- [BAI00] S. K. Baik, M. H. Sohn, D. Y. Park, J. B. Ahn, Y. K. Kwon, K. S. Ryu, Y. -S. Jo, I. Muta, and T. Hoshino, "A 30 kVA superconducting generator development and basic tests," *IEEE Trans. Appl. Supercond.*, vol. 10, no. 1, pp. 947-950, Mar. 2000.
- [BAI05] S. K. Baik, M. H. Sohn, E. Y. Lee, Y. K. Kwon, Y. S. Jo, T. S. Moon, H. J. Park, and Y. C. Kim, "Design considerations for 1MW class HTS synchronous motor," *IEEE Trans. Appl. Supercond.*, vol. 15, no. 2, pp. 2202-2205, Jun. 2000.
- [BAI09] W. O. S. Bailey, M. Al-Mosawi, Y. F. Yang, K. Goddard, and C. Beduz, "The design of a lightweight HTS synchronous generator cooled by subcooled liquid nitrogen," *IEEE Trans. Appl. Supercond.*, vol. 19, no. 3, pp. 1674-1677, Jun. 2009.
- [BAI11] W. Bailey, H. M. Wen; M. Al-Mosawi, K. Goddard, and Y. F. Yang, "Testing of a lightweight coreless HTS synchronous generator cooled by subcooled liquid nitrogen," *IEEE Trans. Appl. Supercond.*, vol. 21, no. 3, pp. 1159-1162, Jun. 2011.
- [BAI13] W. O. S. Bailey, Y. Yang, C. Beduz, and K. F. Goddard, "Short circuit tests on a coreless HTS synchronous generator," *IEEE Trans. Appl. Supercond.*, vol. 23, no. 3, pp. 5201505, Jun. 2013.
- [BAR05] P. N. Barnes, M. D. Sumption, and G. L. Rhoads, "Review of high power density superconducting generators: Present state and prospects for incorporating YBCO windings," *Cryogenics*, vol. 45, no. 10/11, pp. 670-686, Oct. 2005
- [BEJ77] A. Bejan and P. Thullen, "Thermal performance of the rotor of the MIT-EPRI 3 MVA superconducting," *IEEE Trans. Magn.*, vol. 13, no. 1, pp. 763-766, Jan. 1977.
- [BER14] J. Berk, P. DeMarzo, D. Stangeland, "Corporate Finance", Third Canadian Edition, 2014
- [BHO97] Bhowmik, S.; van Zyl, A.; Spee, R.; Enslin, J.H.R., "Sensorless current control for active rectifiers," in *Industry Applications*, IEEE Transactions on , vol.33, no.3, pp.765-773, May/June 1997
- [BIS89] H. Bischof, W. Engl, H. -P. Groter, H. W. Lorenzen, and J. Schaller, "Practical experience on the operation of a 320 kVA synchronous generator with a superconducting field winding," *IEEE Trans. Magn.*, vol. 25, no. 2, pp. 1791-1794, Mar. 1989.
- [BLA77] R. D. Blaugher, J. H. Parker, and J. McCabria, "High speed superconducting generator," *IEEE Trans. Magn.*, vol. 13, no. 1, pp. 755-758, Jan. 1977.
- [BLA10] Blaabjerg, F.; Iov, F.; Chen, Z.; Ma, K., "Power electronics and controls for wind turbine systems," *Energy Conference and Exhibition (EnergyCon), 2010 IEEE International*, vol., no., pp.333,344, 18-22 Dec. 2010
- [BLA13] Blaabjerg, F.; Ke Ma, "Future on Power Electronics for Wind Turbine Systems," *Emerging and Selected Topics in Power Electronics, IEEE Journal of*, vol.1, no.3, pp.139,152, Sept. 2013
- [BOS06] B.K. Bose, "Power Electronics and Motor Drives: Advances and Trends", Academic Press, 2006
- [BRA84] T. Bratoljic, D. Huttenloher, H. W. Lorenzen, and H. P. Zerbes, "Tests on a 320 kVA superconducting generator," *IEEE Trans. Power Eng. Rev.*, vol. RER-4, no. 4, pp. 32-33, Apr. 1984.

- [BRE73] W. C. Brenner, D. W. Deis, R. F. Edwards, H. E. Haller, C. J. Mole, C. C. Sterrett, M. S. Walker, and L. N. Wedman, "Development of a 5 MVA superconducting generator – electrical design and performance," *IEEE Conf. Winter Power Meeting*, Jan., 1973.
- [BRU79] Y. Brunet, J. Mazuer, and M. Renard, "First electrical tests on a 500 kW hypersynchronous alternator," *IEEE Trans. Magn.*, vol. 15, no. 1, pp. 723-726, Jan. 1979.
- [BRU86] Y. Brunet, J. L. Sabri, and P. Tixador, "Electrical design of air-cored synchronous generators using superconducting field and armature windings," *Proc. IEE. Electric Power Applications*, vol. 134, no. 1, pp. 47-52, Jan. 1987.
- [BRU89] Y. Brunet, P. Tixador, and P. Vedrine, "Experimental results of an experimental three-phase AC superconducting armature," *IEEE Trans. Magn.*, vol. 25, no. 2, pp. 1811-1814, Mar. 1989.
- [CHA74] Y. W. Chang, C. K. Jones, S. Karpathy, D. C. Litz, A. Patterson, and M. S. Walker, "Development of a 5 MVA Superconducting Generator Testing and Evaluation," *IEEE Trans. Power App. Syst.*, vol. PAS-93, no. 2, pp. 496-499, Mar. 1974.
- [CHE95] H. Chen and O. Tsukamoto, "Stability characteristics of fully superconducting and damperless generator with excitation control in fault condition," *IEEE Trans. Appl. Supercond.*, vol. 5, no. 2, pp. 449-452, Jun. 1995.
- [CHE09] Z. Chen, J.M Guerrero, F. Blaabjerg, "A Review of the State of the Art of Power Electronics for Wind Turbines," *IEEE Transactions on Power Electronics*, vol.24, no. 8, pp. 1859-1875, 2009.
- [CHE14] Ming Cheng, Ying Zhu, The state of the art of wind energy conversion systems and technologies: A review, *Energy Conversion and Management*, Volume 88, December 2014, Pages 332-347
- [CHO14] K. Choi, S. Park, Y. Kim, S. Lee, W. Kim, J. Lee, and J. Lee, "Characteristics of rotating armature type high temperature superconducting generators with dual field windings for the wind turbine," *IEEE Trans. Appl. Supercond.*, vol. PP, no. 99, 2014.
- [CHU99] Y. D. Chun, H. -W Lee, J. Lee, Y. K. Kwon, K. S. Ryu, and J. P. Hong, "Transient analysis of a superconducting AC generator using the compensated 2-D model," *IEEE Trans. Magn.*, vol. 35, no. 5, pp. 4085-4087, Sept. 1999.
- [CRA11] A. D. Crane, "Exciter assembly," US Patent 7 969 123 B2, Jun. 28, 2011.
- [DRO05] Uwe Drofenik, Johann W. Kolar. "A General Scheme for Calculating Switching- and Conduction Losses of Power Semiconductors in Numerical Circuit Simulations of Power Electronic Systems." *Proceedings of IPEC'05*.
- [ETA97] The electricity training association, "Power system protection", 1997
- [FAG73] T. J. Fagan, Jr., D. C. Litz, J. H. Murphy, A. Patterson, C. C. Sterrett, D. Stoner, and A. Ulke, "Development of a 5 MVA Superconducting Generator – Mechanical and Cryogenic Design," *IEEE Conf. Winter Power Meeting*, Jan., 1973.
- [FAI12] R. Fair, *Superconductivity for large scale wind turbines*, Available: snf.ieeecsc.org/sites/ieeecsc.org/files/STP307.pdf
- [FAN14] H. Fang, R. Qu, J. Wang, Z. Zhu, and H. Chen, "Design of a Novel Torque Tube for a Direct-Drive Superconducting Wind Generator," *IEEE Trans. Appl. Supercond.*, vol. PP, no. 99, 2014.
- [FEA85] J. A. Fealey, W. D. Jones, T. A. Keim, and T. E. Laskaris, "Comprehense test and evaluation of a 20 MVA superconducting generator," *IEEE Trans. Power App. Syst.*, vol. PAS-104, no. 6, pp. 1484-1491, Jun. 1985.
- [FLI81] C. Flick, W. R. McCown, and J. H. Parker, "General design aspects of a 300 MVA superconducting generator for utility application," *IEEE Trans. Magn.*, vol. MAG-17, no. 1, pp. 873-879, Jan. 1981.
- [FRA03] M. Frank, J. Frauenhofer, P. V. Hasselt, W. Nick, H. -W. Neumueller, and G. Nerowski, "Long-term operational experience with first Siemens 400 kW HTS machine in diverse configurations," *IEEE Trans. Appl. Supercond.*, vol. 13, no. 2, pp. 2120-2123, Jun. 2014.
- [FRA06] M. Frank, P. V. Hasselt, P. Kummeth, P. Masek, W. Nick, H. Rothfischer, H. Schmidt, B. Wacker, H. -W. Neumuller, G. Nerowski, J. Frauenhofer, R. Hartig, and W. Rzdaki, "High-temperature superconducting rotating machines for ship applications," *IEEE*

Trans. Appl. Supercond., vol. 16, no. 2, pp. 1465-1468, Jun. 2006.

- [FRA08] J. Frauenhofer, J. Grundmann, G. Klaus, and W. Nick, "Basic concepts, status, opportunities, and challenges of electrical machines utilizing high temperature superconducting (HTS) windings," *J. Phys., Conf. Ser.*, vol. 97, no. 1, p. 012189, 2008.
- [FUK11] S. Fukui, J. Ogawa, S. Takao, O. Tsukamoto, N. Kashima, and S. Nagaya, "Study of 10 MW-Class Wind Turbine Synchronous Generators With HTS Field Windings," *IEEE Trans. Appl. Supercond.*, vol. 21, no. 3, pp. 1151-1154, Jun. 2011.
- [GAM11] B. Gamble, G. Snitchler, and T. MacDonald, "Full power test of a 36.5MW HTS propulsion motor," *IEEE Trans. Appl. Supercond.*, vol. 21, no. 3, pp. 1083-1088, Jun. 2011.
- [GAM02] B. Gamble, S. Kalsi, G. Snitchler, D. Madura, and R. Howard, "The status of HTS motors," presented at *IEEE Power Engineering Soc. Meeting*, Chicago, IL, 2002.
- [GAM06] B. Gamble, G. Snitchler, and S. S. Kalsi, "HTS generator topologies," in *Proc. IEEE Power Eng. Soc. Gen. Meet.*, Montreal, QC, Canada, 2006, pp. 1-5
- [GAM80] B. B. Gamble and T. A. Keim, "High power density generator," presented at the *15th Intersoc. Energy Conversion Engineering Conf.*, Seattle, WA, 1980.
- [GE96] W. Q. Ge and S. D. Tang, "Development and test of a 300 kW superconducting homopolar generator," *IEEE Trans. Magn.*, vol. 32, no. 4, Jul. 1996.
- [GIE08] J. F. Gieras, *Advancements in Electric Machines (Power Systems)*. New York, NY, USA: Springer-Verlag, 2008
- [GIL81] R. Gillet, J. Goyer, Y. Laumond, A. Marquet, and M. Berthet, "Electricite de France - Alstom-Atlantique superconducting turbogenerator development program," *IEEE Trans. Magn.*, vol. 17, no. 1, pp. 890-893, Jan. 1981.
- [GOD09] K. F. Goddard, B. Lukasik, and J. K. Sykulski, "Alternative Designs of High-Temperature Superconducting Synchronous Generators," *IEEE Trans. Appl. Supercond.*, vol. 19, no. 6, pp. 3805-3811, Dec. 2009.
- [GOL02] C. Gold, "Exciter and electronic regulator for rotating machinery," U.S. Patent 6 420 842 B1, Jul. 16, 2002
- [HIT09] "High voltage IGBT module application manual", Hitachi power semiconductor device, Ltd., Dec 2009
- [HIR96] H. Chibe, N. Uno, T. Ichikawa, S. Meguro, K. Takahashi, T. Saitou, S. Sakai, and S. Akita, "R&D of superconductors for 70 MW class generators," *IEEE Trans. Magn.*, vol. 32, no. 4, pp. 2343-2356, Jul. 1996
- [HOJ13] H. Hojabri, H. Mokhtari and L. Chang, "Reactive power control of permanent-magnet synchronous wind generator with matrix converter", *IEEE Trans. Power Delivery.*, vol. 28, no. 2, pp. 575-584, April 2013
- [HUL73] J. K. Hulm, E. F. McCann, C. J. Mole, and J. H. Parker, "Development of a 5 MVA Superconducting Generator - General Aspects," *IEEE Conf. Winter Power Meeting*, Jan., 1973.
- [HWA13] Y. J. Hwang, S. Choi, J. Y. Jang, J. Lee, Y. S. Yoon, H. M. Kim, Y. D. Chung, Y. S. Jo, M. H. Jang, E. A. Al-Ammar, and T. K. Ko, "A study on the superconducting synchronous generator with the fixed-type field coil," *IEEE Trans. Appl. Supercond.*, vol. 23, no. 3, pp. 5200305, Jun. 2013.
- [HWA14] Y. J. Hwang, M. C. Ahn, J. Lee; Y. S. Yoon, H. M. Kim, Y. D. Chung, Y. S. Jo, T. J. Kim, and T. K. Ko, "Electromagnetic design of a 15 MW-class HTS flux switching synchronous generator considering mechanical stress of the rotor core," *IEEE Trans. Appl. Supercond.*, vol. 24, no. 3, pp. 1-5, Jun. 2014.
- [IBA12] E. Ibarra, I. Kortabarria, J. Andreu, I M. de Alegria, J. L. Martin and P. Ibañez, "Improvement of the design process of matrix converter platforms using the switching state matrix averaging simulation method", *IEEE Trans. Ind. Electron.*, vol. 59, no. 1, pp. 220-234, January 2012
- [INN14] INNWIND, "Deliverable D3.32 Converter designs based on new components and modular multilevel topologies", September 2014
- [INN14a] INNWIND, "Deliverable 1.11. Database of existing Wind parameter Measurements for tall atmospheres across Europe", August 2014
- [INO94] K. Inoue, T. Tokumasu, K. Nakanishi, T. Hamajima, K. Ito, and S. Oshima, "Study on the coil for quick response superconducting generator," *IEEE Trans. Magn.*, vol. 30, no.

4, pp. 2403-2406, Jul. 1994.

- [INT83] L. Intichar and D. Lambrecht, "Technical overview of the German program to develop superconducting AC generators," *IEEE Trans. Magn.*, vol. MAG-19, no. 3, pp. 536-540, May 1983.
- [IOV08] F. Iov, M Ciobotaru, F. Blaabjerg. "Power Electronics Control of Wind Energy in Distributed Power System", in Proceedings of 11th International Conference on Optimization of Electrical and Electronic Equipment Optim'08, pp. 16, May 24-26, Brasov, Romania, ISBN 1-4244-1545-4.
- [ISH88] T. Ishigohka, A. Ninomiya, T. Okada, T. Nitta, T. Shintani, I. Muta, and E. Mukai, "An experimental study on a superconducting generator with dual machine shield system," *IEEE Trans. Magn.*, vol. 24, no. 2, pp. 1481-1484, Mar. 1988
- [ISH08] S. Ishmael, C. Goodzeit, P. Masson, R. Meinke, and R. Sullivan, "Flux pump excited double-helix rotor for use in synchronous machines," *IEEE Trans. Appl. Supercond.*, vol. 18, no. 2, pp. 693-696, Jun. 2008
- [IWA07] M. Iwakuma, A. Tomioka, M. Konno, Y. Hase, T. Satou, Y. Iijima, T. Saitoh, Y. Yamada, T. Izumi, and Y. Shiohara, "Development of a 15 kW Motor With a Fixed YBCO Superconducting Field Winding," *IEEE Trans. Appl. Supercond.*, vol. 17, no. 2, pp. 1607-1610, Jun. 2007.
- [JEN12] B. B. Jensen, N. Mijatovic, and A. B. Abrahamsen, "Development of superconducting wind turbine generators," Available: proceedings.ewea.org/annual2012/.../919_EWEA2012presentation.ppt
- [J000] Y. S. Jo, J. P. Hong, J. Lee, Y. K. Kwon, and K. S. Ryu, "An approach to the shape optimum design of superconducting synchronous generator," *IEEE Trans. Appl. Supercond.*, vol. 10, no. 1, pp. 939-942, Mar. 2000.
- [J014] H. C. Jo, W. S. Lee, Y. D. Chung, K. Y. Yoon, H. Kim, Y. S. Jo, T. K. Ko, and Y. S. Yoon, "Numerical analysis and design of damper layer for MW-Class HTS synchronous wind turbine generator," *IEEE Trans. Appl. Supercond.*, vol. 24, no. 3, pp. 1-5, Jun. 2014.
- [KAL02] S. S. Kalsi, "Development status of superconducting rotating machines," in *Proc. IEEE PES Meet.*, New York, NY, USA, 2002, pp. 27-31.
- [KAL11] S. S. Kalsi, Applications of high temperature superconductors to electric power equipment, Hoboken, John Wiley & Sons, Inc., 2011.
- [KAL14] S. S. Kalsi, "Superconducting wind turbine generator employing MgB₂ windings both on rotor and stator," *IEEE Trans. Appl. Supercond.*, vol. 24, no. 1, pp. 47-53, Feb. 2014.
- [KAR14] H. Karmaker, M. Ho, E. Chen, and D. Kulkarni, "Direct drive HTS winding generator design for commercial applications," *2014 Int. Conf. Electrical Machines*, Sept. 2014, pp. 491-495.
- [KEI85] T. A. Keim, T. E. Laskaris, J. A. Fealey, and P. A. Rios, "Design and Manufacture of a 20 MVA Superconducting Generator," *IEEE Trans. Power Eng. Rev.*, vol. RER-5, no. 6, pp. 56-56, Jun. 1985.
- [KEY11] O. Keysan and M. A. Mueller, "A homopolar HTSG topology for large direct-drive wind turbines," *IEEE Trans. Appl. Supercond.*, vol. 21, no. 5, pp. 3523-3531, Oct. 2011.
- [KIM14] J. H. Kim, S. I. Park, T. D. Le, K. L. Kim, H. Lee, Y. -S. Jo, Y. S. Yoon, and H. M. Kim, "Characteristic analysis of various structural shapes of superconducting field coils," *IEEE Trans. Appl. Supercond.*, accepted 2014.
- [KIR73] J. L. Kirtley, J. L. Smith, P. Thullen, and H. H. Woodson, "MIT-EEL program on large superconducting machines," *Proc. IEEE*, vol. 61, no. 1, pp. 112-115, Jan. 1973.
- [KLA07] G. Klaus, M. Wilke, J. Fraunhofer, W. Nick, and H. -W. Neumuller, "Design challenges and benefits of HTS synchronous machines", *IEEE Power Engineering Society General Meeting*, 24-28 June 2007, pp.1-8.
- [KOU10] S. Kouro, M. Malinowski, K. Gopakumar, J. Pou, L. G. Franquelo, B. Wu, J. Rodriguez, M. A. Perez, J. I. Leon, "Recent Advances and Industrial Applications of Multilevel Converters," *IEEE Transactions on Power Electronics*, vol. 57, no. 8, pp. 2553 - 2580, 2010
- [KOS12] D. Kostopoulos, H. Polinder, and A. Brink, Available:

- proceedings.ewea.org/annual2012/.../1559_EWEA2012presentation.pdf
- [KUM86] M. Kumagai, T. Tanaka, K. Ito, Y. Watanabe, K. Sato, and Y. Gocho “Development of superconducting AC generator,” *IEEE Trans. Energy Convers.*, vol. EC-1, no. 4, pp. 122-129, Dec. 1986.
- [KUM87] M. Kumagai, M. Tari, K. Ito, and Y. Watanabe, “Electrical and cryogenic characteristics of 3000kVA superconducting generator,” *IEEE Trans. Magn.*, vol. 23, no. 5, pp. 3539-3541, Sept. 1987.
- [KW005] Y. K. Kwon, M. H. Sohn, S. K. Baik, E. Y. Lee, J. M. Kim, T. S. Moon, H. J. Park, Y. C. Kim, and K. S. Ryu, “Development of a 100 hp synchronous motor with HTS field coils,” *IEEE Trans. Appl. Supercond.*, vol. 15, no. 2, pp. 2194-2197, Jun. 2014.
- [LAS81] T. E. Laskaris, “High-performance superconducting windings for AC generators,” *IEEE Trans. Magn.*, vol. 17, no. 1, pp. 884-889, Jan. 1981.
- [LEW07] C. Lewis and J. Muller, “A direct drive wind turbine HTS generator,” in *Proc. IEEE Power Engineering Society General Meeting*, Jun. 2007, pp. 1–8.
- [LIA14] Y. C. Liang, M. D. Rotaru, and J. K. Sykulski, “Electromagnetic simulations of a fully superconducting 10-MW-class wind turbine generator,” *IEEE Trans. Appl. Supercond.*, vol. 23, no. 6, pp. 46-50, Dec. 2013.
- [LIU14a] Y. Z. Liu, R. Qu, and J. Wang, “Comparative analysis on superconducting direct-drive wind generators with iron teeth and air-gap winding,” *IEEE Trans. Appl. Supercond.*, vol. 24, no. 3, pp. 1-5, Jun. 2014.
- [LIU14b] Y. Z. Liu, R. Qu, Z. Zhu, J. Wang, and H. Y. Fang, “Analysis on the performances of a rotor screen for a 12 MW superconducting direct-drive wind generator,” *IEEE Trans. Appl. Supercond.*, vol. 24, no. 5, pp. 1-5, Oct. 2014.
- [LIU14c] Y. Liu, S. Niu, S. L. Ho, W. N. Fu, and T. W. Ching, “Design and analysis of a new HTS double-stator doubly-fed wind generator,” *IEEE Trans. Appl. Supercond.*, Accepted, 2014.
- [LUD12] Ludois, D.C.; Venkataramanan, G., "Modular multilevel converter as a low inductance machine drive," Power and Energy Conference at Illinois (PECI), 2012 IEEE , vol., no., pp.1,4, 24-25 Feb. 2012
- [LUK08] B. Lukasik, K. F. Goddard, and J. K. Sykulski, “Finite-element assisted method to reduce harmonic content in the air-gap flux density of a high-temperature superconducting coreless rotor generator,” *IET Trans. Science, Measurement & Technology*, vol. 2, no. 6, pp. 485-492, Nov. 2008.
- [LUK09] B. Lukasik, K. F. Goddard, and J. K. Sykulski, “Finite element assisted method of estimating equivalent circuit parameters for a superconducting synchronous generator with a coreless rotor,” *IEEE Trans. Appl. Supercond.*, vol. 45, no. 3, pp. 1226-1229, Mar. 2009.
- [MAK80] N. Maki, T. Sanematsu, and H. Ogata, “Design and component development of a 50 MVA superconducting generator,” *IEEE Trans. Power App. Syst.*, vol. PAS-99, no. 1, pp. 185-194, Jan./Feb. 1980.
- [MAK87] N. Maki, K. Yamaguchi, M. Takahashi, and T. Sanematsu, “Test results of 50 MVA superconducting generator,” *IEEE Trans. Magn.*, vol. 23, no. 5, pp. 3536-3538, Sept. 1987.
- [MAT94] H. Matsumoto, T. Kitajima, K. Ito, H. Moriyama, J. Shibuya, Y. Tsuda, and N. Suzuki, “Development of major technologies for superconducting generator with quick response excitation,” *IEEE Trans. Magn.*, vol. 30, no. 4, pp. 1805-1808, Jul. 1994.
- [MEL12] Z. Mel, High temperature superconductors (HTS) for energy applications, Cambridge, UK, Woodhead Publishing Limited, 2012.
- [MIN81] J. V. Minervini, K. Tepper, and J. L. Jr. Smith, “Model test coil for a 10 MVA superconducting generator field winding,” *IEEE Trans. Magn.*, vol. 17, no. 1, pp. 123-126, Jan. 1981.
- [MIN07] Minshull, S.R.; Bingham, C.M.; Stone, D.A.; Foster, M.P., "A back to back multilevel converter for driving low inductance brushless AC machines," Power Electronics and Applications, 2007 European Conference on , vol., no., pp.1,9, 2-5 Sept. 2007
- [MON03] Mondal, S.K.; Bose, B.K.; Oleschuk, V.; Pinto, J.O.P., "Space vector pulse width modulation of three-level inverter extending operation into overmodulation region," Power Electronics, IEEE Transactions on, vol.18, no.2, pp.604,611, Mar 2003
- [MOS05] M. K. Al-Mosawi, C. Beduz, and Y. Yang, “Construction of a 100 kVA high temperature

- superconducting synchronous generator," *IEEE Trans. Appl. Supercond.*, vol. 15, no. 2, pp. 2182-2185, Jun. 2005.
- [MOS07] M. K. Al-Mosawi, K. Goddard, C. Beduz, and Y. Yang, "Coreless HTS synchronous generator operating at liquid nitrogen temperatures," *IEEE Trans. Appl. Supercond.*, vol. 17, no. 2, pp. 1599-1602, Jun. 2007.
- [MOU] www.uk.mouser.com
- [MUT83] I. Muta, T. Nitta, T. Shintani, I. Muta, T. Ishigohka, and H. Fujino, "Electrical characteristics of fully superconducting synchronous generator in persistent excitation mode," *IEEE Trans. Magn.*, vol. MAG-19, no. 3, pp. 1043-1046, May. 1983.
- [MUT92] I. Muta, H. Tsukiji, T. Hoshino, E. Mukai, "Electrical characteristics of fully superconducting synchronous generator in persistent excitation mode," *IEEE Trans. Magn.*, vol. 28, no. 1, pp. 434-437, Jan. 1992.
- [MUT94] I. Muta, H. Tsukiji, N. Nanda, T. Hoshino, and E. Mukai, "The effect of excitation methods on electrical characteristics of fully superconducting generator model," *IEEE Trans. Magn.*, vol. 30, no. 4, pp. 2030-2033, Jul. 1994
- [NEL13] V. Nelson, "Wind energy: Renewable energy and the environment, 2nd edition", CRC Press 2013
- [NIC07] W. Nick, M. Frank, G. Klaus, J. Frauenhofer, and H. -W. Neumüller, "Operational experience with the world's first 3600 rpm 4 MVA generator at siemens," *IEEE Trans. Appl. Supercond.*, vol. 17, no. 2, pp. 2030-2033, Jun. 2007.
- [NIS03] K. Nishijima, M. Asada, A. Izumi, R. Takahashi, H. Sato, and S. Maeda, "A new project for superconducting generator (SCG)," *IEEE Trans. Appl. Supercond.*, vol. 13, no. 2, pp. 2124-2127, Jun. 2003.
- [NOM02] Y. Nomoto, A. Ninomiya, and T. Ishigohka, "Fabrication and test of a superconducting generator with ring windings," *IEEE Trans. Appl. Supercond.*, vol. 12, no. 1, pp. 863-867, Mar. 2002.
- [OHA91] S. Fuchino, H. Fukuda, T. Ogawa, K. Shimizu, Y. Nakabayashi, Y. Kobayashi, M. Ogihara, Y. Kamisada, N. Maki, A. Ueda, and T. Matsuda, "Development of 70 MW class superconducting generators," *IEEE Trans. Magn.*, vol. 28, no. 1, pp. 279-282, Jan. 1992.
- [OKA85a] T. Okada, T. Nitta, T. Shintani, I. Muta, T. Ishigohka, and H. Fujino, "The basic test on the 20 KVA superconducting synchronous generator," *IEEE Trans. Magn.*, vol. 19, no. 3, pp. 1043-1046, May 1983.
- [OKA85b] T. Okada, T. Nitta, and T. Shintani, "On-load test of the 20kVA superconducting generator," *IEEE Trans. Magn.*, vol. 21, no. 2, pp. 668-671, Mar. 1985.
- [OKA87] T. Okada, T. Nitta, T. Shintani, "Transient performances of the 20 kVA superconducting synchronous generator in power systems," *IEEE Trans. Magn.*, vol. 23, no. 2, pp. 1340-1343, Mar. 1987.
- [ONL14a] Available: www.magnetlab.com
- [ONL14b] *SeaTitan™ 10MW wind turbine*, Available: www.amsc.com/documents/seatitan-10-mw-wind-turbine-data-sheet/
- [PAR75] J. H. Parker, R. D. Blaugher, A. Patterson, P. D. Vecchio, and J. L. McCabria, "A high speed superconducting rotor," *IEEE Trans. Magn.*, vol. MAG-11, no. 2, p. 640-645, Mar. 1975.
- [PAR79] J. H. Parker and R. A. Towne, "Design of large superconducting generators for electric utility application," *IEEE Trans. Power App. Syst.*, vol. PAS-98, no. 6, p. 2241-2250, Nov./Dec. 1979.
- [POD05] Podlesak, T.F.; Katsis, D.C.; Wheeler, P.W.; Clare, J.C.; Empringham, L.; Bland, M., "A 150-kVA vector-controlled matrix converter induction motor drive," *Industry Applications*, IEEE Transactions on , vol.41, no.3, pp.841,847, May-June 2005
- [QU13] R. H. Qu, Y. Z. Liu, and J. Wang, "Review of superconducting generator topologies for direct-drive wind turbines," *IEEE Trans. Appl. Supercond.*, vol. 23, no. 3, pp. 5201108-5201108, Jun. 2013.
- [REZ14] Reznik, A.; Simoes, M.G.; Al-Durra, A.; Muyeen, S.M., "Filter Design and Performance Analysis for Grid-Interconnected Systems," *Industry Applications, IEEE Transactions on*, vol.50, no.2, pp.1225,1232, March-April 2014
- [ROD07] J. Rodriguez, S. Bernet, Wu Bin, J. O. Pontt, S. Kouro, "Multilevel Voltage-Source-Converter Topologies for Industrial Medium-Voltage Drives," *IEEE Transactions on*

- [ROD12] Industrial Electronics, vol. 54, no. 6, pp.2930-2945, 2007.
Rodriguez, J.; Rivera, M.; Kolar, J.W.; Wheeler, P.W., "A Review of Control and Modulation Methods for Matrix Converters," *Industrial Electronics, IEEE Transactions on*, vol.59, no.1, pp.58,70, Jan. 2012
- [SEK00] S. Sekine, A. Ninomiya, and T. Ishigohka, "Fabrication and test of superconducting generator with ring windings," *IEEE Trans. Appl. Supercond.*, vol. 10, no. 1, pp. 943-936, Mar. 2000.
- [SEN09] O. S. Senturk, L. Helle, S. Munk-Nielsen, P. Rodriguez, R. Teodorescu, "Medium voltage three-level converters for the grid connection of a multi-MW wind turbine," in *Proc. EPE*, pp: 1- 8, 2009.
- [SEO14] J. H. Seo, K. J. Han, H. S. Choi, S. -H. Lee, S. Hahn, and H. Lee, "Comparison study on harmonic loss of MW-class wind generators with HTS field winding," *IEEE Trans. Appl. Supercond.*, vol. 24, no. 3, pp. 1-5, Jun. 2014.
- [SHA13] R. Shafaie and M. Kalantar, "Design of a 10-MW-class wind turbine HTS synchronous generator with optimized field winding," *IEEE Trans. Appl. Supercond.*, vol. 23, no. 4, pp. 5202307, Aug. 2013.
- [SHA14a] R. Shafaie, M. Kalantar, and A. Gholami, "Thermal analysis of 10-MW-class wind turbine HTS synchronous generator," *IEEE Trans. Appl. Supercond.*, vol. 24, no. 2, pp. 90-98, Apr. 2014.
- [SHA14b] R. Shafaie and M. Kalantar, "Comparison of theoretical and numerical electromagnetic 125odelling for HTS synchronous generator," *IEEE Trans. Appl. Supercond.*, Accepted, 2014.
- [SHI02] K. S. Ship, K. F. Goddard, and J. K. Sykulski, "Field optimisation in a synchronous generator with high temperature superconducting field winding and magnetic core," *4th Int. Conf. Computation in Electromagnetics*, Apr. 2002, pp. 8-11.
- [SHI04] K. S. Ship and J. K. Sykulski, "Field simulation studies for a high temperature superconducting synchronous generator with a coreless rotor," *IEE Proc. Sci. Measurement and Technology*, vol. 151, no. 6, pp. 414-418, Nov. 2004.
- [SHI99a] T. Shimada, M. Shibuya, R. Takahashi, Y. Imai, H. Kusafuka, R. Shiobara, K. Yamaguchi, M. Takahashi, K. Suzuki, and K. Miyaike, "Recent progress on 70 MW class superconducting generators," *IEEE Trans. Appl. Supercond.*, vol. 9, no. 2, pp. 1189-1192, Jun. 1999.
- [SHI99b] K. Shimohata, I. Kodera, M. Morita, T. Inaguchi, H. Yoshimura, S. Nakamura, S. Maeda, K. Suzuki, A. Ueda, and T. Hirao, "Cryogenic and electrical performance at a factory test of a rotor for 70 MW class slow-response excitation type superconducting generator," *IEEE Trans. Appl. Supercond.*, vol. 9, no. 2, pp. 1213-1216, Jun. 1999.
- [SHI13] M. F. Hsieh, C. K. Lin, and I. H. Lin, "Design and analysis of high temperature superconducting generator for offshore wind turbines," *IEEE Trans. Magn.*, vol. 49, no. 5, pp. 1881-1884, May 2013.
- [SIV09] K. Sivasubramaniam, T. Zhang, M. Lokhandwalla, E. T. Laskaris, J. W. Bray, B. Gerstler, M. R. Shah, and J. P. Alexander, "Development of a high speed HTS generator for airborne applications," *IEEE Trans. Appl. Supercond.*, vol. 19, no. 3, pp. 1656-1661, Jun. 2009.
- [SMI79] J. L. Smith. G. L. Wilson, J.L. Kirtley, "MIT-DOE program to demonstrate an advanced superconducting generator," *IEEE Trans. Magn.*, vol. MAG-15, no. 1, pp. 727-730, Jan. 1979.
- [SMI95] J. L. Smith, J. L. Kirtley, S. Sunder, and S. Umans, "Performance of MIT 10 MVA superconducting generator rotor," *IEEE Trans. Appl. Supercond.*, vol. 5, no. 2, pp. 445-448, Jun. 1995.
- [SNI05] G. Snitchler, B. Gamble, S. S. Kalsi, "The performance of a 5 MW high temperature superconductor ship propulsion motor," *IEEE Trans. Appl. Supercond.*, vol. 15, no. 2, pp. 2206-2209, Jun. 2005.
- [SNI10] G. Snitchler, "Progress on high temperature superconductor propulsion motors and direct drive wind generators," in *Proc. IPEC, 2010*, pp. 5-10.
- [SNI11] G. Snitchler, B. Gamble, C. King, and P. Winn, "10 MW class superconductor wind turbine generators," *IEEE Trans. Appl. Supercond.*, vol. 21, no. 3, pp. 1089-1092, Jun.

- 2011.
- [STA13] W. Stautner, R. Fair, K. Sivasubramaniam, K. Amm, J. Bray, E. T. Laskaris, K. Weeber, M. Douglass, L. Fulton, S. Hou, J. Kim, R. Longtin, M. Moscinski, J. Rochford, R. Rajput-Ghoshal, P. Riley, D. Wagner, and R. Duckworth, "Large scale superconducting wind turbine cooling," *IEEE Trans. Appl. Supercond.*, vol. 23, no. 3, pp. 520084, Jun. 2013.
- [STE64] Z. Stekly and H. H. Woodson, "Rotating machinery utilizing superconductors," *IEEE Trans. Aerosp.*, vol. 2, no. 3, pp. 1104-1105, Jul. 1964.
- [SUN13] H. J. Sung, G. H. Kim, K. Kim; S. J. Jung, M. Park, I. K. Yu, Y. G. Kim, H. Lee, and A. R. Kim, "Practical design of a 10 MW superconducting wind power generator considering weight issue," *IEEE Trans. Appl. Supercond.*, vol. 23, no. 3, pp. 520185, Jun. 2013.
- [TAK89] M. Takahashi, M. Watanabe, N. Takahashi, M. Kitamura, N. Maki, and M. Ooi, "Performance evaluations of 50 MVA airgap winding stator for superconducting generator," *IEEE Trans. Energy Conv.*, vol. 4, no. 2, pp. 264-272, Jun. 1989.
- [TAK95] H. Takigami, K. Nakanishi, H. Nakamura, S. Meguro, S. Akita, and S. Ohshima, "Development of a double stranded cable superconductor for 70 MW class superconducting generator with quick response type," *IEEE Trans. Appl. Supercond.*, vol. 5, no. 2, pp. 980-983, Jun. 1995.
- [TER12] Y. Terao, M. Sekino, and H. Ohsaki, "Electromagnetic design of 10 MW class fully superconducting wind turbine generators," *IEEE Trans. Appl. Supercond.*, vol. 22, no. 3, pp. 520194, Jun. 2012.
- [THU70] P. Thullen, J. L. Smith, and H. H. Woodson, "Economic and operational aspects of the application of superconductors in steam turbine generator field windings," 1970 *IEEE Winter Power Meeting*, Jan. 1970.
- [THU71] P. Thullen, J. C. Dudley, and D. L. Greene, "An experimental alternator with a superconducting rotating field winding," *IEEE Trans. Power App. Syst.*, vol. PAS-90, pp. 611-619, Mar./Apr. 1971.
- [TIX91] P. Tixador, Y. Brunet, P. Vadrine, Y. Laumond, J. L. Sabrie, "Electrical tests on a fully superconducting synchronous machine," *IEEE Trans. Magn.*, vol. 27, no. 2, pp. 2256-2259, Mar. 1991.
- [TON10] W. Tong, *Wind power generation and wind turbine design*, Southampton, UK:MIT, 2010, pp. 328.
- [TSU92] O. Tsukamoto, N. Amemiya, T. Takao, S. Akita, K. Ohishi, H. Shimizu, Y. Tanaka, and Y. Uchikawa, "Development of 30 kVA class fully superconducting generator," *IEEE Trans. Magn.*, vol. 28, no. 1, pp. 283-286, Jan. 1992.
- [TSU93] O. Tsukamoto, J. Chen, S. Akita, "Stability characteristics of fully superconducting and damperless generator connected to power grid," *IEEE Trans. Appl. Supercond.*, vol. 3, no. 1, pp. 377-380, Mar. 1993.
- [TSU97a] H. Tsukiji, T. Hoshino, E. Mukai, and I. Muta, "Fabrication and excitation testing of a fully superconducting brushless generator with magnetic flux pump," *Elect. Eng. Jpn.*, vol. 118, no. 4, pp. 35-45, Mar. 1997.
- [TSU97b] H. Tsukiji, T. Hoshino, I. Muta, and E. Mukai, "Electrical characteristics of a fully superconducting brushless generator equipped with a magnetic flux pump," *Elect. Eng. Jpn.*, vol. 120, no. 3, pp. 64-72, Aug. 1997.
- [UED99] K. Ueda, R. Shiobara, M. Takahashi, and T. Ageta, "Measurement and analysis of 70 MW superconducting generator constants," *IEEE Trans. Appl. Supercond.*, vol. 9, no. 2, pp. 1193-1196, Jun. 1999.
- [ULA80] A. H. M. S. Ula, J. L. Kirtley, J. L. Smith, "Demonstration of advanced concepts in a 10 MVA superconducting generator," *Proc. Int. Conf. Electrical Machines*, Sep. 1980.
- [UMA02] S. D. Umans and D. J. Driscoll, "Excitation system for rotating synchronous machines," U.S. Patent 6 362 588, Mar. 26, 2002.
- [UMA06] S. D. Umans and B. A. Shoykhet, "Quench in high-temperature superconducting motor field coils: experimental results," *IEEE Tran. Ind. Appl.*, vol. 42, no. 4, pp. 983-989, Jul./Aug. 2006.
- [WAN09] Y. Wang, R. Chen, J. Tan and M. Su, "An optimal PID control of wind generation based on matrix converter", in Proc. IEEE 6th International Power Electronics and Motion Control Conference (IPEMC), May 2009.
- [WAN14a] J. Wang, R. Qu, Y. Liu, J. He, Z. Zhu, and H. Fang, "Comparison study of

- superconducting wind generators with HTS and LTS field windings," *IEEE Trans. Appl. Supercond.*, Accepted 2014.
- [WAN14b] J. Wang, R. Qu; Y. Liu, and J. Li, "Study of multiphase superconducting wind generators with fractional-slot concentrated windings," *IEEE Trans. Appl. Supercond.*, vol. 24, no. 3, pp. 1-6, Jun. 2014.
- [WEI10] Xing Wei; Lan Xiao; Zhilei Yao; Chunying Gong, "Design of LCL filter for wind power inverter," *World Non-Grid-Connected Wind Power and Energy Conference (WNWEC)*, 2010, vol., no., pp.1,6, 5-7 Nov. 2010
- [WEN09] H. Wen, W. Bailey, K. Goddard, M. Al-Mosawi, C. Beduz, and Y. Yang, "Performance test of a 100kW HTS generator operating at 67K-77K," *IEEE Trans. Appl. Supercond.*, vol. 19, no. 3, pp. 1652-1655, Jun. 2009.
- [WEN11] H. Wen, W. Bailey, M. K. Al-Mosawi, K. Goddar, C. Beduz, and Y. Yang, "Further testing of an "iron-cored" HTS synchronous generator cooled by liquid air," *IEEE Trans. Appl. Supercond.*, vol. 21, no. 3, pp. 1163-1166, Jun. 2011.
- [WEN14] C. Wen, H. Yu, T. Hong, M. Hu, L. Huang, Z. Chen, and G. Meng, "Coil shape optimization for superconducting wind turbine generator using response surface methodology and particle," *IEEE Trans. Appl. Supercond.*, vol. 24, no. 3, pp. 1-4, Jun. 2014.
- [WHE02] Wheeler, P.W.; Rodriguez, J.; Clare, J.C.; Empringham, L.; Weinstein, A., "Matrix converters: a technology review," *Industrial Electronics, IEEE Transactions on* , vol.49, no.2, pp.276,288, Apr 2002
- [WON05] N. J. Won, S. Jeong, H. Kim, J. Jung, and Y. K. Kwon, "Investigation of on-board hybrid pulse tube cryocooler for high temperature superconducting rotor," *IEEE Trans. Appl. Supercond.*, vol. 15, no. 2, pp. 2190–2193, Jun. 2005.
- [WOO71] H. H. Woodson, J. L. Smith, P. Thullen, and J. L. Kirtley, "The application of superconductors in the field windings of large synchronous machines," *IEEE Trans. Power App. Syst.*, vol. PAS-90, pp. 620-627, Mar./Apr. 1971.
- [WU11] D. Wu and E. Chen, "Stator design for a 1000 kW HTSC motor with air-gap winding," *IEEE Trans. Appl. Supercond.*, vol. 21, no. 3, pp. 1093–1096, Jun. 2011
- [XU14] Y. Xu, N. Maki, and M. Izumi, "Electrical Design Study of 10-MW Salient-Pole Wind Turbine HTS Synchronous Generators," *IEEE Trans. Appl. Supercond.*, vol. 24, no. 6, pp. 1-6, Dec. 2014.
- [YAM84] K. Yamaguchi, N. Maki, S. Numata, H. Ogata, and T. Sanematsu, "Superconducting rotor development for a 50 MVA generator," *IEEE Trans. Power Eng. Rev.*, vol. PER-4, no. 7, pp. 53-54, Jul. 1984.
- [YAM89] K. Yamaguchi, N. Maki, and R. Shiobara, "Rotor design of a 1000MW superconducting generator," *IEEE Trans. Energy Convers.*, vol. 4, no. 2, pp. 244-249, Jun. 1989.
- [YAM93] K. Yamaguchi, Y. Yagi, R. Shiobara, S. Ohashi, H. Sato, K. Nakanishi, K.;Tanaka, M. Ohi, Y. Matsunobu, H. Tomeoku, N. Maki, and M. Ogihara, "Field winding model test of 70 MW class superconducting generator," *IEEE Trans. Appl. Supercond.*, vol. 3, no. 1, pp. 383-387, Mar. 1993.
- [YAM14] H. Yamasaki, N. Natori, and M. Furuse, "Evaluation of heat inleak in a model superconducting coil module for a wind turbine generator with iron cores," *IEEE Trans. Appl. Supercond.*, Accepted, 2014.
- [YIN81] A. Ying, P. W. Eckels, D. C. Litz, W. Moore, "Mechanical and thermal design of the EPRI/Westinghouse 300 MVA superconducting generator," *IEEE Trans. Magn.*, vol. 17, no. 1, pp. 894-899, Jan. 1981.
- [YOS91] H. Yoshimura, A. Ueda, M. Morita, S. Maeda, M. Nagao, K. Shimohata, Y. Matsuo, Y. Nagata, T. Yamada, and M. Tanaka, "Heater-induced quenches in a model field winding for the 70 MW class superconducting generator," *IEEE Trans. Magn.*, vol. 27, no. 2, pp. 2088-2091, Mar. 1991.
- [ZEN07] Xiangjun Zeng; Zhe Chen; Blaabjerg, F., "Design and comparison of full-size converters for large variable-speed wind turbines," *Power Electronics and Applications, 2007 European Conference on*, vol., no., pp.1,10, 2-5 Sept. 2007
- [ZHA00] B. Zhang, D. Driscoll, and V. Dombrovski, "Development status of a 1,000 HP superconducting motor," *IEEE Cement Industry Technical Conf.*, 2000, pp. 81-85.
- [ZHU13a] Z.Q. Zhu, Jiabing Hu, (2013) "Electrical machines and power-electronic systems for high-power wind energy generation applications: Part I – market penetration, current

- technology and advanced machine systems", COMPEL - The international journal for computation and mathematics in electrical and electronic engineering, Vol. 32 Iss: 1, pp.7 - 33
- [ZHU13b] Z.Q. Zhu, Jiabing Hu, (2013) "Electrical machines and power-electronic systems for high-power wind energy generation applications: Part II – power electronics and control systems", COMPEL - The international journal for computation and mathematics in electrical and electronic engineering, Vol. 32 Iss: 1, pp.34 - 71
- [ZHU14] Z. Zhu, R. Qu, and J. Wang, "Conceptual design of the cryostat for a direct-drive superconducting wind generator," *IEEE Trans. Appl. Supercond.*, vol. 24, no. 3, pp. 1-4, Jun. 2014.

APPENDIX I. CHARACTERISTIC OF SC MATERIAL

Table 43. *Current density – flux density characteristic of SC material (30K)*

Normal flux density (T)	Critical current density (A/mm ²)	Normal flux density (T)	Critical current density (A/mm ²)
0.5	736.8	2.357	347.5
1	528.3	2.5	333.6
1.5	430.9	3.5	278.0
2	375.3	4.5	237.7

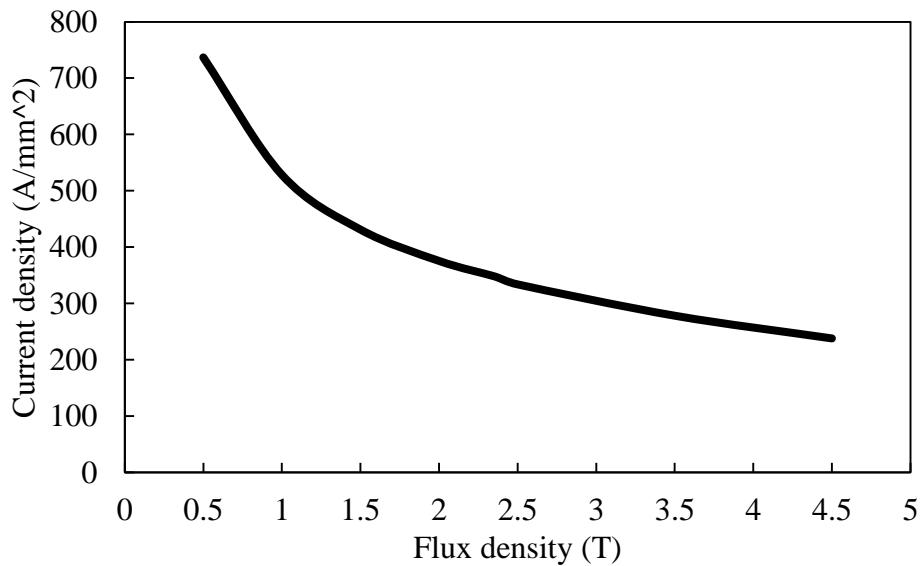


Fig. 93 Variation of engineering critical current with normal flux density in SC material, temperature=30K.

APPENDIX II. SPECIFICATIONS OF LAMINATION

A. Loss characteristic

Table 44. Loss characteristic of lamination 50JN600

B(T)	W/m ³ 50Hz	W/m ³ 60Hz	W/m ³ 100Hz
0	0	0	0
0.3	/	/	5000
0.4	/	/	7750
0.5	5250	7250	12000
0.6	7100	9100	15750
0.7	9250	11000	20750
0.8	11000	13850	26250
0.9	13000	17250	32250
1	15750	20000	39000
1.1	19000	23800	46250
1.2	22250	27500	56000
1.3	25500	32500	65250
1.4	30000	38250	76150
1.5	35500	44750	90000
1.6	41000	51000	
1.7	47500	58600	

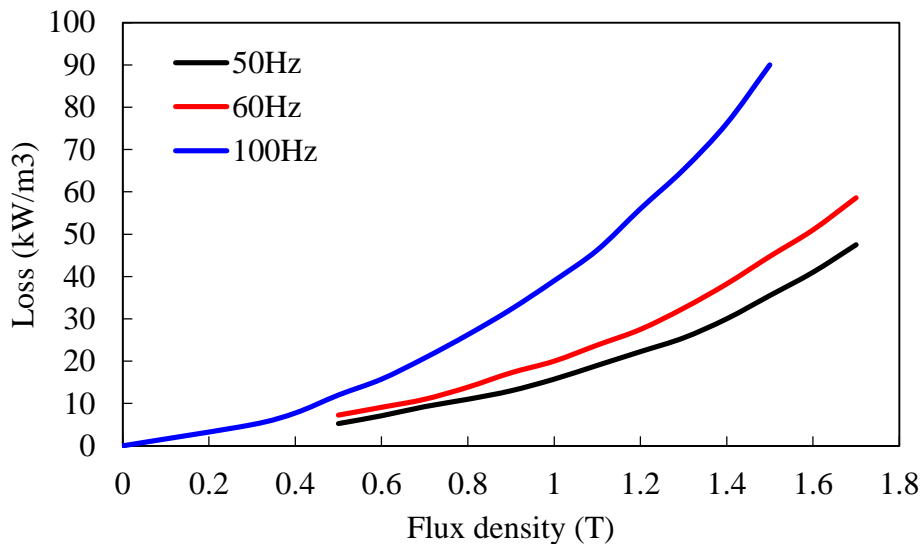


Fig. 94 Variations of losses with flux density of 50JN600

B. B-H characteristic

Table 45. *B-H characteristic of lamination*

B (T)	H (A/m)	B (T)	H (A/m)	B (T)	H (A/m)
0	0	0.9	112.3638	1.8	8032.124
0.1	12.48487	1	127.3051	1.9	13680.28
0.2	24.96974	1.1	147.5272	2	24355.32
0.3	37.45462	1.2	177.8143	2.1	44047.03
0.4	49.93949	1.3	229.0948	2.2	79659.84
0.5	62.42436	1.4	342.6318	2.3	143727.9
0.6	74.90923	1.5	697.926	2.4	223305.4
0.7	87.3941	1.6	1793.44	2.5	302882.9
0.8	99.87897	1.7	4046.7		

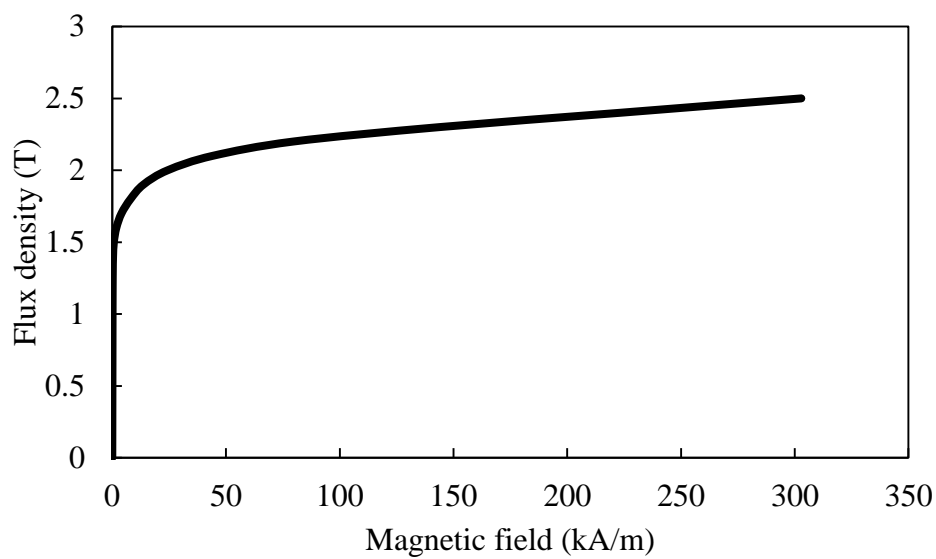


Fig. 95 *B-H curve of lamination.*

APPENDIX III. REQUIREMENTS OF 10MW DIRECT-DRIVE SC GENERATORS

Table 46. Requirements and limitations of SC wind power generation drive train

System output power (MW)	10 (to be scaled up to 20 @ 6.8rpm)
Rotor speed (rpm)	9.6
Estimated air gap torque (MNm) - based on 95% efficiency	10.5
Mechanical air gap (mm)	0.1% of air gap diameter
Target energy cost (€/MWh/yr)	53.3
Current density in stator winding (A/mm ²)	3.5
Current density in SC coils (A/mm ²) - it is significantly affected by temperature.	See Fig. 96
Torque ripple	<1% rated
Maximum field voltage	3300V
DC link voltage/power ripple	<1%
Cost of energy (€/kW)	0.05

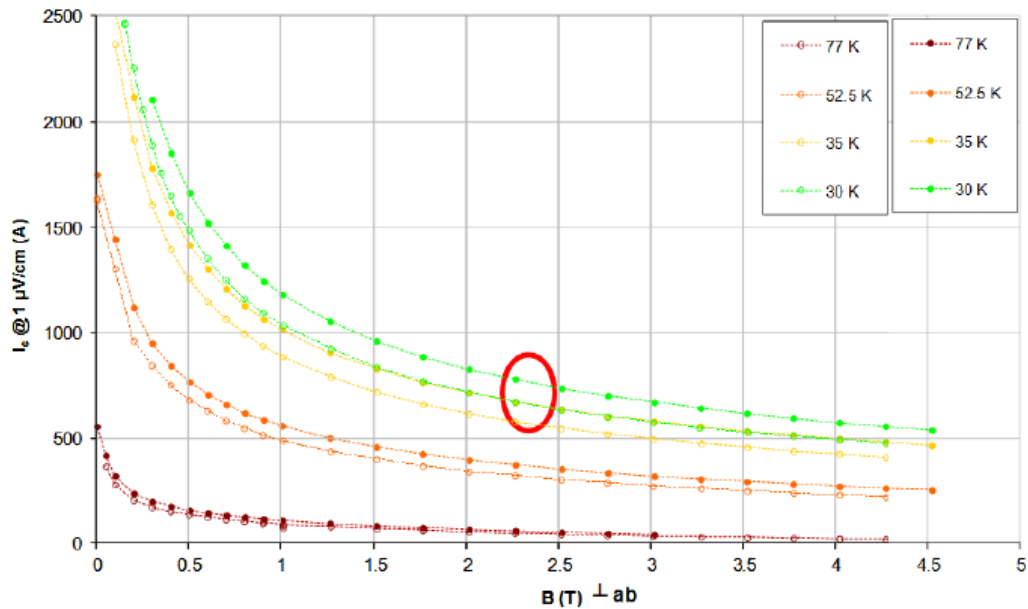


Fig. 96 Variation of critical current with temperature and perpendicular field.

For each design, only b_s changes and other parameters are not changed. The maximum possible b_s is preferable to improve the torque.

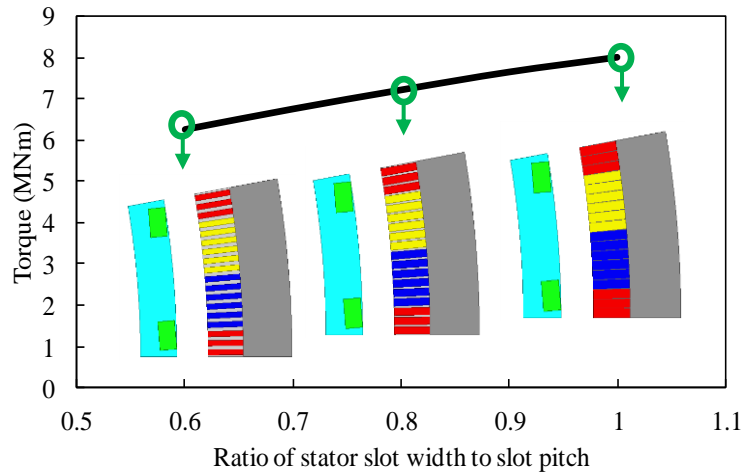


Fig. 98 Variation of torque with ratio of stator slot width to slot pitch. The optimized parameters include b_{sc} , h_{sc} , h_s , and h_{yi} ; Optimization condition: $P_{Cu}=85\text{kW}$, $S_{Sc}/\text{pole}=3000\text{mm}^2$, $J_{Sc}=300\text{A}/\text{mm}^2$.

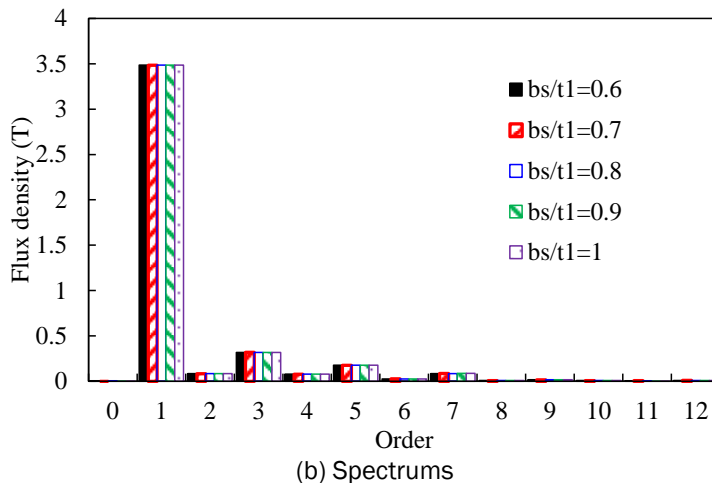
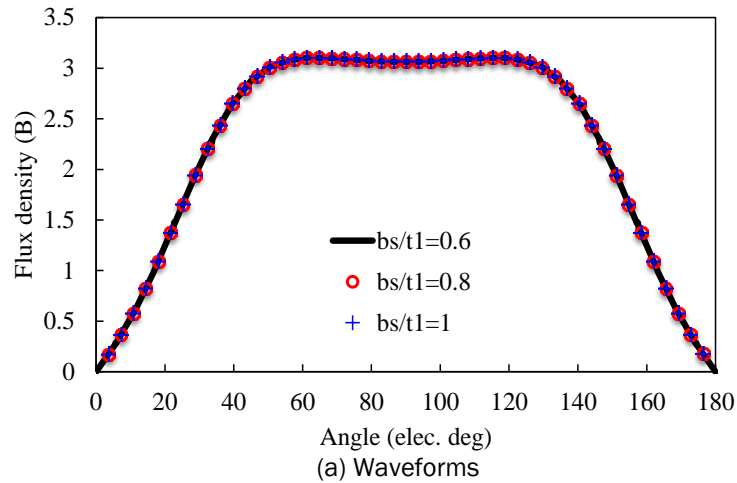


Fig. 99 Waveforms and spectrums of flux density in the middle of airgap.

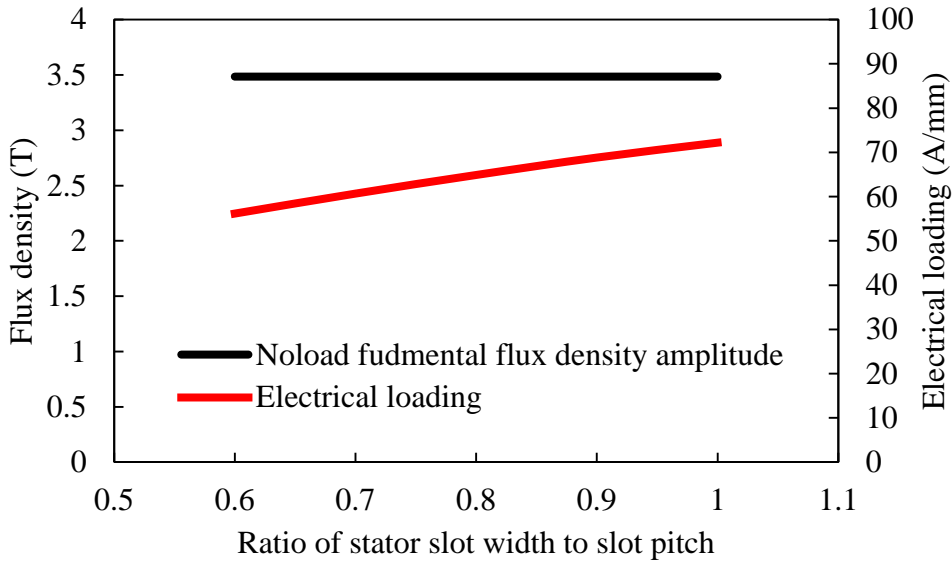


Fig. 100 Variations of amplitude of fundamental flux density in the middle of airgap and electrical loading with ratio of stator slot width to slot pitch.

IV.3 Influence of stator slot width

For each h_s , the parameters b_{sc} , h_{sc} , b_s , h_{yi} are optimized globally to maximize the torque. The variation of torque with h_s is shown in Fig. 101. There exists an optimal h_s to achieve the maximum possible torque. As h_s increases, the effective airgap (airgap between SC coils and stator yoke) increases, Fig. 101, thus, flux density in the airgap decreases, Fig. 102. However, the electrical loading increases with h_s , Fig. 103. Consequently, there exists an optimal h_s to achieve the maximum torque.

The optimal h_s and h_{yi} for each design are interrelated, seen from Fig. 101.

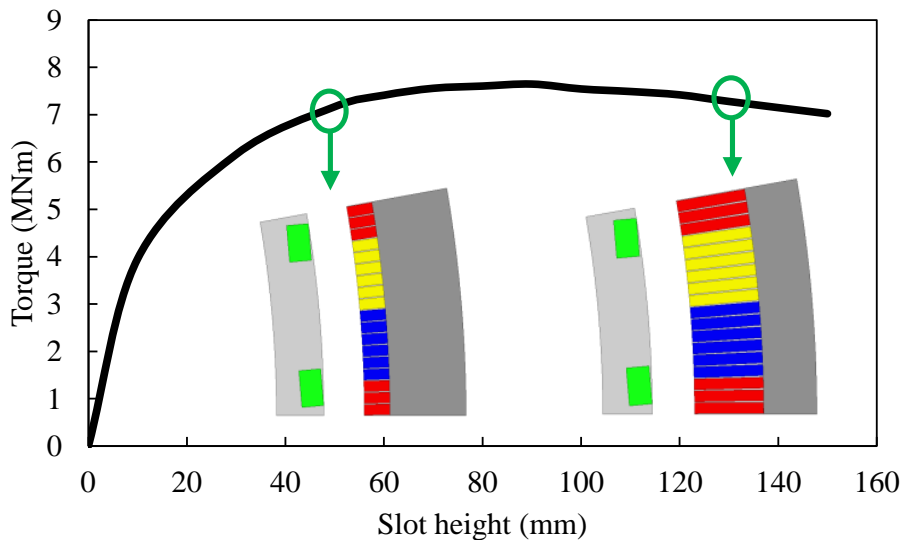


Fig. 101 Variation of torque with stator slot height. The optimized parameters include b_{sc} , h_{sc} , b_s , and h_{yi} ; Optimization condition: $P_{cu}=85\text{kW}$, $S_{sc}/\text{pole}=3000\text{mm}^2$, $J_{sc}=300\text{A}/\text{mm}^2$.

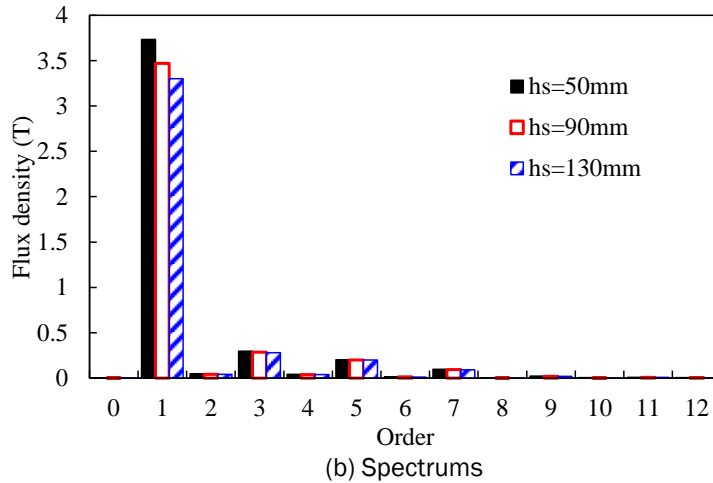
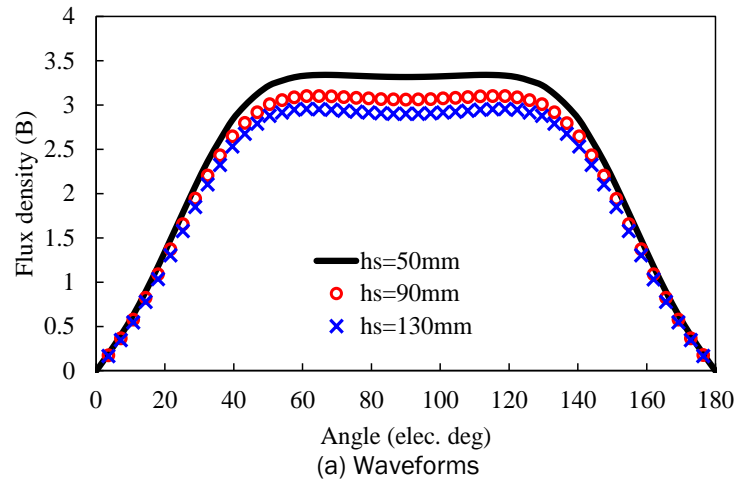


Fig. 102 Waveforms and spectrums of flux density in the middle of airgap.

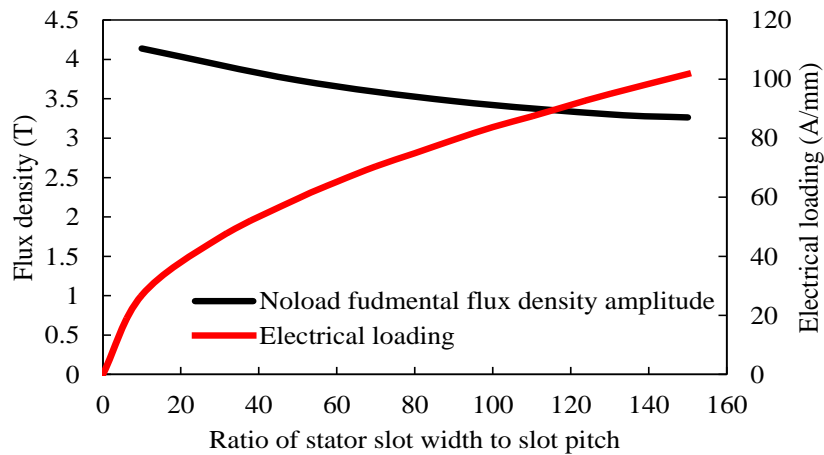


Fig. 103 Variations of amplitude of fundamental flux density in the middle of airgap and electrical loading with stator slot height.

IV.4 Influence of stator yoke thickness

For each h_{yi} , the parameters b_{sc} , h_{sc} , b_s , h_s are optimized globally to maximize the torque. The variation of torque with h_{yi} is shown in Fig. 104. There exists an optimal h_{yi} to achieve the maximum possible torque. As h_{yi} increases, the flux density in the airgap increases, Fig. 105. However, the electrical loading decreases, Fig. 106, because the stator slot area decrease, Fig. 104. Consequently, there exists an optimal h_{yi} to achieve the maximum torque.

The optimal h_s and h_{yj} for each design are interrelated, seen from the cross sections in Fig. 104.

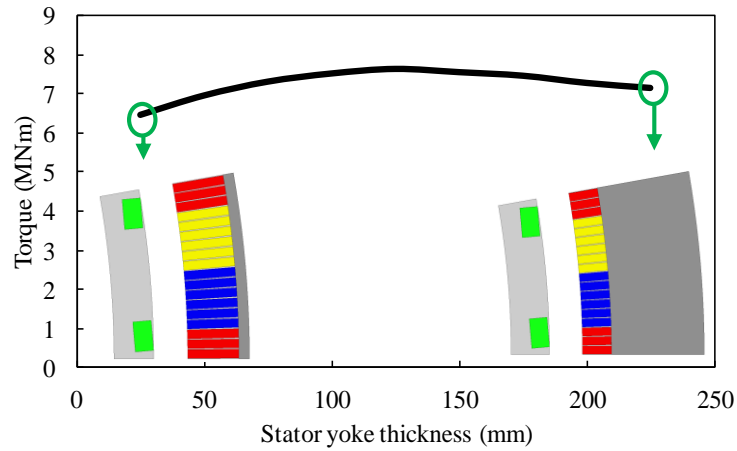


Fig. 104 Variation of torque with stator yoke thickness. The optimized parameters include b_{sc} , h_{sc} , b_s , and h_s ; Optimization condition: $P_{Cu}=85\text{kW}$, $S_{Sc}/\text{pole}=3000\text{mm}^2$, $J_{sc}=300\text{A}/\text{mm}^2$.

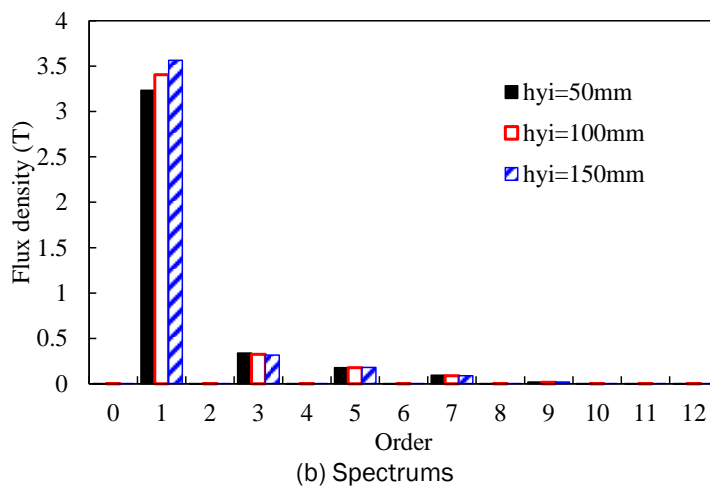
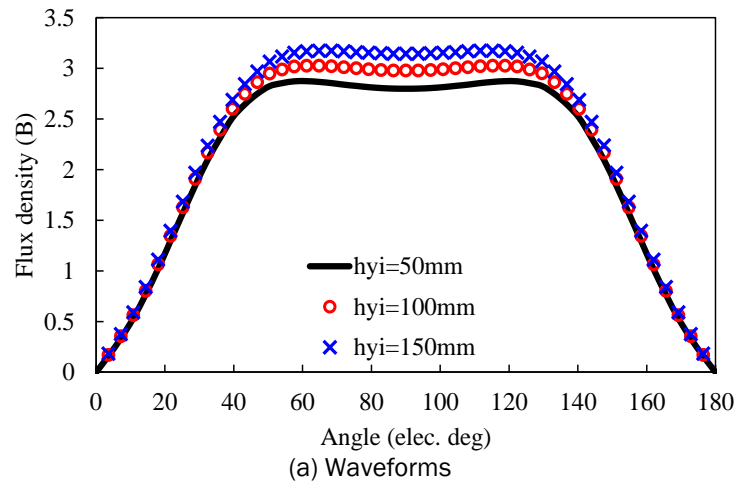


Fig. 105 Waveforms and spectrums of flux density in the middle of airgap.

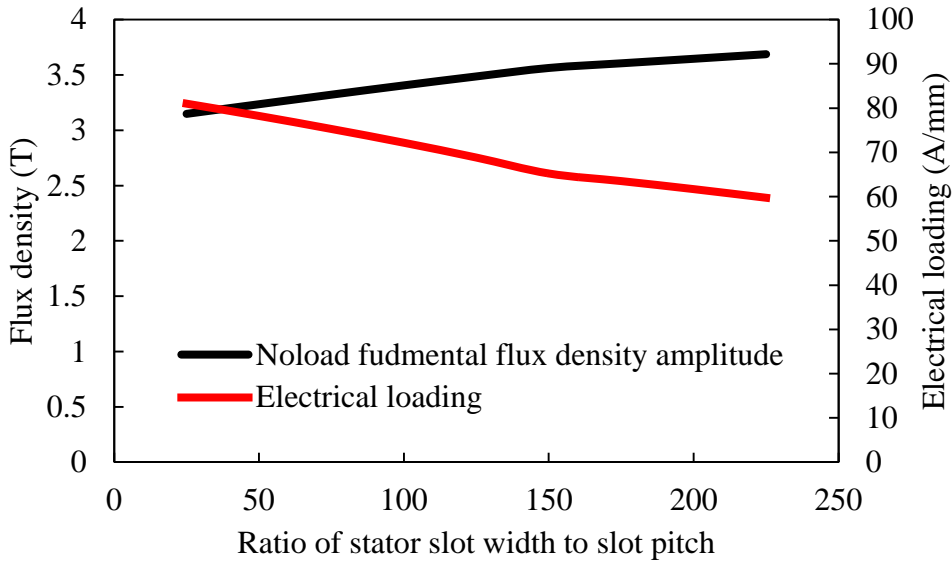


Fig. 106 Variations of amplitude of fundamental flux density in the middle of airgap and electrical loading with stator yoke thickness.

IV.5 Influence of SC Coil Pitch

For each SC coil pitch, the parameters b_{sc} , h_{sc} , b_s , h_{yi} are optimized globally to maximize the torque. The variation of torque with SC coil pitch is shown in Fig. 107. The torque increases with SC coil pitch. As SC coil pitch increases, the flux density in the airgap increases, Fig. 108. The electrical loading does not vary with SC coil pitch, Fig. 109. Consequently, torque increases with SC coil pitch. The maximum possible SC coil pitch is desirable to maximize torque capability.

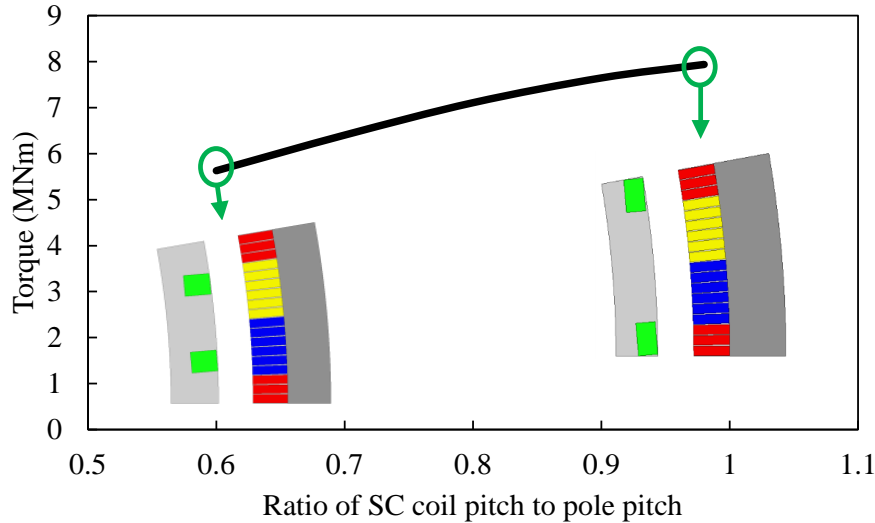


Fig. 107 Variation of torque with SC coil pitch. The optimized parameters include b_{sc} , h_{sc} , b_s , and h_{yi} ; Optimization condition: $P_{cu}=85\text{kW}$, $S_{sc}/\text{pole}=3000\text{mm}^2$, $J_{sc}=300\text{A}/\text{mm}^2$.

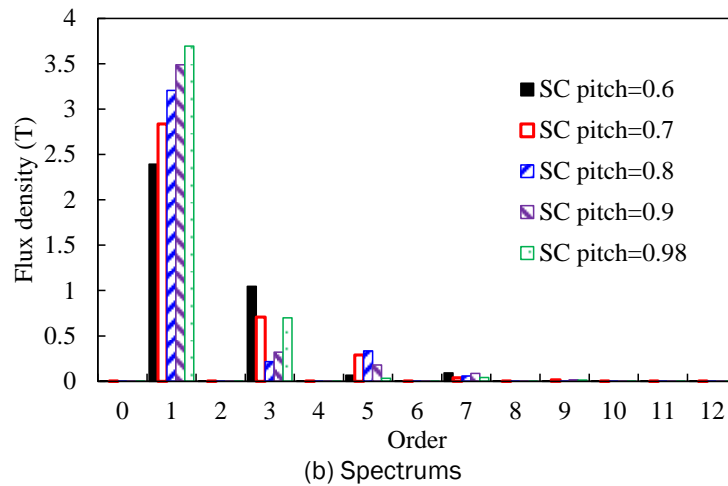
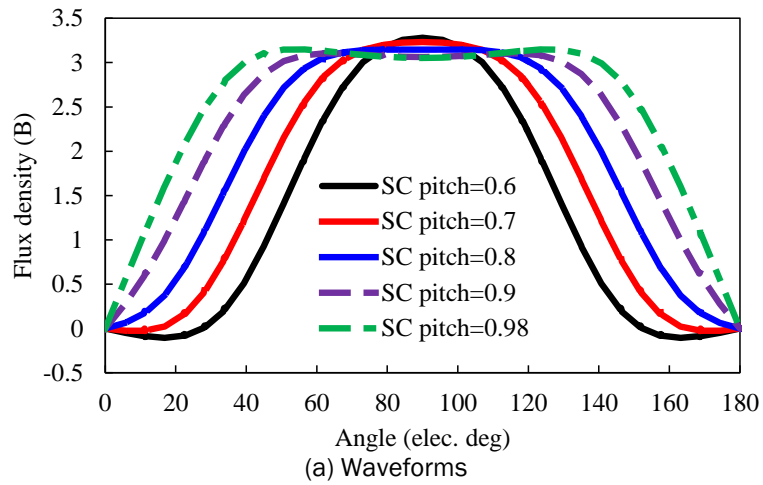


Fig. 108 Waveforms and spectrums of flux density in the middle of airgap.

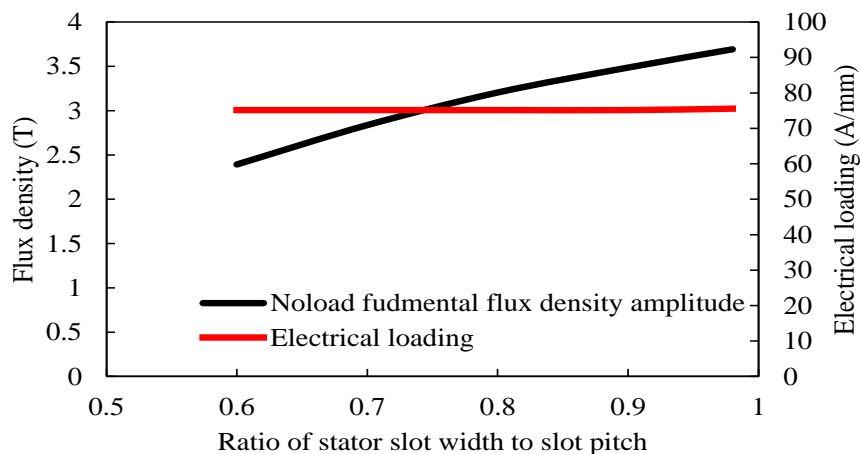


Fig. 109 Variations of amplitude of fundamental flux density in the middle of airgap and electrical loading with SC coil pitch.

IV.6 Influence of Copper Loss

For each P_{Cu} , the parameters b_{sc} , h_{sc} , b_s , h_s , h_{yi} are optimized globally to maximize the torque. The variation of torque with SC coil pitch is shown in Fig. 110. The torque increases with P_{Cu} . The reason can be easily explained, and it is due the increase of electrical loading.

The SC generators optimized with different P_{Cu} have identical geometry, Fig. 110.

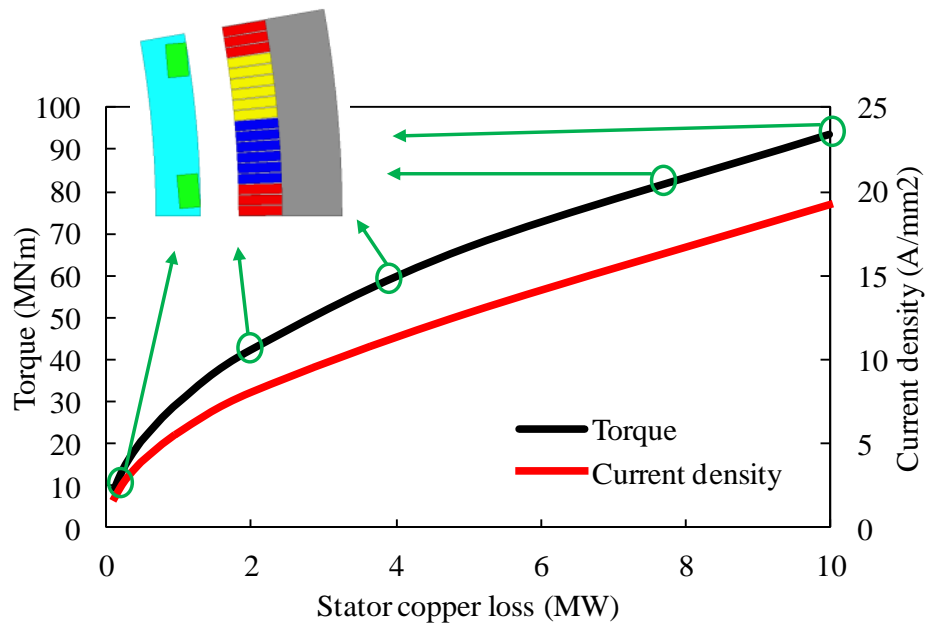


Fig. 110 Variation of torque with stator copper loss. The optimized parameters include b_{sc} , h_{sc} , b_s , h_s , and h_{yl} ; Optimization condition: $P_{cu}=85\text{kW}$, $S_{sc}/\text{pole}=3000\text{mm}^2$, $J_{sc}=300\text{A}/\text{mm}^2$.

IV.7 Influence of Pole Number

IV.A. Determination of SC current density

For each $2p$, the total S_{sc} of the whole cross section of SC generator is fixed, which is 2916cm^2 . Thus, the cross section area of each SC coil varies with $2p$. The varied SC coil cross section area has a significant influence on the self-induced field in SC coils. For a SC material, the critical engineering current density, flux densities (components perpendicular and parallel to the surface of SC tapes respectively) and temperature are always interrelated. Consequently, the S_{sc} and J_{sc} are closely related and correct J_{sc} should be imposed on SC coil. In this optimization, the temperature is assumed to be 30K , and only the perpendicular flux density B_{\perp} is considered, since B_{\perp} is more dominant for the influence on current density.

The variation of induced maximum B_{\perp} in SC with J is shown as the blue dashed line in Fig. 111, which is linear and termed as load $J-B_{\perp}$. The red dashed line in the figure is the $J-B_{\perp}$ characteristic of SC involving a 22% safety margin. The J for the cross point of load $J-B_{\perp}$ and $J-B_{\perp}$ characteristic is determined as the operation current density of SC coil, in order to fully and safely utilize the SC material.

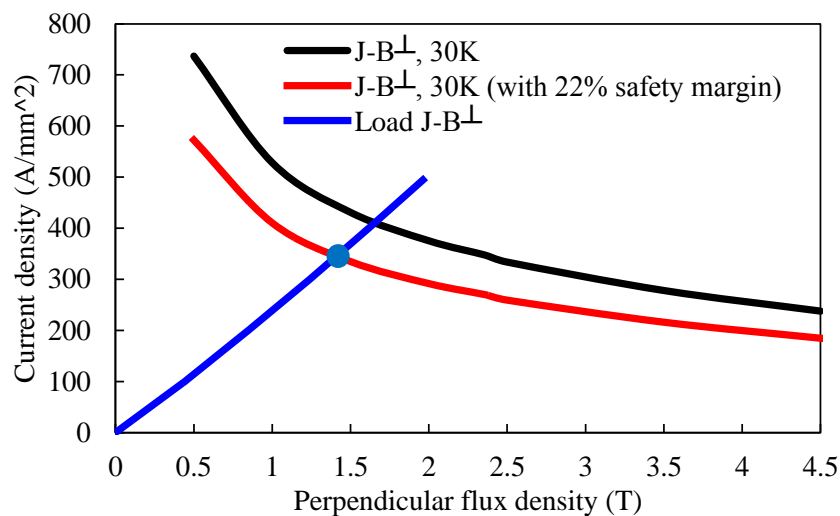


Fig. 111 Variations of current density with perpendicular flux density in SC, B_{\perp} is the amplitude of flux density perpendicular to the surface of SC tapes, Load $J-B_{\perp}$ is the variation of current density with maximum self-induced B_{\perp} in SC.

IV.B. Influence on torque

For each $2p$, P_{Cu} (without end winding) and total S_{SC} are fixed, which are 200 kW and 2916 cm² respectively. The parameters h_s , h_{yi} , J_{SC} are optimized globally to maximize the torque. The variation of torque with $2p$ is shown in Fig. 112. As $2p$ increases, the ratio of g to pole pitch increases, consequently, more flux produced by SC coils is leaked, as shown in the flux line figures in Fig. 112. Thus, the torque decreases as $2p$ increases.

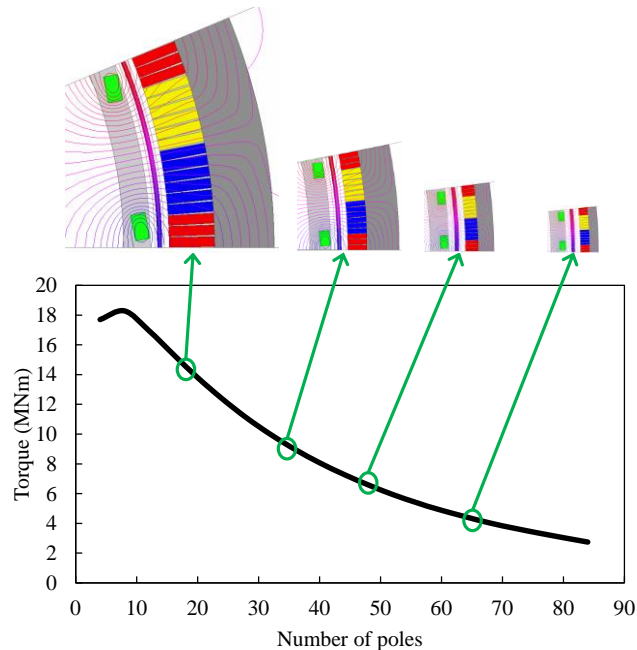


Fig. 112 Variation of torque with pole number. The optimized parameters include b_s , h_s , and J_{SC} ; Optimization condition: $b_{sc}/h_{sc}=2$, $P_{Cu}=200\text{kW}$, $S_{SC}/\text{pole}=291600/(2p)\text{ mm}^2$.

IV.C. Influence on torque per generator volume

As $2p$ increases, the axial length of armature winding decreases, further the total axial length of generator decreases, as shown in Fig. 113, which means the total volume of generator decreases. When the torque in Fig. 112 is divided by the volume, the torque per generator volume is obtained, as shown in Fig. 114. There exists an optimal $2p$ for the torque per generator volume. The optimal $2p$ (for torque per generator volume) is larger than $2p$ (for torque).

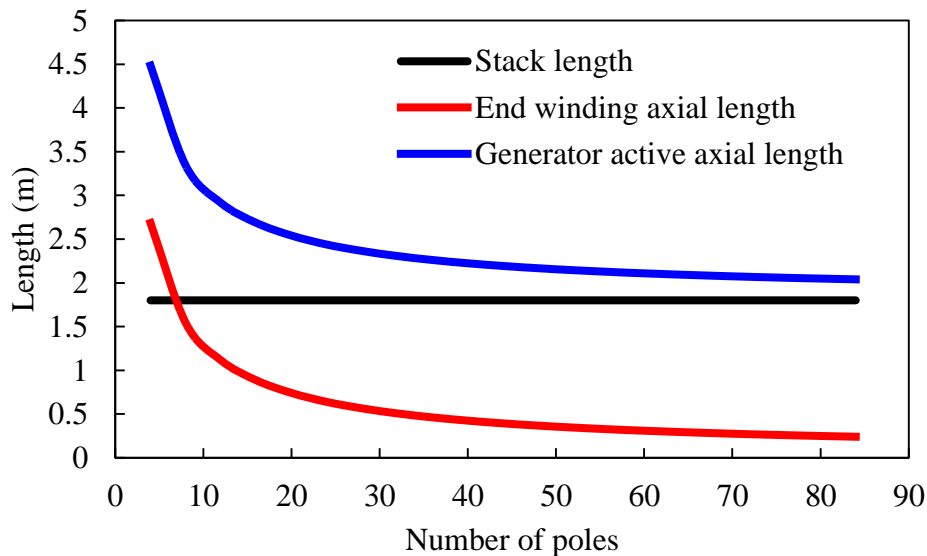


Fig. 113 Variation of armature winding axial length with pole number.

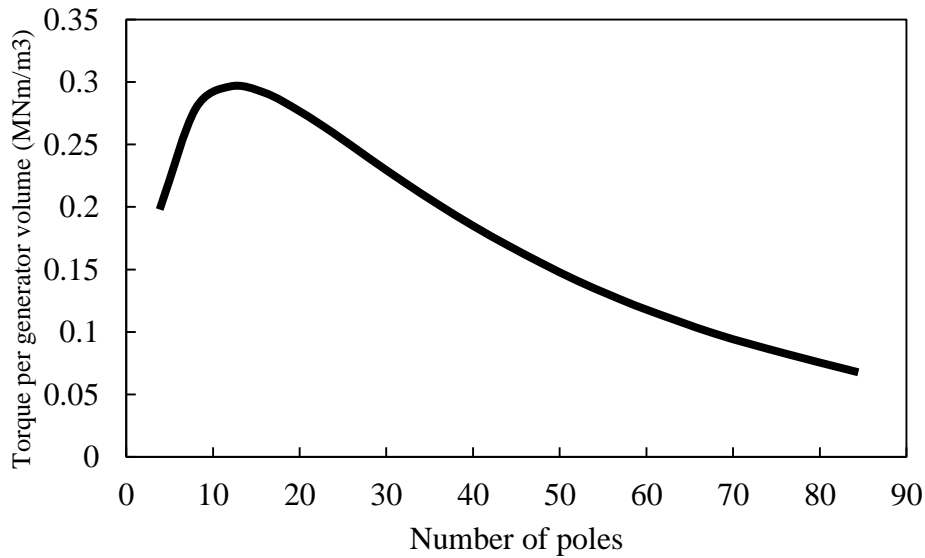


Fig. 114 Variation of torque per generator volume with pole number.

IV.D. Influence on torque per SC volume

During the investigation, the volume of SC coil straight section is not changed, because the total S_{SC} in the cross section of whole generator is fixed. However, the volume of end coil decreases as $2p$ increases. Consequently, the total volume of SC coils decreases, Fig. 115. When the torque in Fig. 112 is divided by SC volume in Fig. 115, the torque per SC volume is obtained, as shown in Fig. 116. There exists an optimal $2p$ for torque per SC volume. The optimal $2p$ (for torque per SC volume) is larger than $2p$ (for torque).

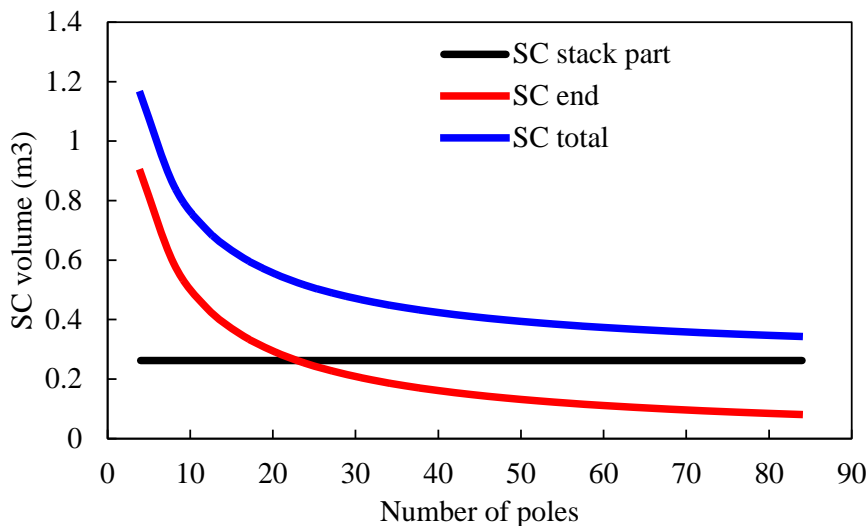


Fig. 115 Variation of SC material volume with pole number, SC stack part is the straight section of SC coil, SC end is the end section of SC coil, SC total means the whole SC coil.

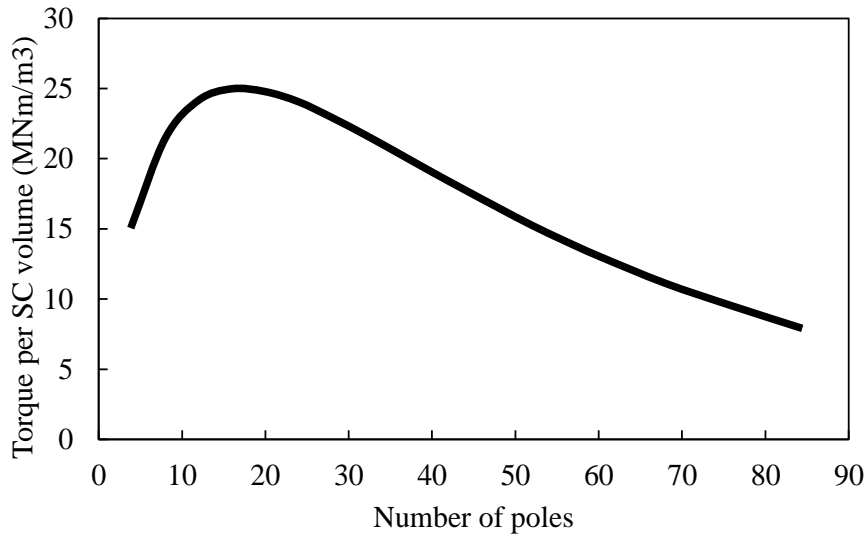


Fig. 116 Variation of torque per SC volume with pole number.

IV.E. Influence on torque per iron mass

The variation of iron mass with pole number is shown in Fig. 117. As $2p$ increases, the iron mass reduces, because the thickness of stator yoke decreases. When the torque in Fig. 112 is divided by the iron mass, the torque per iron mass is obtained, as shown in Fig. 118. There exists an optimal $2p$ for torque per iron mass. The optimal $2p$ (for torque per iron mass) is larger than $2p$ (for torque).

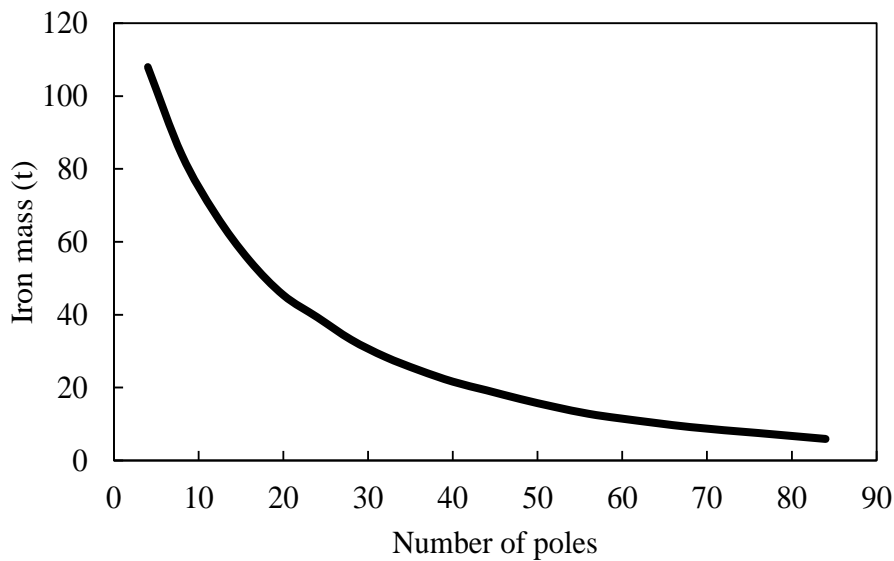


Fig. 117 Variation of iron mass with pole number.

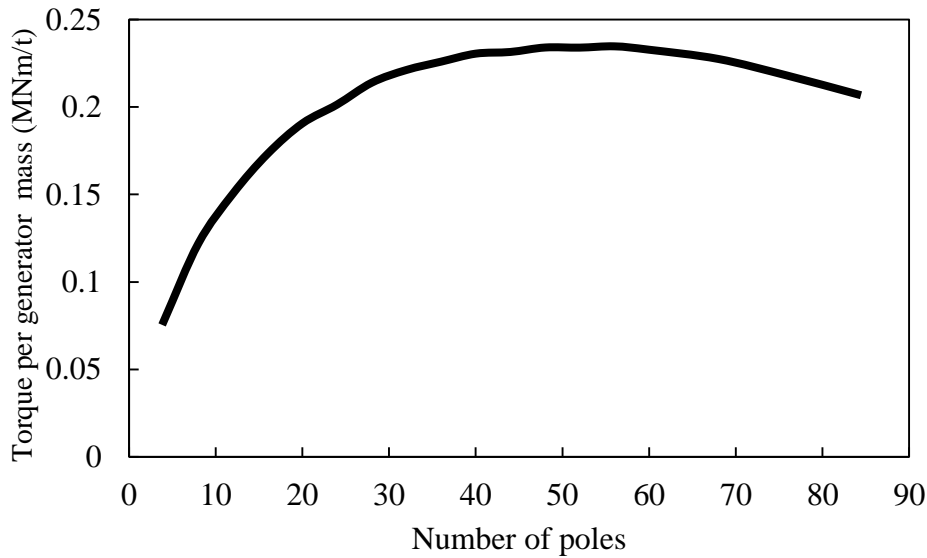


Fig. 118 Variation of torque per generator mass with pole number.

IV.F. Summary

The scaled torque per generator volume, torque per generator mass (only iron mass included), torque per SC volume and efficiency are shown in Fig. 119. A lower $2p$ is preferable (12~16), from the view of torque per generator volume, SC utilization and efficiency, etc. A higher $2p$ favours to reduce the generator mass. This conclusion is close to that of Converteam project and some studies conducted in Japan, which showed the optimal pole number for SC generator for direct-drive wind turbines is 16~20 [TON10].

The pole numbers of SC generator designs in literature are summarized in Fig. 120 ([FAI12] [LIU14a] [LIU14b] [KAL14] [SUN13] [TON10] [TER12] [FUK11] [SHA13]). The choices of $2p$ of different affiliations are quite different.

In this report, the influence of pole number on performances is carried out with the condition that the total S_{sc} of the cross section of generator is fixed. It is worth conducting the investigation with a different condition that the S_{sc} per pole is fixed. It is not conducted in this project due to the large amount of work.

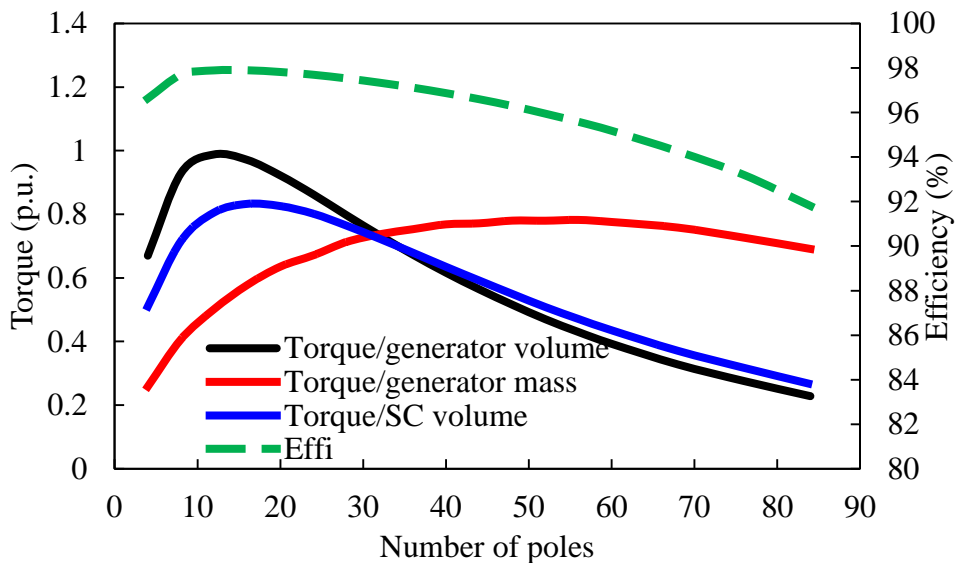


Fig. 119 Variations of torque per generator volume, torque per generator mass (only iron mass included), torque per SC volume and efficiency with pole number. The base values for torque per volume, per mass and per SC volume are 0.3MNm/m^3 , 0.3MNm/t , 30MNm/m^3 respectively.

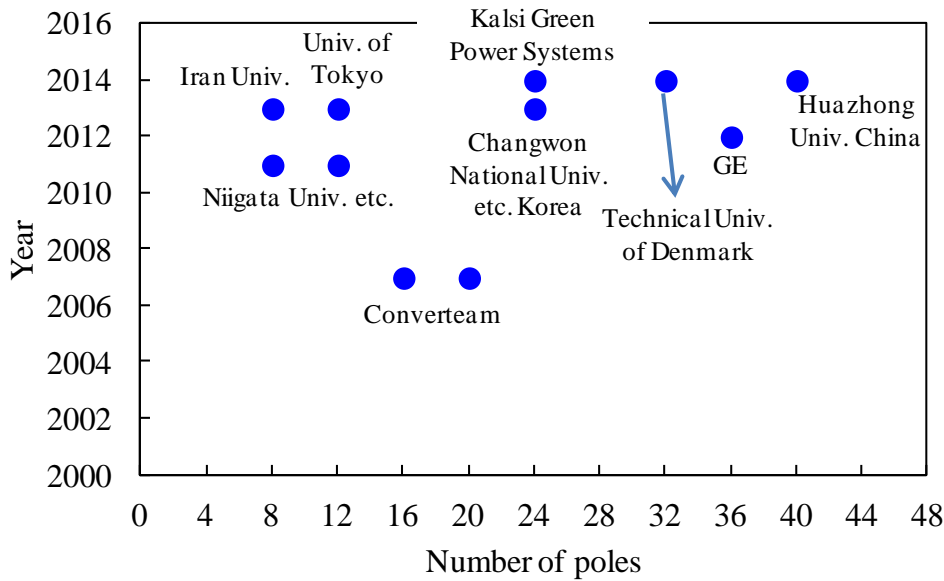


Fig. 120 Summary of the pole numbers of SC generator in literature.

IV.8 Influence of SC Coil Width to Height

The variation of torque with ratio of SC coil width to height is shown in Fig. 121. As the ratio increases, the SC coil becomes closer to armature winding, which favours to reduce the effective airgap length and increase the torque, but the SC coil pitch decreases as well, which tends to reduce the torque capability, as shown in section 0. Thus, there exists an optimal b_{sc}/h_{sc} to achieve the maximum torque. However, the ratio does not affect the torque significantly over a large range. In order to reduce the number of parameters and simplify the optimization process, the ratio can be fixed between 1 and 2.

During the investigation, the B_{\perp} related J_{sc} is considered, as shown in Fig. 122.

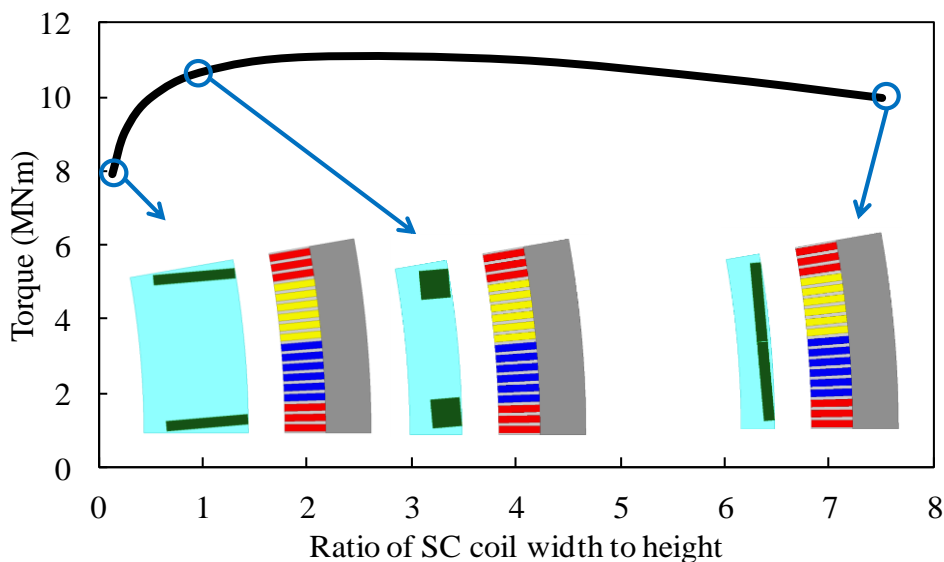


Fig. 121 Variation of torque with ratio of SC coil width to height. The optimized parameters include b_s , h_s , and J_{sc} ; Optimization condition: $P_{Co}=200\text{kW}$, $S_{Sc}/\text{pole}=8090\text{mm}^2$.

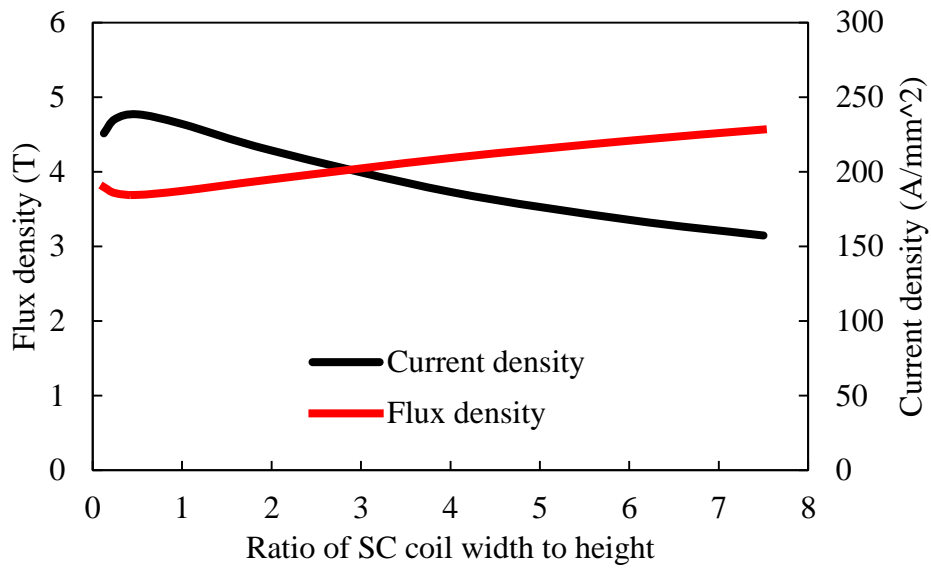


Fig. 122 Variation of maximum B_{\perp} and current density in SC with ratio of SC coil width to height.

APPENDIX V. COMPARISON BETWEEN SC GENERATORS WITH IRON-CORE STATOR AIR-CORE ROTOR AND AIR-CORE STATOR AIR-CORE ROTOR TOPOLOGIES

In this chapter, 10MW SC generators with iron-core stator air-core rotor and air-core stator air-core rotor topologies are designed respectively, to satisfy the requirements in Appendix III. The stator outer diameter and pole number are 5 m and 32 respectively, without optimization. The optimization process of other parameters is the same as that for iron-core stator and rotor topology in Chapter 2, section 3.1.1. The flowchart of optimization is shown in Fig. 23.

The cross sections of optimized SC generators are shown in Fig. 123. The flux density distributions are shown in Fig. 124. The highest flux density is 5.6~5.9T. For SC material, the perpendicular flux density is more dominant for the influence on SC material performance. The perpendicular flux density distributions are shown in Fig. 125. The positions of maximum perpendicular is 4.5~4.7T.

The parameters are listed in Table 48. When iron is utilized as stator teeth, the flux density in the air gap can be improved, as shown in Fig. 126, further the torque density can be improved. Consequently, the stack length of iron-core stator topology is shorter, as listed in Table 48 (1.26m vs 1.59m). However, due to the non-continuity of air gap reluctance, the cogging of iron-core stator is much larger, as shown in Fig. 128, and the no load voltage is not as sinusoidal as that of air-core stator topology Fig. 127. In addition, the torque ripple of iron-core stator topology is much larger, Fig. 129 (13.7% vs 0.6%). For the design of iron-core stator topology, some strategies have to be adopted to reduce the torque ripple.

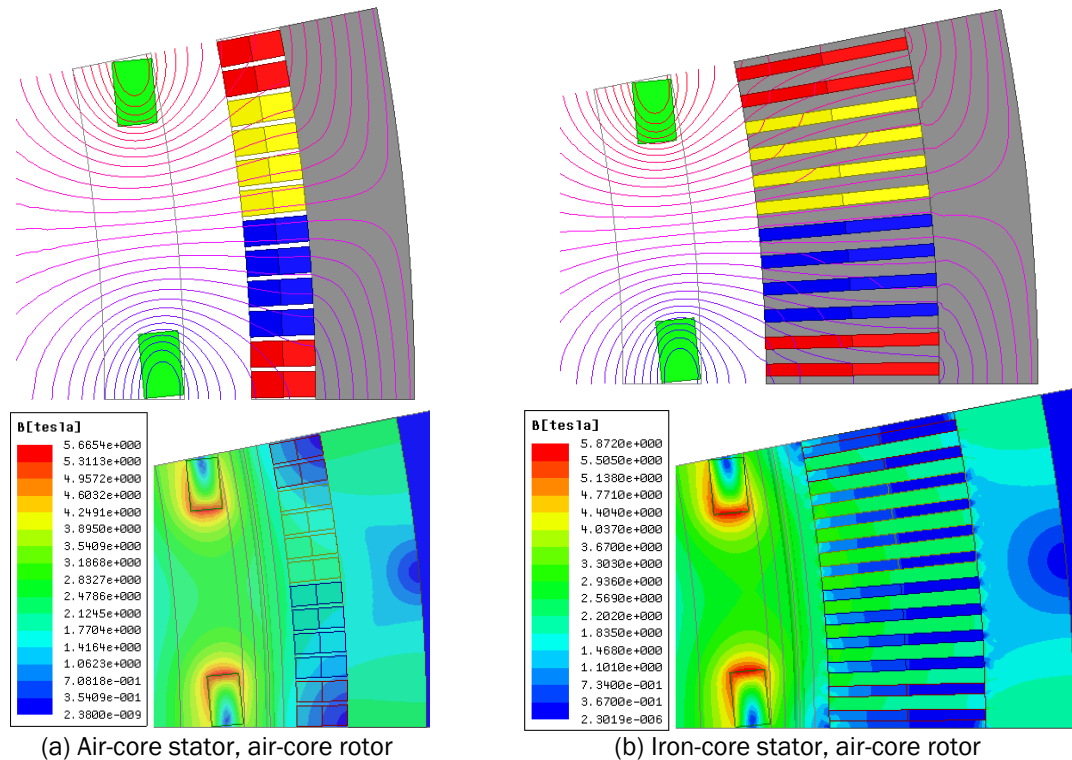


Fig. 123 Flux lines and flux density distributions, no load.

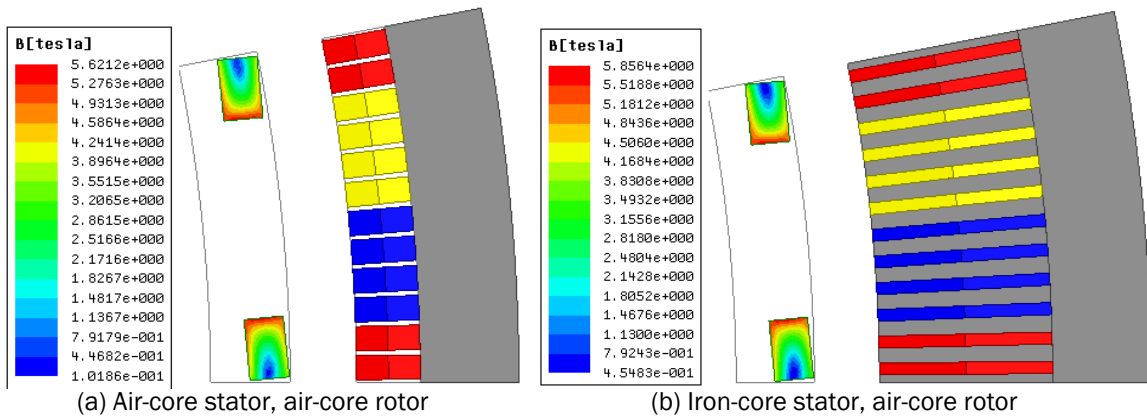


Fig. 124 Flux density distributions in SC coil, no load.

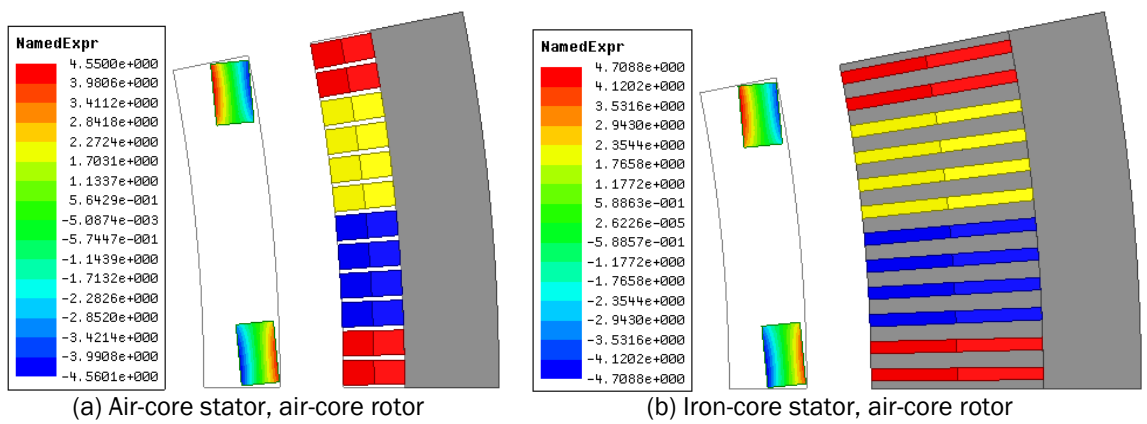


Fig. 125 Perpendicular flux density distributions in SC coil, no load.

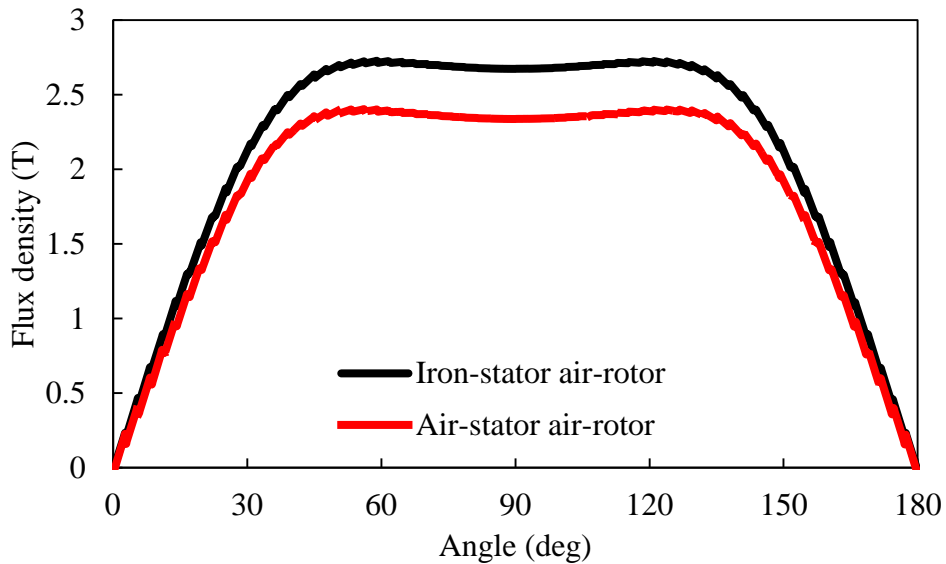


Fig. 126 Flux density in the middle of air gap.

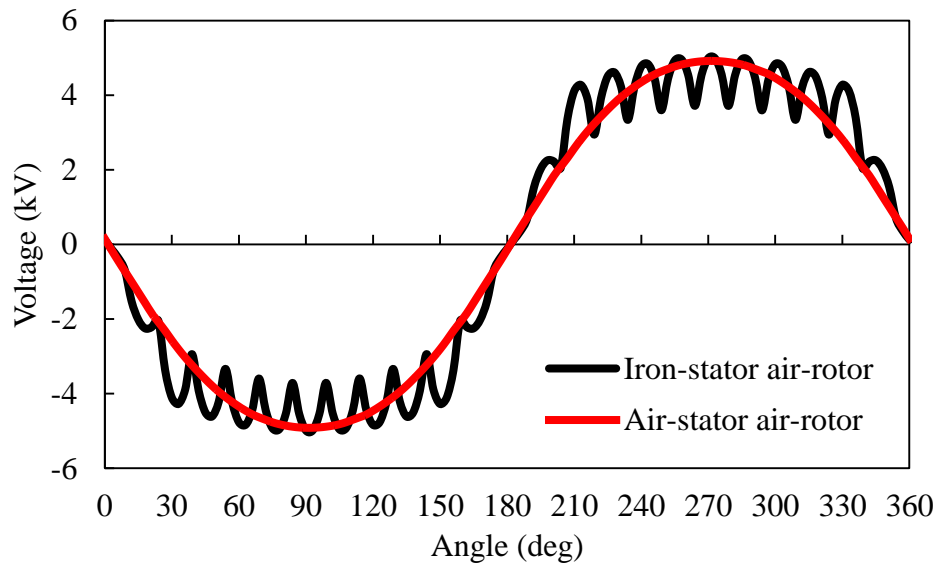


Fig. 127 Phase voltage.

Table 48. Parameters of 10MW SC generator

	Air-core stator Air-core rotor	Iron-core stator Air-core rotor
Stator outer diameter D	5m	5m
Stack length L	1.59m	1.26m
Speed n	9.6rpm	9.6rpm
Torque T_{em}	10.5MNm	10.5MNm
Line voltage U_{ab} (no load)	3.27Vrms	3.2Vrms
Stator phase current I_a	1806Arms	1982Arms
Stator current density J_s	3.5A/mm ²	3.5A/mm ²
Stator phase resistance R_s	0.0759 Ω	0.0662 Ω
Copper loss P_{Cu} (DC loss)	454Kw	454Kw
Stator slot packing factor	0.6	0.6
Number of poles $2p$	32	32
Number of stator slots Q	384	384
Air gap length g	9mm	9mm
SC current density J_{sc}	186A/mm ²	186A/mm ²
SC area per pole	8000mm ²	8000mm ²
Length of SC wire	270km	196km
Dimensions of cross section of SC coil	80mm×50mm	80mm×50mm
Stator yoke thickness h_{yl}	125mm	125mm
Stator slot dimension	31.9mm×80.8mm	15.8mm×224mm
Ampere turns of SC per pole	744,000AT	744,000AT
Max. B_{\perp} in SC	4.55T	4.7T
Torque ripple (peak to peak)	0.6%	13.7%
Number of conductions per slot	22	30
Number of parallel branches	8	8
Cost of SC (million €)	24	19.6
Cost of Cu (million €)	0.098	0.098
Cost of iron (million €)	0.059	0.062
Cost of total (million €)	24.127	19.75

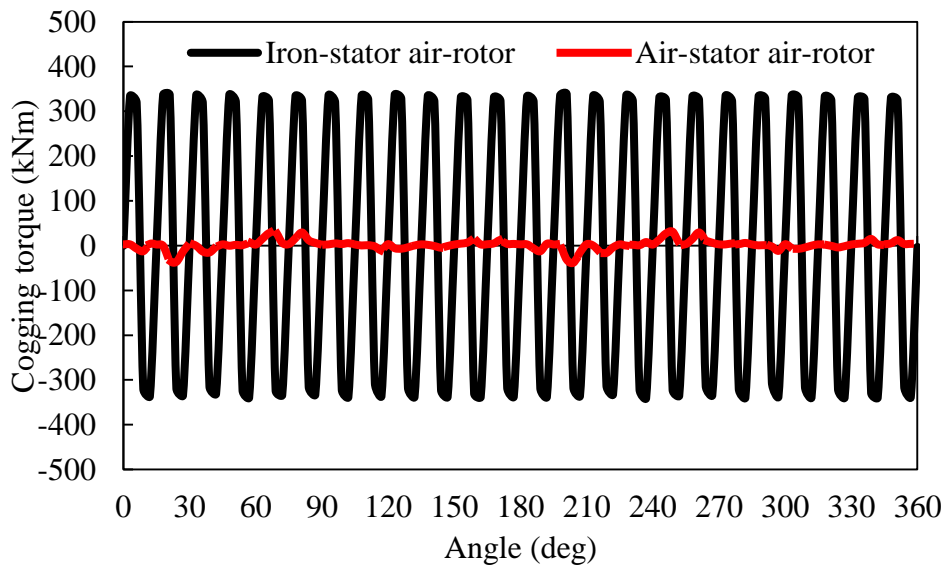


Fig. 128 Cogging torque.

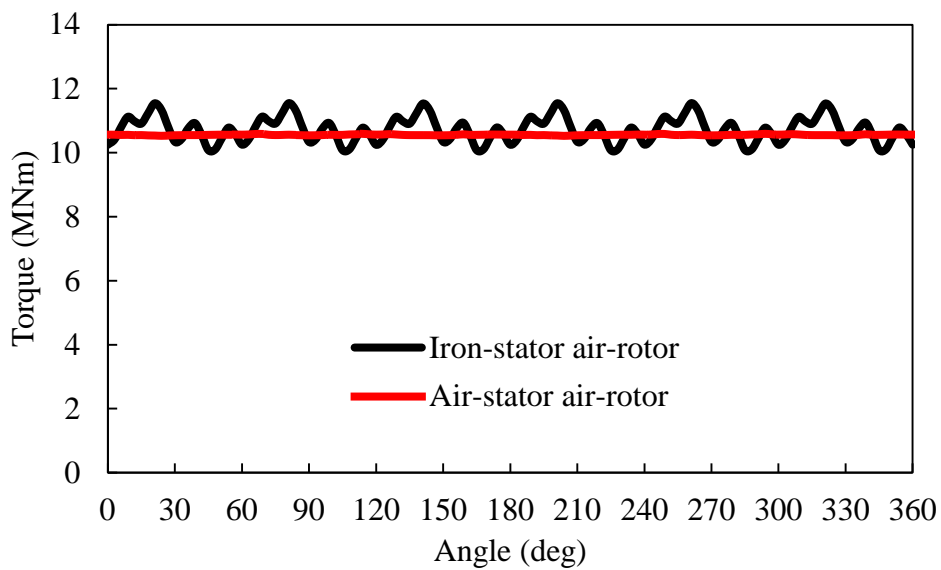


Fig. 129 Rated torque.

APPENDIX VI. ANALYSIS OF SC GENERATORS WITH IRON-AIR-COMBINED TEETH

The analysis for two different topologies, i.e. air-cored rotor and iron-cored rotor.

VI.1 SC Generator with Air-Cored Rotor

The cross section of air-cored rotor SC generator with iron-air-combined tooth topology is shown in Fig. 130. If the ratio of iron to total tooth height is 0.5, the waveform and spectrum of rated torque are shown in Fig. 131. It is found that the average torque is decreased a little, while the torque ripple is reduced a lot. The waveform and spectrum of cogging torque are shown in Fig. 132. The cogging torque is decreased significantly, because the discontinuity is reduced as parts of teeth are replaced by air. The variations of average torque and torque ripple with iron tooth height are shown in Fig. 133.(a). The ratio of iron to total tooth height influences average torque a little bit, but affects the torque ripple a lot. There exists a knee point for the variation of torque ripple. The variations of major torque ripple components (6th and 36th) and cogging torque with the ratio are shown in Fig. 133 (b). It shows that the large torque ripple is mainly due to 36th component, which is caused by cogging torque. The knee point for the variation of torque ripple is also due to the knee point for cogging torque.

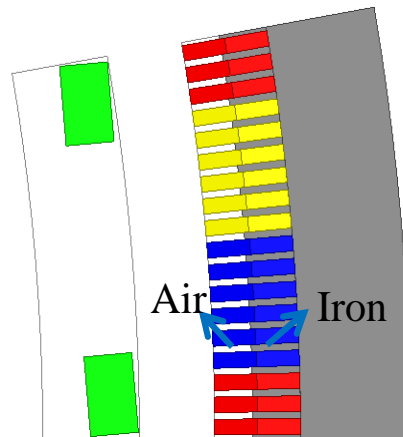


Fig. 130 Cross section of air-cored rotor SC generator with iron-air-combined teeth.

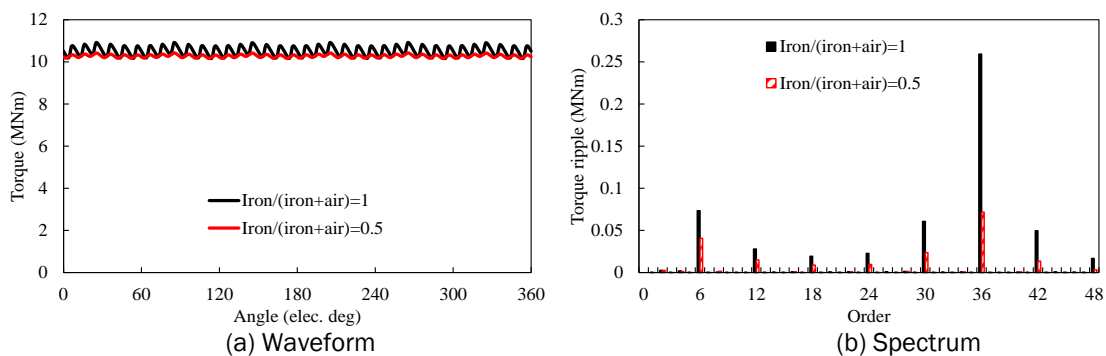


Fig. 131 Waveforms and spectrums of torque ripple, iron/(iron+air) is the ratio of iron tooth height to total tooth height.

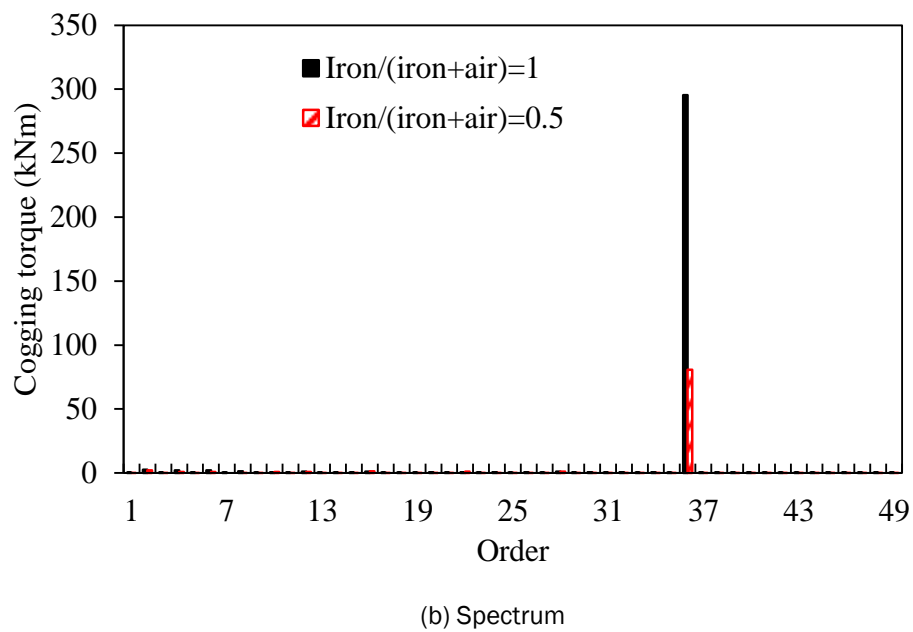
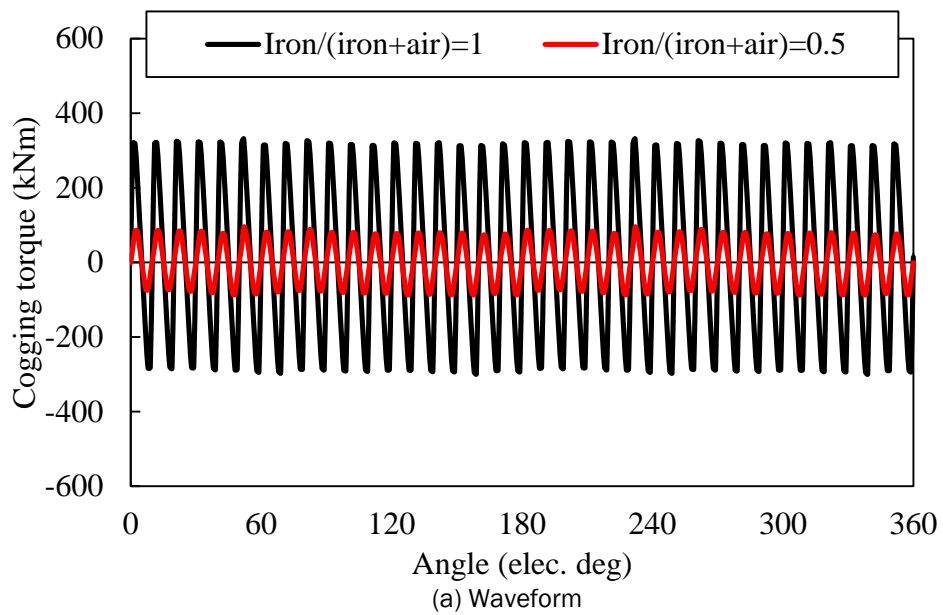
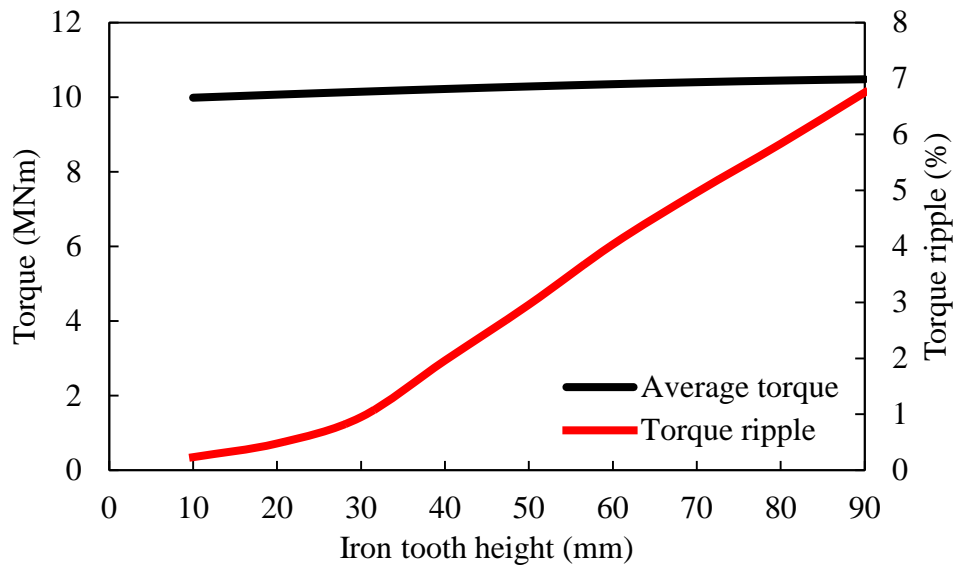
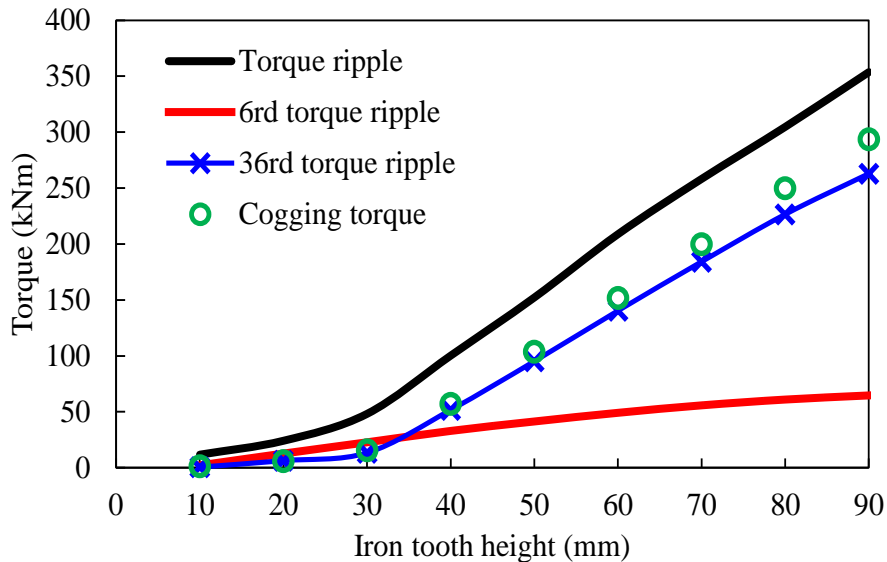


Fig. 132 Waveforms and spectrums of cogging torque.



(a) Average torque and peak to peak torque ripple



(b) Peak to peak torque ripple, 6th and 36th torque ripple and cogging torque
 Fig. 133 Variations of average torque and torque ripple with iron tooth height.

VI.2 SC Generator with Iron-Cored Rotor

The cross section of iron-cored rotor SC generator with iron-air-combined tooth topology is shown in Fig. 134. The waveforms and spectrums of rated torque, cogging torque of iron-cored rotor SC generator with the ratio of iron to total tooth height 0.94 are shown in Fig. 135 and Fig. 136. The variations of average torque and torque ripple with iron tooth height are shown in Fig. 133. The influence of combined tooth topology for iron-cored rotor SC generator on average torque is much larger than that for air-cored rotor topology, because the saturation level of teeth of air-cored rotor topology is higher than that of iron-cored rotor topology, 2T vs 3T. Thus, the less saturated teeth influence reluctance a lot, further affects torque capability a lot. Although the combined tooth can still reduce torque ripple a lot, it may not be suitable for iron-cored rotor topology.

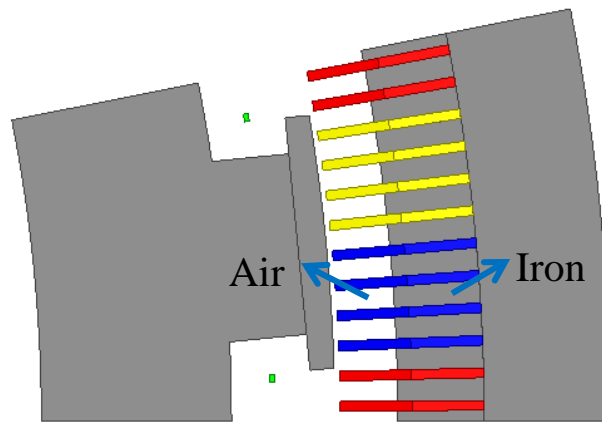
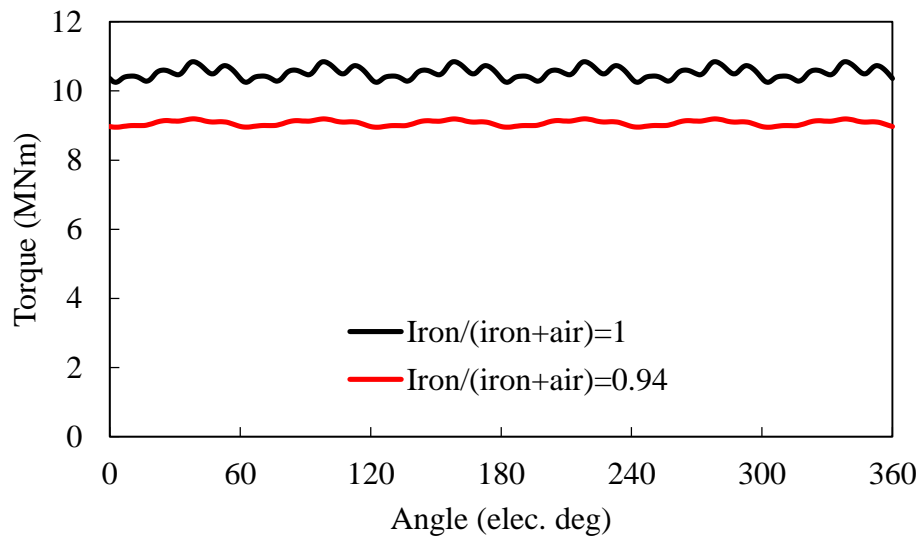
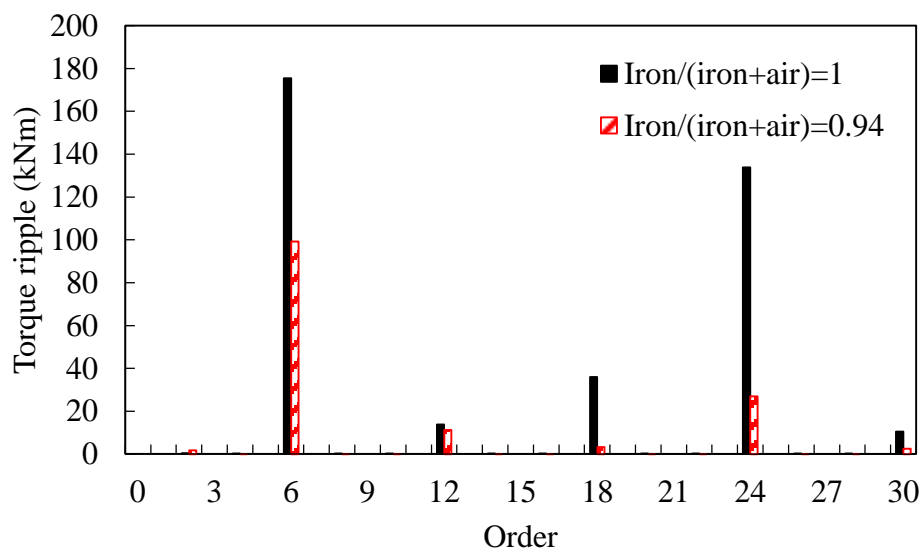


Fig. 134 Cross section of air-cored rotor SC generator with iron-air-combined teeth.

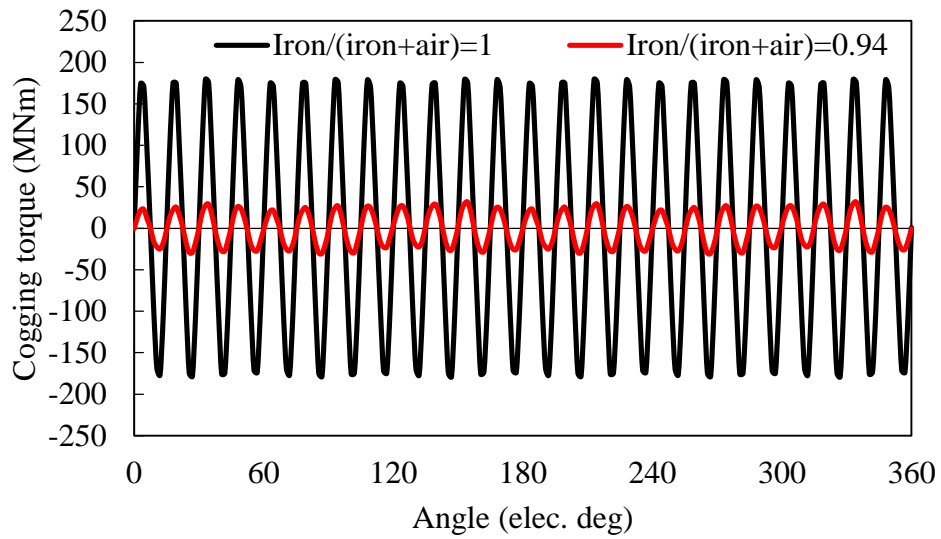


(a) Waveform

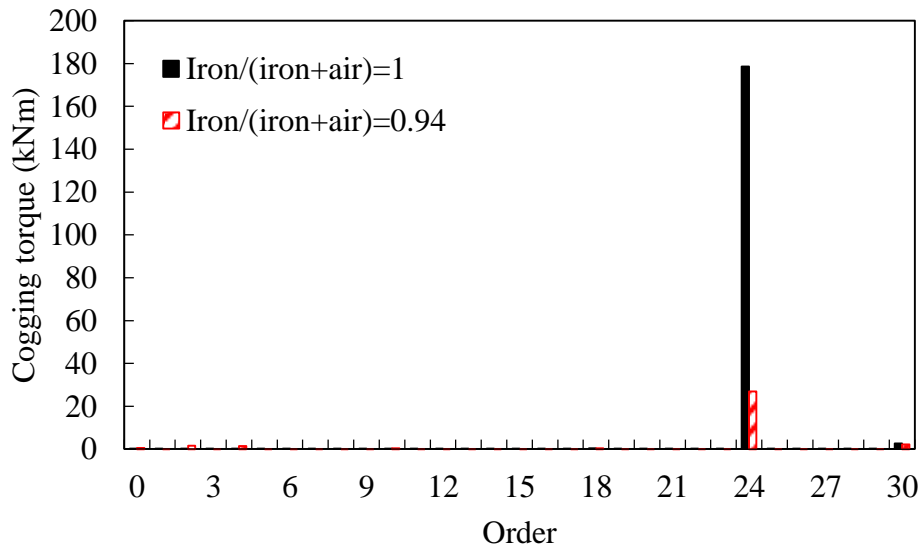


(b) Spectrum

Fig. 135 Waveforms and spectrums of torque ripple, iron/(iron+air) is the ratio of iron tooth height to total tooth height.

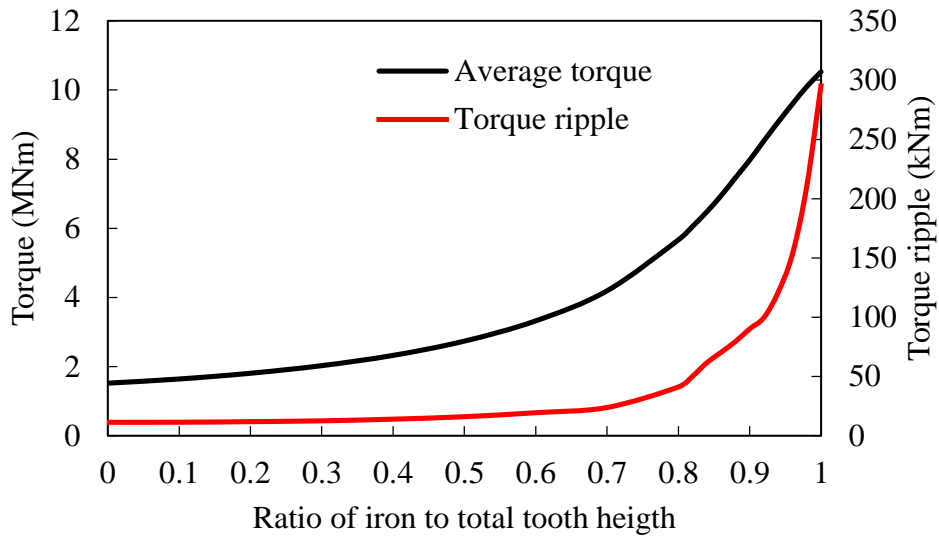


(a) Waveform

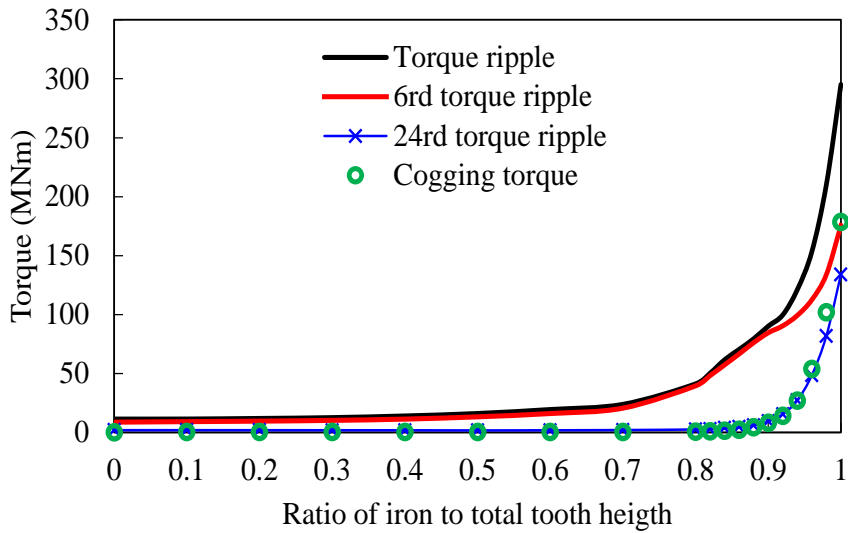


(b) Spectrum

Fig. 136 Waveforms and spectrums of cogging torque.



(a) Average torque and peak to peak torque ripple



(b) Peak to peak torque ripple, 6th and 36th torque ripple and cogging torque
Variations of average torque and torque ripple with iron tooth height.